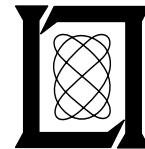# The FLOWS (FAA-Lincoln Laboratory Operational Weather Studies) Automatic Weather Station Network in Operation

M. M. Wolfson
J. T. DiStefano
B. E. Forman

26 March 1987

Lincoln Laboratory

MASSACHUSETTS INSTITUTE OF TECHNOLOGY

LEXINGTON, MASSACHUSETTS

1. Report No. DOT/FAA/PM-85-27	2. Government Accession No.	3. Recipient's Catalog No.
4. Title and Subtitle The FLOWS (FAA-Lincoln Laboratory Operational Weather Studies) Automatic Weather Station Network in Operation		5. Report Date 26 March 1987
		6. Performing Organization Code
7. Author(s) M.M Wolfson, J.T. DiStefano, B.E. Forman		8. Performing Organization Report No. ATC-134
9. Performing Organization Name and Address Lincoln Laboratory, MIT P.O. Box 73 Lexington, MA 02173-0073		10. Work Unit No. (TRAIS)
		11. Contract or Grant No. DTFA-01-80-Y-10546
12. Sponsoring Agency Name and Address Department of Transportation Federal Aviation Administration Systems Research and Development Service Washington, DC 20591		13. Type of Report and Period Covered Project Report
		14. Sponsoring Agency Code

15. Supplementary Notes

16. Abstract

This report describes in detail the FLOWS automatic weather station network as a wind shear data collection system, describes the post-data collection processing and analysis procedures, and presents an evaluation of the performance of the network after its first field test and an illustration of how the data are actually used in analysis. Preliminary results of an investigation into correcting wind speed measurements for the effects of anemometer site obstructions are also presented. The goal has been to describe all facets of the weather station system, data processing, and preliminary performance results in sufficient detail so as to allow current and future users to understand the experimental utility of the weather station data and the limitations, the characteristics of the meteorological sensors, and the possible improvements that could be made to the weather station system.

17. Key Words		18. Distribution Statement

automatic weather station
mesonet
meteorological
  instrumentation
microburst
low-altitude wind shear
	Doppler weather radar
	anemometer site obstructions
	wind speed
	  corrections
	PROBE station
		Document is available to the public through the National Technical Information Service, Springfield, VA 22161.

19. Security Classif. (of this report) Unclassified	20. Security Classif. (of this page) Unclassified	21. No. of Pages 266	22. Price

FORM DOT F 1700.7 (8-69)

NOTICE

Mention of a commercial company or product does not constitute an endorsement by the Federal Aviation Administration or by MIT Lincoln Laboratory. Use for publicity or advertising purposes of information from this publication concerning proprietary products or the tests of such products is not authorized.

ABSTRACT

This report describes in detail the FLOWS* automatic weather station network as a wind shear data collection system, describes the post-data collection processing and analysis procedures, and presents an evaluation of the performance of the network after its first field test and an illustration of how the data are actually used in analysis. Preliminary results of an investigation into correcting wind speed measurements for the effects of anemometer site obstructions are also presented. The goal has been to describe all facets of the weather station system, data processing, and preliminary performance results in sufficient detail so as to allow current and future users to understand the experimental utility of the weather station data and the limitations, the characteristics of the meteorological sensors, and the possible improvements that could be made to the weather station system.

---

*FAA-Lincoln Laboratory Operational Weather Studies.

CONTENTS

LIST OF ILLUSTRATIONS

LIST OF TABLES

ACKNOWLEDGMENTS

LIST OF ACRONYMS AND ABBREVIATIONS

ASCII   American Standard Code for Information Interchange

ATC   Air Traffic Control

AWS   Air Force Air Weather Service

BCH   Bose, Ray-Chaudhuri, Hocquenghem (authors of error detecting
            bit code)

CCOPE   Cooperative Convective Precipitation Experiment

CIDF   Common Instrument Data Format

DCP   data collection platform

ETI   Electronic Techniques, Incorporated

FAA   Federal Aviation Administration

FL-1   FAA-Lincoln Laboratory Weather Radar System No. 1

FL-2   FAA-Lincoln Laboratory Weather Radar System No. 2

FLOWS   FAA-Lincoln Laboratory Operational Weather Studies

GOES   Geostationary Operational Environmental Satellite

HP   Hewlett-Packard

ID   Identification

LAWS   low-altitude wind shear

LLWAS   Low Level Wind Shear Alert System

MCM   Master Control Module, part of Synergetics DCP

M.I.T.   Massachusetts Institute of Technology

MLS   Maximum Linear Sequence (bit code)

MRI   Meteorological Research, Incorporated

NCAR   National Center for Atmospheric Research

NEMA   National Electrical Manufacturers' Association

LIST OF ACRONYMS AND ABBREVIATIONS (Continued)

NESDIS   National Environmental Satellite, Data, and Information Service
          (part of NOAA)

NESS   National Earth Satellite Service

NEXRAD   Next Generation Doppler Weather Radars

NOAA   National Oceanic and Atmospheric Administration

NWS   National Weather Service

PAM   Portable Automated Mesonet

PROBE   Portable Remote Observations of the Environment
          (name for original automatic weather stations)

TDWR   Terminal Doppler Weather Radar

I. INTRODUCTION

A. The FLOWS Project

The Lincoln Laboratory Weather Radar Project is concerned with identifying and resolving the technical issues associated with meeting unique Federal Aviation Administration (FAA) needs for real-time hazardous weather information used by pilots, air traffic controllers, and meteorologists. The weather radar has the potential to be a primary source of this information, but the radars now in use have a number of deficiencies, and the data from these radars are currently available only to the meteorologists. The FAA, the National Weather Service (NWS), and the Air Force Air Weather Service (AWS) have joined together to fund a national network of "next generation" weather radars (NEXRAD) that will have advanced capabilities. In particular, the radars will be capable of sensing wind speed and direction by Doppler processing. These Doppler radars can detect rain, hail, turbulence, and low-altitude wind shear (LAWS) and can measure the wind characteristics as a function of altitude.

The FAA is currently planning to procure additional NEXRAD-like Terminal Doppler Weather Radars (TDWR) that can be devoted to detecting weather hazards at a number of airports. The NEXRAD and TDWR radar data will become part of the new enroute and terminal weather information system currently being developed by the FAA to provide real-time Doppler radar information to the ATC users identified above.

Under FAA sponsorship, Lincoln Laboratory has initiated long term study called the FLOWS (FAA-Lincoln Laboratory Operational Weather Studies) Project that places emphasis on automated hazardous weather detection in the airport terminal area with a NEXRAD-like Doppler weather radar (Evans and Turnbull, 1985). Most fatal aircraft accidents for which weather has been cited as the cause have occurred in the airport terminal area. From investigations of these accidents, it has been determined that low-altitude wind shear specifically has often been the cause (see Table I-1). Understandably, the FAA is especially interested in knowing more about the causes and the characteristics of low-altitude wind shear. Thus, the FLOWS radar studies of aviation-hazardous weather focus on the automatic detection and warning of low-altitude wind shear in the airport terminal area.

B. FLOWS Measurements

The primary FLOWS measurement sensor is a relocatable S-band Doppler weather radar designed and assembled by Lincoln Laboratory (Evans and Johnson, 1984; see Figure I-1). Because only the radial component of the true windfield can be measured by Doppler radar, other support sensors are needed to confirm the radar-based detections of wind shear hazards. Data from a second Doppler radar can provide the orthogonal wind components when the geometry is favorable and thus allow for the derivation of true horizontal winds in these cases. The FAA has funded the University of North Dakota to use its C-band Doppler radar during part of FLOWS to provide support measurements of this kind.

Table I-1. Aircraft accidents and incidents related to low-altitude wind shear (1964-1982). Taken from National Research Council (1983).

No	Year & Date	Time (LST)	Location	Airline Flt No (Aircraft type)	T/O or LDG (Runway)	Fat/Inj	Wind Shear Experienced	Weather Systems and References( )
1	1964 MAR 01	1129	Lake Tahoe NV	Paradise 901A (L-1049)	●LDG ---	85/0	During climbout after a missed approach	Strong mountain lee wave during snowstorm (1) (3) (9)
2	1964 JUL 01	2134	JFK New York NY	AA 64 (B-720B)	●LDG 31R	0/0	Windshift from headwind to cross-wind	Thunderstorm with a sharp pressure rise(1)
3	1965 MAR 17	1858	Kansas City MO	TWA 407 (B-727)	●LDG 36	0/0	Wind direction change on final, 310°-21kts to 280°-22kts	Unstable moist air(1)
4	1968 JUN 08	1351	Salt Lake Cty UT	UAL 8327 (B-727)	●LDG 34L	0/1	260°-13kts at 1351 to 280°-12kts at 1354	Heavy thunderstorm with suspected gust front(1)
5	1970 JUL 20	1136	Naha AB Okinawa	FLY TIG 45 (DC-8)	●LDG 18	4/0	10kts tailwind near threshold	Heavy rainshower one mile in diameter(1)
6	1970 DEC 10	1926	St Thomas VI	Carib-Atl (CV-640)	●LDG 09	NA	Landing in 080°-20kts wind	Lee side flow in rainshower(1)
7	1971 JAN 04	1832	LGA New York NY	FAA N-7 (DC-3)	●LDG 04	0/2	Tailwind changed into headwind.	Frontal Shear(1) (9)
8	1972 MAY 18	1421	Ft Lauderdale FL	EAL 346 (DC-9)	●LDG 09L	0/3	180°-10kts at 1418 to 130°-12kts at 1426	Heavy thunderstorm(1)
9	1972 JUL 26	1406	New Orleans LA	NA 32 (B-727)	●LDG 28	0/0	IAS dropped 162 to 122kts	Intense rainstorm and thunderstorm(1)
10	1972 DEC 12	2256	JFK New York NY	TWA 669 (B-707)	●LDG 04R	0/0	42kts tailwind at 1500'to 5kts headwind at the surface	Frontal shear(10); Fog and drizzle (1) (9)
11	1973 MAR 03	1250	Wichita KS	TWA 315 (B-727)	●LDG 19R	0/0⁻	100°-10kts at 1240:00 to 170°-10 kts to 070°-10kts at 1249:10	Thunderstorm(1)
12	1973 JUN 15	1403	ORD Chicago IL	Airlift 105 (DC-8)	●LDG 22R	0/0	Estimated downdraft 50fps at 3000', 13fps at 500' AGL	Heavy rainstorm(1)
13	1973 JUL 23	1643	St Louis MO	OZ 809 (FH-227B)	●LDG 30L	38/6	Up- and downdrafts	Outflow shear(4); Thunderstorm, sharp pressure rise(1)
14	1973 NOV 27	1851	Chattanooga TN	DL 516 (DC-9)	●LDG 20	0/42	Low-altitude wind shear	Outflow shear(4); Thunderstorm outflow (1) (9)
15	1973 DEC 17	1543	Boston MA	Iberia 933 (DC-10)	●LDG 33L	0/16	200°-24kts at 500', 260°-12kts at 200', 315°-08kts at surface	Frontal shear(4), Rain and fog(1) (9)
16	1974 JAN 30	2341	Pago Pago SAMOA	PAA 806 (B-707)	●LDG 05	96/5	Decreasing headwind and/or down-draft during the final 4 seconds	Outflow shear(4), Heavy rainshower (1) (9)
17	1975 JUN 24	1457	JFK New York NY	EAL 902 (L-1011)	OLDG 22L	---	8kts headwind to 6kts tailwind with 20fps downdraft	Small downburst or microburst(5); Strong thunderstorm(1) (9)
18	1975 JUN 24	1505	JFK New York NY	EAL 66 (B-727)	●LDG 22L	112/12	14kts headwind to 1kt headwind with 21fps downdraft	Small downburst or microburst(5); outflow shear(4); Strong thunderstrom (1) (9)
19	1975 AUG 07	1511	Denver CO	CO 426 (B-727)	●T/O 35L	0/15	IAS decreased 158 to 116kts in 5 seconds	Small downburst or microburst(6); Outflow shear(4); Thunderstorm(1) (9)
20	1975 NOV 12	2002	Raleigh NC	EAL 576 (B-727)	●LOG 23	0/1	10° windshift, gust up to 21kts	3 inch per hour rain fall rate(1) (9)
21	1975 DEC 31	1056	Greer SC	EAL (DC-9)	●LDG 03	0/0	200° change in wind direction	Light rain and fog(1)
22	1976 JUN 23	1612	Philadelphia PA	AL 121 (DC-9)	●LDG 27R	0/87	65kts headwind to 20kts tail-wind	Microburst(7), Outflow shear(4), Fast-moving thunderstorm(1) (9)
23	1976 DEC 12	2326	Cape May NJ	Atl Cty 977 (DHC-6)	●LDG 19	3/7	Gust to 50kts	Frontal shear(1) (9)
24	1977 JUN 03	1258	Tucson AZ	CO 63 (B-727)	●T/O 21	0/0	30kts headwind to 30kts tail-wind	Microburst(7); Outflow shear(4); Downdraft in thunderstorm(9)
25	1979 AUG 22	1412	Atlanta GA	EAL 693 (B727)	OLDG 27L	---	strong downdraft and headwind	Microburst(8), Thunderstorm rainshower(9)
26	1982 JUL 09	1509	New Orleans LA	PAA 759 (B-727)	●T/O 10	153/9	Headwind tailwind and downdraft shear	Microburst with heavy rain(9)
27	1982 JUL 28	1521	LGA New York NY	TWA 524 (B-727)	OLDG 22	---	Severe wind shear at 20-100' AGL	Strong thunderstorm with gusty winds(2)

TOTAL: ● 24 Accidents, O 3 Incidents, 491 fatalities / 206 Injuries

SOURCES: (1) Shrager, 1977; (2) NTSB letter to FAA, March 25, 1983; (3) Wuttele, 1970; (4) FAA Wind Shear Program, December 1982; (5) Fujita and Byers, 1977; (6) Fujita and Caracena, 1977; (7) Fujita, 1978; (8) Fujita, 1980; (9) NTSB Accident/Incident Reports; (10) Sowa, Private Communication.
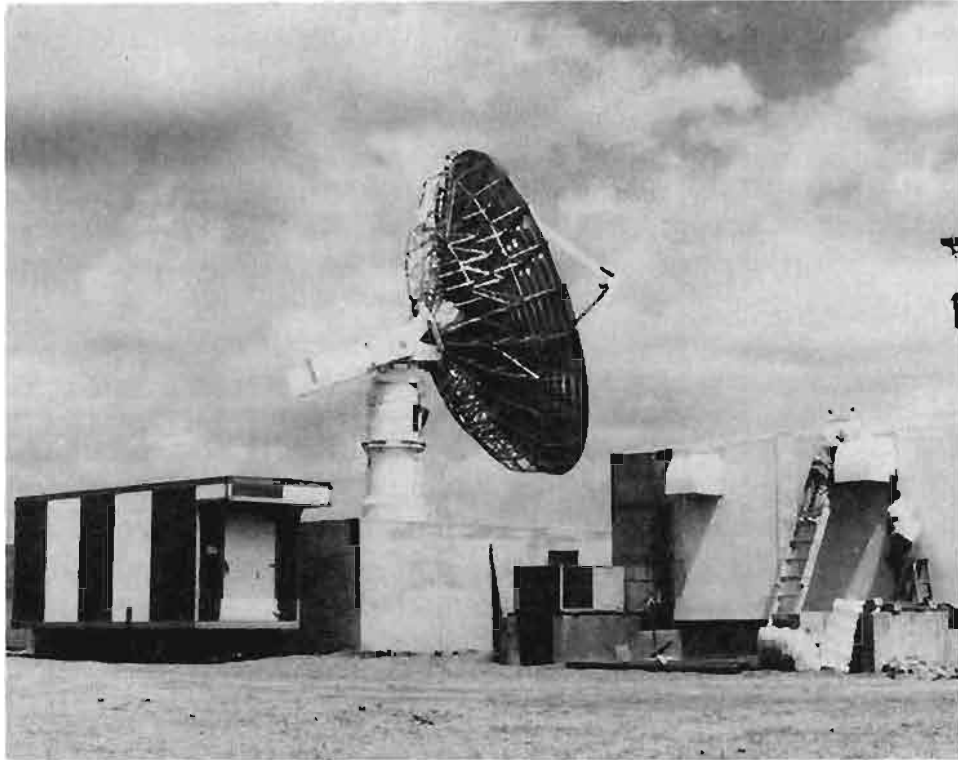
Figure I-1. FL-2, the FAA-Lincoln Laboratory S-band Doppler radar, is shown without its radome. The antenna is 28' in diameter and the phase center height is 25'.

The FLOWS automatic weather station network, called a mesonet, is being operated by Lincoln Laboratory for the FAA as a major additional source of support measurements. The surface meteorological data collected continuously by the 30 stations will be compared with FL-2 Doppler radar data both to validate low-altitude wind shear and other possibly hazardous weather detected by radar and to provide an indication of undetected wind shear events. Table I-2 lists the meteorological variables measured by the network and the required accuracies needed to support the FLOWS program objectives. All of the meteorological data collected by the weather station network will be used to help gain a better understanding of the causes and characteristics of low-altitude wind shear.

In addition to the mesonet data, surface wind speed and direction data from the 6-anemometer FAA Low Level Wind Shear Alert System (LLWAS) are recorded. The possibility that these measurements could be used in conjunction with single-Doppler radar data in real-time to provide more accurate estimates of runway headwind/tailwind shear or as part of a large database of different types of data to be used as part of an expert system is being explored.

In-situ measurements of wind shear, liquid water content, and turbulence are obtained with an instrumented Cessna Citation II aircraft owned and operated by the University of North Dakota. Qualification of the relationship between radar-detected and aircraft-experienced turbulence and wind shear also forms a fundamental part of the FLOWS program objectives.

The humid southeast part of the country was selected for the first data collection operation because the frequency of thunderstorms and convection there is high and because the frequency of commercial air traffic is high there as well. Also, no high resolution measurements capable of revealing small scale low-altitude wind shear had been collected there before. The FL-2 radar was moved to a selected site in Olive Branch, MS approximately 17 km southeast of the Memphis International Airport in late July 1984 (Figure I-2), and began making measurements in 1985. The locations of all of the FLOWS sensors are shown in Figure I-3.

C. Purpose and Overview of this Report

The purpose of this report is to describe in detail the automatic weather station network as a wind shear data collection system, to describe the post-data collection processing and analysis procedures, and to evaluate the performance and utility of the system after its first field test.

In the following chapter (II), some basic information on the problem of low-altitude wind shear for aviation is presented. It is shown that the microburst, a small scale intense downdraft which hits the surface and causes a strong divergent outflow of wind, has a particularly hazardous pattern of wind shear. Also some background on the automatic weather stations and a description of the 1984-85 FLOWS network near Memphis are presented.

Variable	Required Accuracy	Driving Factors
Temperature	± 1.0°C	Thunderstorm outflow front detection, temperature
Relative Humidity	± 2% above 50%	~ 1.0° accuracy in equivalent potential temperature
Pressure	± 1.0 mb absolute ± 0.2 mb tendency	Resolve pressure jump (~1 mb) associated with outflow
Wind Speed	± 1.0 m/s	Resolve natural variations of wind speeds $\geq$ 1.0 m/s across network
Wind Direction	± 5°	Resolve significant ($\geq$ 50°) wind direction changes to within 10%
Precipitation	± 0.2 mm (per min.)	Resolve significant accumulations (> 0.25 mm in 1 min.) of rainfall

Table I-2. Required mesonet variable accuracies needed to support the FLOWS program objectives with brief statement of the specific driving factors. Accuracies meet or exceed standards set by the World Meteorological Organization (WMO,1983).

153197-N-01

MEMPHIS
INTERNATIONAL
AIRPORT

TENNESSEE

MEMPHIS

ARKANSAS

LOCATION OF
FLOWS
PROJECT
1984 - 1985

MISSISSIPPI

Figure I-2. Location of the 1984-85 FLOWS data collection operation near Memphis, TN.
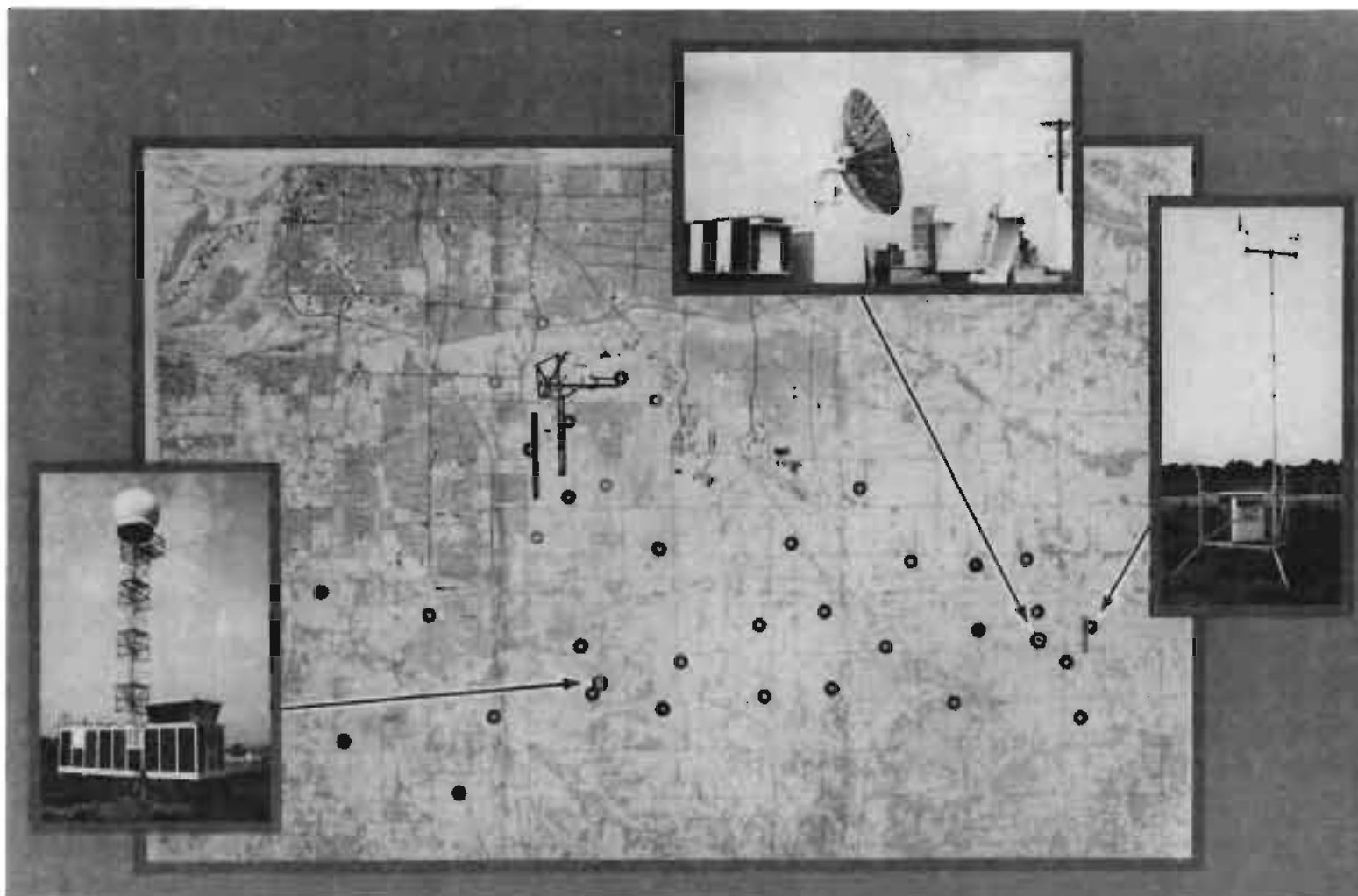
Figure 1-3. Map showing location of FL-2 S-band Doppler weather radar (top) relative to Memphis International Airport (dark lines near center of map). The location of the University of North Dakota C-band Doppler weather radar (left) is also shown. Other circles on the map show the locations of the automatic weather stations (right) and, near the airport, the FAA Low Level Wind Shear Alert System (LLWAS).

Substantial changes have been made to the weather stations since June of 1983 when they were furnished to Lincoln Laboratory. Although the same sensors are still being used, some of them have been modified and the Data Collection Platforms are entirely new. Technical information on the weather station system, including the instrumentation, hardware, and Data Collection Platforms is given in Chapter III, and a complete description of the transmitted data is given in Chapter IV. The post-data collection processing and analysis are described generally in the two subsequent chapters. A technique for mathematically correcting wind speed measurements for site obstructions which can help compensate for less than perfect anemometer locations is given in Chapter V, and the software data processing system is described in Chapter VI. In Chapter VII, the overall performance of the automatic weather station system is evaluated and in Chapter VIII an analysis of a microburst that occurred over the Memphis International Airport is presented to demonstrate the utility of the mesonet data. Chapters IX and X present, respectively, a summary of the report and recommendations for improvements in both the weather station system and the data processing system.

II. BACKGROUND

In this chapter some basic information on the hazard of low-altitude wind shear for aviation is presented. Some background on this subject is necessary to appreciate the overall design of the FLOWS measurement program as well as the need for an automatic weather station network. A brief history of the automatic weather stations and a description of the 1984-85 FLOWS network near Memphis, TN are also presented.

A. Low-Altitude Wind Shear

Low-altitude wind shear, in its various forms, has long been known as a hazard to aviation for it influences aircraft at probably the most vulnerable time during their entire flight. The wind shear encountered on take-off or landing has caused several tragic accidents, including the Pan Am 759 crash in July 1982 just outside of the New Orleans International Airport. Most recently, Delta Flight 191 crashed on landing at Dallas/ Ft. Worth International Airport on 2 August 1985 after entering a quickly-developing isolated thunderstorm. Although the exact causes of this crash have yet to be determined by the National Transportation Safety Board, the plane landing just before Delta 191 encountered wind shear leading to a 25-knot loss of airspeed and a rapid loss of altitude. The rain within the storm was very heavy, and had apparently intensified very rapidly (Ott, 1985).

Low-altitude wind shear is a broad category encompassing several distinct meteorological phenomena. The most common of these is the "gust front", the boundary between cool air flowing out from beneath a mature thunderstorm and the surrounding warm environmental air. Although a gust front is created by a particular storm cell, it can propagate miles away from the parent cell and can last for hours, as well as merge and mix with outflow currents from other neighboring cells.

The main dangers for aircraft encountering a gust front are the sudden change in both horizontal and vertical wind speed and direction across the front, together with the strong turbulence in the "nose" of the gust front. Figure II-1 shows the structure of a mature thunderstorm with an overlay showing a typical aircraft glideslope penetrating the shear zone associated with the gust front and Figure II-2 depicts in detail the structure of the outflow leading edge. Since the shear zone associated with the gust front is spatially large in the along-front direction (10 km or more), is fairly persistent (lifetimes greater than 20 min), and is advected horizontally in the low level flow, the task of automatically predicting gust fronts will be manageable as long as they can be detected some distance away from the airport.

A more recently discovered, but possibly also common meteorological phenomenon contributing to low-altitude wind shear is the "downburst". The downburst is defined as a divergent outflow of damaging wind (>18 meters per second, 35 nautical miles per hour) of spatial extent greater than 4 km

TYPICAL STRUCTURE OF A SEVERE
THUNDERSTORM CELL IN THE MATURE STAGE

UPPER WINDS ⟹

ALTITUDE (ft)

IIII TURBULENCE

ICE CRYSTALS

SNOW (and Hail)

SHEAR ZONE

SNOW

WATER DROPLETS

RAIN

GUST FRONT
(First Gust)

SHEAR
ZONE

GLIDESLOPE

SURFACE RAIN

SURFACE

40,000
35,000
30,000
25,000
20,000
15,000
10,000
5,000

HORIZONTAL SCALE   0 ½ 1 mi

DRAFT VECTOR SCALE   0 30 ft s
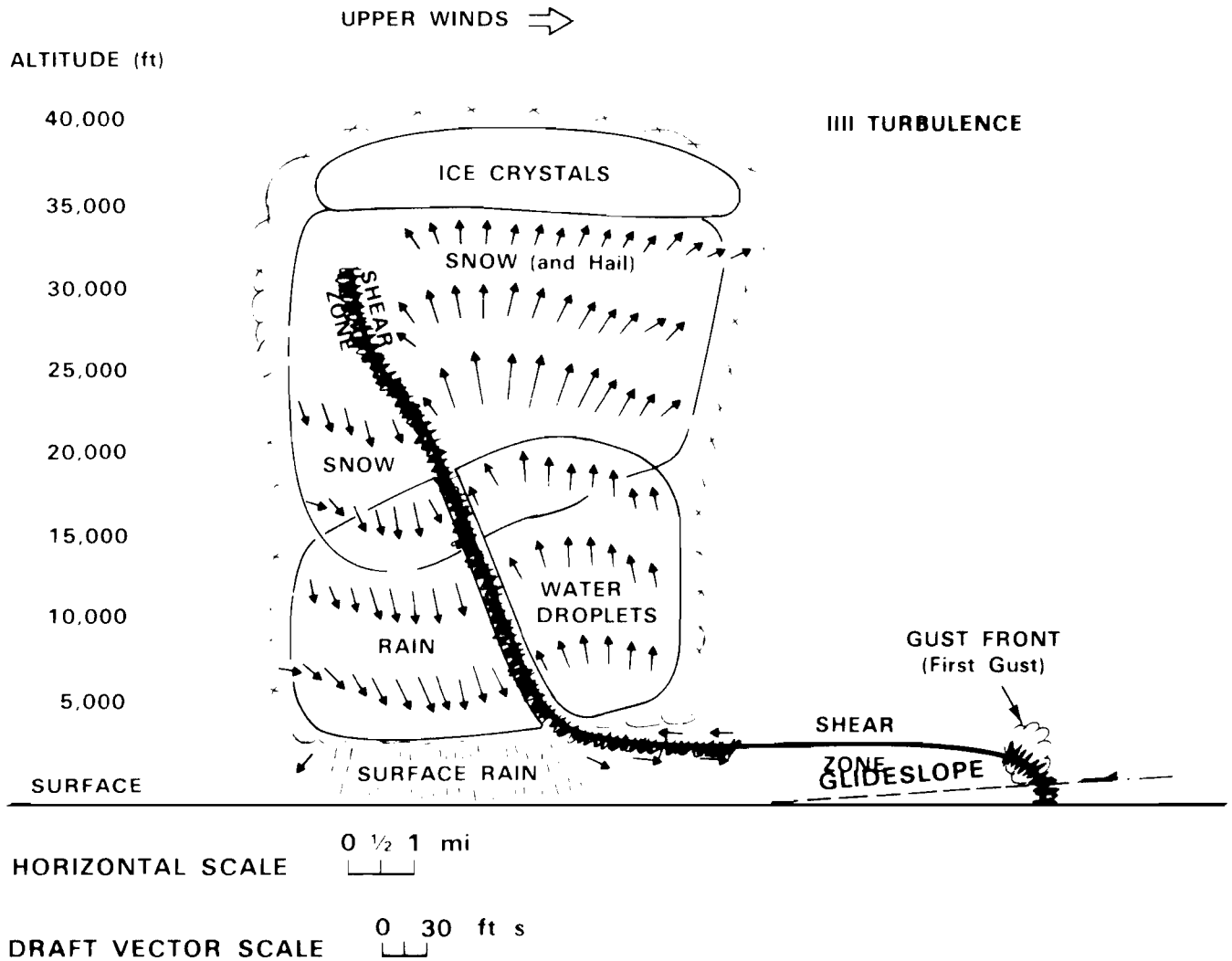
Figure II-1. Typical structure of a mature storm cell. The solid line, separating updraft from downdraft inside the cell and outflow from inflow in front of the cell, represents the turbulent shear zone.

120056-N 01

TURBULENT AREA

GUST FRONT ENVELOPE

RAIN

MULTIPLE SURGES

HEAD

WAKE

WAKE

WARM AIR INFLOW

GUST FRONT

COLD AIR OUTFLOW

NOSE

BACKFLOW

TURBULENT AREA

3000

2000

1000

HEIGHT AGL (m)

DISTANCE FROM GUST FRONT (km)

20   15   10   5   0   5

2-3
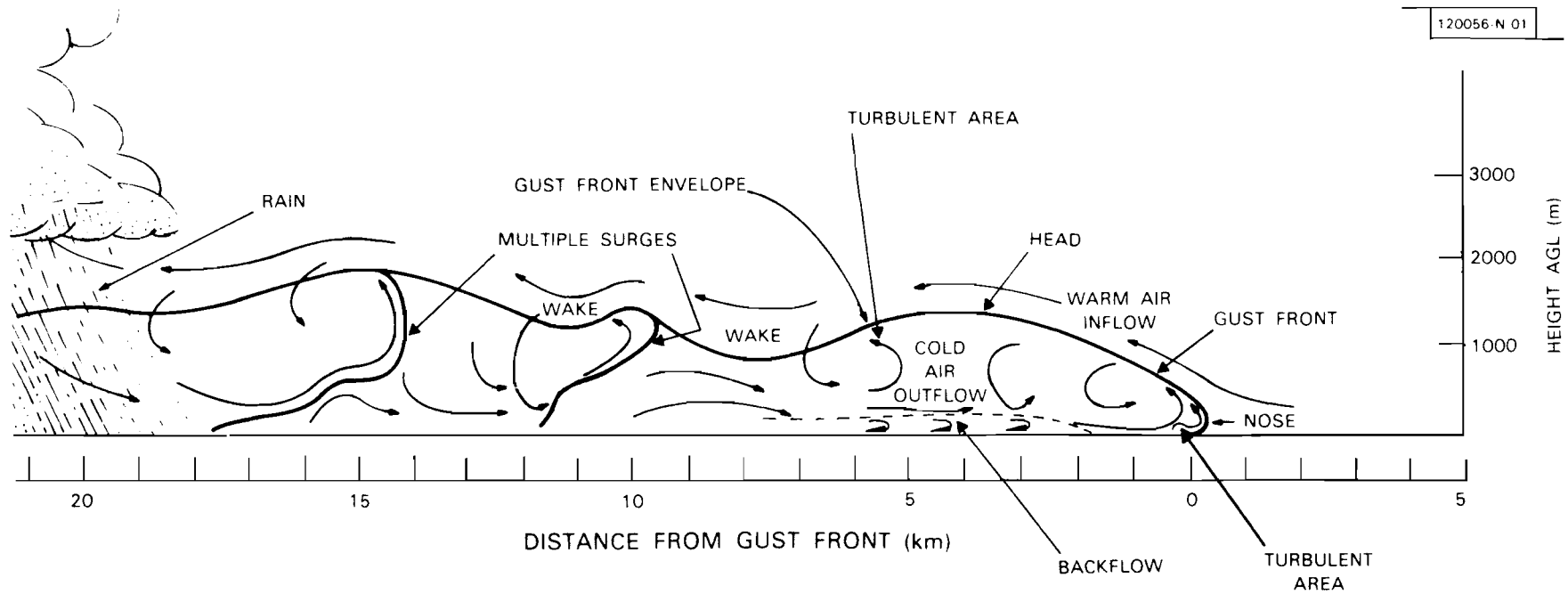
Figure II-2. Schematic diagram of the vertical structure of a thunderstorm outflow and gust front. Depicted motion is gust front relative. After Goff (1976).

across. If the outflow is less that 4 km across, it is called a "microburst". Although downbursts and microbursts are the result of downdrafts of various sizes impacting the ground and spreading, the explanations for the downdrafts themselves differ.

The downburst or microburst, unlike the gust front, is a small scale highly divergent wind shear event. The temporal scale of a microburst can be characterized by the time from initial low-altitude divergence to the time of maximum velocity differential. Case studies based on the 1984 FLOWS Memphis mesonet data (Wolfson, et al, 1985) suggest that this time scale is approximately 4-5 minutes. This is essentially in agreement with time scales found for microbursts in the Denver area (Wilson, et al, 1984) and in the Chicago area (Fujita, 1985), although the parent storm types differ considerably. However, the peak outflow winds may last only one minute and be 25% to 50% stronger than those in the preceding or following minute. These features, compounded with the fact that downbursts descend from aloft rather than propagate horizontally into an area, will make them extremely difficult to predict and detect.

The downburst/microburst is a significant aircraft hazard because a plane may experience increased lift when first encountering the downburst outflow but the central downdraft and increased tailwind on the far side force the aircraft to lose airspeed and sink rapidly (Figure II-3). An analysis of the Pan Am Flight 759 accident which occurred at New Orleans in July 1982 revealed that a microburst was responsible for the wind shear that caused the plane to crash. Figure II-4 shows a vertical cross section of the low-altitude winds at the time that accident took place (Fujita, 1983).

In addition to the hazard posed by the divergent outflow itself, another hazard exists in the microburst. As the downdraft air spreads radially outward along the ground, it forms its own small gust front at the leading edge, but the outflow air moves so rapidly that it soon overtakes the gust front. The air recirculates in a vertical spiral at the leading edge of the outflow causing the development of a deeper "head" and locally strong downdrafts well away from the microburst. An analysis of the Delta 191 accident which occurred at Dallas/Ft. Worth in August 1985 by Fujita (1986) suggests that the aircraft encountered a microburst with this type of outflow "wave" structure while it was trying to land (Figure II-5). The waves within the outflow are capable, in their own right, of causing a rapid loss of altitude of a plane flying through them. Since this turbulent spinning region of air can also be some distance away from the heaviest rain it is, in some ways, as great a hazard as the main microburst since conventional airborne radars could not possibly detect it. Often, the microburst itself is coincident with a local maximum in the radar reflectivity field representing a region of intensified rainfall.

Other sources of low-altitude wind shear are squall lines, cold fronts, low level jet streams, tornadoes, and any strong localized convection which

AIRCRAFT ENCOUNTER WITH A MICROBURST
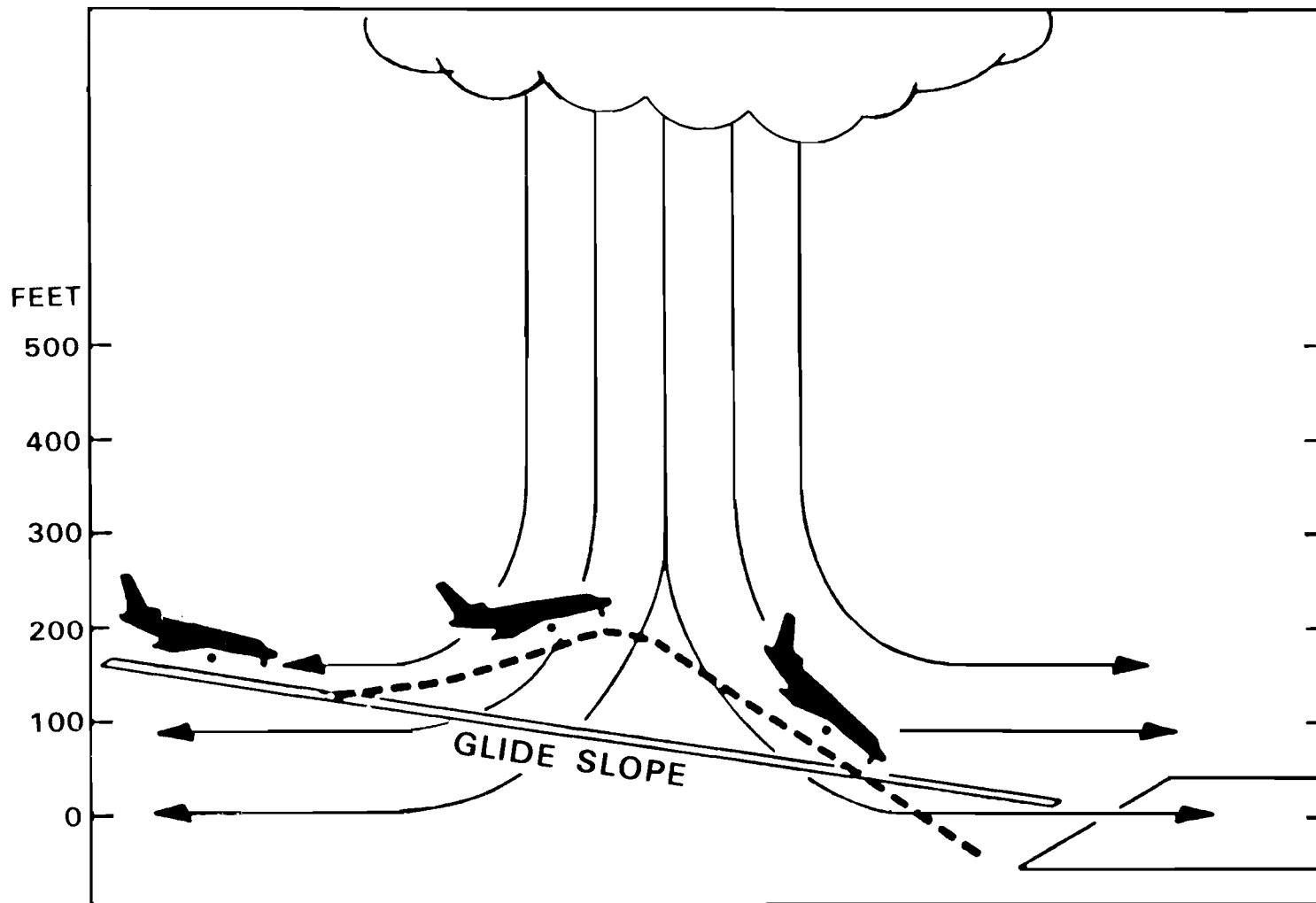
Figure II-3. Schematic drawing of an aircraft encounter with a microburst, a particularly hazardous form of low-altitude wind shear. Notice how the increased headwind lifts the plane above its intended glideslope while the increased tailwind causes the plane to fall below its intended glideslope.

VERTICAL CROSS SECTION OF MICROBURST WINDS
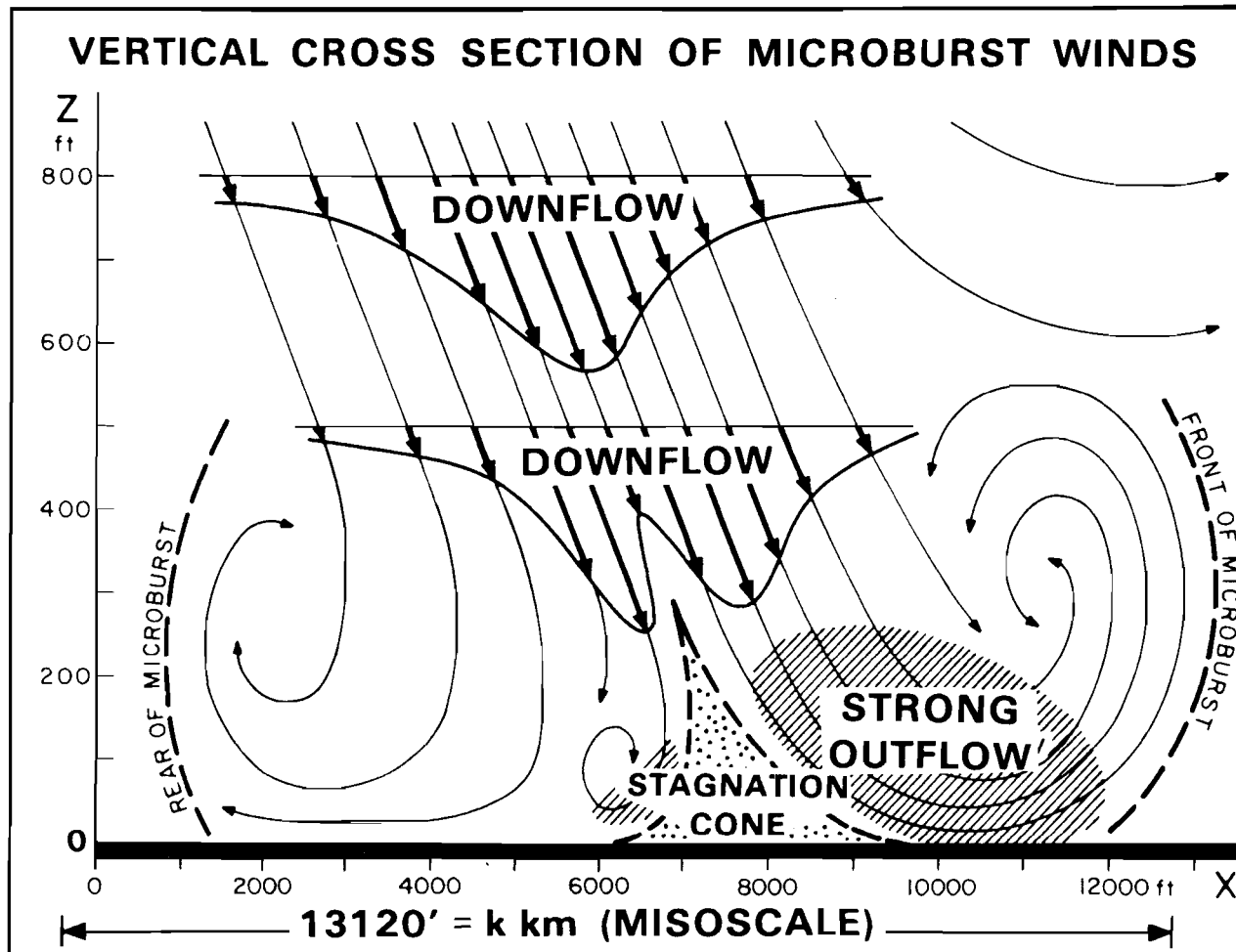
Figure II-4. Vertical cross-section of microburst winds at the time of
the Pan Am Flight 759 take-off from New Orleans International Airport
on 9 July 1982. The downflow combined with the strong outflow caused
the plane to lose lift and crash in a residential neighborhood near
the airport. After Fujita (1983).
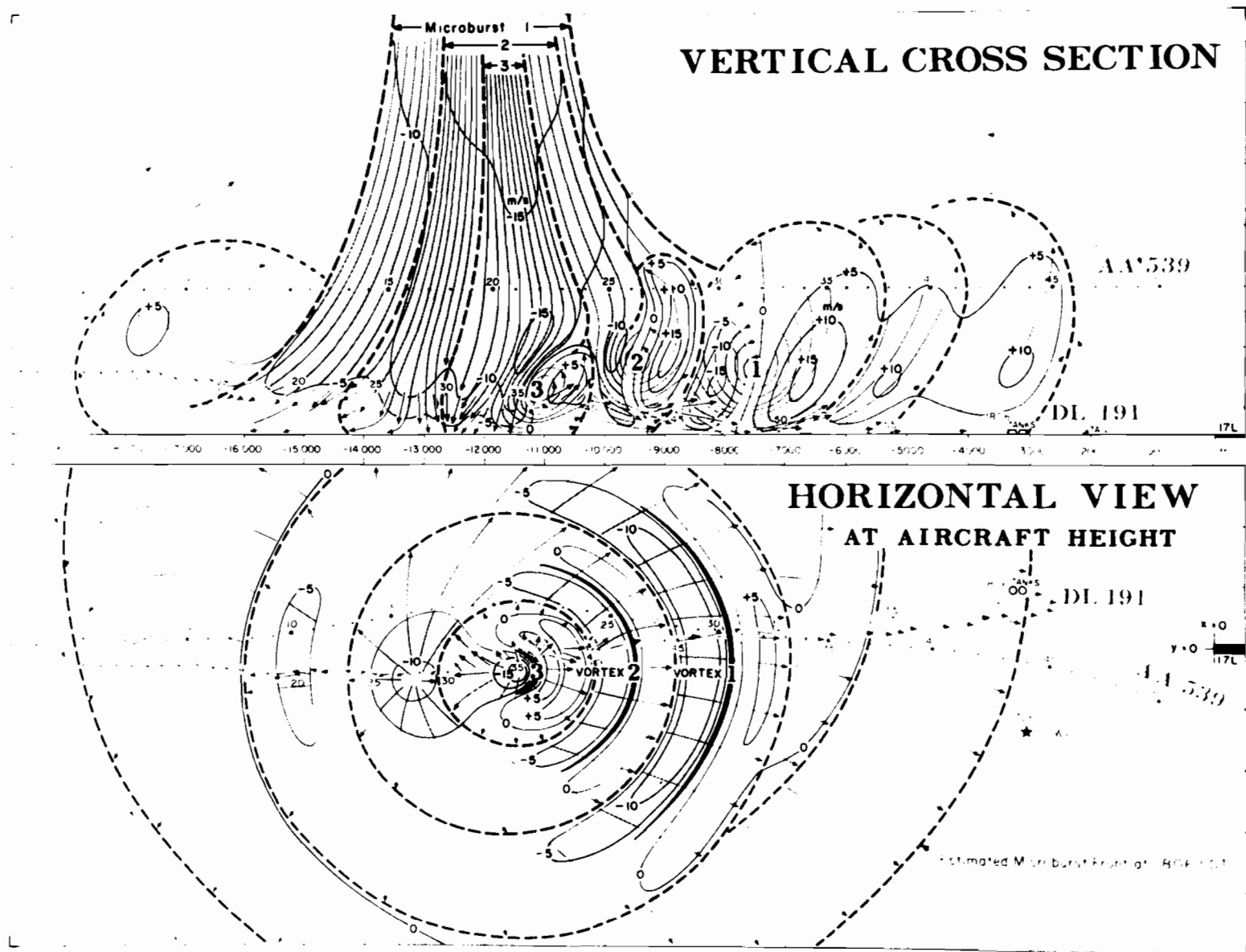
Figure II-5. A vertical cross-section and a horizontal view of the Delta
191 microburst at 1806 CDT on August 2, 1985. This microburst, approxima-
tely 3.5 km in diameter, is characterized by three major internal vortices
which are surrounded by an older vortex encircling the entire event (from
Fujita, 1986).

produces gusty winds and low-altitude turbulence. In the FLOWS wind shear studies the emphasis is placed on downbursts and microbursts for they appear to be common (at least near Memphis), are not well understood, and may be the most aviation-hazardous form of low-altitude wind shear.

B. History of the Automatic Weather Stations

The automatic weather stations that were first used by Lincoln Laboratory in the summer of 1983 were developed by the US Department of the Interior Bureau of Reclamation's Office of Atmospheric Resources Management in the late 1970's (Harrison, et al, 1979). These stations were given the name PROBE, standing for Portable Remote OBservations of the Environment - exactly what they were designed to provide. There was a basic research need at that time for a meteorological data collection network that would allow short term predictions of convective activity, could provide good time resolution, and could be installed and operational in very little time without the need for laying power or telephone data lines.

The stations, shown in Figures II-6 and II-7, were designed to measure temperature, relative humidity, barometric pressure, wind speed, wind direction, and precipitation amounts. The measurements are averaged, stored in memory, and transmitted at regularly-timed intervals to the Geostationary Operational Environmental Satellite (GOES). The data are relayed by the satellite back to earth where they are collected by the NOAA National Environmental Satellite, Data, and Information Service's (NESDIS's) ground station on Wallops Island and by anyone with a receiving station tuned to the correct channel. An additional advantage to collecting the data this way is that the sites almost never have to be visited if they are working properly. The power for the stations is pro-vided by a 12V deep cycle battery which is continuously trickle-charged during daylight hours by the solar panels.

The FAA arranged for the Bureau of Reclamation to furnish 25 of these PROBE stations to Lincoln Laboratory to be operated in the vicinity of Hanscom Field (Bedford, MA) in support of the FAA-Lincoln Laboratory Summer 1983 Doppler radar experiments with FL-1, the Lincoln-built system at MIT (Wolfson, et al, 1984). Unfortunately, a number of problems caused by the use of mesonet equipment that had become old and trouble prone, and to poor sensor calibration procedures prevented the successful collection of data that summer. We did, however, achieve one of our primary objectives which was to learn what would be needed to successfully collect mesonet data in 1984!

During the winter months, new Data Collection Platforms were purchased for each station that are highly reliable, microprocessor-based systems with great flexibility. The sensors were repaired and calibrated at Lincoln Laboratory in order to insure the accuracy of the measurements. Also, the number of stations in the network was increased from 25 to 30 to allow expansion of the spatial coverage without extending the average inter-station spacing.
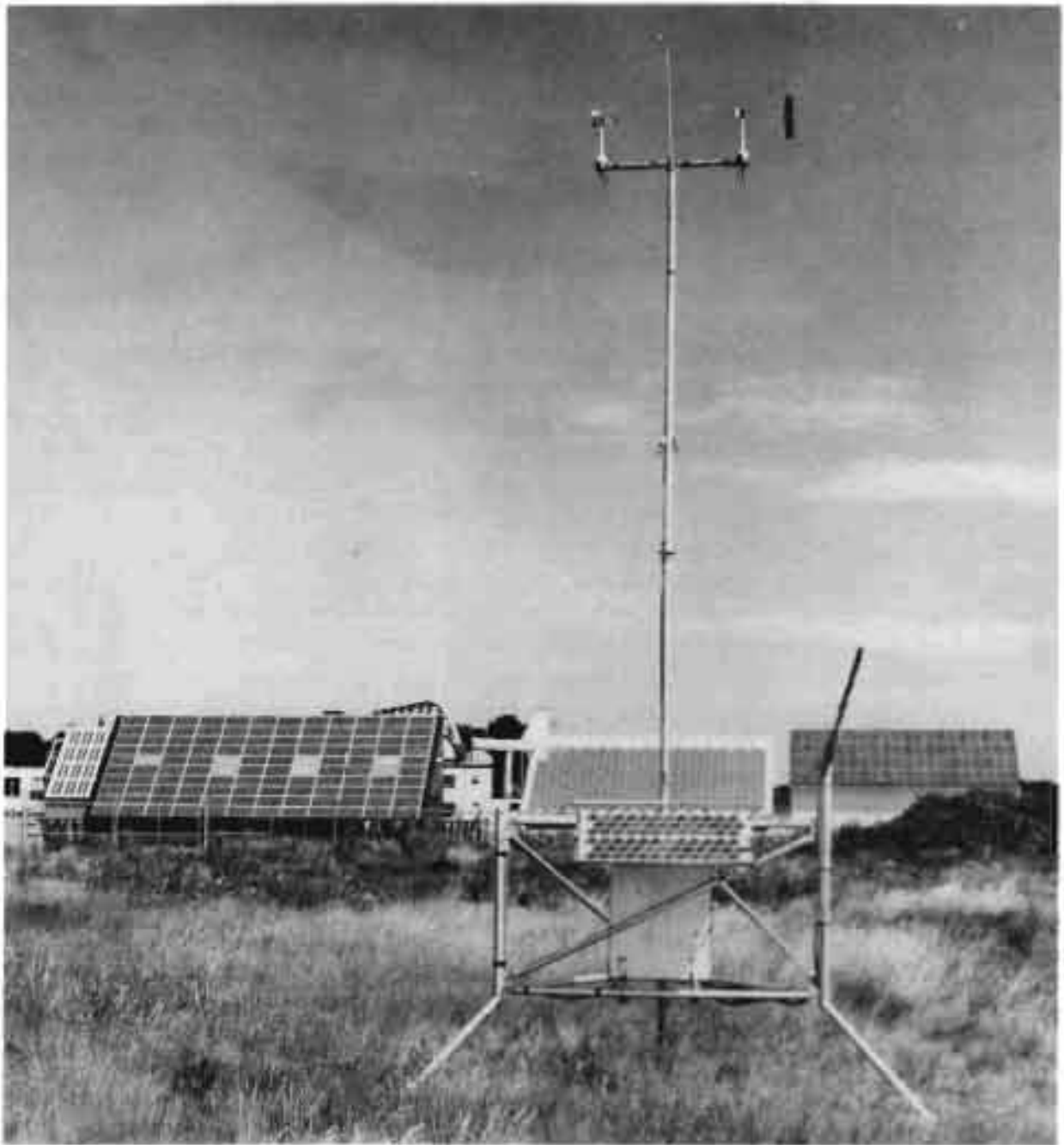
Figure II-6. FLOWS automatic weather station. Solar panels are
visible above white armored box. Vane aspirator is at left (white
tube with fin) and antenna is at right.

Figure II-7. View of automatic weather station features not shown in Figure II-6. Technician is working on antenna. Notice wind sensor mast is self-guyed.

C. The 1984-85 Network

The Memphis International Airport was chosen as the focus for the initial FLOWS FL-2 Doppler radar tests for a number of reasons. First, it has a complex runway pattern, it has air traffic that is light enough to enable a research aircraft to use the airport but heavy enough to be considered one of the major U.S. airports, and the airport is scheduled to receive a NEXRAD system to be operated on an interim basis as a Terminal Doppler Weather Radar. The desire to collect Doppler radar data in a region of the country in which it had not been collected previously was a factor, as was the high thunderstorm frequency in the spring, summer, and fall. Once the airport was decided upon and the testbed radar site was chosen, the mesonet sites were selected. Some stations were sited near the airport to effectively increase the density and spatial extent of the LLWAS system, some were sited around the FL-2 radar (see Figure I-3), and the others were placed between the radar and the airport to fill out the network. Five additional stations were placed southwest of the airport so that surface data could be gathered on approaching storms.

The 1984 FLOWS automatic weather station network in the Memphis area is depicted in Figure II-8 and the 1985 network, with a couple of minor changes (station Nos. 4 and 27), is shown in Figure II-9. The entire network has an oval shape because the northern extent was limited by the heavily built up areas east and west of the airport. Most of the weather stations are south of the Tennessee-Mississippi state line.

The station spacing was determined by the size and scale of the low-altitude wind shear to be measured. The horizontal scale of a microburst is initially less than 4 km across. Thus, the stations were sited approximately 3 km apart, with a maximum allowable distance of 5 km. It is sometimes difficult to justify siting the stations this close together, for if they were farther apart the total network could cover a much larger area and the probability of measuring a low-altitude wind shear event would be greater. However, with that approach the low resolution data collected would not reveal important features of the wind shear and would therefore be of doubtful value. Detailed guidelines for selecting new mesonet sites as well as logistical requirements for deployment of the network are given in Appendix A.

Each Memphis mesonet site has been studied for possible wind obstructions as advised by wind shear expert Dr. T. Fujita of the University of Chicago. Panoramic photographs taken from each site as well as wind speed and direction comparisons between the stations have been used in analyzing the windfields. When serious blockage was found, an attempt was made to relocate the station. In less serious cases, it has been found that mathematical correction factors can help compensate for station blockage (Chapter V).

THIS PAGE INTENTIONALLY LEFT BLANK.

FAA / LINCOLN LAB WIND-SHEAR MESONET AT MEMPHIS, TENNESSEE

DATA SOURCES: USGS 7 1/2 MIN MAPS 1973-1982
1982 AERIAL PHOTOS BY FUJITA
MAPPING & CARTOGRAPHY: T. THEODORE FUJITA

JULY 1984
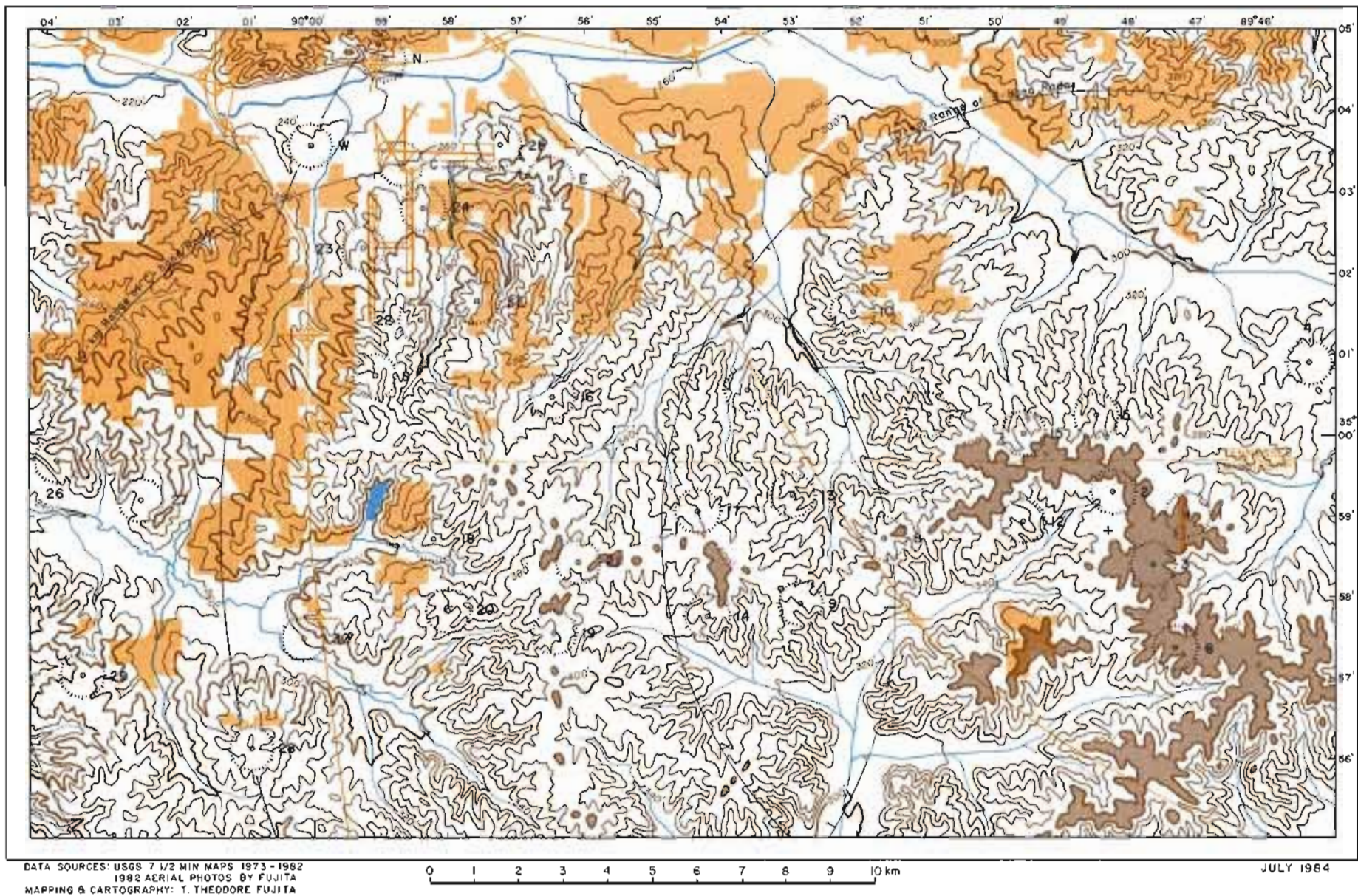
Figure II-8. 1984 FLOWS Automatic Weather Station Network. Mesonet stations are indicated by an open circle surrounded by a compass rose, with the station number just to the right.

FLOWS MESONET AT MEMPHIS
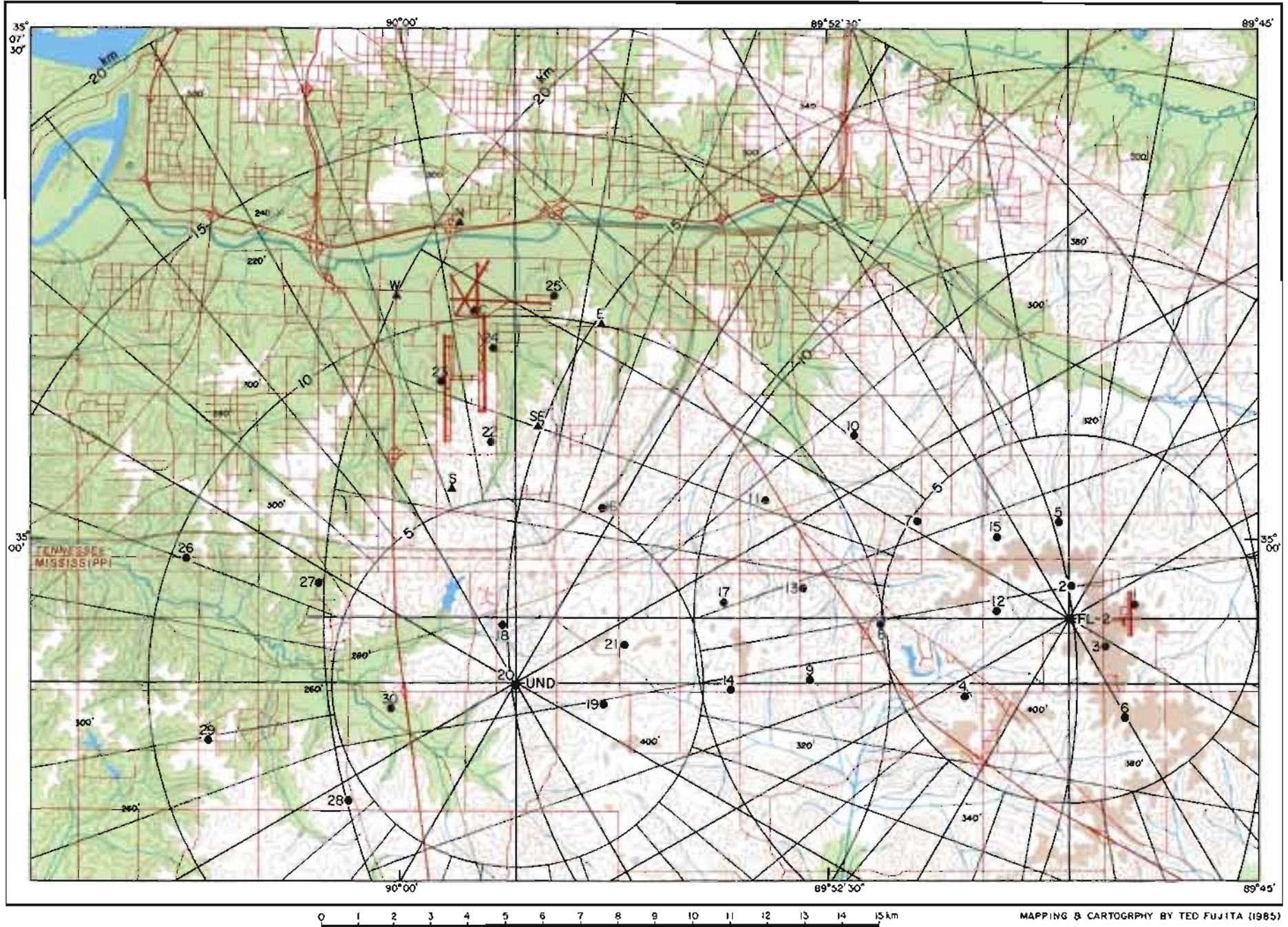
Figure II~9.   1985 FLOWS Automatic Weather Station Network.

MAPPING & CARTOGRPHY BY TED FUJITA (1985)

III. WEATHER STATION SYSTEM

This chapter presents a detailed description of all parts of the FLOWS automatic weather station system. In the first section, the sensors and their maintenance and calibration procedures are described. In the second section, the hardware and mechanical parts of the system are described and in the final section, details on the overall design of the new Data Collection Platforms, the transmission format, and the internal processing software are presented. A complete discussion of the weather station data is given separately in Chapter IV.

A. Instrumentation

For each sensor on the automatic weather stations, a brief technical description is presented. The sensor types and measurement specifications, including the range and resolution of each, are listed in Table III-1. The realized accuracy of the measurements from each sensor depends heavily on the calibration, but the manufacturer-specified accuracies together with the accuracies required to meet the FLOWS program objectives (from Table I-2) are presented in Table III-2.

1. Anemometer

a. Description

The FLOWS automatic weather stations are equipped with the MRI model 1022 wind speed sensors. The instrument consists of a cup anemometer mounted on a common cross arm with the wind vane (see Section III.A.2.) The cross arm height on the station is 6.8 meters above ground level (see Figure II-7).

Wind speed is derived from a photo chopper disk assembly attached to the lower end of the anemometer shaft. As the cups turn, the chopper disk breaks the light beam from a light emitting diode exactly 100 times per revolution. The output signal is a sine wave that has the same frequency as these light pulses, and this frequency is directly proportional to the wind speed.

b. Modifications

i. Fouled Bearings

The Bureau of Reclamation found that many of the anemometers developed bearing problems throughout the course of their deployment due to corrosion by moisture, which obviously prevented an accurate wind speed measurement. Apparently water could migrate up the outside of the anemometer shaft under the anemometer cup assembly, and foul the top set of bearings which are not sealed. Although the manufacturer (Meteorological Research, Inc.) developed a remedy for this problem known as the "Water-Slinger", the personnel from the company which we had calibrate our sensors and set up our stations in

Variable	Sensor	Manufacturer	Range	Resolution
Wind Speed	cup anomometer	Meteorological Research, Inc. (MRI) Model 1022 Modified to prevent water leakage	0.2-54.0 m/s	0.05 m/s
Wind Direction	wind vane	Meteorological Research, Inc. (MRI) Model 1022 with sin-cos output	0°-360°	0.4°
Relative Humidity	thin-film capacitive sensor	Weathertronics model 5121-99 (Vaisala model HMP-14A)	0-100%	2%
Temperature	2-element thermistor	Weathertronics model 5121-99 (Yellow Springs Instrument (YSI) Sensor)	$-30°-^{+}50°$	0.1°C
Pressure	strain gage bridge pressure transducer	Weathertronics model 7115	900-1100 mb	0.1 mb
Precipitation	weighing bucket	Bellfort Instrument Co. Model 5915R	0-300 mm	0.2 mm

Table III-1. Measurement specifications of FLOWS automatic weather station sensors.

Variable	Manufacturer Specified Accuracy	Required Accuracy
Wind Speed	±0.1 m/s or 1% of WS	±1.0 m/s
Wind Direction	±3.6°	±5°
Relative Humidity	hysteresis, linearity < 1% (0-80%)	±2% above 50%
Temperature	0.15°C	±1.0°C
Pressure	0.1% at constant temperature	±1.0 mb absolute ±0.2 mb tendency
Precipitation	½ of 1% FS (1.5 mm) (resolution 0.2 mm)	±0.2 mm (per min.)

Table III-2. Comparison of manufacturer-specified sensor accuracies with those required to meet the FLOWS program objectives (from Table I-2). In every case the specified accuracies meet or exceed those required.

June of 1983 (Electronics Techniques, Inc.) felt that the application of a few turns of black electrical tape around the top of the shaft was simpler and preferable. Apparently, the "Water Slinger" greatly increased the frictional torque required to start the cups spinning. However, it was found by Lincoln that during hot summer days the tape would swell so much that it would partially or completely restrict the cups from turning.

There are three main design flaws in the MRI anemometer that allow water to reach the top bearing assembly:

1) the bearings are not sealed,

2) the shaft is smooth so that path of water up the shaft is unhindered (apparently the water can travel up because a low pressure region is created as the cups spin) and,

3) the body of the hub of the anemometer cup assembly is not long enough to shield the bearing assembly completely from horizontally blowing rain.

Modifications, described below, have been made to the sensor to correct the latter two design flaws. Installing sealed bearings would also greatly increase the starting threshold, so the cleaning or replacement and lubrication of the loose bearings have been made part of the routine maintenance procedure for the anemometer. New bearings were installed in all of the anemometers at the end of the 1985 data collection period, and should henceforth be replaced at two year intervals.

The first modification made was to cut a circular notch near the top of the anemometer shaft. In this notch is seated a black rubber O-ring which effectively acts as a rim or lip on the shaft (Figure III-1). Second, a Teflon bushing was added to the hub of the cup assembly which extended down completely over the O-ring (Figure III-2). There is ample room between the outside edge of the O-ring and the inside edge of the Teflon bushing to allow the cups to turn freely even if the rubber ring were to swell significantly. The O-ring will be in direct contact with water whenever it rains, so the lifetime of this particular piece is significant. A conservative procedure would be to replace it every 3-4 months while the sensor is in the field. If the O-ring were allowed to remain longer, there would be a danger of it splitting or cracking, in which case it would surely prevent the cups from turning freely. It may be that the Teflon bushing alone is enough protection for the bearings, in which case the O-rings could be omitted entirely. This should be tested when the network is next deployed.

ii. Loose Cups

It was found that the MRI anemometer cups were not held securely in the cup hub assembly and were able to twist so that their faces were not perfectly vertical. The cups are held into the hub with hex-key set screws
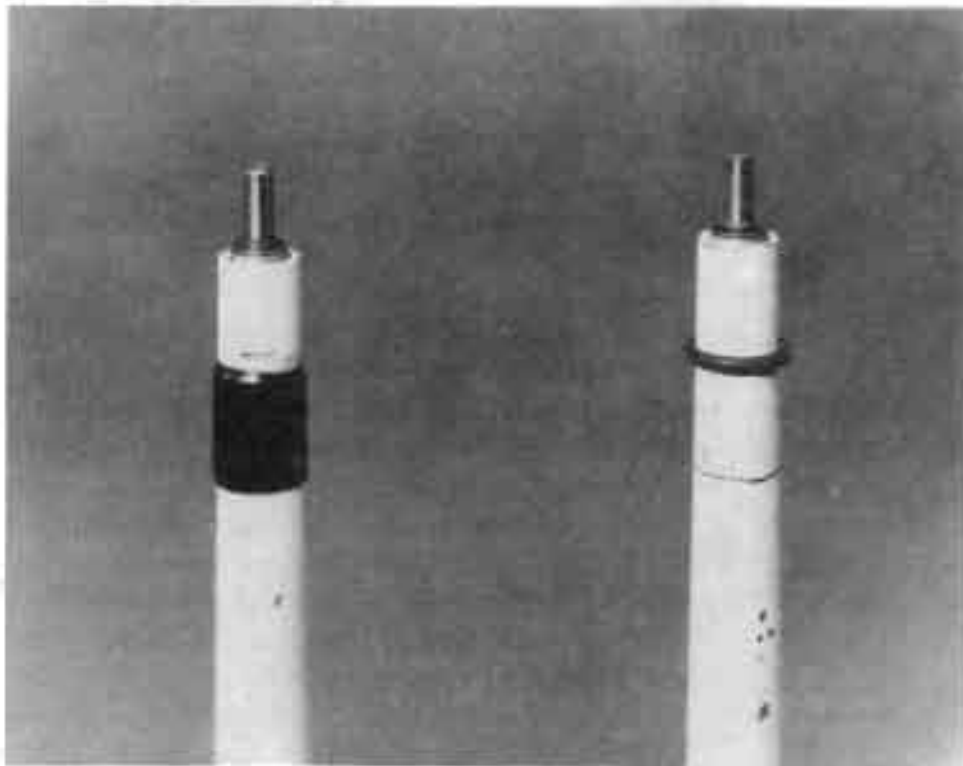
Figure III-1. Top of anemometer shaft is shown both before (left) and after (right) modification. Before, black electrical tape prevented water from reaching the top; after, an O-ring seated in a notch is used.

Figure III-2. Anemometer hubs, to which cups are attached, are shown both before (left) and after (right) modification. Notice at right how the white Teflon bushing extends down from the black hub and covers the O-ring (shown in Figure III-1).

which, when tightened, press down on the stem coming from each cup. In the original manufacturer's design this stem is hollow. Since the stem is made of aluminum, the act of tightening the screw to secure the cup dents the stem which reduces the tightness of the cups. Once the stem was badly dented, there was no way to securely tighten the cups.

To remedy this problem, each stem was straightened out and a small aluminum plug was inserted into the end (Figure III-3). This half-inch long plug prevents the stem from collapsing when the screws are tightened down. In order to make sure that the face of each cup was oriented vertically (parallel with the vertical axis of the center hub), a special device was created for assembling the three cups into each hub. After tightening, the cup assemblies were extremely rigid and there was no tendency for the cups to twist in position.

iii. Spurious Peak Winds

During the 1984 data collection period, both the one-minute averaged wind speed and the peak wind speed (5 s sample) within the minute were transmitted. In low wind conditions, four of the anemometers recorded spuriously high peak wind values. Although the chopper disk was barely moving the circuitry was detecting a high frequency of light pulses. It is likely that the chopper disk was nearly stationary and positioned such that light was just getting through one of the slots. The light detection circuitry oscillated rapidly between detections, giving rise to the spuriously high values.

The manufacturer of the anemometer recommended the replacement of the "R12" 100K resistor with a 1.0M resistor and the "C5" 0.1 µf capacitor with a 0.01 µf capacitor. This essentially creates a low-pass filter in the circuitry and makes it less sensitive to the marginal detections that give rise to the peak wind "chatter". The anemometers exhibiting this problem were all fixed during January 1985, and subsequent tests showed their sampled frequencies to be true.

c. Maintenance

Routine maintenance on the anemometer consists of disassembling the shaft, carefully checking the bearings for any signs of wear, cleaning the bearings in an ultra-sonic cleaner, and checking the chopper disk to see that it is glued in place properly and shows no signs of wear. It was found in maintaining these anemometers for the first time in at least 12 months (Spring 1984), that almost all of the bearings badly needed cleaning, and that a number of chopper disks had come unglued and were rubbing on the electronics assembly in the base of the anemometer.

However, after seven full months in the field in 1984 with the new anemometer modifications, the bearings were found to be in very good shape. None of the anemometers had "frozen up" as they did when water could come into contact with the top bearings, and the bearing were still quite clean and lubricated. Also, the chopper disks were all intact.
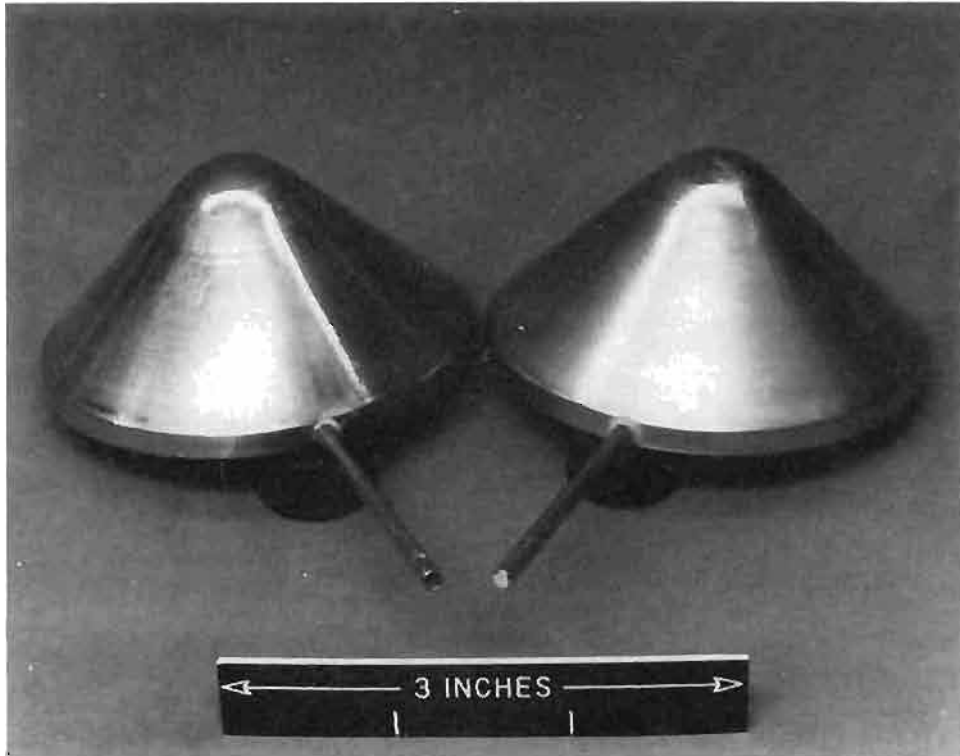
Figure III-3. Anemometer cup stems, by which the cups are held with set screws in the hub, are shown both before (left) and after (right) modification. Before, the hollow stem could be flattened as the cup was tightened in place; after, an aluminum plug prevents collapse of the stem.

d. Calibration

The M.I.T. Wright Brothers wind tunnel was rented for one day (April 12, 1984) to accomplish the anemometer calibration tests (Figure III-4). Before using the tunnel, all of the sensor modifications and routine maintenance had been completed. At the suggestion of Frank Durgin, associate director of the M.I.T. Wright Brothers wind tunnel, four anemometers were placed across the tunnel during each test (see Figure III-5). The test section of the wind tunnel is 10 feet wide and 7 feet tall, and the anemometers were placed 21 inches apart.

The goal was to use the tunnel to measure two aspects of the sensor performance. The first of these was the "friction velocity" or the overall difference in wind measurement between our sensors and the wind tunnel. The second was the effect of flow angles off-horizontal on the wind measurement.

i. Starting Threshold

The sensor threshold velocity, or the velocity at which the anemometer first starts to spin as the wind velocity increases, was measured in the NCAR wind tunnel for new and used sensors by the Bureau of Reclamation (Holman and McInerney, 1983). They found that a "starting torque" of 0.003 oz-in to begin rotating the anemometer shaft ensured that the sensors met the design specification of a starting threshold of 0.22 m/s. The new sensors easily met this criteria while the used sensors had a starting threshold around 0.8 m/s. Those sensors that required a starting torque greater than 0.003 oz-in were dismantled and their bearings were cleaned.

While the starting threshold of the anemometers was not measured in the M.I.T. wind tunnel, the routine maintenance procedure already involves cleaning and lubricating the bearings on each sensor. When Holman and McInerney (1983) measured the anemometer starting torques after a season in the field, those anemometers whose bearings were not actually frozen required starting torques of between 0.003 and 0.015 oz-in. Even this higher value is not sufficient to stop the anemometer cups from turning in a very light wind.

ii. Friction Velocity (and Flow Coefficient)

The friction velocity of the anemometers was measured to determine the difference between the true and ideal calibration curves. The output of a set of four anemometers was measured at approximately 3, 5, 7, 15, 20, 30, and 35 meters/second. The corresponding measured mean and standard deviation of the four sensors are given in Table III-3. The last two rows of the table, labelled "Discrepancy", show the difference between the anemometer measured mean wind speed and that measured by the wind tunnel Barotron.
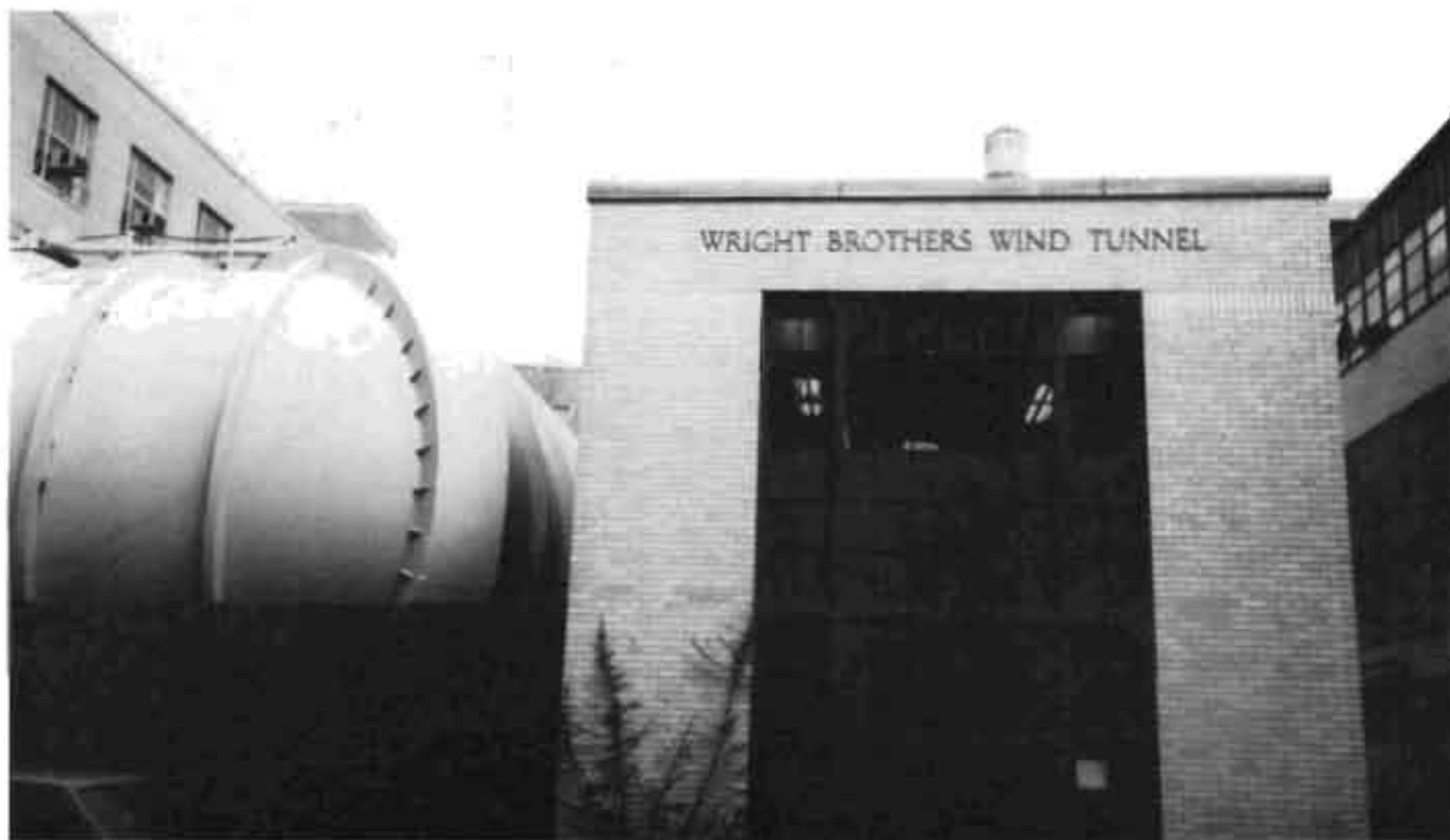
Figure III-4. Wright Brothers Wind Tunnel on M.I.T. campus in Cambridge, Massachusetts. A section of the tunnel can be seen at left.
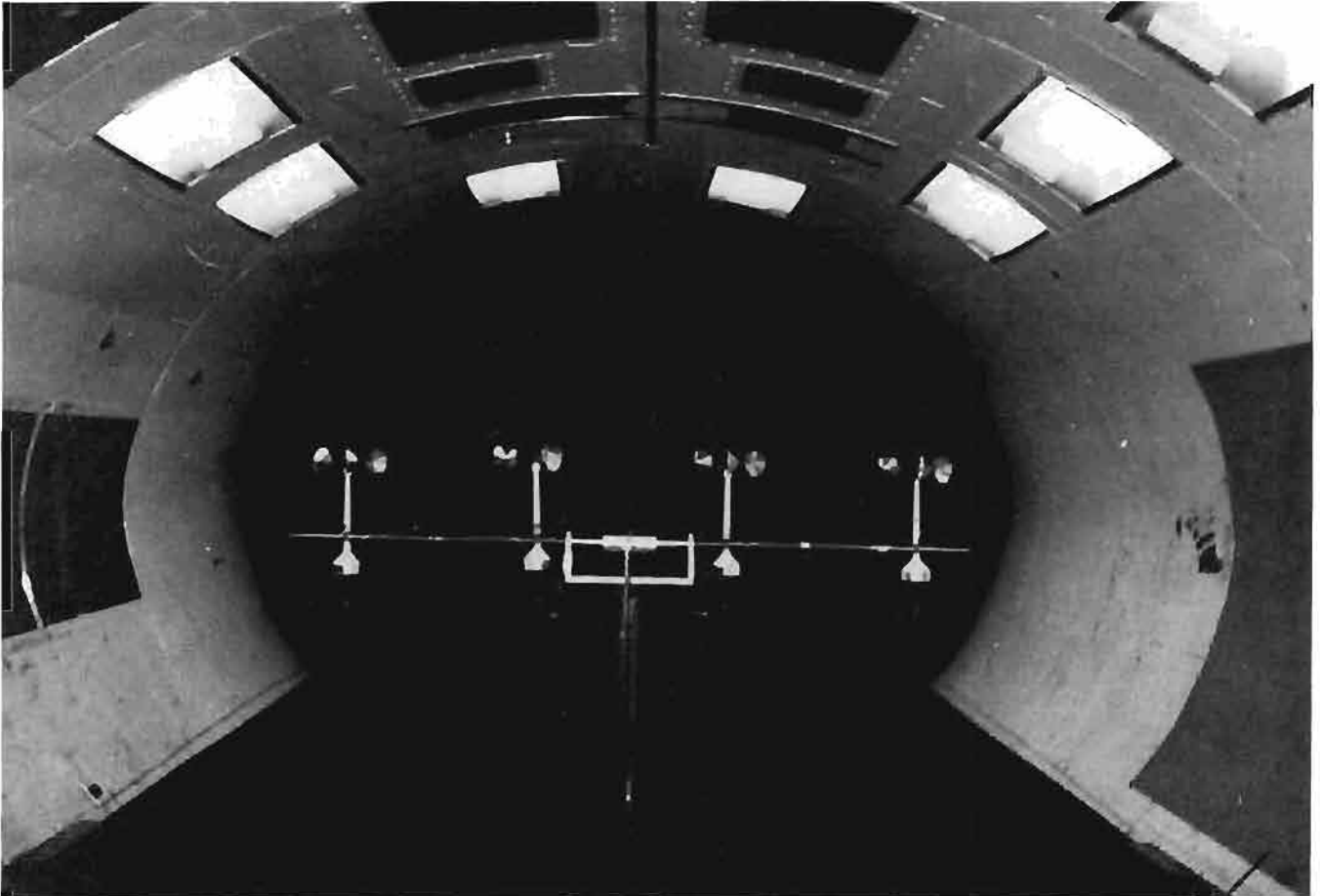
Figure III-5. Test section of the M.I.T. wind tunnel is shown with four Lincoln anemometers in position. The section is 7' tall and 10' wide and the anemometers are 21" apart.

Nominal Wind Speed	3	5	7	10	15	20	30	35
Wind Tunnel Speed	2.75 ±.02	5.31 ±.11	6.91 ±.08	9.88 ±.07	14.89 ±.01	19.61 ±.09	30.06 ±.03	35.06 ±.02
Mean Anemometer Speed	2.98	5.75	7.44	10.55	15.72	20.74	31.58	36.83
Mean Anemometer Standard Deviation	.04	.06	.07	.04	.08	.17	.27	.46
Discrepancy (absolute)	+.23	+.44	+.53	+.67	+.83	+1.13	+1.52	+1.77
Discrepancy (percent)	8.4	8.3	7.7	6.8	5.6	5.8	5.1	5.0

TABLE III-3. Comparison of M.I.T. Wright Brothers wind tunnel and MRI anemometer indicated wind speeds at 8 nominal levels. All wind speed units are meters per second.

There is a systematic, nearly linear (Figure III-6) increase with wind speed of this discrepancy and it is always positive. Typically, the sensor-measured velocity is less than the true velocity by a small constant amount which is thought to be due to bearing friction and might vary with the individual unit or over time but not with wind speed. The discrepancy measured in wind speed is also in the wrong sense to be caused by bearing friction.

One possible explanation for this "overspeeding" of between 5.0% and 8.5% is that the fluctuations in the actual wind speed in the tunnel (time scale ~5 sec) produced a net positive contribution to the mean anemometer torque. Because of the anemometer cup geometry, a "gust" gives a positive torque of greater magnitude than the negative torque of a "lull", so the overspeeding effect is most pronounced in fluctuating wind conditions. The values recorded for the anemometer-measured wind speeds were 30-second averages of the sensor outputs, a procedure necessitated by the persistent wind fluctuations in the tunnel.

Another possible explanation, in addition to known overspeeding effects from cup geometry, is that the four anemometers (Figure III-5) may have produced their own local turbulence effects upon each other, thus magnifying the overspeeding phenomena.

It is also possible that the manufacturer specified flow coefficient of 1.8 m/revolution, used in the equation to relate sensor output frequency (100 pulses/revolution) to wind speed, is slightly too large. Since Figure III-6 shows a linear dependence of the wind speed discrepancy on the actual wind speed (slope $\cong$ .044), multiplication of the flow coefficient by (1-.044=.956), making it 1.72 m/revolution, would bring the sensor output into agreement with the wind tunnel speeds. Use of a flow coefficient of 1.7 m/revolution is recommended for the 1986 network.

It is interesting to note that a comparison between the 1981 CCOPE mesonet wind speed data taken with the NCAR PAM stations (Brock and Govind, 1977) and the Bureau of Reclamation PROBE stations showed the PROBE winds to be stronger and the difference between them to be increasing with wind speed (Figure III-7). This discrepancy was attributed to the difference in wind speed sensor height of 2.8 m (PROBE was higher) but at least part of it may have been due to overspeeding of the PROBE anemometers.

iii. Off-Axis Response

Anemometers are generally mounted with their vertical axes parallel to the gravitational vector so that they optimally measure the flow of wind parallel to the plane of rotation of the cups. However, because of local topography or the presence of updrafts or downdrafts, the flow itself will not always be purely horizontal. Thus it is important to characterize the anemometers' "off-axis response", defined as the ratio of the actual response of the anemometer at various angles of attack to the true response at zero angle of attack. The off-axis response can alternatively be
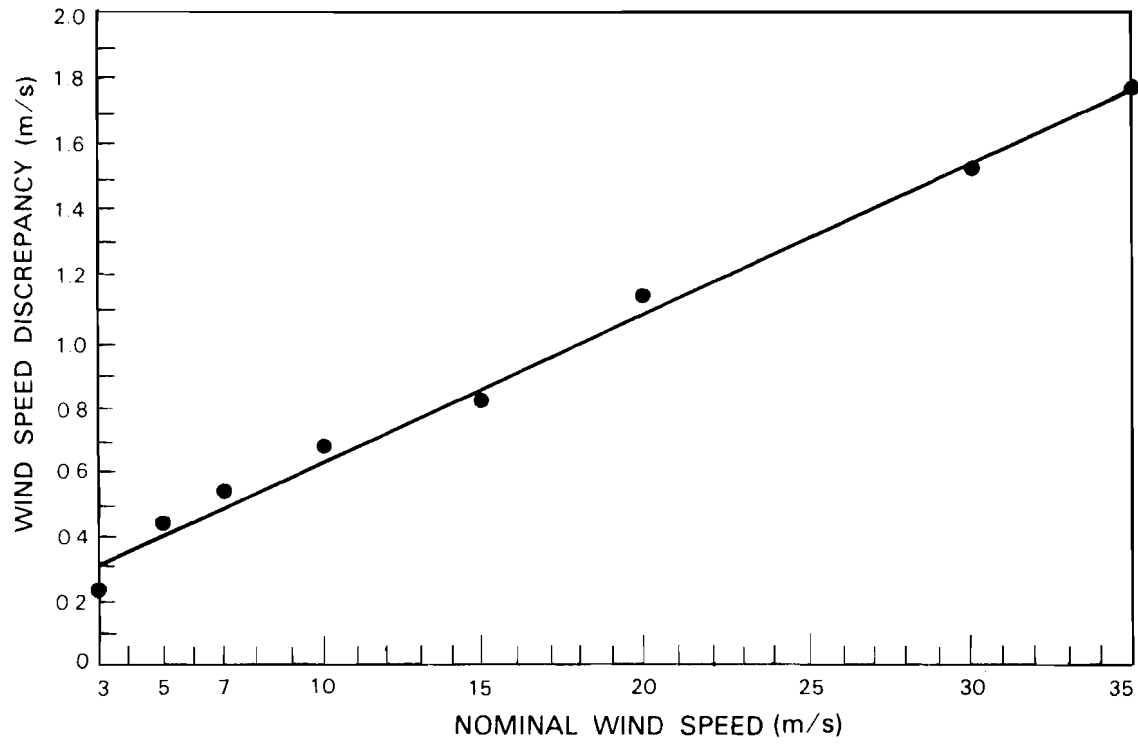
153728-N

Figure III-6. Plot of the difference between anemometer measured wind speed and tunnel (Baratron) measured wind speed ("Discrepancy") versus the tunnel measured speeds. Overspeeding of the anemometers always occurred.
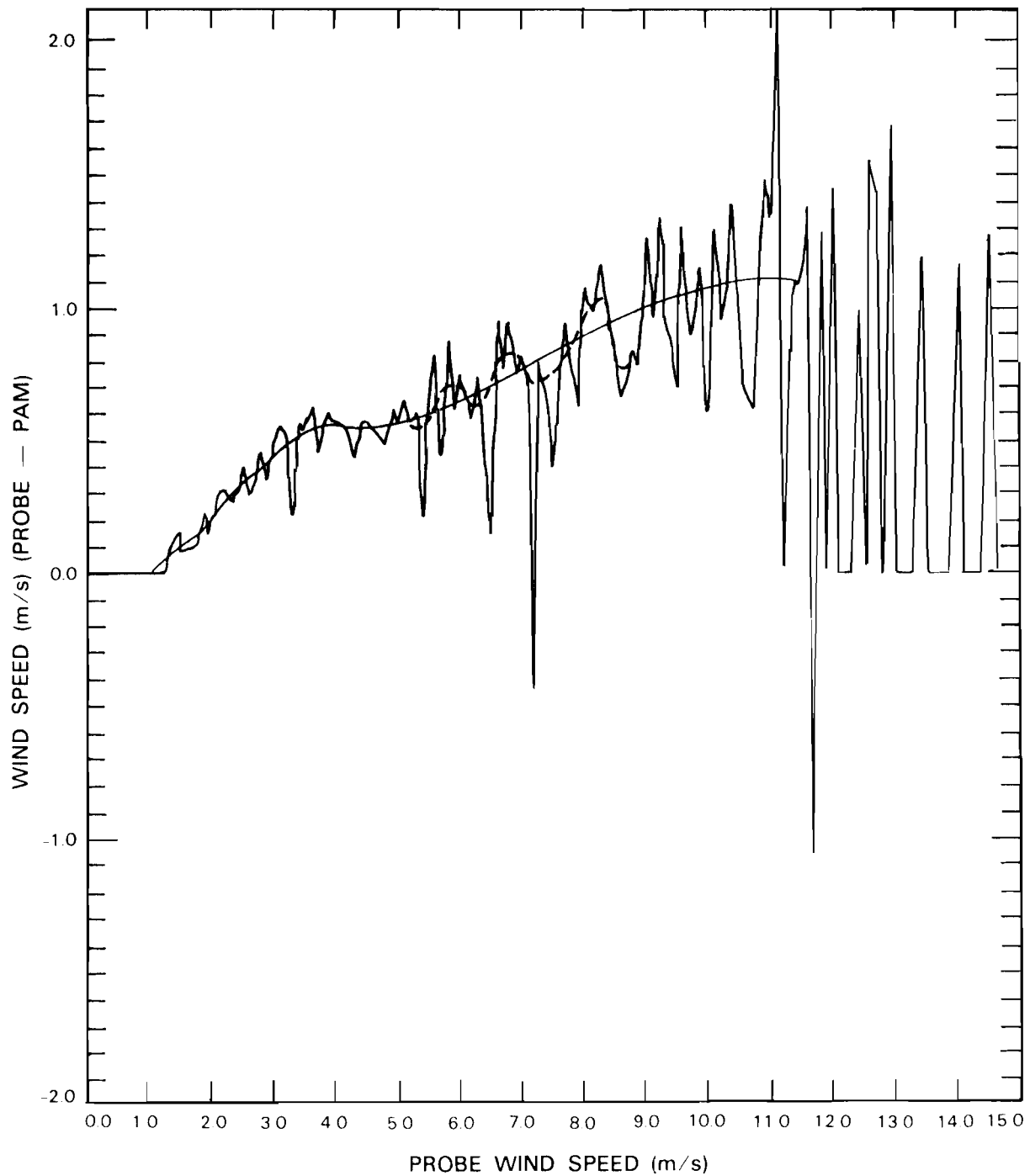
153727-N

Figure III-7. Plot of wind speed difference between the PROBE (now used by Lincoln) and PAM anemometers versus PROBE wind speed. Data were collected during the 1981 CCOPE project, and show that the PROBE winds (6.8 m anemometer height) were systematically stronger than PAM winds (4.0 m anemometer height). Origins or explanations for the "spikes" in the wind discrepancies are unknown. Data provided by C. Wade at NCAR.

defined as the ratio of the actual response to the "ideal" response, the wind value in the normal position times the cosine of the angle of attack. The former definition is used for the results presented here.

Figures III-8 and III-9 show the results of flow angle tests at 5 and 10 m/s, respectively, for the four anemometers shown in Figure III-5. The results are basically the same for the two wind speeds. Cup anemometers are known for their "overspeeding" at flow angles off the horizontal (MacCready, 1966) but this is true for the PROBE MRI anemometers only at positive flow angles (updrafts). The asymmetry about purely horizontal flow is due to the influence on the wind field by the anemometer housing. For negative flow angles (downdrafts) overspeeding does not occur.

The measurements presented here were taken at roughly 5° intervals to ±25°. It was not possible to test the anemometer response at greater flow angles because of the lack of equipment. However, Figure III-10, taken from MacCready (1966), shows the response of a "standard small cups" anemo- meter. The results for curve 3 in that figure are representative of the response that can be expected at flow angles between 25° and 60°.

2. Wind Vane

a. Description

The FLOWS automatic weather stations are equipped with the MRI model 1022 wind direction sensors. The instrument consists of a wind vane mounted on a common cross arm with the anemometer. The cross arm height on the station is 6.8 meters above ground level (see Figure II-7).

The wind direction transducer is a sine/cosine potentiometer which provides the orthogonal components of the wind direction vector. This potentiometer eliminates the ambiguity that can arise from averaging the wind direction over time with a straight 0-360° potentiometer.

b. Maintenance

Maintenance on the wind vane consists of two primary operations. The first is checking the sine-cosine potentiometer in the base of the vane for any signs of wear. The second is making sure the vane itself is balanced about its mounting point and that neither the weight nor the fin have come loose. This latter operation is straightforward while the former requires the use of an oscilloscope.

The oscilloscope is put into "X-Y" mode, so that the sine and cosine signals coming from the potentiometer trace out a perfect circle on the display when the vane is spun. In Spring of 1984, five bad potentiometers were found out of 33. Often the vane had to be spun very quickly in order to reveal the "drop-outs" around the circle.
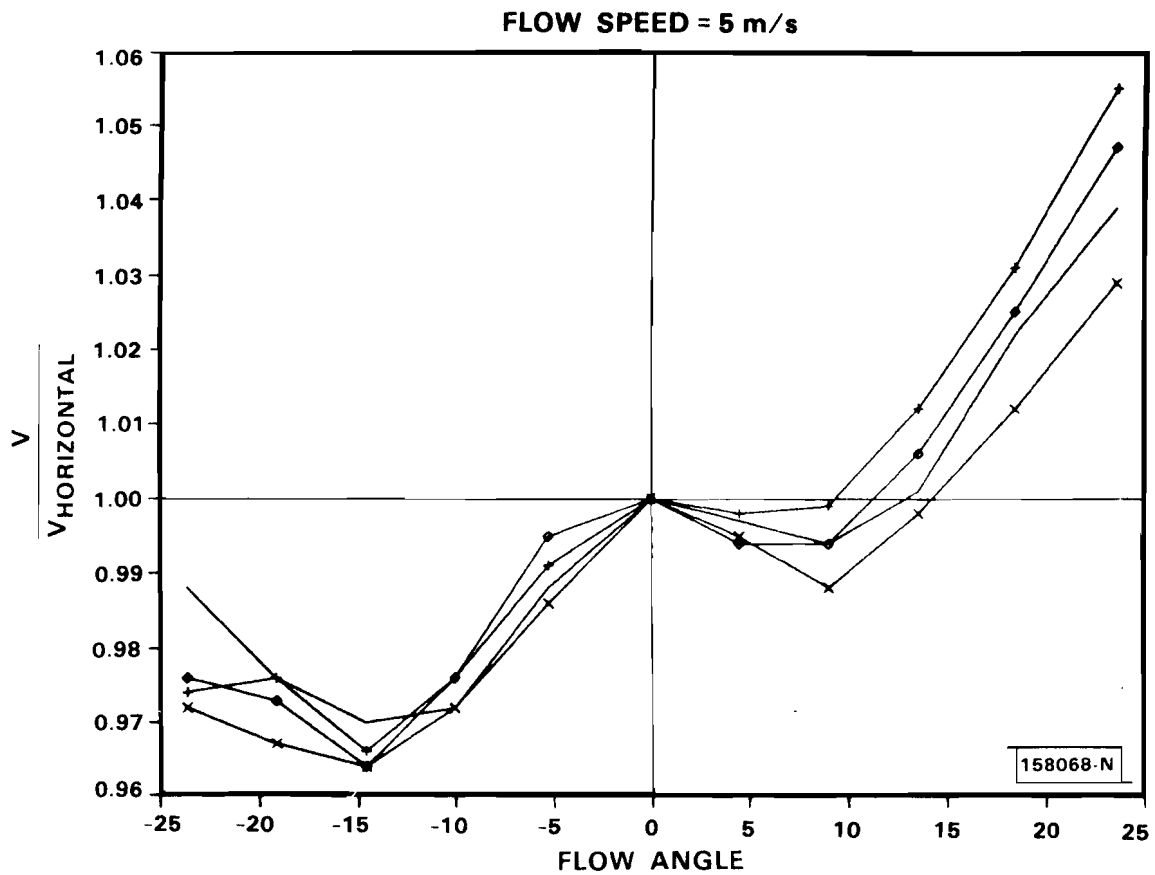
Figure III-8. Results of flow angle experiment to determine anemometer off-axis response for 5 m/s wind speed. Overspeeding is evident at positive flow angles (updrafts) but not at negative flow angles (downdrafts).
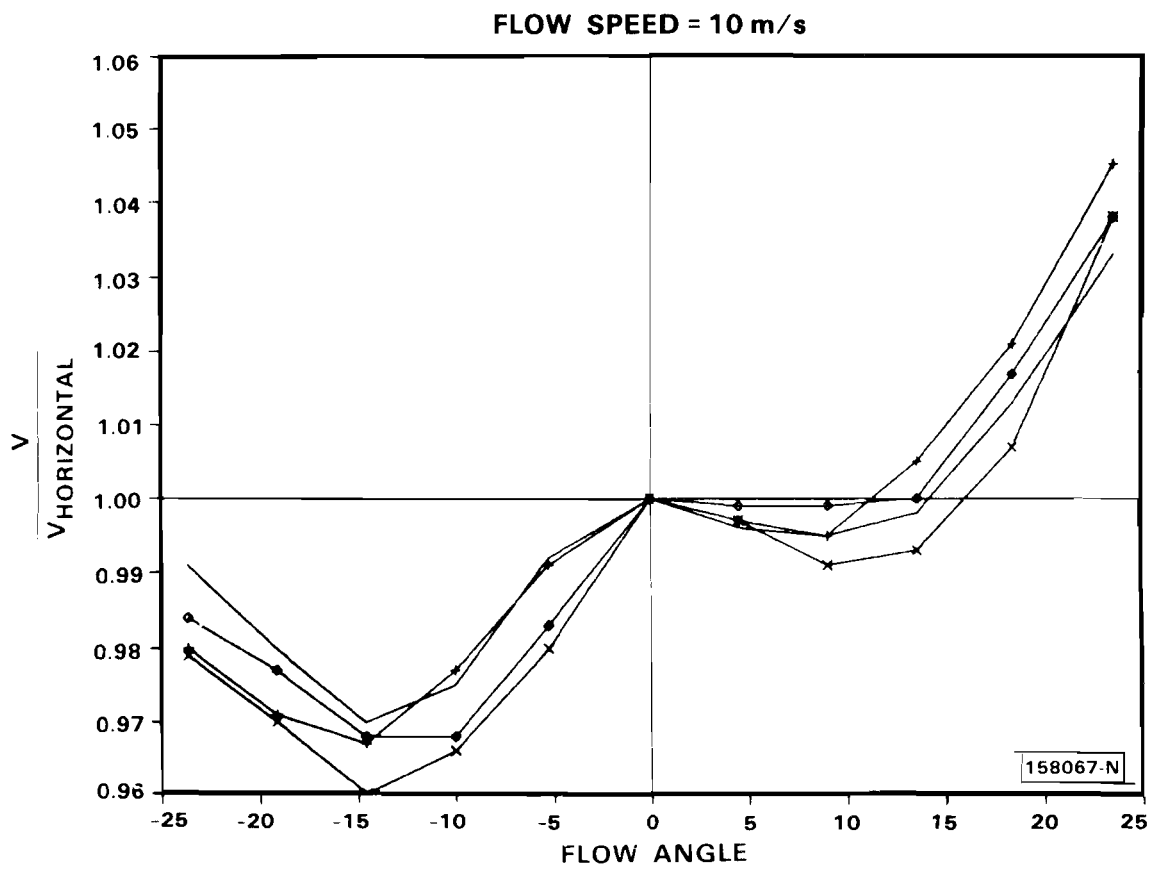
Figure III-9. Same as Figure III-8 but for 10 m/s wind speed.
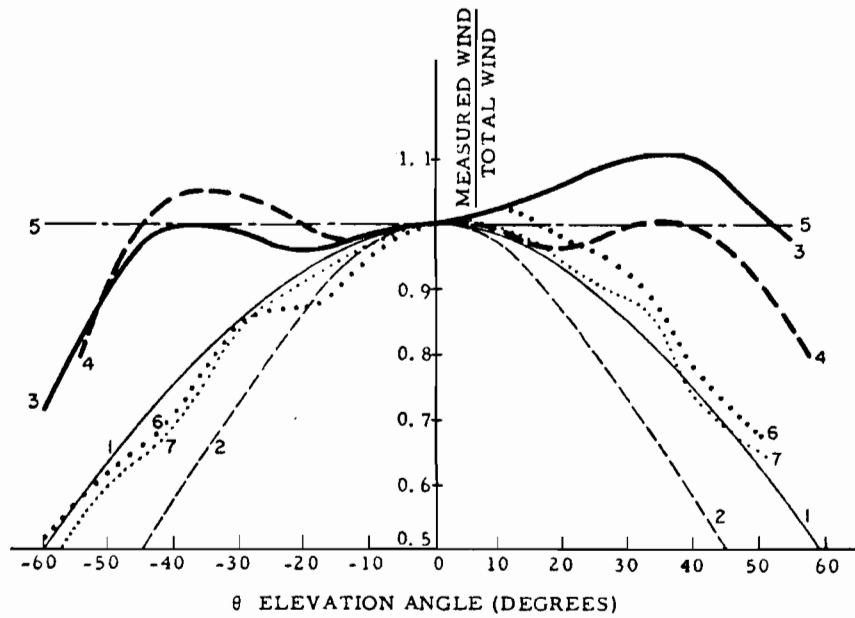
Figure III-10. Wind speed sensor sensitivity to wind elevation (flow) angle. Ratio of measured wind to total wind for various sensor responses as a function of elevation angle. Taken from MacCready (1966).

3. Humidity Probe

a. Description

The relative humidity sensor in the Weathertronics temperature-relative humidity probe is the Vaisala Humicap. The Humicap is a thin film capacitive sensor. A very thin (1 micron) dielectric polymer layer absorbs water molecules that readily pass through a thin metal electrode causing a change in capacitance as a function of relative humidity. This function is essentially linear and independent of temperature. A solid state electronic circuit located in the probe body provides the voltage output directly proportional to relative humidity, over the range from 0 to 100%.

The temperature - relative humidity probe is situated on one corner of the weather station inside a vane aspirator (Figure II-6, left corner). The vane aspirator (described in III.B.1) shields the probe from direct sunlight, and provides good airflow over the sensors at most times (particularly important for the thermistor).

b. Modifications

The only modification made to the relative humidity probes was to replace the 37 micron sintered filter caps with with the 216 micron caps. This allows better airflow over the Humicap and permits the probe to dry more quickly after reaching saturation. Apprarently, the 37 micron filter caps are best used with probes located in fan-aspirated radiation shields which provide a constant airflow; since the FLOWS automatic weather stations are equipped with vane aspirators which provide airflow only by remaining pointed into the wind, the more porous caps are more appropriate.

c. Maintenance

The Humicap element can be cleaned, if necessary, by first removing the sintered filter cap and then blowing air gently (not compressed air) over the sensor. Washing of the sensor is not recommended. In humid environments, under exposure to atmospheric pollutants and high ambient temperatures, the useful life of the Humicap is at most two years. All of the Humicaps in the FLOWS probes were replaced by Vaisala, Inc. in January 1985.

The sintered filter caps themselves should be cleaned annually, for they can trap natural aerosols and pollutants and become clogged. Compressed air may be used for this procedure.

d. Calibration

The recommended calibration procedure for the Weathertronics (Vaisala) relative humidity probe is to use two saturated salt solutions to produce known constant relative humidity conditions and to adjust the two probe potentiometers until the output signal (in mv) matches the actual relative humidity (in percent). The two recommended salt solutions were LiCl (12%)

and NaCl (75%), neither of which has strong saturation vapor pressure dependence on temperature. The probes should then be sealed in airtight chambers with the solution until equilibrium is reached (at least 2 hours). For indoor use, or for outdoor use in a typically dry environment, this "low-end" calibration may be appropriate. However, for outdoor use in humid environments a "high-end" calibration, requiring in addition the measurement of relative humidity at 97% (K_2SO_4) and an adjustment period of 8 hours to reach the high-end equilibrium, is necessary. With this "high-end" calibration, the relative humidity measurement will be accurate at low and high relative humidities and about 2% too low in mid-ranges. The alternative "low-end" calibration is accurate at low and mid-ranges but gives saturation relative humidities of 120% or greater.

During the Spring 1984 sensor calibration, the manufacturer-recommended "low-end" calibration procedure was performed, and during the 1984 data collection period, maximum relative humidities well over 100% were recorded. During January 1985 Vaisala, Inc. calibrated the probes for high humidity conditions.

This calibration performed by Vaisala has proven to be very accurate ($\pm$2%) over the full humidity range. Vaisala was also able to provide a correction that could be applied to erroneously high relative humidities (due to "low-end" calibration) greater than 75%

$$U_{LIN} = -41.4 + 2.165 \, U_p - 0.00814 \, (U_p{}^2)$$

where

U_{LIN} = linearized value for relative humidity (%)

U_p = relative humidity value from probe (%).

This correction was used in processing the 1984 dataset, but was not required for the 1985 data.

4. Temperature Probe

a. Description

The temperature and relative humidity probe is packaged by Weathertronics, and contains the Vaisala Humicap relative humidity sensor and the Yellow Springs Instrument (YSI) temperature sensor.

The YSI temperature sensor is a two element precision thermistor. Circuitry is provided in the probe for an output voltage inversely proportional to temperature, accurate over the range from -30 to +50°C. The new probes purchased from Vaisala, Inc. (model HMP-14A) are accurate over the range from -20 to +80°C.

b. Maintenance

The maintenance on the thermistor consists simply of measuring the indicated voltage at known temperatures to be sure it is still functioning properly. If not, the entire thermistor must be replaced. Temperature comparisons against digital thermometers as well as mercury thermometers were performed and it was found that the good thermistors indicated the temperature very accurately while those that had gone bad indicated temperatures at least 5° from true.

5. Barometer

a. Description

The pressure sensor used in the FLOWS automatic weather station is a modified version of the Weathertronics 7115 strain gage bridge pressure transducer. The strain gage bridge has a good linear response with pressure and wears very well because it has no moving parts. Its one main drawback is the strong dependence of output on temperature of at least .12%/°C (see Figure III-11).

ETI, the company that developed the original PROBE data collection package, chose to keep the barometer at a constant temperature of 90°F as a method of temperature compensation. This was accomplished by installing a heater next to the sensor, then wrapping it in insulating foam, putting that package inside a thermos bottle and placing the thermos inside a large styrofoam cylinder (see Figures III-14 and III-16). A thermistat was put in line with the heater so that the temperature would not rise above 95°F.

One of the problems with this system is the excess power it needs to keep the barometers warm, but once the sensor has reached a constant temperature, the power consumption is minimal. The main problem is that the heater cycle is evident in the barometer output signal as it causes the temperature to change near the strain gage bridge. This contamination is difficult to edit manually, and almost impossible to edit automatically; it can make the data essentially unusable (see Chapter VII.B.3.c for examples of this).

The barometer is located inside the large white armored box hanging on one side of the station triangle (see Figures II-6 and II-7). This box only partially shields the barometer from the wind, which is a source of dynamic pressure fluctuations.

b. Modifications

No modifications have been made to the barometers, but some are definitely needed. For example, if the barometer signal output were characterized during calibration as a function of not only pressure but temperature too, the necessary temperature compensation could be performed
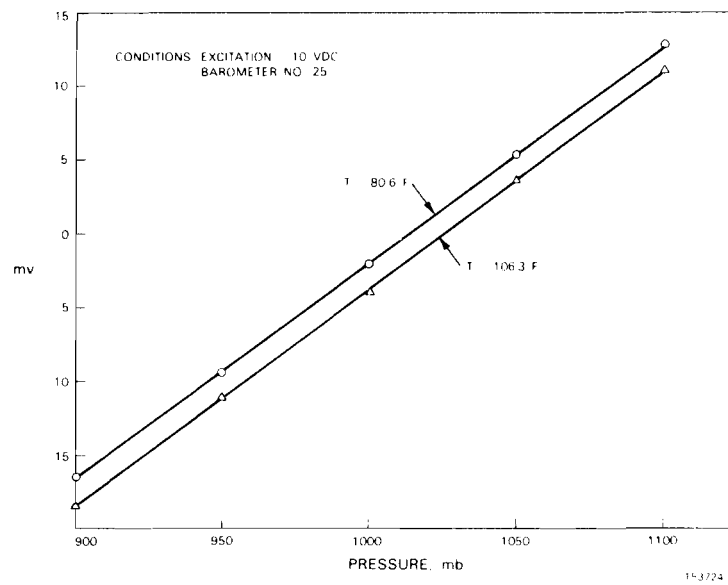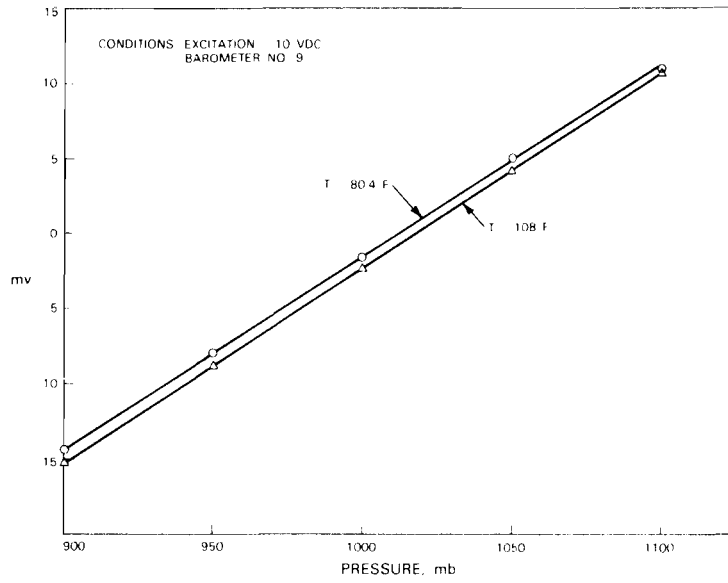
Figure III-11. Plots of barometer output versus pressure at two constant temperatures approximately 27°F apart, for two barometers (Nos. 9 and 25). Notice how different the output change with temperature is for the two barometers.

mathematically. A special test facility with a temperature-controlled pressure chamber would be required. A temperature sensor would also need to be installed next to the strain gage bridge and sampled along with the barometer for each pressure measurement.

Also, the low signal output on the barometer is amplified before it is digitally measured, but this process equally amplifies the noise component. If new barometers were considered, a design characterized by larger output signal range for the limited input voltage should be selected.

The wind-induced dynamic pressure fluctuations can be nearly elimi-nated through the use of a specially designed pressure port on the baro-meter. This should be considered after other modifications have been made to increase the accuracy of the signal.

c. Calibration

Some initial hysteresis and comparison tests were performed to deter-mine first, whether the accuracy of these barometers was acceptable and if so, what calibration procedure should be performed. Table III-4 shows that for the two barometers tested using 10 V excitation that the discrepancy between pressure measured as pressure was increased and that measured as pressure was decreased was at most 0.5 mv or 3.8 mb over the 200 mb range. Since atmospheric pressure changes over the same 10 minute time interval might be at most 10 mb, an estimate of the discrepancy due to the barometer hysteresis would be 0.2 mb. This is roughly equal to the limit in resolu-tion and so was deemed acceptable.

A second test was performed to compare the calibration slopes (mv/mb) for these same two barometers at constant temperature. As shown in Figure III-12 the slopes differed considerably by up to 5 mb for the same differential voltage output at typical atmospheric sea level pressures (950-1050 mb). Thus, the linear equation relating output voltage to pressure had to be determined specifically for each barometer.

All of the barometer tests and the calibration runs were performed in the Ultek vacuum chamber located in the Lincoln Laboratory Space Lab, shown at the right in Figure III-13. The pressure was measured with the very accurate Baratron gage and the data were collected with the Hewlett Packard 3054A Automatic Data Acquisition System shown at the left in Figure III-13.

The calibration runs were done with 10 barometers at a time mounted in the pressure chamber (Figure III-14). During the 1984 calibration, a 5 V excitation voltage was used to match the reference voltage available on the Synergetics Data Collection Platforms (DCPs) that would be used in the field. The voltage used in January 1985 was 9 V to match that now available from the new Lincoln-built voltage regulators. The excitation voltages were supplied during the tests with a Vishay 2120 bridge excita-tion amplifier and the output voltages were measured directly.

	UNIT 9			UNIT 25		
PRESSURE (mb)	DOWN (mv)	UP (mv)	Δ (mv)	DOWN (mv)	UP (mv)	Δ (mv)
900	-14.3	-14.6	+ 0.3	-15.3	-15.8	+0.5
950	- 7.8	- 7.9	+ 0.1	- 8.0	- 8.3	+0.3
1000	- 1.5	- 1.6	+ 0.1	- 0.8	- 0.8	--
1050	5.2	5.0	- 0.2	6.6	6.4	-0.2
1100	11.2	11.2	--	14.0	14.0	--

Table III-4. Data recorded during barometer hysteresis check are presented. The sensor outputs were sampled at the same 5 pressure levels as the pressure was decreased (DOWN) and then immediately increased (UP). The difference (UP-DOWN), Δ) is given for each pressure level for the two sensors.
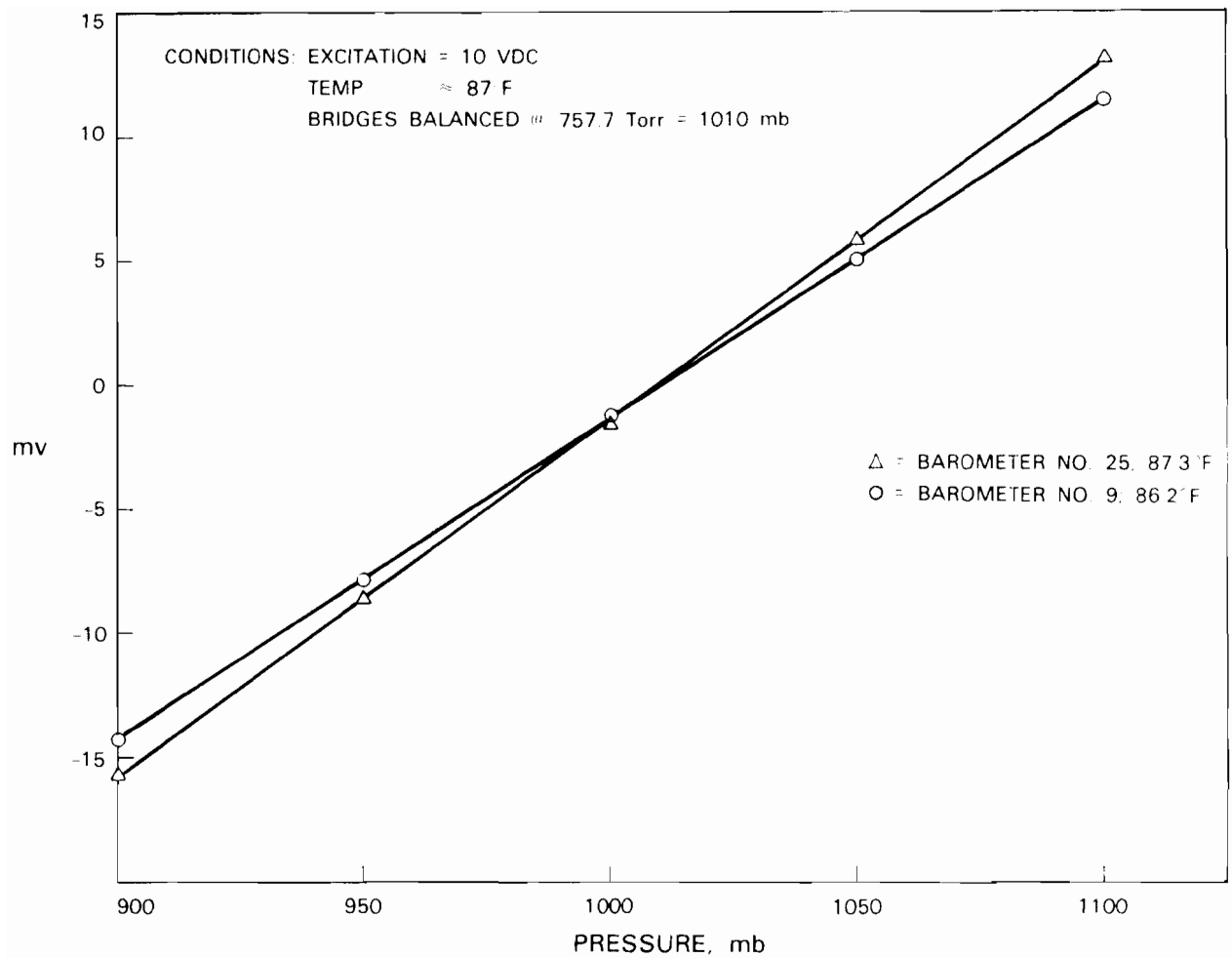
Figure III-12. Plot showing the barometer output as a function of pressure for two barometers (Nos. 9 and 25). Notice how different the slopes of the two lines are.

Figure III-13. View of Ultek pressure (vacuum) chamber at M.I.T. Lincoln Laboratory. Chamber is sealed and in operation. Operator at keyboard is using the HP Automatic Data Acquisition System.
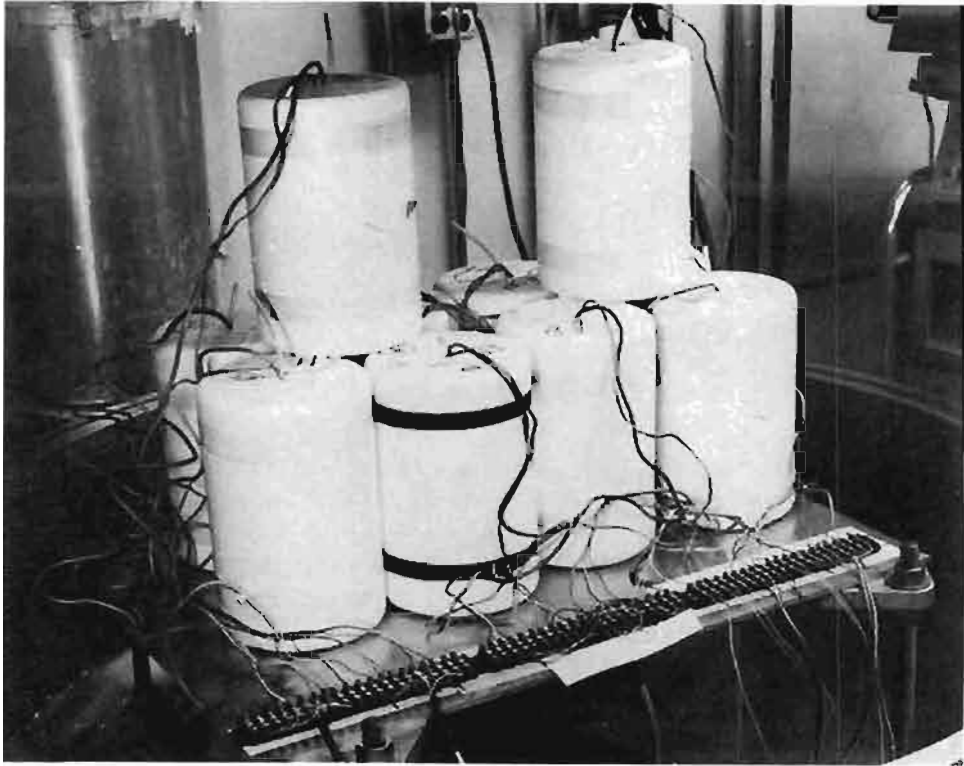
Figure III-14. View of 10 barometers mounted in pressure chamber just prior to testing. Visible are the styrofoam cylindrical containers providing the barometer thermal insulation. Tygon tubing input ports can be seen at the tops of the cylinders, next to wiring.

The calibration procedure began by sealing the pressure chamber and evacuating it to a pressure below 900 mb. The pressure was then slowly increased using dry nitrogen. The inflow of nitrogen was slowed and finally stopped as each 10 mb point was reached from 900 to 1100 mb. At that time a data scan of all 10 barometers and the Baratron gage was initiated, taking approximately 3 seconds.

As soon as the barometers were mounted in the chamber and connected, the heaters were turned on (Figure III-15). When the thermistats caused the heaters to turn off, the chamber was sealed and the pressure measurements began. However, subsequent tests have shown that the internal barometer temperature does not reach the designed limit of 90°F for a couple of hours, during which time the heater may be turned on and off many times. Thus some error was introduced because the calibration was not performed at the infield temperature of 90°F, but at approximately 80°F instead. As Figure III-11 shows, this will influence the offset but not the slope of the pressure-voltage calibration equation. Thus the calibrated absolute pressures still required an additive correction.

6. Rain Gage

a. Description

The rain gages being used are the "weighing bucket" type, which do not have the high resolution of, for example, the "tipping bucket" variety but can resolve changes in precipitation amounts to within 0.2 mm and are stable even in very heavy rain. The gage is simply a calibrated weighing scale on which a bucket sits; whatever falls into the bucket will get weighed as if it were rain. For that reason and also because of evaporation, precipitation amount differences from minute to minute are used to determine net rainfall within a given period of time.

b. Maintenance

Maintenance on the rain gages consists of visually inspecting the weighing mechanism in action to make sure it operates freely. If any binding occurs, the rack can be recentered or readjusted. The weighing mechanism is chrome plated and thus does not need lubrication; in fact lubrication is discouraged for it can easily attract and hold dirt. The potentiometers should also be checked for dropouts or wear.

c. Calibration

The raingage calibration is performed in the field for each rain gage using the DCP to read the output voltages. First, a weight equalling the weight of the bucket is placed on the "scale" and the output voltage is noted (typically 0-400 mv). Then, a stack of weights plus holder, equalling the weight of the water it would take to fill the bucket plus the bucket itself, is placed on the scale and the voltage is again noted (approximately 4.7-5.0 V).
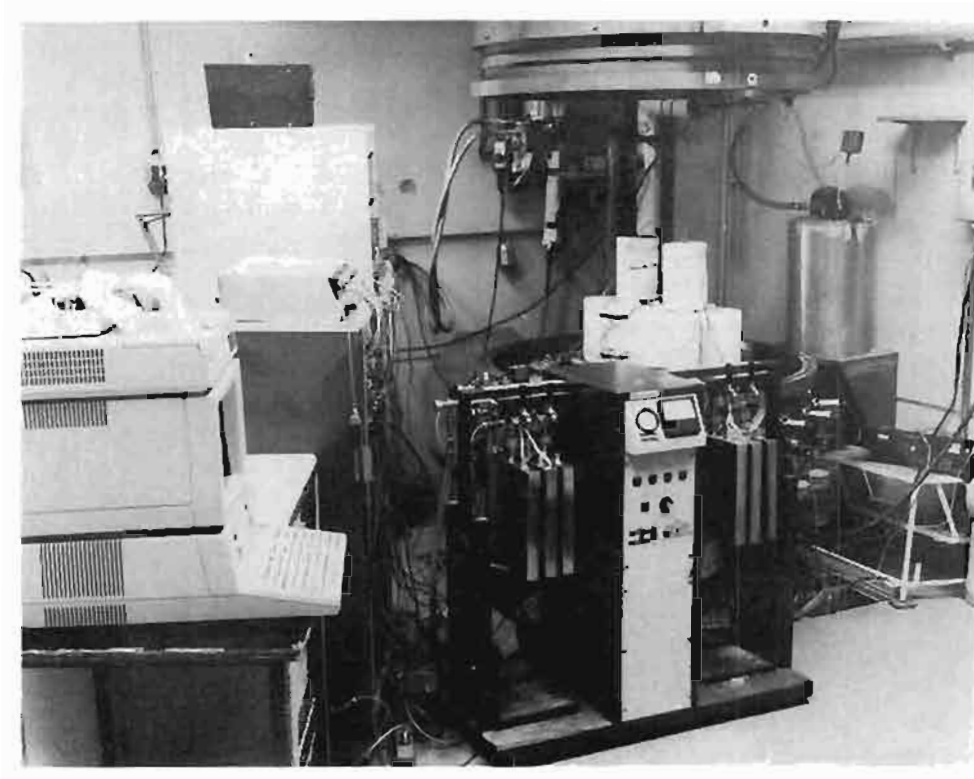
Figure III-15. View of pressure chamber, with barometers placed inside, just prior to being sealed.

The slope of the linear equation is the total bucket capacity (300 mm) divided by the voltage range (e.g., 4.7 -0.4 = 4.3) while the intercept is simply the voltage measured with an empty bucket. The equation is programmed into the DCP and the accuracy is checked by adding each weight, equivalent to 25 mm of rain, and noting the output. If inaccuracies exist, the slope and offset are adjusted.

B. Hardware

In this section, the mechanical hardware portions of the weather station system and the self-sufficient solar power system are described.

1. Vane Aspirator

a. Description

The vane aspirator is basically a reflective tube to shield the thermistor from direct sunlight with a fin to keep the body of the tube aligned into the wind to allow adequate airflow over the thermister and the relative humidity sensor. The outside of the aspirator is painted white to reflect the sun, and the tube itself is mounted on a shaft surrounded with bearings so that it can turn freely.

b. Modifications

During light wind conditions when the sun is near the horizon and the opening of the vane aspirator is pointed toward the sun, the absorption of radiation by the black inner surface of the aspirator can cause a positive temperature error on the order of 1.0°C (Fredrickson, 1984). It may be possible to eliminate this source of error by painting the inner surface near the front opening of the aspirator white. This modification should be made on one unit and comparison temperature tests should be performed in the early morning and/or late evening on a clear day with the aspirators pointing toward the sun and prevented from turning. The modification should be made on all aspirators if it proves effective.

c. Maintenance

The maintenance on the aspirator consists mainly of checking the paint coat to make sure that it had not chipped or peeled and, if it has, repainting it and cleaning and lubricating the bearings to made sure the vane can turn freely.

2. Tower

The tower consists of the Synergetics Model 1 tripod with a crossarm for wind sensor mounting at the top of the 6.8 m mast. The tower is a self-guyed, free standing structure capable of withstanding 50 m/s winds

and limiting the mast whip to less than ±5 cm. The mast tips down to allow easy access to the wind sensors and lightning rod. The structure easily supports up to 200 kg and has adjustable legs to provide leveling on uneven terrain. The large foot pads reduce the footprint loading of the tower itself to less than 75 g/cm^2. The station is shown in Figures II-6 and II-7.

3. Electronics Enclosure

The station has an environmental enclosure meeting NEMA Type 12 specifications. The DCP and the barometer are located within the NEMA enclosure (see Figure III-16).

The NEMA enclosure is itself surrounded by nearly 3/8 inches of steel plate. This white armor box is configured in two half-boxes which support and completely surround the environmental enclosure (See Figures II-6, II-7, and III-16). The battery is stored in the bottom of this outer box.

In the years since these steel boxes were new, the paint has chipped badly and serious rusting has begun to occur. It is probable that the stations will be deployed continuously throughout at least the summer months of 1986 and 1987, and so it is recommended that the boxes all be stripped and repainted at the end of the 1985 data collection period when they are removed from the field.

4. Solar Power System

a. Solar Panels

The solar panels are mounted on the south side of the tripod and are set at a favorable angle for receiving the sun's rays. Two Arco model 16-1200 panels are used per station. These panels each contain 36 three-inch single-crystal silicon cells enclosed in a weather-proof assembly with a rigid, self-supporting frame. The power output is an average of 1.2 amperes at 16.2 VDC. With two panels in parallel the peak power provided is nearly 40 watts.

The solar panels that were broken or stolen during the summer of 1983 were replaced with the new, more powerful version from Arco. The new solar panels are 12" x 48" with roughly 75 watts output and have rectangular photo cells instead of circular ones so that little surface area is wasted.

b. Battery

The battery used is a Delco model 1150 (or model 2000 or similar model) heavy duty maintenance-free battery designed for cycling applications. The battery provides 105 amp-hour capacity which could power a typical station for about two weeks without charging. The battery is trickle-charged continously during daylight hours by the solar panels.
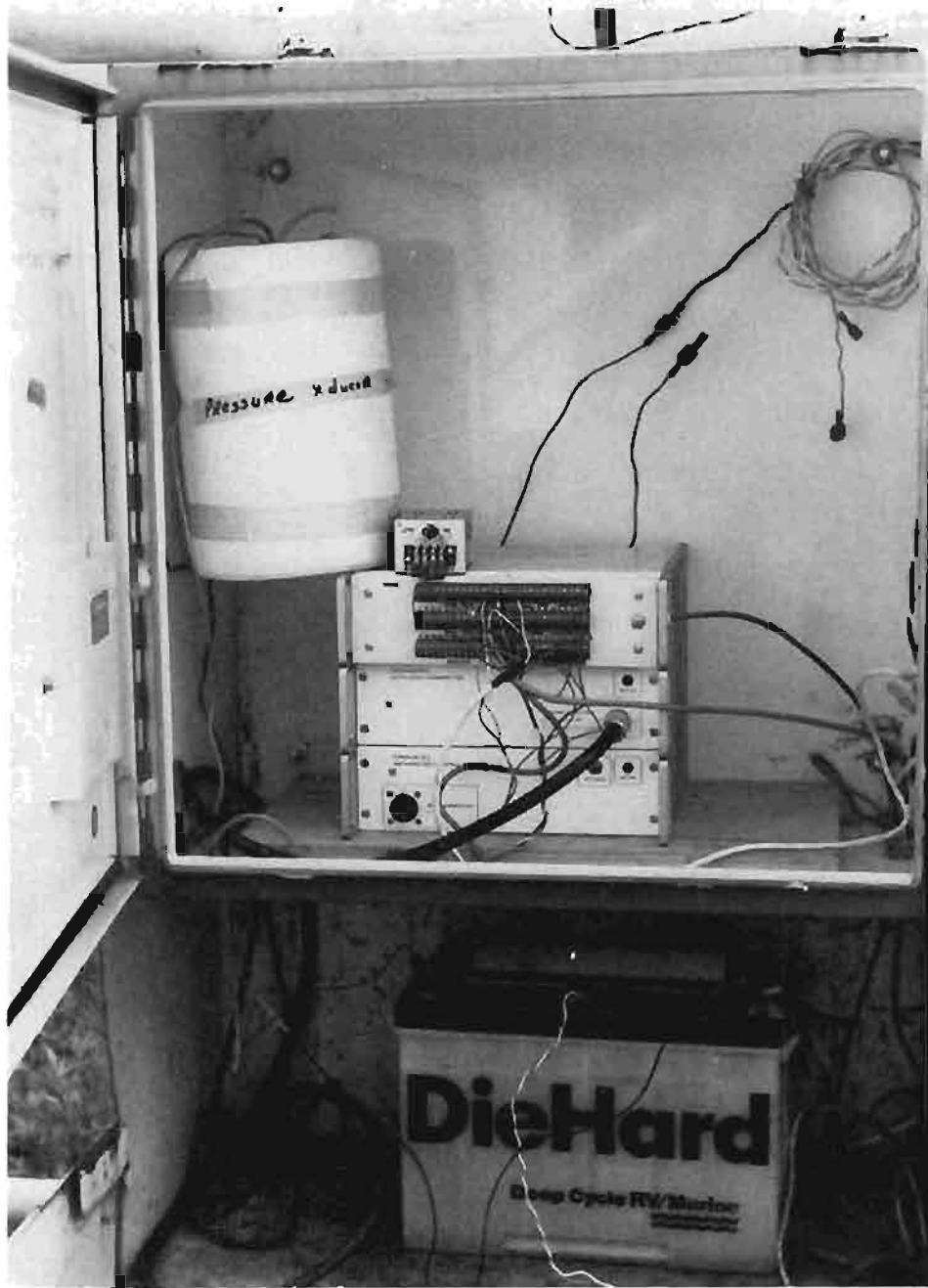
Figure III-16. White armored box containing environmental NEMA enclosure and battery is shown. Inside the NEMA enclosure, the barometer (pressure transducer) and the DCP can be seen. The Lincoln-built voltage regulator is the small box on top of the DCP.

c. Voltage Regulators

The new Data Collection Platforms have available reference voltages of 1.25 V and 5 V. However, a 3.6 ± 0.1 V source is needed for the temperature-relative humidity probes. Also, since the barometer output voltage is proportional to the input voltage, it is preferable to use a 9.0 V soure (about the highest possible off the 12 V battery) rather than the DCP's 5 V source to achieve better resolution.

Low power voltage regulators have been built (using the National Semiconductor LM 117 3-terminal adjustable regulators) that take as input the unregulated 12 V from the battery and provide the required 3.6 and 9.0 V sources. Both regulators are contained in the same small box (Figures III-16 and III-17). Only the 3.6 V regulators were used in 1984, and the 9 V regulators were added in January of 1985.

5. Lightning Protection

The lightning protection consists simply of an aluminum rod, mounted at the top of the station and wired to a ground rod buried near one of the tripod footpads. The lightning rod can be seen in Figures II-6 and II-7 between the anemometer and wind vane at the top of the wind sensor mast. Additional lightning protection has been added to the sensor interface module on the DCP (see III.C.3.b.).

C. Data Collection Platforms

The data from the meteorological sensors consist of analog voltage signals or, in the case of wind speed, of frequency outputs which need to be sampled, averaged, scaled, stored, and finally transmitted to the GOES satellite. All of these functions are performed by the Synergetics 3400 series Data Collection Platform (DCP) shown in Figure III-17. The DCPs are modular in design to allow greater system flexibility. The system being used in the FLOWS automatic weather stations consists of a sensor interface module designed specifically for meteorological sensors (top module in Figure III-17), a communications module that relays the digitally encoded data to the satellite (middle module in Figure III-17), and a microprocessor-based control module that regulates the collection, conver-sion, and transmission of the data (bottom module in Figure III-17). Each module is described in somewhat more detail below.

1. Control Module

The "Master Control Module" (MCM) is basically a programmable general purpose microprocessor (MC6802) that controls the overall workings of the DCP and the data processing. The high level programing language/operating system used is a version of FORTH called "S-FORTH" which was modified by Synergetics to include real-time multitasking features. S-FORTH is a stack-oriented, threaded interpretive language. Using S-FORTH, the DCP can
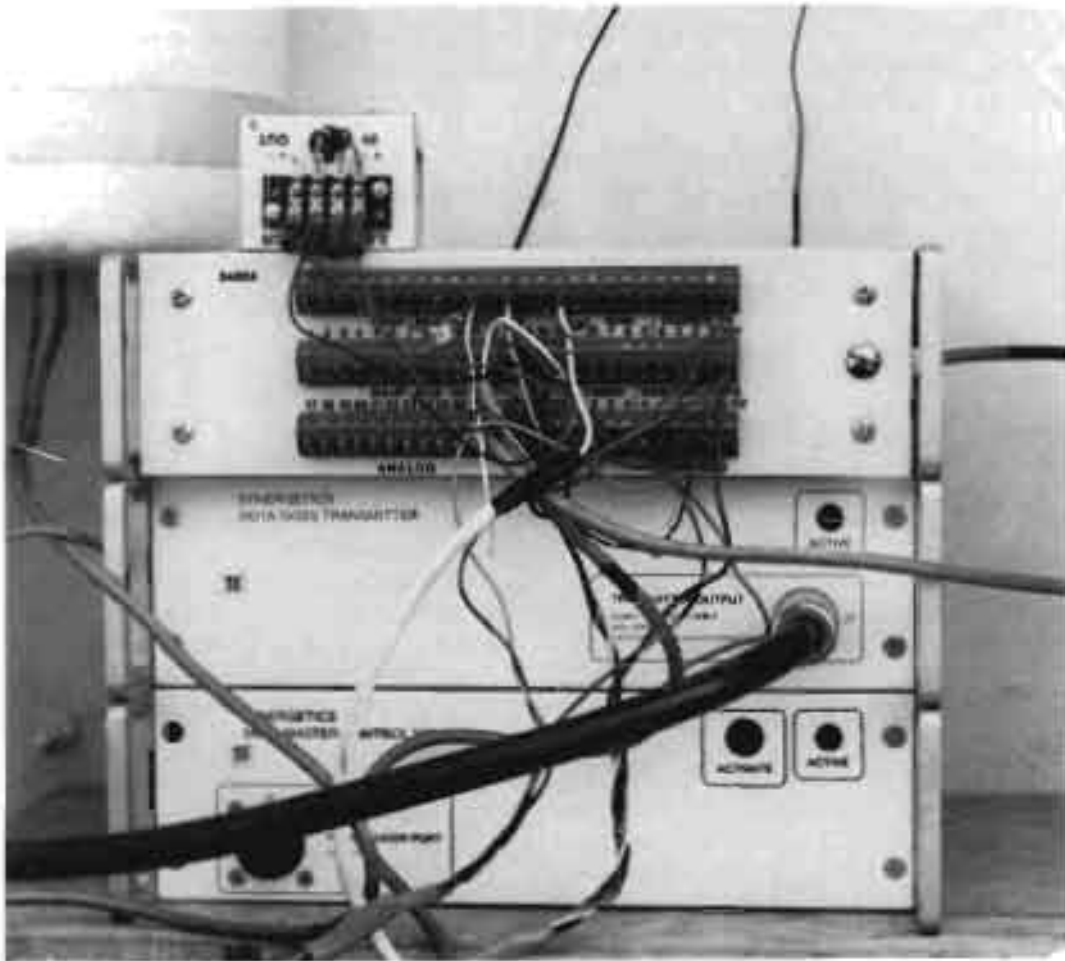
Figure III-17. Synergetics Data Collection Platform in use in the field. On top is the sensor interface module to which all the different sensor wires are connected. In the middle is the GOES transmitter to which the large antenna cable is connected. On the bottom is the control module which can be programmed through the port just visible in the lower left corner.

be programmed to execute the fairly complicated equations needed to convert the sensor voltages into engineering units. The language also allows the user to perform lower level operations such as system timing control and bit manipulation. Any RS-232 terminal can be used to program the MCM through the serial port on the front panel. Power (5 VDC) is available on this port for the portable terminals used in the field.

The MCM controls the timing for the entire DCP. It has a long term (128 year) calendar clock plus a very stable temperature compensated crystal oscillator that is accurate to within 30 seconds per year. The MCM is also capable of performing several self-diagnostics, including measuring its power supply and internal temperature.

2. Communications Module

a. Description

The GOES transmitter module can transmit on all 266 domestic and international channels (frequency range 401.7010 - 402.0985 MHz). These channels are software selectable so that the transmitter module need never be opened. The transmitter module has a built-in monitoring system that can provide performance information such as forward and reflected RF power, selected frequency channel, and various other status and error flags.

b. Transmission Format

Data is transmitted by the DCP in the NOAA-NESS self-timed operational mode in binary format. A specific channel on GOES-EAST was assigned by NESS solely for FLOWS automatic weather station transmissions, and designated transmission times were established without restrictions (see Section IV.A.1 for the selected schedule). Each station has a BCH address assigned by NESS as a platform identification code.

Each transmission begins with a preamble of unmodulated carrier for carrier acquisition in the demodulator phase-lock loop circuit, then alternating bits for bit synchronization in the demodulator, and a Maximum Linear Sequence (MLS) code for frame synchronization. In the original format supported by the GOES system, the preamble took 6.75-8.0 seconds to transmit. This, now called the "long" preamble, has been supplemented by a "short" preamble, taking 1.45-1.50 seconds to transmit. The Synergetics DCP supports both long and short preamble formats; the FLOWS weather stations use the short preamble. The only limitation is that the ground station must be capable of capturing the faster preamble.

After transmission of the preamble and the station ID code, the data are transmitted. The decimal data are output in either ASCII mode, which takes the individual values and converts each integer digit into the equivalent ASCII character, or the binary encoded mode, which takes each number and converts it into three bytes that together represent the 16-bit

signed value. Each group of sensor data in binary encoded format is pre-
ceded by a 1-byte header number. The Synergetics DCP supports both ASCII
and binary data formats. The FLOWS weather stations use the binary encoded
format because it is approximately 2-3 times more efficient; however a com-
puter program is required to interpret the down-linked data.

3. Sensor Interface Module

a. Description

The sensor interface module is a general purpose interface for a wide
variety of sensors. The sensor inputs (screw terminal connectors) can be
set up to measure analog AC or DC (single-ended or true differential) voltage
signals, digital signals, and frequency signals from 0.125 Hz to 65 KHz.
The interface module contains outputs that can be used to control pro-
cesses, turn on sensors, and supply sensor power. Regulated reference
voltages of 1.25 V and 5 V, each with 10 mA of current, are available to
power the sensors.

b. Modification

Small gas discharge tubes were added to all the I/O lines on the sen-
sor interface to provide additional protection against lightning damage.
Any strong surge that travels along the sensor input lines will ionize the
gas in the tubes and break the connection, preventing damage to the
electronics. When this does occur, the site must be visited to replace the
blown gas tube.

4. Software

The software that is running in the Synergetics DCP consists of two
"scans" which are executed once each "interval", a scan dependent, user
selectable amount of time. Within each scan are numbered equations, like
executable statements or variable assignments in FORTRAN, which are exe-
cuted in the order in which they are entered. A maximum of 60 may be used
altogether.

The first scan sets up the sensor interface input port assignments,
the type of input signals expected on each port, the sample rate, and the
processing to be applied to the samples within each scan interval (e.g.,
average, maximum, etc.). The second scan converts the processed samples
(e.g., 1-minute averages) into engineering units and stores them in arrays
for transmission. Higher-level software in which scans 1 and 2 are con-
tained controls and executes the user-specified transmission schedule on
the selected channel, and automatically supplies the necessary preamble,
the platform identification code, and the DCP self-diagnosed status for
each transmission.

The software language used is called "S-FORTH", a version of FORTH
modified by Synergetics. The FORTH language uses a last-in, first-out

stack and "Reverse Polish Notation" syntax for equations. The Synergetics DCP manual describes the language in detail; Appendix B contains an abbreviated glossary which will help in understanding this specific programs currently being run in the DCPs. These programs are described in detail and listed in Appendix C.

All of this software can be written in advance of field installation and recorded on a microcassette tape. The "generic" software can then be downloaded in the field and any site-specific or sensor-specific constants can be entered at that time. This software recording capability has proven essential to efficient site installation.

IV. WEATHER STATION DATA

In this chapter, the FLOWS automatic weather station data, both transmitted and archived, are described. The limited real-time data access procedure is also described.

A. Transmitted Data

1. Transmission Format and Schedule

Each mesonet station transmits data twice an hour, 24 hours a day. For each of the 7 meteorological variables, there is one 3-byte binary encoded 16-bit data value generated per minute. Thus, 633 bytes of data alone are transmitted ((30 min x 7 variables + DCP status word) x 3 bytes). Each group of 30 sensor data values must have a one-byte header, and these plus the data plus the required short preamble and final end of transmission character take 52.8 seconds to transmit at the GOES established rate of 100 baud. This allows an interstation gap of 7.2 seconds each minute before the next transmission begins. Since there are 30 stations in the network, a transmission is taking place every minute. The transmission schedule was selected according to station number, so that station No. 1 begins its transmissions at 1 minute and 31 minutes after every hour, station No. 2 at 2 and 32 minutes after, and so on with station No. 30 transmitting on and half past every hour.

2. Variables

The variables transmitted by the FLOWS automatic weather stations are listed in Table IV-1. The data units and the DCP sensor sampling times are given as well as the "digital resolution" of the data. The digital resolution is the engineering units equivalent of the sensor output resolvable with the 13-bit A/D converters in the DCP sensor interface. For all sensors except the barometer the digital resolution is not a limitation; the barometer output signal is so weak with 9 V excitation (5-15 mv differential) that the final resolution of the pressure data is 0.2 mb.

3. Wind Direction

The wind direction itself is not transmitted but the information necessary for its calculation is. The wind vane output consists of signals representing both the sine and the cosine of the wind angle, thus determining the angle unambiguously. However, transmission of both signals would double the amount of data sent for the wind direction. In 1984 the cosine signal only was transmitted and information about the sine signal was included as part of the average wind speed. By determining whether the sine of the wind angle was positive, negative, or equal to zero and sending that information as the most significant digit of the average wind speed,

Variable	Units	Sample Time	Digital Resolution
Temperature	Degrees C x 100	10 s	.04°C
Relative Humidity	Percent x 100	10 s	.02% RH
Pressure	Millibars x 10	10 s	.2 mb
Avg. Wind Speed	m/s x 100 (and Wind direction information, see IV.A.3.)	5 s	.02 m/s
Peak Wind Speed	m/s x 100	5 s	.02 m/s
Cosine or Sine of Wind Direction	Millivolts (0-5000) (See IV.A.3.)	5 s	.04°
Precipitation	Milimeters x 10	10 s	.1 mm
DCP Status	Binary Code	30 min	(16 bits)

Table IV-1. The variables transmitted by the FLOWS automatic weather stations are listed, along with their units, sample times, and digital resolution.

it was possible to recover the wind direction angle and still only transmit one of the wind vane outputs. The problem was that when the cosine signal was near its limits, the resolution in terms of degrees of azimuth was greatly decreased.

The transmitted "cosine" actually represents the output cosine signal (in mv) from the wind vane. When this signal is near the middle of the 0-5000 mv range, a 1 mv difference represents 0.02 degrees of azimuth. But when the signal is near the limits of its range (cosine near ±1), a 1 mv difference represents 1.62 degrees of azimuth. The data collected in 1984 showed very few measurements at all from a 15° range around 0° (360°) and 180°. (The range of angles around 0° and 180° that was undersampled depended upon the particular wind vane sensor being used; the average was about 15°.) When measurements were recorded in these directions, the wind was much lighter than usual, and there were no measurements at all at 0° and 180° exactly as is illustrated in Figure IV-1.

To remedy this situation, the sine instead of the cosine is now transmitted when the winds are from the north or the south. The changes occur at 45°, 135°, 225°, and 315°. Thus the sine is transmitted when the winds are from 135° - 225°, the cosine is transmitted when the winds are from 225° - 315°, and so on. In this way, the transmitted signal is always in the middle of its possible voltage range, and a 1 mv discrepancy will result in an error of only 0.04° at worst.

A constant of 10,000 is added to the wind direction signal (0-5000 mv) only when it represents the sine; otherwise the true cosine will be transmitted and the value will be less than 5000. The signal that is not transmitted (i.e., the cosine if the wind direction value is greater than 10000; the sine otherwise) is tested to determine whether it is positive, negative, or equal to zero. Constants of 100, 200, or 0, respectively are added to the average wind speed to signify the results of the test. See Appendix C for the DCP software implementation of this logic and Appendix D for the algorithm used in decoding the transmitted data into wind direction and some examples.

Some matching problem is still evident (Figure IV-2) but now the angles affected are 45°, 135°, 225° and 315°. As before, the severity of the problem is a function of the specific sensor. But now, while occasionally apparent in a long term average, the problem is much less severe than it was, and is not noticeable from minute to minute. It may still be possible to improve the matching problem by testing each wind vane individually to determine the exact signal values when the sine is equal to the cosine. The DCP software can easily be tailored for each site. Another possibility is to procure all new 0°-360° or 0°-540° potentiometers for the wind vanes which would involve some additional expense.
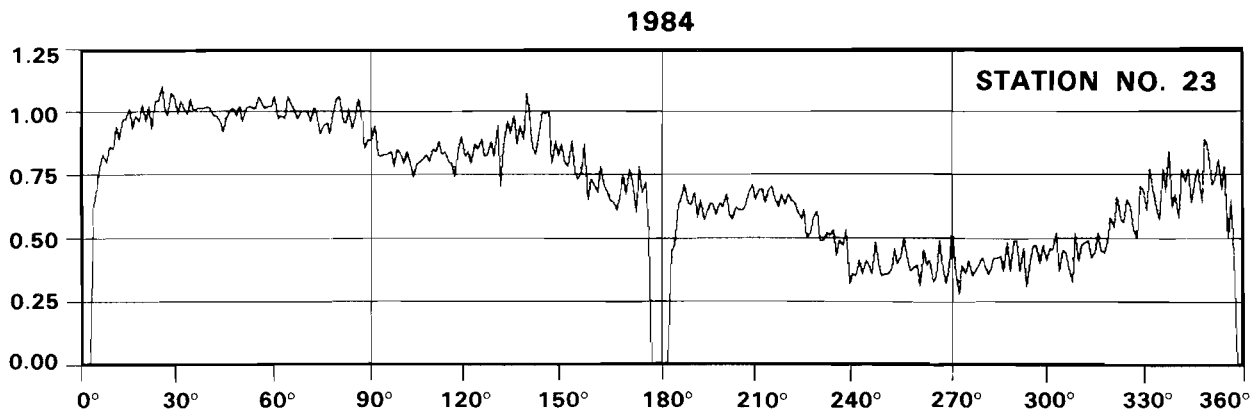
1984

Figure IV-1. Normalized mean wind speed for station No. 23 averaged for the entire month of July 1984. No winds were measured at 180° and 360° exactly.
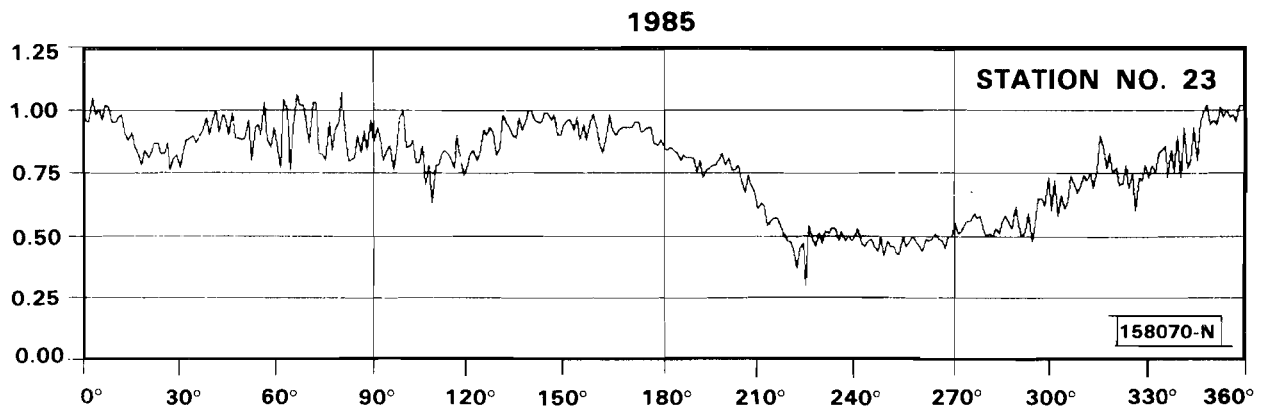
1985

Figure IV-2. Normalized mean wind speed for station No. 23 averaged for the entire month of July 1985. Fewer winds were measured at 45°, 135°, 225° and 315° than at other azimuths and when they were measured, they were lighter than usual.

4. DCP Status Word

The DCP status word contains 16 bits of encoded information about the platform internal temperature, the forward power, the battery voltage, and error codes. One status word is transmitted with every message which represents the DCP status just prior to the transmission. Information on the interpretation of the status word is given in Appendix E.

B. Archived Data

Two methods of collection and archival of the mesonet data were explored during the initial tests in 1983: 1) dissemination of the data via 1200-baud telephone communications with the NOAA-NESDIS Data Collection Service and 2) reception of the data on magnetic tape from a private company that collected it with their own GOES ground station. The latter method proved to be nearly 100% reliable although some cost was incurred, while the former required the daily attention of a Lincoln staff member, provided an incomplete dataset because of NESDIS downtime, system crashes, and lack of storage, but was completely free of charge. The approach of hiring a private company was recommended, and bids were solicited for the 1984 and 1985 seasons. An alternative approach would have been to purchase a GOES ground station and archive the data at Lincoln Laboratory; however the initial cost and the continued personnel requirements could not be justified.

The tapes from our down-link service contain 5 days of data and arrive at Lincoln Laboratory 2 days after the last day's data have been collected. The tapes contain the decoded ASCII data (from 3-byte binary transmission format) in essentially the same order in which they were transmitted.

The data are converted into a common format from which all of the inventory, analysis, and processing programs work. Details of the data processing and analysis software are given in Chapter VI. The translation into common format is immediately followed by editing, calibration, and the calculation of derived products such as dew point and equivalent potential temperature. Both the original raw data and the final data are permanently archived.

C. Real-Time Data Access

A real-time data access capability is provided by our data down-link and archive service via 1200-baud dial-up modem to their computer. While in principle this service is unlimited, the long distance telephone line charges preclude its use for gathering large amounts of data. It is essential, however, for the daily data quality and missed transmission checks performed by the field technicians. Meteorologists involved in the Doppler radar data collection would like to see the mesonet data in real time both

for prediction and confirmation of radar-detectable wind shear, but the transmission schedule on the dedicated GOES channel is so crowded that 30 minutes of data must be transmitted at once by each station. This pattern makes it impossible to achieve simultaneous measurements across the network in a timely manner. If a second satellite channel were available, real time display of the wind data might become useful for the FLOWS radar operations.

1. Daily Data Quality Check

An interactive computer session is initiated once each day to collect at least one hour of data from each station in the network. The data are automatically converted from the binary format in which they were transmitted to decimal form before they are sent over the phone line, although the original raw data can be seen if desired. At the radar site, the received data are stored on disk and later plotted, at which time a comparison is made not only between the stations but to the local hourly National Weather Service observations as well.

In addition to simply listing all the data received for a specified period of time, the data from any one station alone can be selected. This is particularly useful when recurring or persistent problems plague a given site. Also, just the individual transmission headers can be listed, providing an efficient way to check, for each station, the time of transmission (if this drifts more than 5s, another transmission may be garbled), the radiated power and the signal-to-noise ratio (if these are too low, the battery voltage may be low or the antenna could be damaged), and the total number of transmission errors (each byte received is checked).

2. Missing Messages

A very useful utility is available on the down-link computer to list those stations and times for which transmissions were missed. However, in getting this information the entire database is searched and compared with the known schedule of transmissions for the time period selected (usually 24 hours). This can be a very time-consuming operation and expensive to perform on-line. Instead, arrangements have been made for the computer to initiate this search automatically at 0600 GMT every day, and to store the output in a disk file. This file can simply be listed whenever the information is required.

V.   CORRECTING WIND SPEED MEASUREMENTS FOR SITE OBSTRUCTIONS

   A. Rationale

   The slowing or obstruction of wind by local obstacles is a well known
problem to those wishing to make accurate wind speed measurements.
Manufacturers' anemometer mounting instructions generally inform the user
that obtaining good sensor exposure is necessary to assure accurate wind
speed measurements and that selecting a site where there will be, as nearly
as possible, an unobstructed wind flow from all directions that is free
from turbulent eddies is essential. When siting a network of automatic
weather stations, or an array of LLWAS anemometers, often some imperfect
sites must be accepted to maintain a fairly precise overall sensor con-
figuration. In the Memphis, TN area and in extreme northern Mississippi,
the obstructions generally consisted of large rows of trees separating
individual farm fields and, in some cases, of distant low buildings.

   The FLOWS project is interested in the unobstructed wind speed
measurements for two main reasons. First, when analyzing a snapshot of the
wind field over the network for horizontal wind shear and/or for comparison
with Doppler radar data, use of the measured, uncorrected winds would
reveal spurious patterns of divergence or vorticity that depend little on
time but greatly on the prevailing wind direction and that would, in some
cases, obscure the true shear pattern. Second, when using surface wind
measurements to estimate winds aloft that might be encountered by an
aircraft on take-off or landing, a simple power law can be accurately used
(e.g., $V_2 = (H_2/H_1)^{1/7} V_1$) if the original surface wind speed measurements
are representative of the unobstructed flow at that altitude.

   Of course, if the effects of site obstructions on the measured surface
wind fields are insignificant, no corrections would be needed. However,
the results of time averaging the wind speed measurements from mid-February
through August 1985* at each of the FLOWS mesonet and LLWAS stations, shown
in Table V-1 and Figure V-1, reveal substantial differences of up to 50%
(e.g., between station No. 7 and LLWAS Centerfield) that are related to the
degree of obstruction of each station's immediate environment (see Table
V-2; the mean obstruction angle at no. 7 is 8.7° and at LLWAS CF, 0.3°).
Potential errors of this magnitude are certainly a concern, and thus care-
ful attention has been given to correcting them. While manual wind field
analysis, with the aid of panoramic photographs and topographic maps,

---

*The 1985 data were used because of the improved wind direction measure-
ments (see IV.A.3) and because all 30 FLOWS mesonet stations were opera-
tional from the start of data collection.

Station Number	Mean Wind Speed	Number of Measurements
1	3.03	253 323
2	3.05	249 020
3	2.96	254 083
4	2.29	240 464
5	2.18	238 576
6	2.85	249 018
7	1.83	190 602
8	2.79	240 603
9	2.43	224 126
10	1.99	234 554
11	2.31	224 298
12	2.03	237 109
13	2.33	238 168
14	2.42	223 306
15	2.44	249 188
16	2.41	239 755
17	2.48	222 126
18	2.34	250 485
19	2.43	240 849
20	2.86	253 509
21	2.96	252 343
22	3.13	246 738
23	3.24	240 049
24	3.23	251 085
25	3.23	258 999
26	2.83	228 298
27	2.67	226 115
28	2.77	242 522
29	3.01	238 826
30	2.84	228 791
CF	3.56	242 710
N	2.54	233 075
E	2.87	236 518
SE	2.47	231 630
S	2.35	238 991
W	2.65	233 393
NETWORK MEAN	2.67	8 583 245

Table V-1. Mean wind speed values for the FLOWS mesonet sta-
tions and the FAA LLWAS stations for the period 15 February
through 31 August 1985. The number of measurements used in
computing the mean wind speed values are also given.
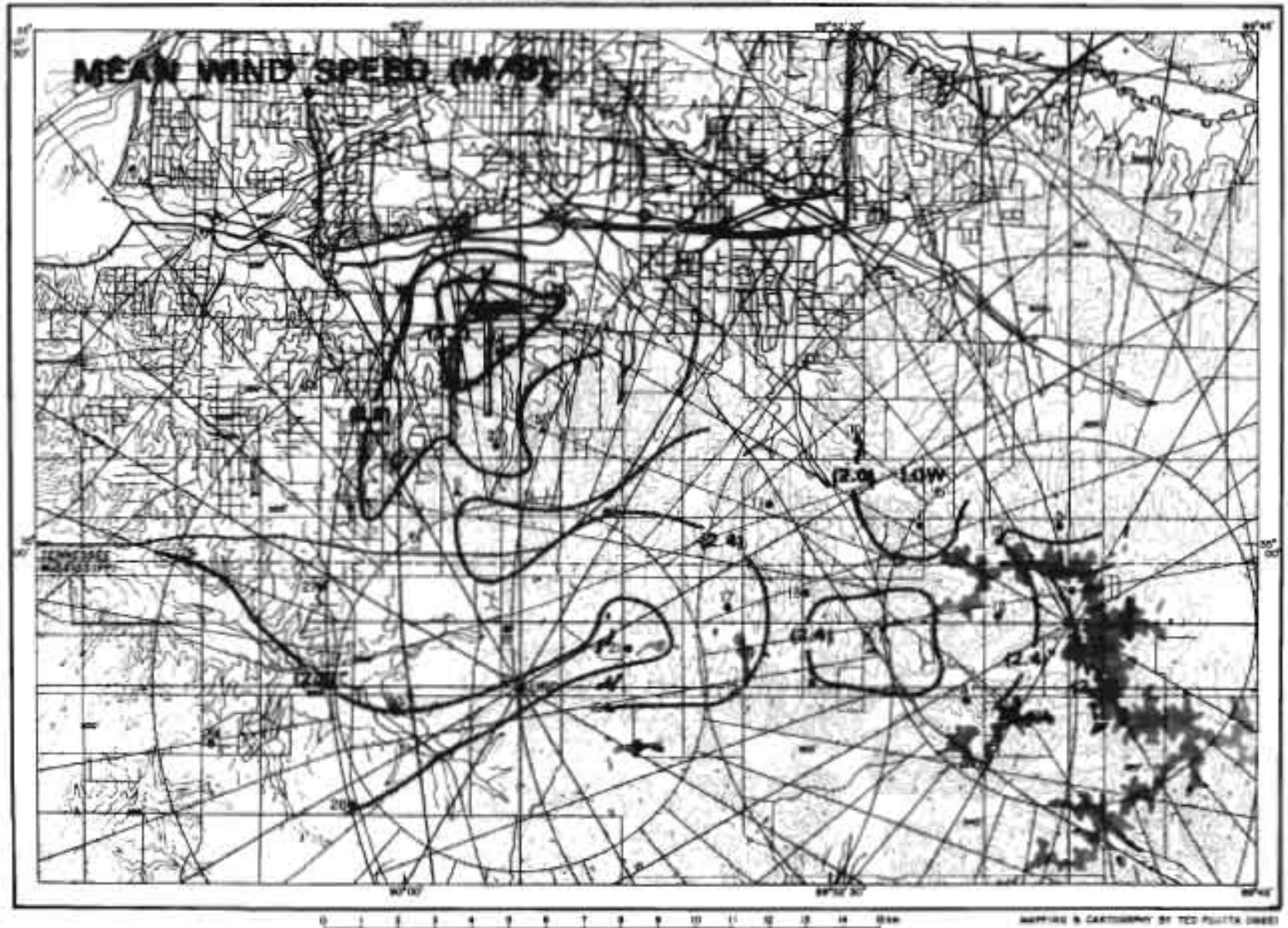
Figure V-1. Mean wind speed averaged over 197 days (15 February-31 August 1985) at 6 Memphis LLWAS stations and 30 FLOWS automatic weather stations. The effects of the open terrain near both the Memphis International Airport and the small Olive Branch, MS airport (near FL-2 radar site) can be seen. Values at station No. 7 (1.8 m/s) and LLWAS Center Field (3.6 m/s) differ by a factor of two. No correction has been made for the greater height of the LLWAS anemometers, but this would give rise to a difference of 0.4 m/s at most and does not appear to be a significant factor in the contoured mean wind speed pattern.

could be used to help correct the problem, an accurate automated procedure is much more desirable. A time-independent site-specific wind speed correction formula that is a function of wind direction is derived using a similar but improved technique to that given by Fujita and Wakimoto (1982), hereafter referred to as FW. The possibility of seasonal or monthly variations of the corrections, especially related to the growth of trees, is explored.

B. Transmission Factors

First, it is assumed that the measured wind speed, V, can be expressed as

$$V = U \psi \tag{1}$$

where U is the unobstructed wind speed at anemometer height and ψ is the fraction of the unobstructed wind "transmitted" into the wake region behind an obstruction. It is quite easy to imagine the character and pattern of the obstruction wake flow varying with the magnitude of the wind, but here, in Eq. (1), it is implicitly assumed that the measured wind speed is linearly proportional to the unobstructed wind speed. This is an imperfect assumption that represents only a first approximation to the true relationship.

The spatial scale over which the unobstructed wind varies is called the macroscale, and is much larger than the FLOWS network (>400 km); thus the value of U can be considered uniform across the network. However, the speed and direction of the unobstructed wind vary with time, as do the speed and direction of the measured wind. But if the ratio of the measured to the unobstructed wind speed, defined as the transmission factor ψ, can be related to the specific site obstructions, then in principle any time variations in ψ would be caused by time variations in the obstructions themselves or by changes in the characteristics of the obstructed wake flow. The wake flow pattern could change, for example, because of changes in the stability of the atmospheric boundary layer or as a function of wind speed. Neglecting these possible time variations, Eq. (1) becomes

$$V(s,d) = U(d) \, \psi(s,d) \tag{2}$$

where s is the particular weather station and d is the measured wind direction. With estimates of $\psi(s,d)$, Eq. (2) can be used to find the unobstructed wind speed at any time.

In the next section, the procedure for deriving time-independent transmission factors for the network is given. The effects of obstructions of different spatial scales on the measured winds are evaluated in section

C. by comparing the observed transmission factors with those predicted from the visible obstructions in panoramic photographs taken at each anemometer site. It is postulated, as in FW, that variations unexplained by visible obstructions are caused by obstructions on scales larger than those visible. A preliminary investigation into the time dependence of the transmission factors on monthly and seasonal time scales is presented in section D., but an in-depth study of possible variations in the wake flow linked to surface stability or to wind speed magnitude variations has been left for future work.

1. Estimating the Unobstructed Wind Speed

The unobstructed wind speed can be estimated as a function of azimuth by assuming it is equal to the highest mean wind speed measured by any of the stations (mesonet and LLWAS) in a given direction over a long-term average. In this case, the data from 15 February through 31 August 1985 (197 days) were used. The five stations nearest the center of the airport accounted for most of these measurements; in all they accounted for 337 out of 360 elements or 94% of the estimated unobstructed wind array. Even without directional considerations, the mean wind speed map (Figure V-1) reveals a significant maxima of 3.0 m/s and higher directly over the airport; if one had to guess in advance where the unobstructed winds might be measured, one might have guessed these same five sites.

This small number of stations is not unreasonable, for the panoramic photographs in Figure V-2 show that at each of these stations, in the directions where the measured winds were the highest, the airflow was essentially unobstructed. Even to the north, towards the city of Memphis, the airport is surrounded by open swamp areas and expressways. The land at the airport, while fairly low, is also very flat and so topography creates little if any obstruction effect. It is very good news indeed that the surface wind measurements that require the least correction are being measured at the airport (only one of these stations was part of the FAA LLWAS system, though). Near the FL-2 radar site at the far east end of the network some stations, such as No. 2 and No. 3, have very open surroundings and are at a somewhat higher elevation than those at the airport (400' vs. 220' MSL). Apparently, though, the hilly, wooded terrain creates enough surface roughness to have a small frictional slowing effect on the winds there.

In computing the time averaged winds as a function of azimuth, from which the unobstructed wind is selected, daily histograms of mean wind speed were computed over azimuth (1° bins) and a record was kept of the number of measurements, or counts at each azimuth for each station. The results from any number of these daily histograms could be averaged together, using the total counts as weighting factors, to produce a time averaged profile of the wind speeds for any desired length of time. It was from this averaged data that the unobstructed winds were estimated. The algorithm for editing the wind speeds (described in VI.D.2.a) rejects, among other things, absolutely calm anemometer readings. The total numbers of wind speed values used in computing the averages are given in Table V-1.
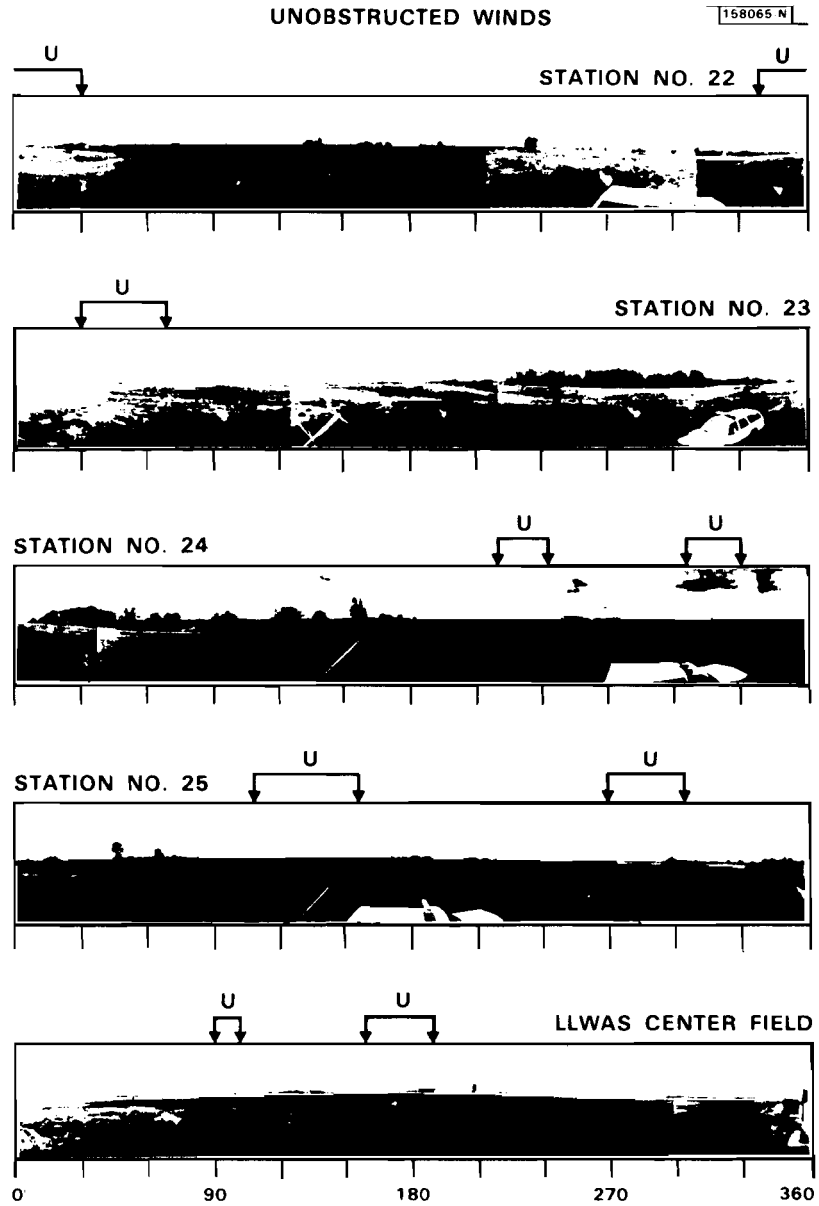
Figure V-2. Panoramic photographs taken at station Nos. 22, 23, 24, 25, and LLWAS Center Field. The azimuths from which maximum wind speeds were used in the unobstructed wind array are marked above each photograph.

Unrealistic variations are present in the unobstructed wind speed array, U(d), when the components are selected every 1° in azimuth as they were here. Following FW, a weighting function was used to smooth azimuthal variations:

$$G = 1 + \cos(n\lambda) \qquad -180° \leq n\lambda \leq +180°. \qquad (3)$$

The results of using G with varying azimuthal widths are illustrated in Figure V-3. The 30° width was found to eliminate unwanted variations while not oversmoothing the data.

The unobstructed wind speed U(d) used for the calculation of the transmission factors was thus defined as

$$U_{30} = \frac{\sum \hat{V} \, G(30°)}{\sum G(30°)} \qquad (4)$$

where $\hat{V}$ is the highest time averaged wind speed in a given direction and $G(30°)$ is the weighting function in Eq. (3) applied with a 30° width. Figure V-4 shows the azimuthal distribution of U_{30}.

2. Computing the Transmission Factors

The time averaged wind speed as a function of azimuth for each station, V(s,d), was also smoothed in azimuth, and after experimenting with weighting functions of varying widths up to 30°, a 16° wide function was selected. Therefore,

$$V_{16} = \frac{\sum V \, G(16°)}{\sum G(16°)} \, . \qquad (5)$$

The transmission factors at each station are then defined as

$$\psi(s,d)_{16} = \frac{V_{16} \, (s,d)}{U_{30} \, (d)} \, . \qquad (6)$$

The transmission, ψ, is a smoothed function since those it is computed from are smoothed; its degree of smoothing is equal to that of the most varying function, 16°. It is also essentially a measured quantity in that a network of time series of the surface winds is all that is needed for its calculation at a particular site.

C. Scale-Dependent Transmission Factors

It is clear from Tables V-1 and V-2, and Figure V-1 that some correlation exists between the visible obstructions above the horizon at a particular site and the mean wind speed measured there. Obstructions on this

SMOOTHED TRANSMISSION FACTORS
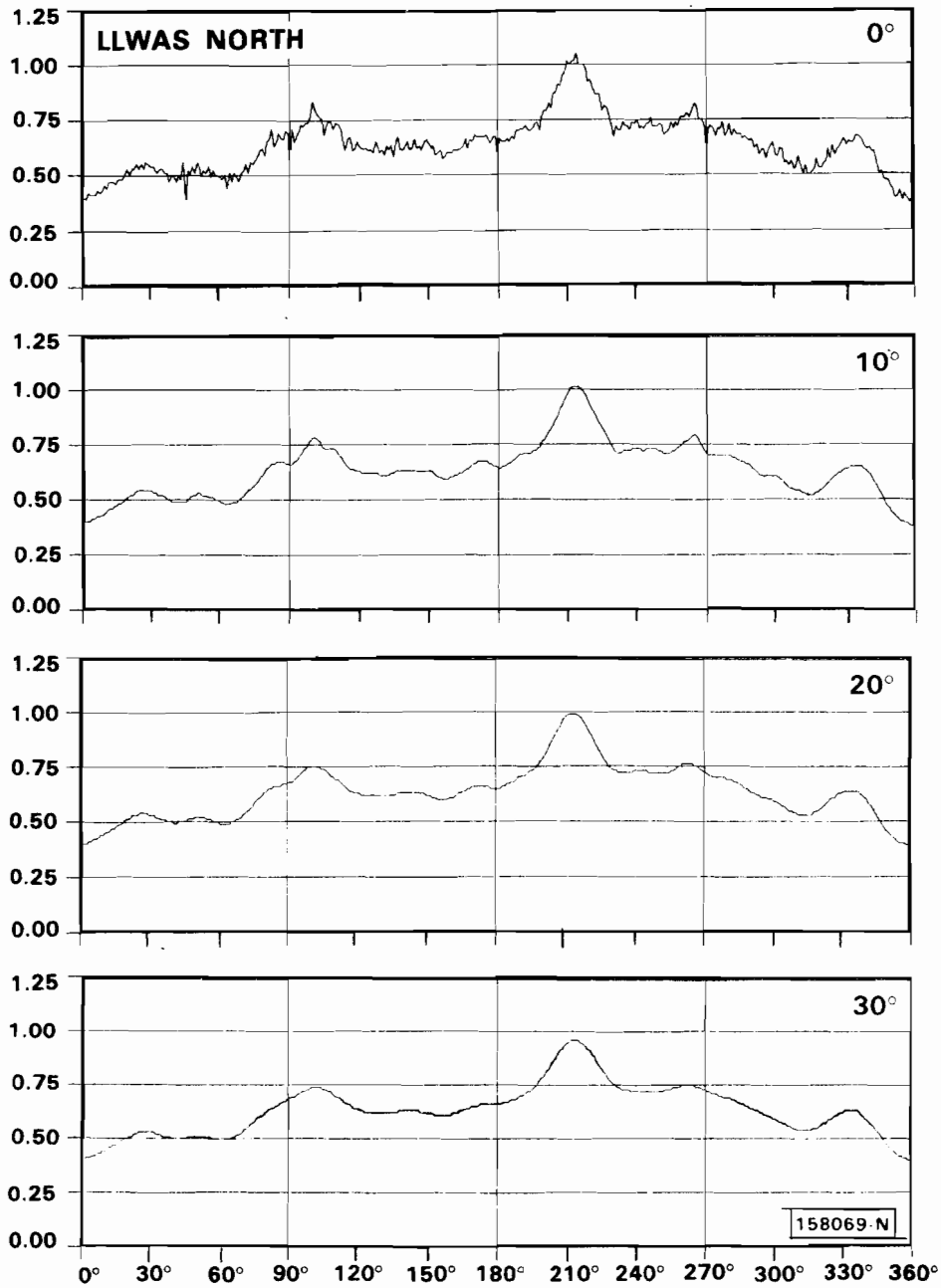
Figure V-3. Illustration of the effects of the weighting function, G (Eq. (3)), with 0°, 10°, 20° and 30° widths, on the transmission factors at LLWAS North.
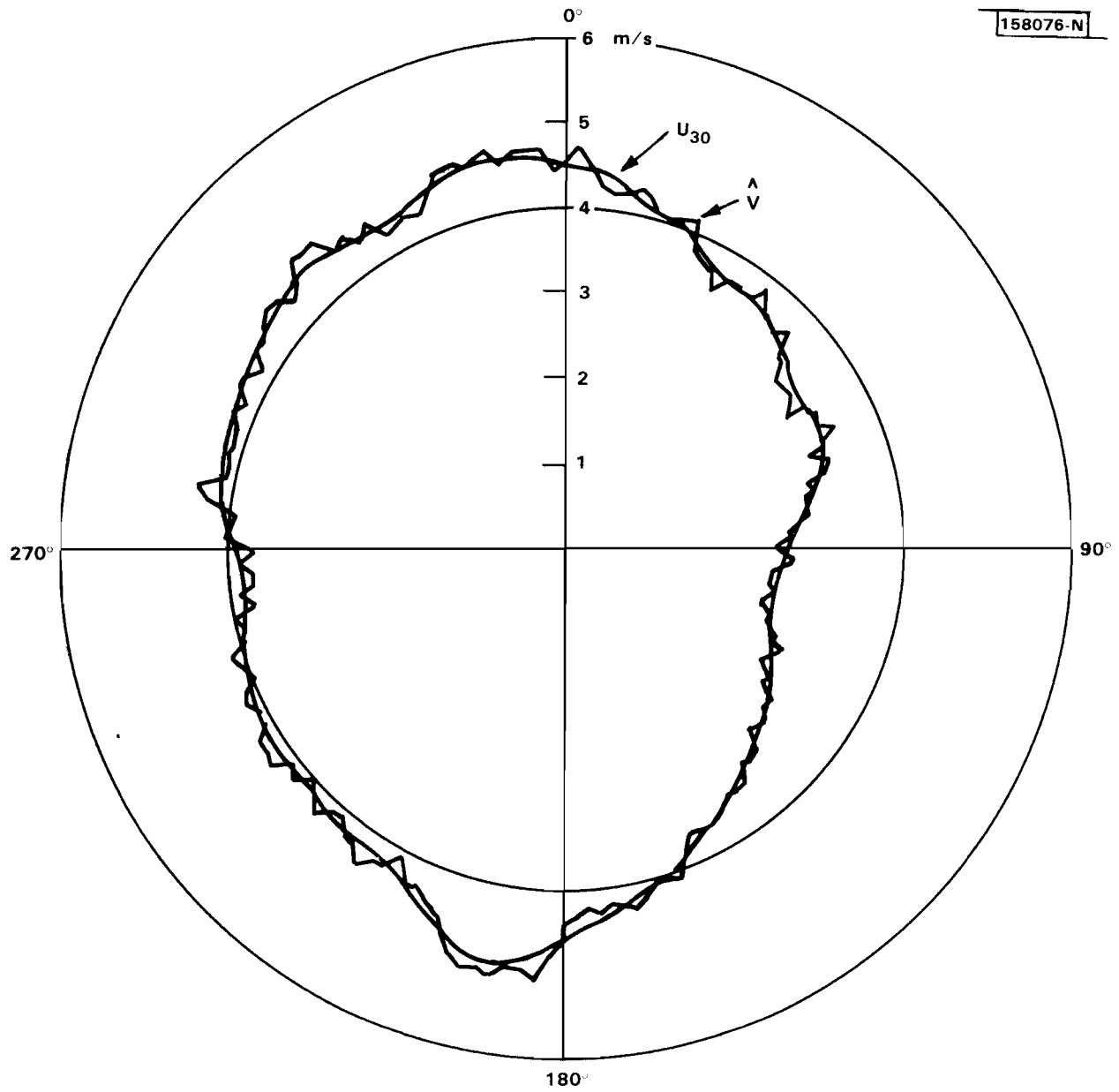
Figure V-4. The smoothed unobstructed wind speed as a function of azimuth for the period 15 February-31 August 1985.

local, visible scale (40 m - 4 km, called microscale in the meteorological literature, misoscale by FW) might well account for most of the observed wind speed transmission at a station. If so, an estimate of the appropriate wind corrections could be given based on the observed obstructions before a complete time series of wind data across a network had been gathered, as long as the function relating obstruction elevation to wind speed transmission is independent of location.

1. Effects of Visible Microscale Obstructions

The effects of the local, visible microscale obstructions on measured wind speeds are estimated by first determining the empirical relationship between them, and then determining how much of the measured transmission at each station can be predicted based on this relationship.

The local obstructions at each site have been characterized by the elevation angles above the horizon of visible objects in a panoramic (360°) photograph taken at the anemometer. The obstruction angles were estimated to the nearest integer for each azimuth from the photographs by Dr. T.T. Fujita (University of Chicago). These values were smoothed in azimuth with a weighting function,

$$\theta(s,d)_{16} = \frac{\sum \theta \ G(16°)}{\sum G(16°)} \tag{7}$$

to match the smoothing of the empirical transmission factors in Eq. (6). The panoramic photographs and the corresponding smoothed obstruction angle curves and transmission factor curves are shown for station Nos. 8 and 23 in Figures V-5 and V-6, respectively. The mean obstruction angles and mean transmission factors for each site are given in Table V-2.

The transmission factors calculated by Eq. (6) were first correlated with the obstruction angles at shifts in azimuth from 0° to ±15° to determine what offset, if any, was needed to align north in the panoramic photos with north on the wind vane directional sleeves. When a shift in azimuth of the obstruction angle data of a few degrees, either clockwise or counterclockwise, resulted in a rapid increase in the magnitude of the correlation and the panoramic photographs suggested a discrepancy might exist between the angles, the obstruction angle data were shifted into alignment with the observed transmission factors.

This correlation, negative at all stations except No. 27, essentially measures the validity of assuming that a functional relationship exists between the observed transmission factors and obstructions at the anemometer sites. The correlation values are listed in Table V-2 for each of the stations; they range in value from -0.12 to -0.91 with a mean value (excluding station No. 27) of -0.51. Assuming the logarithm of ψ varies linearly with the obstruction angle at any given azimuth, the "null" hypothesis that these variables are independent must be rejected, even for the worst case correlation of -0.12 at LLWAS station CF, better than 98% of the time.
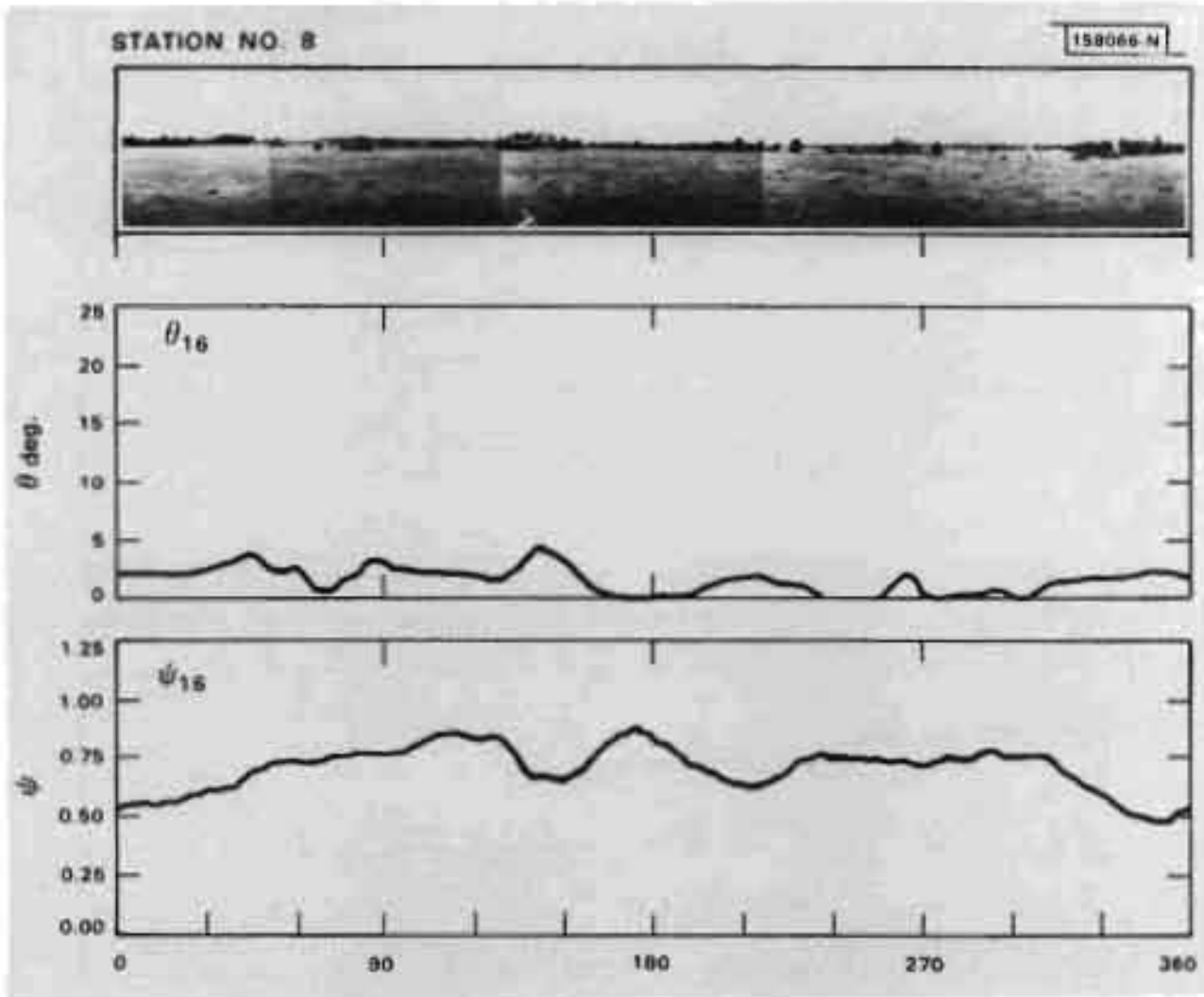
Figure V-5. Panoramic photograph, smoothed obstruction angles θ_{16}, and smoothed transmission factors ψ_{16} for station No. 8.

STATION NO. 23
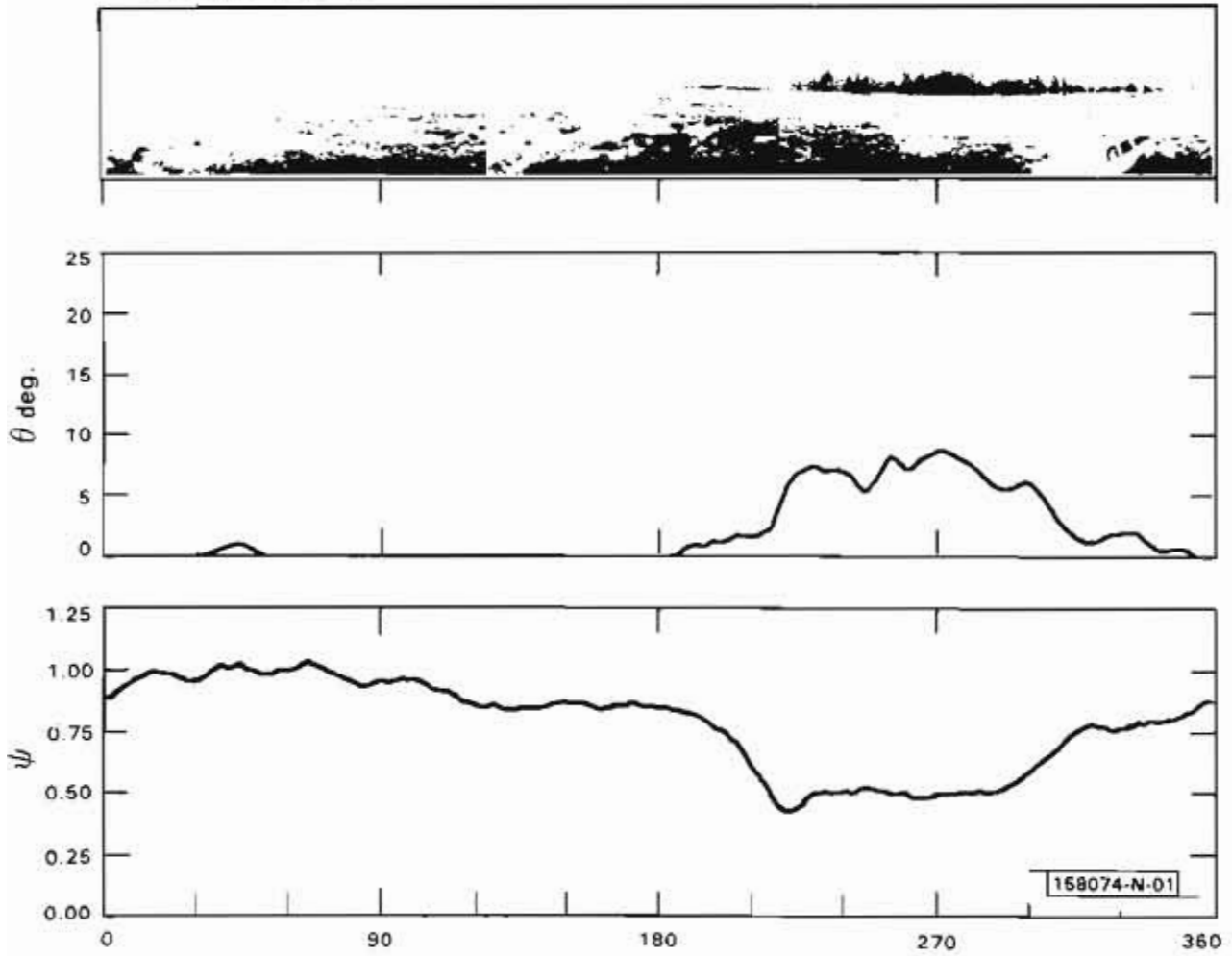
Figure V-6. Panoramic photograph, smoothed obstruction angles θ_{16}, and smoothed transmission factors ψ_{16} for station No. 23.

Station	Mean Obstruction Angle (degrees)	Mean Transmission Factor	Correlation between Obstruction Angles and Transmission Factors (Azimuth shift)
1	2.1	0.75	-0.74
2	1.0	0.75	-0.34 (-6°)
3	1.4	0.73	-0.37
4	3.7	0.56	-0.49
5	4.3	0.56	-0.83 (+4°)
6	1.1	0.73	-0.16 (-10°)
7	8.7	0.47	-0.84 (-6°)
8	1.6	0.70	-0.44
9	3.0	0.61	-0.49
10	4.7	0.51	-0.22
11	8.9	0.50	-0.64 (-7°)
12	6.8	0.49	-0.50 (-5°)
13	3.6	0.59	-0.44 (-3°)
14	2.4	0.61	-0.62
15	6.1	0.60	-0.46
16	3.8	0.62	-0.70
17	2.3	0.65	-0.45
18	3.2	0.59	-0.62 (+5°)
19	2.4	0.59	-0.52
20	1.7	0.74	-0.55 (-3°)
21	0.9	0.73	-0.65
22	0.7	0.82	-0.44
23	2.0	0.78	-0.91
24	1.9	0.81	-0.84
25	2.0	0.82	-0.75
26	2.8	0.71	-0.28
27	1.6	0.68	+0.67
28	2.8	0.70	-0.40 (-6°)
29	0.8	0.74	-0.55
30	1.8	0.75	-0.40
CF	0.3	0.88	-0.12
N	0.3	0.63	-0.42
E	0.3	0.73	-0.37
SE	0.1	0.58	-0.43
S	0.4	0.62	-0.55
W	0.3	0.66	-0.32
Mean	2.5	0.67	-0.48 [-0.51]

Table V-2. The mean obstruction angle (θ) averaged over 360° azimuth, the mean observed transmission factor from 15 February - 31 August 1985 (ψ), and the correlation between the θ and ψ at all azimuths after any wind direction corrections (azimuthal shifts) had been accomplished, for each of the mesonet and LLWAS stations.

Once the azimuth corrections (given in Table V-2) were applied, the values of θ_{16} and ψ_{16} for each station, for every degree of azimuth were plotted against each other. Since many measurements exist at low obstruction angles (Figure V-7), the mean value of the transmission factors for every 0.1° in elevation angle was computed and the results plotted in Figure V-8. The variance of the points increases with increasing elevation angle because fewer of these higher angles were observed. The best exponential curve, fit using all of the data points, (not just the mean at every 0.1°), is also plotted in Figure V-8. It represents the functional relationship between ψ and θ for the FLOWS network:

$$\psi = 0.42 + 0.35 \ e^{-0.18 \ \theta} \tag{8}$$

where θ is in degrees.

Notice that when $\theta=0°$, ψ does not equal 1 but is offset at 0.77. Yet, in an otherwise uniform environment, the transmission factor should increase to 1 an infinite distance downwind of the obstruction where the visible obstruction angle, actually the tangent of the angle*, approaches 0°. Apparently, obstruction effects on scales too large to be visible from the weather station sites are included in the observed transmission factors.

Following FW, it is assumed that

$$\psi = \psi_e \ \psi_i \tag{9}$$

where ψ_e accounts for large-scale (4 km - 400 km, mesoscale) obstruction effects and ψ_i, for microscale obstruction effects as illustrated in Figure V-9. It is assumed that $\psi_i=1$ when $\theta=0°$; ψ_e then is equal to the remaining value of ψ when $\theta=0°$, that is:

$$\psi = 0.77 \ \psi_i \tag{10}$$

Combining Eqs. (8) and (10), the relationship between the visible scale obstructions and the microscale wind speed transmission is found to be:

$$\psi_i = .545 + .455 \ e^{-0.18 \ \theta} \tag{11}$$

Notice that, no matter how large the obstruction angle θ, ψ_i is never less than 0.545 and ψ never less than 0.42, representing correction factors (the reciprocals) of 1.83 and 2.38, respectively, to the measured wind speeds. The exponential decay with elevation angle is quite sharp, the contribution being 0.455 when $\theta=0°$, down to 0.10 when $\theta=8°$, and down to 0.005 when $\theta=25°$ (Figure V-8, curve A).

---

*Most studies have shown that the transmission factor decreases exponentially as the ratio of obstruction height to the downwind distance ($\tan\theta$) increases. The use of θ as an approximation to $\tan\theta$ is valid for these purposes up to angles of 25° where the error is roughly 6%. The largest observed angle in the FLOWS network was 24°.
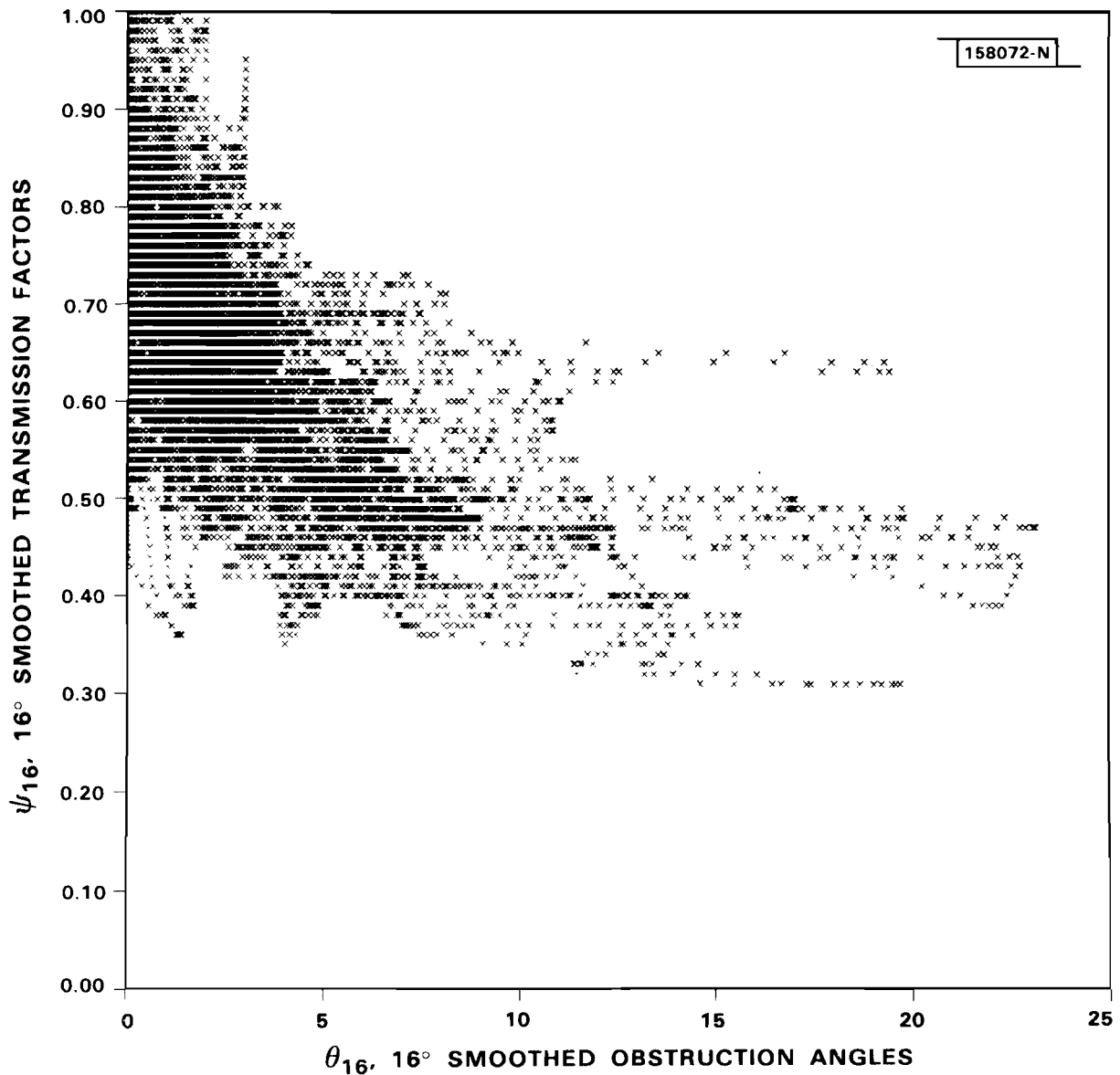
Figure V-7. Plot of smoothed transmission factors (ψ_{16}) versus smoothed obstruction angles (θ_{16}), in degrees, for all stations at all azimuths.
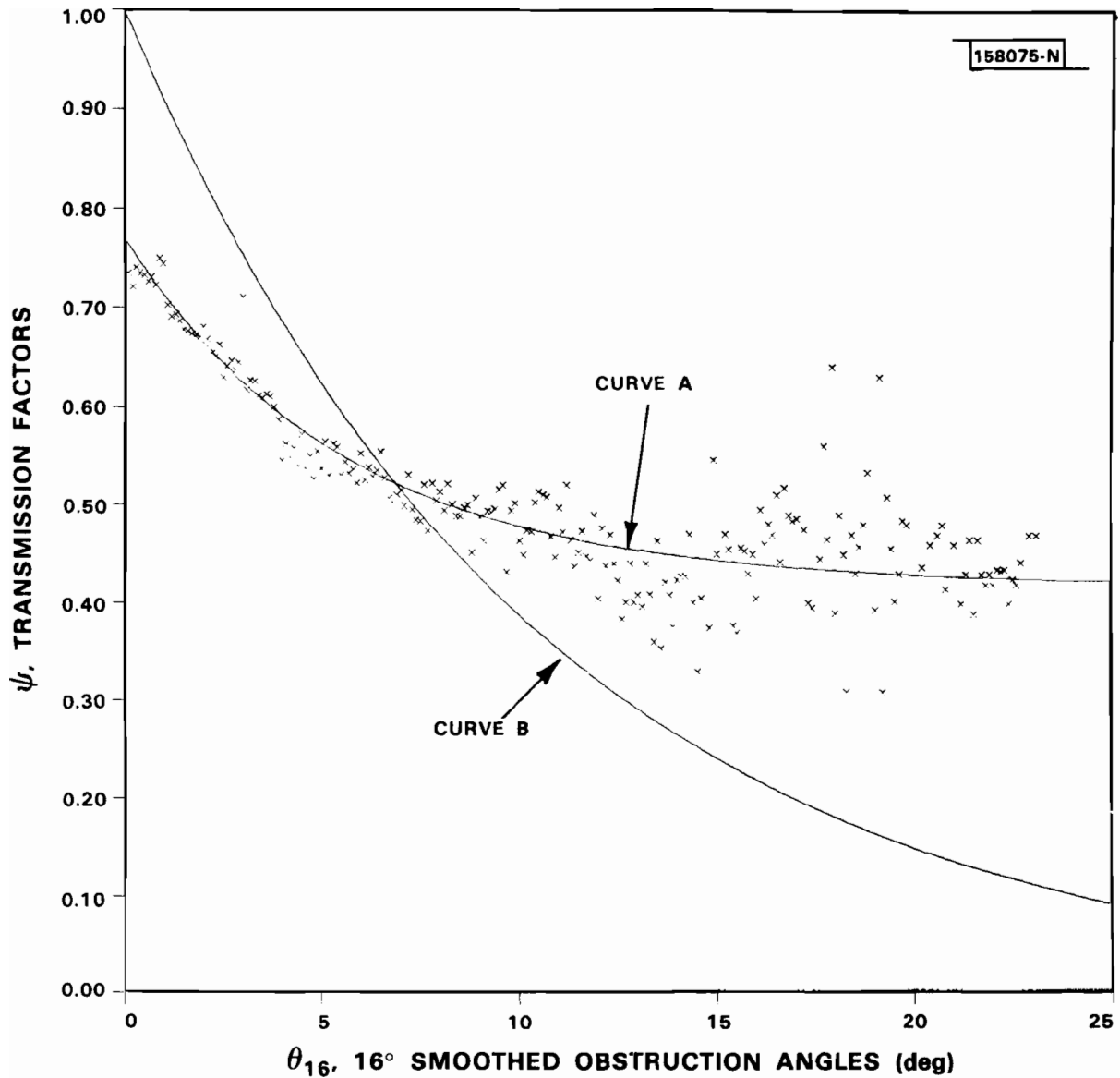
Figure V-8. Plot of the mean of all the transmission factors (ψ_{16}) for each $0.1°$ step in obstruction angle (θ_{16}). A best fit exponential curve (curve A, given by Eq. (8)), is plotted through these points. A mark appears at the bottom of the graph at those angles which did not occur in the dataset. The other curve shown (curve B) was the exponential fit used by Fujita and Wakimoto (1982): $\psi = \exp(-0.0948\ \theta)$.
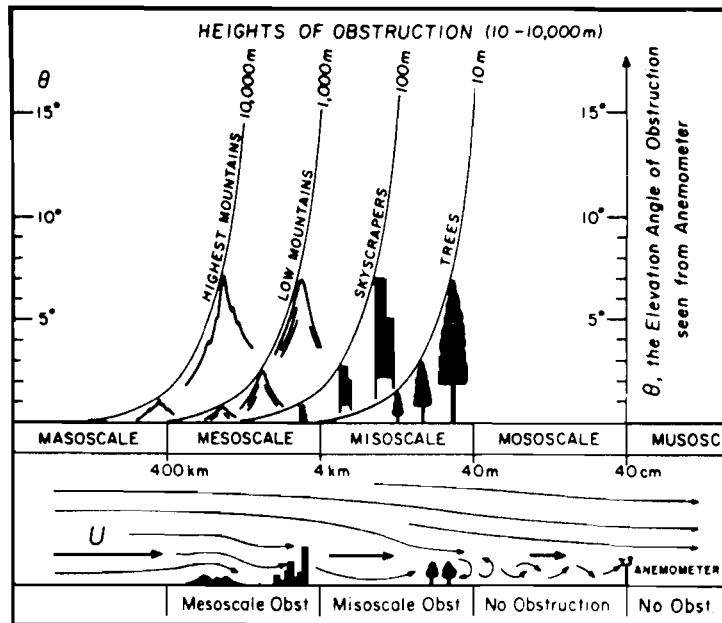
Figure V-9. The obstruction angles (the elevation angles of the obstructions seen from an anemometer) of terrestrial objects located in the multiple-scale environment are shown. The microscale obstructions are caused mainly by trees and buildings, while smaller-scale obstructions are reduced to near zero by choosing the best possible weather station site. Taken from Fujita and Wakimoto (1982).

A similar equation derived by FW had no additive term but had an exponential decay constant of -0.0948, roughly half of that observed here. Thus, their exponential decay was less severe but continuous (Figure V-8, curve B); at $\theta=25°$ the total mesoscale transmission would be only 0.09, implying a correction factor of over 10 to the measured wind speeds. The data collected in the FLOWS experiment reveal that as the obstruction angles increase above 10°-20°, there is little change in observed transmission with further increases in angle. A similar result, obtained by Naegeli (1953) for the small end of the microscale range (4-40 m), is illustrated in Figure V-10. The transmission reaches a minimum of 0.32 at about $\theta=10°$; as θ increases further the transmission increases back up to about 0.75 at $\theta=90°$, directly next to the obstruction. A similar effect would certainly be revealed here if measurements had been made at larger obstruction angles.

Before leaving the subject of deriving a functional relationship between ψ and θ, it is perhaps useful to reconcile the approach used by FW with that used here. FW assumed that

$$\psi_i = e^{-k\theta} \tag{12}$$

and
$$\psi = \psi_e \, \psi_i = C \, e^{-k\theta} \tag{13}$$

where C is a constant for all obstruction angles (but varies in azimuth at each site). ψ_i was first derived by finding the value of k which caused the correlation between θ and

$$\frac{\psi}{\psi_i} = \psi \, e^{+k\theta} \tag{14}$$

to approach zero. But this is just the equation for ψ_e! The exponential constant, k, is just the value that explains all of the variation of ψ with θ, and allows C in Eq. (13) to be fully independent of θ, that is, to be a constant. Furthermore, successively testing values of k that minimize the correlation at each site between θ and ψ_e as given in Eq. (14) or, equivalently, that maximize the negative correlation between ψ and θ, simply amounts to finding approximate solutions that minimize the error in a regression problem that, in this case, can be solved exactly.

Taking the logarithm of Eq. (13)

$$\ln \psi = \ln C - k\theta \tag{15}$$

or

$$Y = A + BX \tag{16}$$

where A=ln C and B=-k are constants. With this linear relationship, the method of least squares provides a simple formula for the "best" estimates of A and B. The correlation is a measure of the relationship between two variables and so is B in Eq. (16).
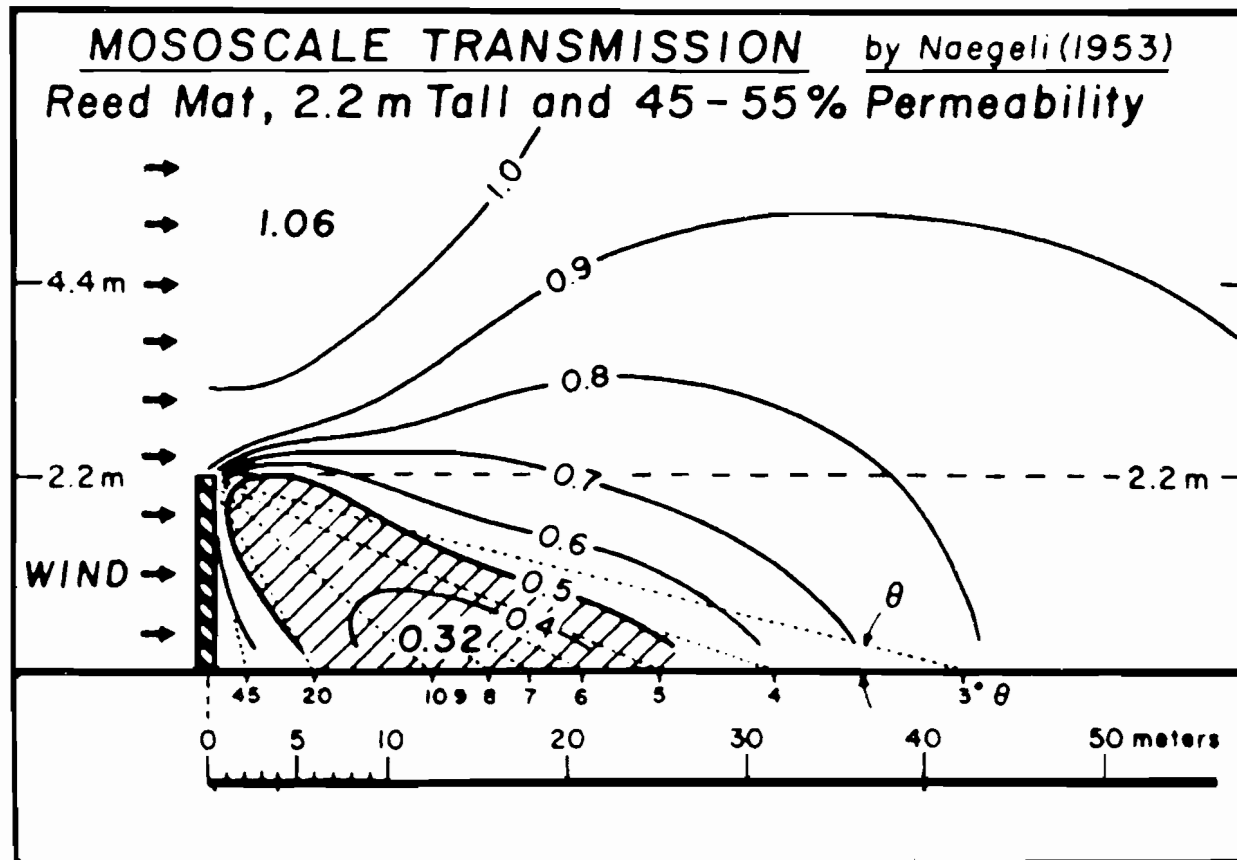
Figure V-10. Wind break effects of a 2.2 m tall reed mat. The fractional transmission or the wind speed deficit can be seen in the wake as far as 50 m behind the mat. Taken from Fujita and Wakimoto (1982).

In FW, the value of k that minimized the correlation between ψ_e and θ was found for each station and these values of k were averaged together, each weighted with the correlation between ψ and θ at that site, to derive a value of k for the network. This is equivalent to finding the best fit line (Y=A+BX) at each station, and then finding the mean value of the slopes, B, for the network by weighting each value of B with itself, multiplied by the ratio of the variance in X (θ) to the variance in Y (ln ψ) at that station. Alternatively, one could find the "network" k directly by using the data from all of the stations at once in solving the regression problem.

This latter approach was used here, except the curve being fit was of the form

$$\psi = A + Ce^{-k\theta}. \tag{17}$$

An iterative procedure was used to find the values of A, C, and k which minimized the sum of the squares of the errors between the observed values of ψ at all of the stations and those estimated with Eq. (17).

2. Effects of Larger Mesoscale Obstructions

Once the transmission factors, ψ_i, have been calculated from the obstruction angles at each station according to Eq. (11), the larger, mesoscale transmission factors, ψ_e, can be calculated from Eq. (9). These values are plotted as a function of obstruction angle in Figure V-11 and the mean value at each azimuth is plotted in Figure V-12. It can be seen that the ψ_e are independent of θ, and have a mean of 0.77. But ψ_e is still a function of azimuth specific to each weather station site. Again, following FW the ψ_e are smoothed, this time with a weighting function (Eq. (3)) of 180° to eliminate all but the lowest frequency variations.

$$\psi_e(s,d)_{180°} = \frac{\sum \frac{\psi}{\psi_i} G(180°)}{\sum G(180°)} . \tag{18}$$

This effectively selects the scale represented by this function as equal to or larger than that encompassed by roughly 90° sectors at distances from just beyond those visible from the site (about 4 km, less if obstructions are close-by) to those much farther away.

To see if the measured variations in ψ_{e-180} could be related to the topographical variations or known large-scale obstructions such as the city of Memphis (25-50 km scale), maps of the deviation from the mean value of ψ_e at each station were plotted for winds blowing from the east, south, west, and north (Figures V-13 through V-16). The actual values contoured in these figures are listed in Table V-3. The absolute values of ψ_e were not used because they also represent a kind of "calibration" term for the anemometers; inherently included are things like the condition of the
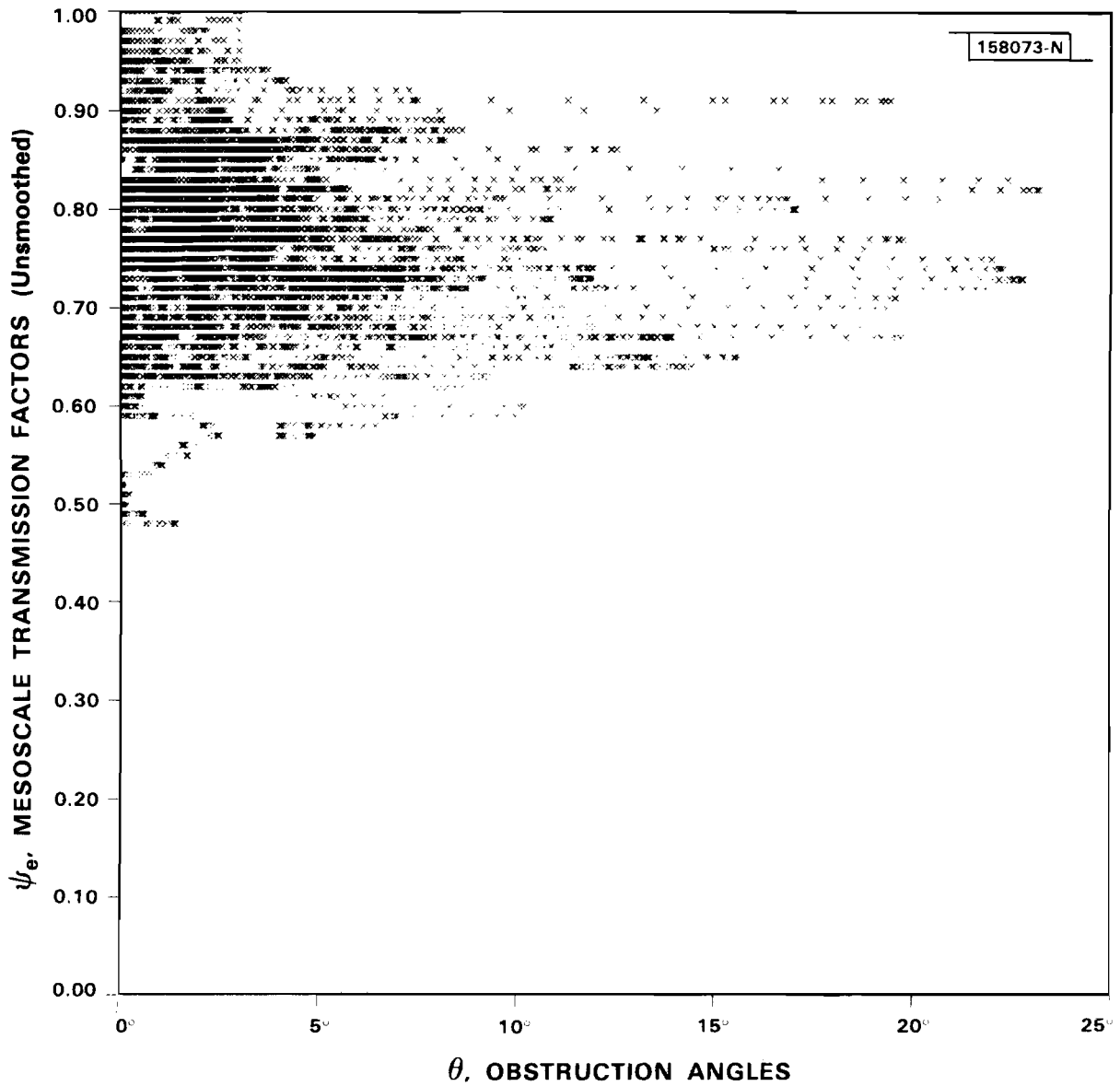
Figure V-11. Plot of the unsmoothed mesoscale transmission factors (ψ_e) versus smoothed obstruction angles (θ_{16}), in degrees, for all stations at all azimuths.
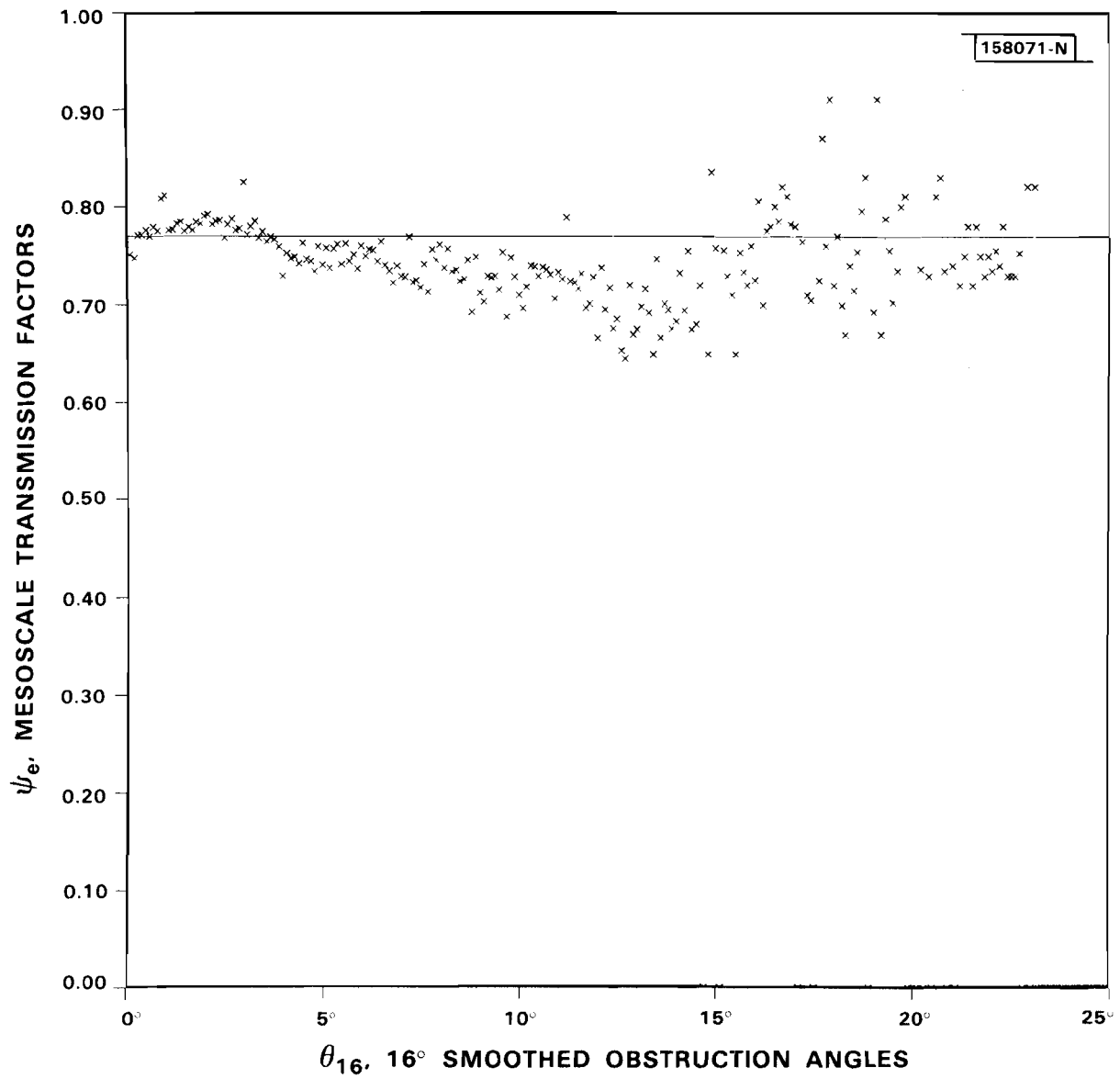
Figure V-12. Plot of the mean of all the mesoscale transmission factors (ψ_e) for each 0.1° step in obstruction angle (θ_{16}). The mean value of 0.77 is shown.
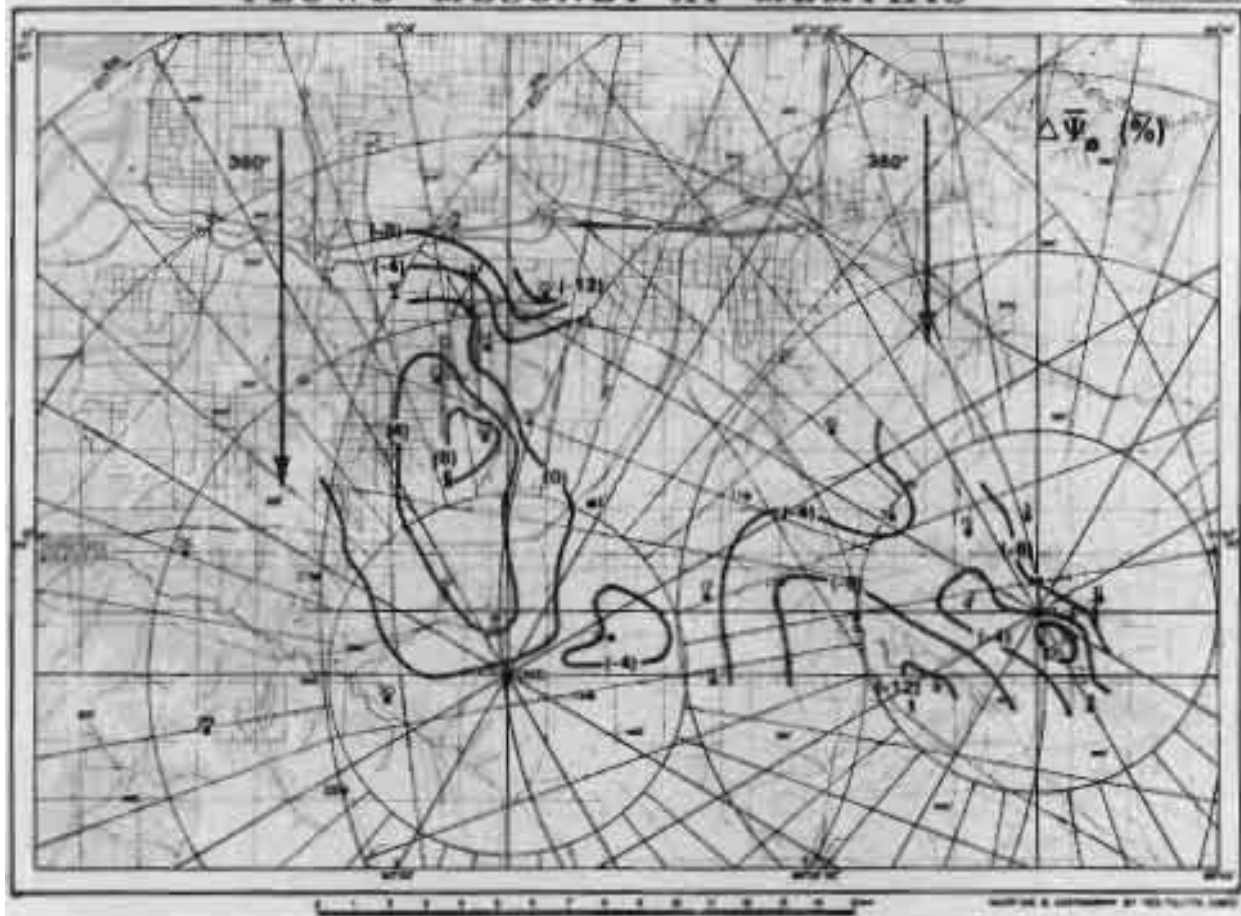
Figure V-13. Contour plot showing $\Delta\psi_e$(%), the difference between ψ_e at a given azimuth and the mean value of ψ_e at all azimuths, for each station in the FLOWS Memphis network. Here, the given azimuth is 90°, revealing the net mesoscale effects of a wind blowing from the east toward the west.
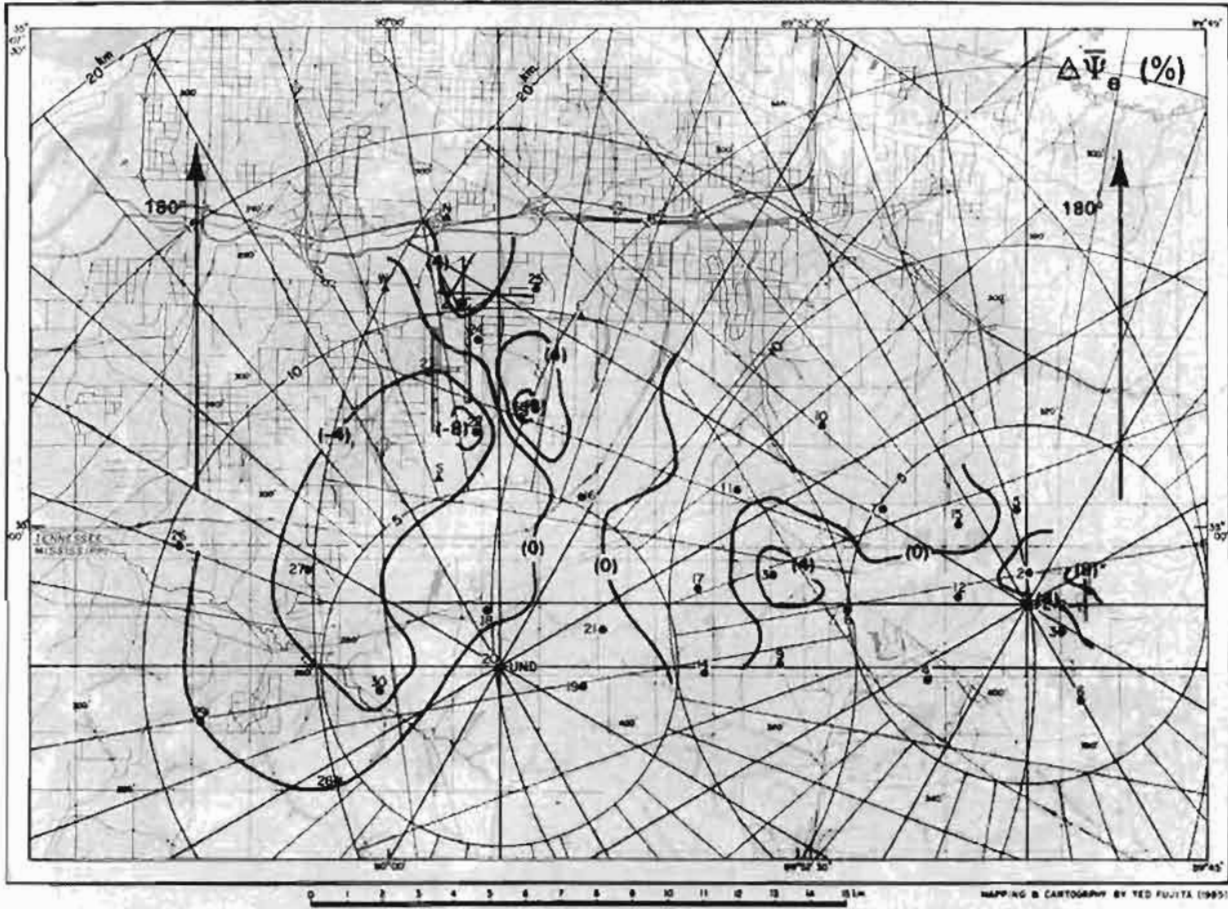
Figure V-14. Contour plot showing $\Delta\psi_e$(%) for a given azimuth of 180°, revealing the net mesoscale effects of a wind blowing from south to north over the FLOWS Memphis network.
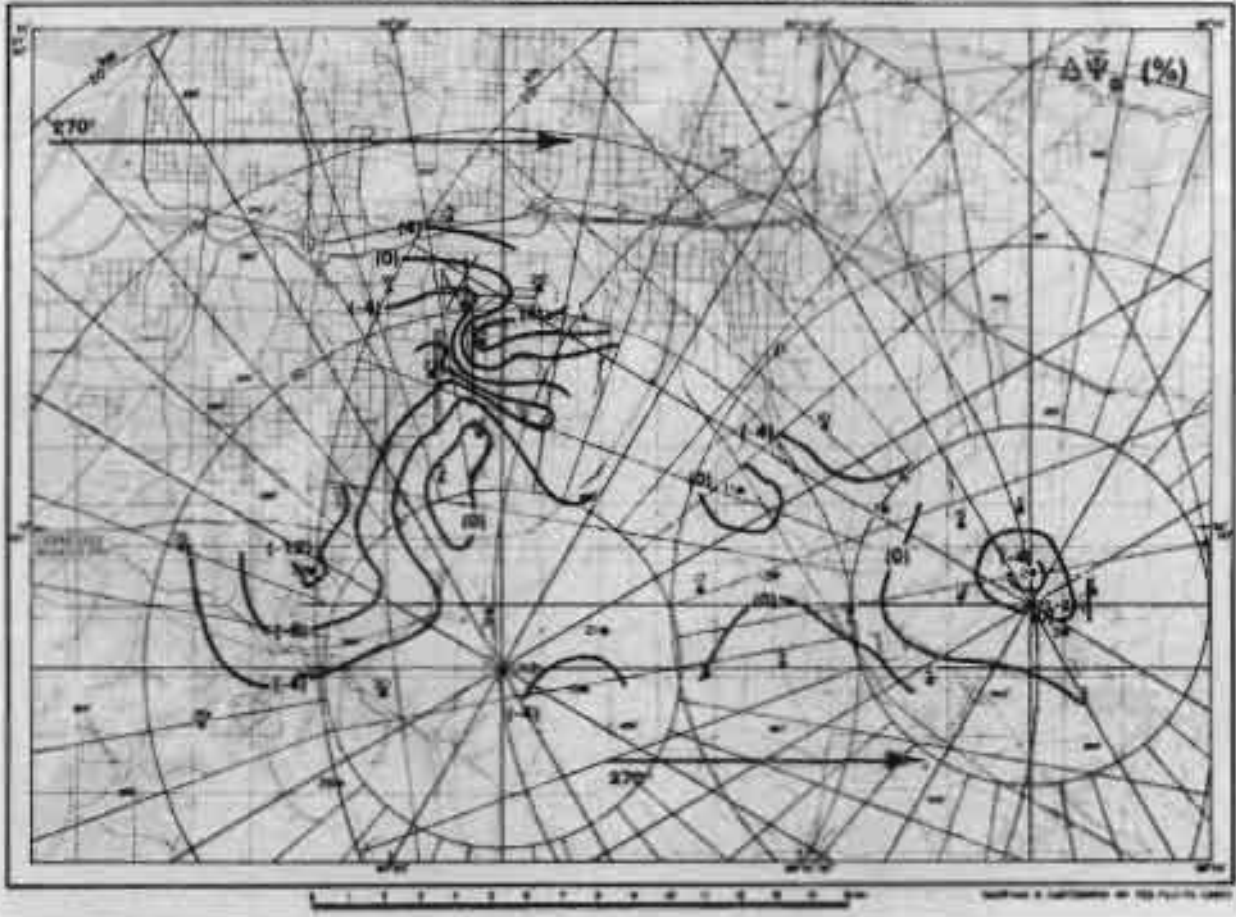
Figure V-15. Contour plot showing $\Delta\bar{\Psi}_e(\%)$ for an azimuth of 270°, revealing the net mesoscale effects of a wind blowing from west to east across the network.
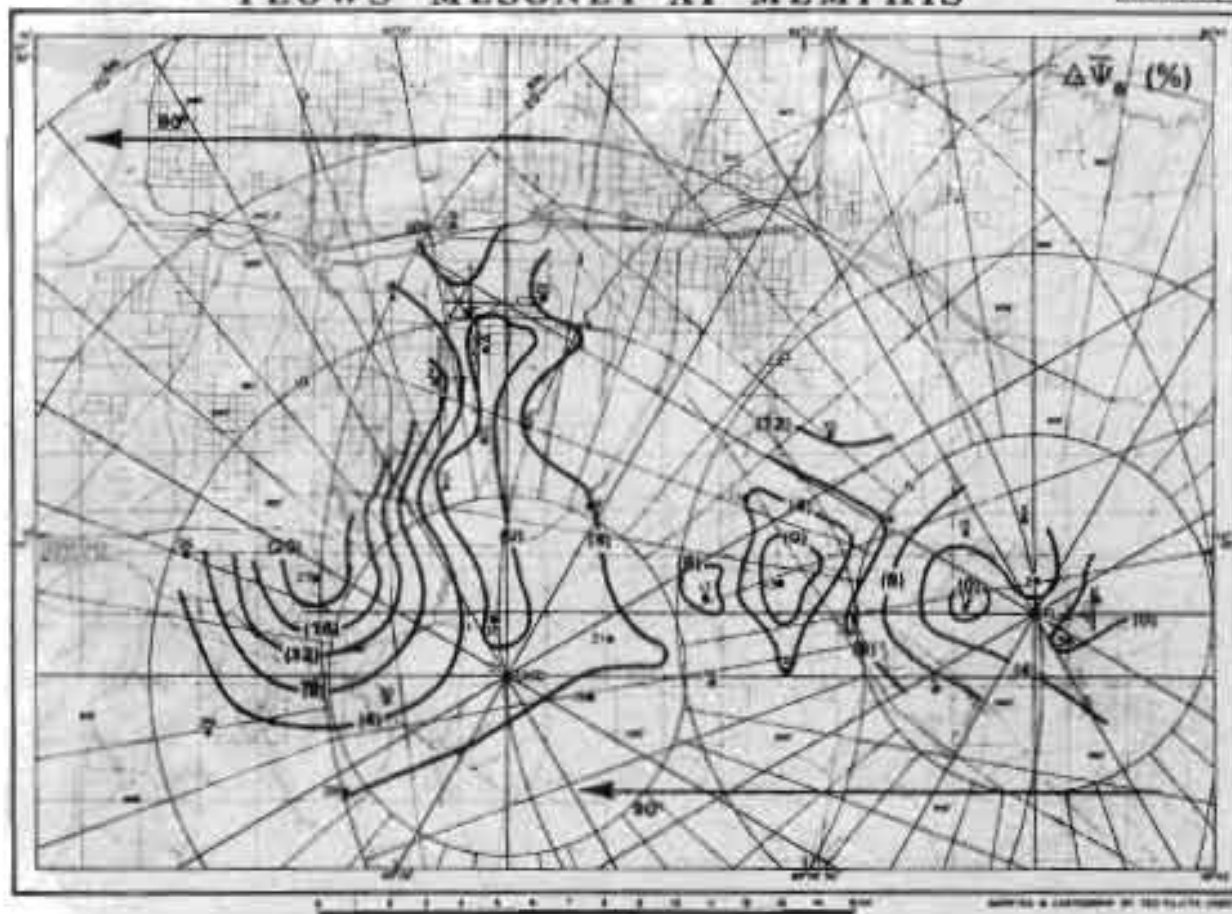
Figure V-16. Contour plot showing $\Delta\phi_e$(%) for an azimuth of 360° or due north, revealing the net mesoscale effects of a wind blowing from north to south over the network.

Station	$\bar{\psi}_e$	90°	180°	270°	360°
1	86	84 (-2)	95 (+9)	90 (+4)	74 (-12)
2	82	88 (+6)	88 (+6)	77 (-5)	74 (-8)
3	81	80 (-1)	83 (+2)	82 (+1)	82 (+1)
4	70	79 (+9)	73 (+3)	69 (-1)	57 (-13)
5	72	77 (+5)	73 (+1)	74 (+2)	63 (-9)
6	79	83 (+4)	79 (0)	79 (0)	76 (-3)
7	70	79 (+9)	67 (-3)	67 (-3)	67 (-3)
8	78	88 (+10)	81 (+3)	77 (-1)	68 (-10)
9	75	79 (+4)	76 (+1)	78 (+3)	67 (-8)
10	68	81 (+13)	65 (-3)	62 (-6)	65 (-3)
11	72	76 (+4)	71 (-1)	73 (+1)	69 (-3)
12	71	70 (-1)	73 (+2)	73 (+2)	69 (-3)
13	74	77 (-3)	80 (+6)	73 (-1)	66 (-8)
14	70	75 (+5)	69 (-1)	70 (0)	67 (-3)
15	83	89 (+6)	81 (-2)	87 (+4)	77 (-6)
16	78	82 (+4)	79 (+1)	74 (-4)	76 (-2)
17	76	85 (+9)	72 (-4)	74 (-2)	73 (-3)
18	72	71 (-1)	71 (-1)	71 (-1)	77 (+5)
19	69	75 (+6)	71 (+3)	63 (-6)	66 (-3)
20	84	85 (+1)	88 (+4)	82 (-2)	81 (-3)
21	79	82 (+3)	81 (+2)	77 (-2)	74 (-5)
22	86	85 (-1)	76 (-10)	87 (+1)	97 (+11)
23	85	94 (+9)	81 (-4)	75 (-10)	91 (+6)
24	90	86 (-4)	92 (+2)	95 (+5)	87 (-3)
25	93	98 (+5)	96 (+3)	95 (+2)	80 (-13)
26	84	90 (+6)	85 (+1)	80 (-4)	81 (-3)
27	77	100 (+23)	71 (-6)	64 (-13)	75 (-2)
28	84	88 (+4)	84 (0)	83 (-1)	82 (-2)
29	79	79 (0)	79 (0)	79 (0)	81 (-2)
30	85	90 (+5)	80 (-5)	84 (-1)	87 (-2)
CF	90	91 (+1)	95 (+5)	85 (-5)	90 (0)
N	65	62 (-3)	71 (+6)	71 (+5)	55 (-10)
E	74	79 (+5)	75 (+1)	69 (+5)	74 (0)
SE	58	63 (+5)	67 (+9)	49 (-9)	54 (-4)
S	64	62 (-2)	59 (-5)	65 (+1)	72 (+8)
W	67	72 (+5)	65 (-2)	64 (-3)	67 (0)
Mean	77	81 (+4)	78 (+1)	75 (-2)	74 (-3)

Table V-3. The mean mesoscale transmission factors (in %), averaged over 360° azimuth, and the values at 90°, 180°, 270°, and 360° for the meso-net and LLWAS stations for the period 15 February - 31 August 1985. Values in parentheses are deviations from the mean value (in %).

bearings, etc. which could produce a transmission value unrelated to obstructions on any scale*.

When the wind is blowing from 90° (Figure V-13), the stations on the upwind side of the airport runways (Nos. 24, 22, and S) have lower transmissions than normal and those on the downwind side (No. 23 and W), higher. The high value at station No. 27 brings the transmission there to 100%, but it is not clear what scale feature, if any, to which it could be attributed. Other patterns appear to be related to exposure at the tops of hills, or shielding by topographical irregularities of 40-100 m in amplitude and 2-10 km in horizontal scale. In general, the flow is quite unobstructed from the east, with a mean mesoscale transmission across the network of 0.81 or +4 above the overall average.

When the wind is blowing from 180° (Figure V-14), the upwind-downwind pattern of decreased-increased transmission over the airport is even more pronounced. A general pattern related to surface elevation is present, with the transmissions in the low wet lands to the west depressed, and those in the central and eastern part of the network elevated. Values here vary much less rapidly in the horizontal than in Figure V-13, suggesting perhaps influence from a larger scale (15-20 km). The network mean is only 1% above normal.

When the wind is blowing from the west (270°, Figure V-15) again, the "dipole" pattern is present over the airport. Only small regions downwind of the airport and over the ridge at the southeast side of the network have positive deviations; the deviation from the mesoscale mean transmission for a westerly wind is 2% below the overall average.

When the wind is blowing from the north (360°, Figure V-16), the largest amplitude upwind-downwind dipole of all four directions exists over the airport, possibly because the winds are slowed significantly over the city of Memphis but then have the full length of the airport, open and unobstructed, as well as the undeveloped area south of there to recover their full speed. Aside from this area south of the airport, no part of the network is showing transmissions above normal and two areas in the southeast part have values 10% or more below normal. The entire network mean deviation was 3% below the overall average for the northerly wind direction.

In each of these figures (V-13 through V-16), there is a such a striking consistency in the mesoscale transmission deviation values from one station to the next, and in the pattern set up over the network, that it

---

*Notice the mean values of ψ_e for each station given in Table V-3 are less than 0.70 for only two mesonet stations (Nos. 10 and 19) but are less than 0.70 for four out of six LLWAS stations (N, SE, S, and W). A comparison of the mean obstruction angles (Table V-2) and the local topography (Figure II-9) for these sites shows that there could possibly be an LLWAS anemometer bearing problem. The mean value of ψ_e for the mesonet is 0.78, and for the LLWAS is 0.70, a difference of 11%. Roughly 6% of this discrepancy may be due to the use of a mesonet anemometer flow coefficient that was too high (see III.A.1.d.ii).

discourages any conclusion that these numbers are simply randomly distributed among the stations. Furthermore, the differences are distinct and sensible between the four figures, suggesting that the observed variations in azimuth are not random, either. Apart from any effects of the visible obstructions at these sites, which were removed in the microscale transmission factors, clearly significant effects of what is assumed to be the larger scale "obstruction horizon" are evident in the data. But what exactly are these scales?

Certainly, the largest contribution to ψ_e is from scales just beyond those visible, as evidenced by the large amplitude variations near and at the airport, typified by an 8 km length scale. Also, topographical variations on the 2-10 km scale and perhaps up to the 20 km scale appear to be important. It is probably fair to also conclude that the smaller the scale of influence, the greater the impact on the observed transmission at the sites. The city of Memphis (20-40 km scale) appears to have a fairly uniform effect of reducing transmission over the network by roughly 3%. The larger amplitude variations in Figure V-16 are attributable to smaller scale topography.

3. Conclusions

It appears, from the evidence presented in the preceding two sections, that the effects of different scale obstructions on winds at a particular site can be quantified. A strong, negative correlation was found between the observed transmission factors and the measured obstruction angles at every site except one. The functional relationship between them was modelled as a decaying exponential plus a constant. It was found that the first 8° of obstruction have the greatest blockage effects; the contributions of higher obstructions become proportionally less great. Even a 2° or 3° high isolated clump of trees can have a measurable, pronounced effect on the measured wind speeds from that direction. The ratio of the observed transmission, ψ, to the calculated microscale transmission, ψ_i, was taken to represent the transmission through obstructions on a scale larger-than-visible, the mesoscale. It was found that contributions from spatial scales from 2-40 km were represented and discernable, with the smaller scales having the greatest impact on the measured winds.

D. Time-Dependent Transmission Factors

The possibility that the observed transmission factors are time dependent at a given site is explored in this section. Since the observed obstructions, namely trees and vegetation, change size, density, and character with the changing seasons, it is plausible that the transmission factors might also change. Using the FLOWS mesonet and LLWAS data from mid-February through August 1985, variability on seasonal and monthly time scales can be investigated.

1. Seasonal Time Scales

Transmission factors for two seasons, spring and summer, were calculated in exactly the same way that the time-independent transmission factors

were calculated in section B. of this chapter. Spring was defined as
February through April and summer as May through August, after testing each
with and without the month of May. Probably the best way of characterizing
the difference between the spring and summer transmission factors and the
"total" ones is with the correlation coefficient. Table V-4 shows that
while the correlations between each of the stations' seasonal transmission
factors and the total were quite high, with mean values for spring and
summer of .86 and .90, respectively, the correlation between spring and
summer transmission factors themselves were considerably lower in every
case (mean value 0.65). However, the correlation between them is far too
high to consider them independent (except perhaps at station No. 28). Thus
while a very slight bit of accuracy might be gained by using seasonal
transmission factors, this procedure is definitely not necessary.

2. Monthly Time Scales

Certainly, if one chooses not to add the complication of seasonal
transmission factors, then one would surely not want to consider an even
finer time scale such as monthly. But the correlations between the indivi-
dual months and the total transmission factors can help answer the prac-
tical question of how much data should be used to accurately estimate the
total transmission factors. From Table V-4 it can be seen that 2.5-4.0
months is probably enough, but is one month enough? Table V-5 lists the
correlations between each month's transmission factors and the total 6.5
month transmission factors. The data for the last 15 days in February was
combined with that for March to make one "month". In general, the correla-
tions are quite similar from month to month, suggesting that one month's
data would allow an accurate estimate of the transmission factors. Sensor
problems could negate this conclusion; see, for example, data for station
No. 3 in July and August (Table V-5).

3. Conclusions

The correlation data presented in the two preceding sections suggest
that wind data from a single month can be used to accurately estimate the
transmission factors as a function of azimuth, barring any sensor malfunc-
tions, at a given site although the more data used in making the estimates,
the better. Different transmission factors for each month or even each
season are unnecessary.

E. Recommended Wind Correction Procedure

In recommending a wind correction procedure, the final use of the data
must be considered. The variations in the wind speed measurements across
the weather station network are quite real; they are partly due to surface
irregularities and obstructions and partly due to actual patterns of
divergence and vorticity in the unobstructed flow. (Of course, part of the
variation could always be due to individual sensor characteristics.) Any
time one wishes to analyze the unobstructed flow, as is the case when the

Correlations between
Transmission Factors:

Station	Spring and Total	Summer and Total	Spring and Summer
1	.88	.96	.78
2	.87	.94	.72
3	.64	.79	.22
4	.98	.97	.92
5	.95	.98	.90
6	.76	.88	.43
7	.94	.92	.85
8	.92	.92	.74
9	.84	.94	.68
10	.97	.87	.80
11	.82	.93	.63
12	.76	.93	.64
13	.78	.93	.61
14	.93	.91	.77
15	.92	.90	.73
16	.84	.93	.65
17	.96	.94	.86
18	.94	.94	.82
19	.93	.91	.77
20	.82	.92	.61
21	.90	.90	.71
22	.87	.94	.69
23	.95	.98	.91
24	.92	.97	.85
25	.94	.98	.89
26	.85	.80	.43
27	.86	.92	.62
28	.64	.57	-.03
29	.71	.74	.31
30	.88	.84	.55
CF	.58	.84	.19
N	.90	.90	.70
E	.81	.93	.61
SE	.92	.92	.78
S	.86	.87	.56
W	.83	.93	.64
Mean	.86	.90	.65

Table V-4. The correlation between the observed transmission factors
for "Spring" (15 February - 30 April 1985) and "Total" (15 February -
31 August 1985), "Summer" (1 May - 31 August 1985 and Total, and
Spring and Summer are given for each of the mesonet and LLWAS stations.

Station	Feb-Mar	April	May	June	July	August
1	.79	.87	.93	.95	.92	.75
2	.57	.89	.82	.85	.74	.84
3	.54	.27	.62	.35	-.13	-.19
4	.93	.96	.90	.93	.93	.92
5	.86	.94	.86	.92	.92	.90
6	.50	.72	.45	.80	.59	.74
7	.86	.87	.86	.89	.90	.78
8	.84	.87	.67	.78	.70	.73
9	.71	.85	.88	.65	.88	.81
10	.87	.80	.84	.83	.80	.74
11	.77	.59	.91	.91	.88	.85
12	.64	.41	.80	.77	.71	.88
13	.61	.72	.82	.80	.78	.75
14	.76	.84	.77	.89	.80	.72
15	.74	.82	.82	.87	.85	.71
16	.59	.83	.87	.75	.77	.83
17	.90	.88	.87	.79	.75	.75
18	.86	.84	.87	.85	.83	.89
19	.90	.84	.80	.74	.70	.84
20	.57	.66	.78	.78	.52	.71
21	.84	.90	.80	.74	.62	.68
22	.31	.78	.78	.89	.65	.72
23	.88	.92	.97	.95	.92	.91
24	.91	.87	.93	.95	.94	.96
25	.87	.93	.94	.97	.94	.96
26	.74	.73	.70	.77	.54	.50
27	.75	.81	.87	.88	.81	.82
28	.63	.42	.59	.40	.13	.15
29	.70	.28	.63	.54	.00	.25
30	.76	.64	.68	.68	.68	.75
CF	.26	.72	.64	.60	.64	.76
N	.74	.88	.79	.86	.76	.93
E	.68	.84	.75	.88	.72	.89
SE	.77	.74	.86	.86	.77	.85
S	.90	.51	.76	.74	.31	.79
W	.79	.78	.90	.84	.79	.89
Mean	.73	.76	.80	.80	.70	.74

Table V-5. Correlation between monthly (15 February - 31 March was considered one month) and total (15 February - 31 August 1985) transmission factors.

measurements are to be compared with Doppler radar data, wind corrections should be applied. Some studies use a correction based on various approximations to the vertical structure of the wind in the lowest turbulent layer to estimate the unobstructed wind (or the wind at 50 m AGL), and some even tailor the profile to the different types of surroundings through the use of a surface roughness parameter. Clearly, though, based on the evidence presented here, the use of a correction scheme that is azimuth-dependent before correcting for boundary layer effects is much more accurate than a scheme that simply increases every measurement at all times by the same percentage predicted by an appropriate logarithmic or power law.

It has been shown here that it is possible to derive scale dependent, azimuth dependent transmission factors, the reciprocals of which can be used as wind speed correction factors. Is it more appropriate to correct wind patterns with spatial variations on small scales (<4 km) for obstruction effects on only that scale, or should all winds be corrected for both visible microscale and larger mesoscale obstructions? The answer to this question may actually be dictated by practical considerations.

Many of the microbursts detected with the automatic weather station network (see Chapter VIII) began as divergent outflows 2-3 km in diameter, and expanded in the course of 15 minutes or so into what might be called "ring" gust fronts with diameters of 20 km or greater. Surely time dependent correction factors corresponding to outflow scale changes could only be specified after detailed analysis of a particular event, and even then their use would definitely be questionable. Part of the intent of deriving a time-independent correction scheme is to avoid detailed study of each wind pattern before the appropriate corrections are made. It is therefore recommended that the winds be corrected according to the scale of phenomena primarily being studied.

Since the FLOWS project is concerned with identifying and understanding microbursts, with horizontal scales by definition less than 4 km, it is recommended that visible correction factors only be used. If gust fronts or larger scale wind shear phenomena were of primary interest, then the measured winds should be corrected for both visible and larger scale obstructions. In either case, the corrected winds should be used for analysis and comparison with Doppler radar data.

Another possibility, not explored in this study, is that the wind correction factors are a nonlinear function of the measured wind speed. This is quite probable considering the complexity of wake flow dynamics. Intuitively, it must be wrong to correct measured wind speeds of 25-30 m/s by the same factor (in some cases more than a factor of 2) used to correct wind speeds of 5-10 m/s. This will be an important consideration in future work.

Another question that may arise is whether it is better to use the reciprocals of the observed transmission factors at each site to correct the measured wind speed, or to use the values of ψ_i, the microscale

factors computed from Eq. (11), with or without the 180° smoothed mesoscale transmission factors, ψ_e, to correct the measured wind speed. The latter procedure is much less susceptible to experimental noise and high-frequency variations in azimuth, and so is recommended.

This suggests that it may be possible to derive wind speed correction factors as a function of azimuth at a new site simply by measuring the elevation angles of the visible obstructions there. Future work should include comparisons of the functional relationship between ψ and θ for new networks with that given here in Eqs. (8) and (11). If strong similarities exist, perhaps this functional relationship can be generalized.

It has been shown that only one set of correction factors or at most seasonally varying factors should be used. The amount of data used in the derivation can be dictated by the computer processing resources available, and how soon after the data are collected that they are to be analyzed.

The final recommended equation for $\psi(s,d)$ to be used in Eq. (2) for microburst studies is:

$$\psi(s,d) = \psi_i(\theta(s,d)_{16°}) \tag{19}$$

while the final recommended equation for gust front studies is:

$$\psi(s,d) = \psi_e(s,d)_{180°} \, \psi_i(\theta(s,d)_{16°}), \tag{20}$$

where ψ_i is given by Eq. (11) and ψ_e is given by Eq. (18). Then, the formula for the unobstructed wind at any station at any time is given by:

$$U(s,time) = \frac{V(s,time) \ (measured)}{\psi(s,d)} \tag{21}$$

VI. DATA PROCESSING AND ANALYSIS SYSTEM

A. Introduction

A software package to analyze and process mesonet and LLWAS data has been implemented, as shown in Figure VI-1. The ultimate purpose of this software is to allow detection and analysis of microbursts and gust fronts. However, before wind shear events can be identified, the data have to undergo several conversion and clean-up processes.

First, the data are converted to a common format to facilitate measurements from a variety of sources (e.g., the mesonet described earlier and the FAA LLWAS). Then erroneous data caused by malfunctioning sensors and wind speed "chatter" (see III.A.1.b.iii) are eliminated. The obstruction correction factors for the winds are computed and the wind speeds can then be corrected for large and small scale obstructions, if desired. These edited and calibrated data are used for the microburst identification.

The software package also contains several plotting programs which allow further analysis of the detected wind shear events, and various utility programs to examine the data in tabular and graphic form. Each part of the mesonet data processing and analysis software system is described in more detail in the following sections of this chapter.

B. Common Data Format

1. Rationale

The raw mesonet and LLWAS data tapes are translated into our Common Instrument Data Format (CIDF) which was developed to serve as a common representation for low volume time-series data. This enables data received from multiple sources to be analyzed using the same software once individual translators have been written. To date, we have utilized data from the FLOWS mesonet and the LLWAS system at the Memphis Airport; we anticipate also processing data from the NCAR mesonet stations which will be deployed near the FLOWS network in Huntsville, AL in 1986.

2. Translators

a. Mesonet

The output from the translator which converts mesonet data collected by the satellite ground station to CIDF format is a file of data for one day. The sensor data included in this file are one minute averages of the surface temperature, relative humidity, barometric pressure, wind speed, wind direction and surface precipitation, as well as the peak (5s sample) wind speed each minute, for 30 mesonet stations. Missing data are represented on the file by a missing data code.

DATA ANALYSIS OVERVIEW
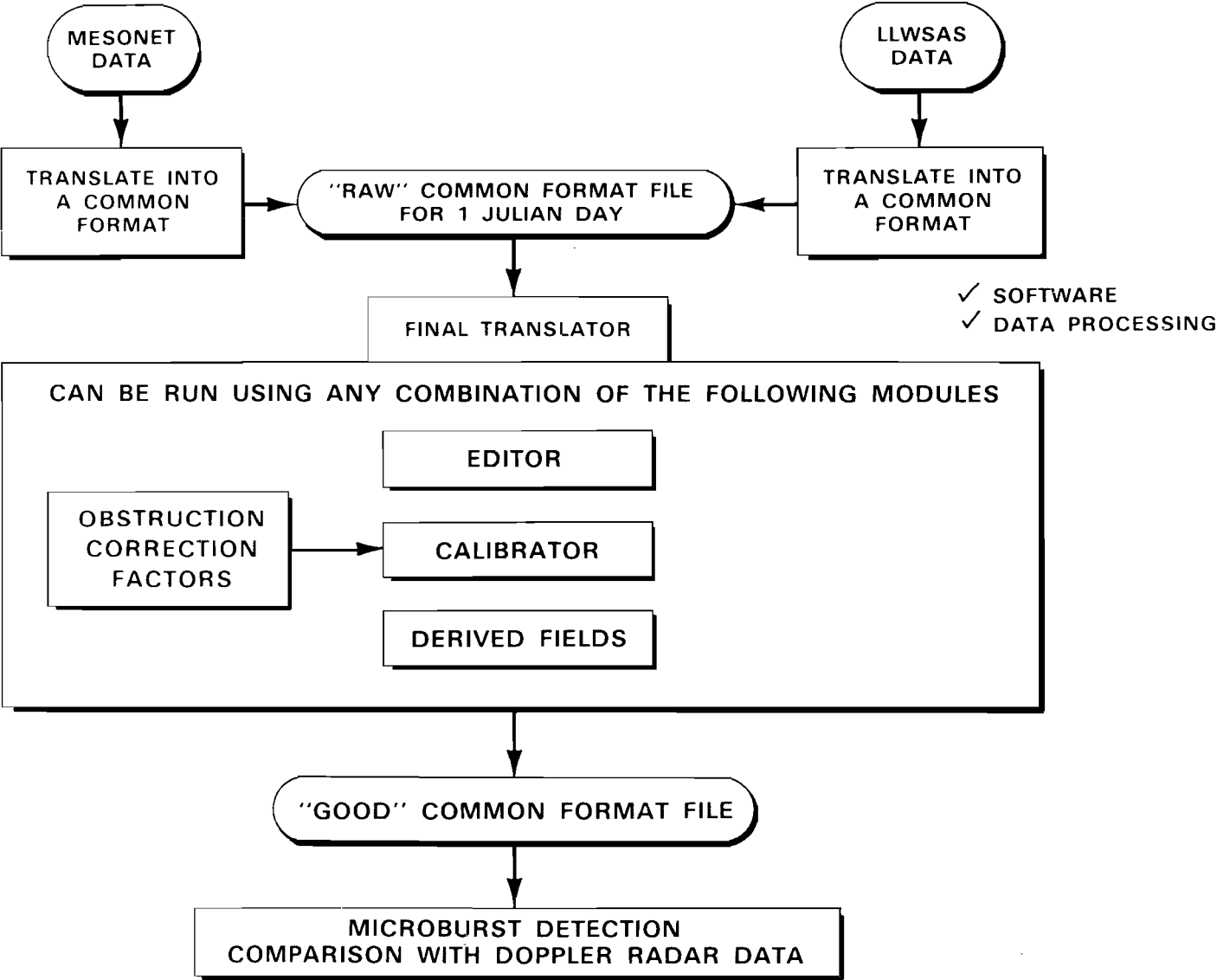
Figure VI-1. Mesonet and LLWAS data analysis overview.

b. LLWAS

The output from the LLWAS translator is a file of data for one day which contains average wind speed, peak wind speed and wind direction data from six stations. The data on the original LLWAS tapes consist of 30-second averaged east and north wind components every 8-9 seconds. In order to make this data compatible with the mesonet data, the one-minute averages of wind speed and direction are calculated.

3. Definition of a Network

A network is a collection of weather stations with specified station codes. The concept of a network was developed in order to segregate data into identifiable units. The 30 FLOWS mesonet stations comprise a network as do the 6 Memphis LLWAS stations. When the testbed moves to Huntsville, a third network, the NCAR weather stations, could be added and additional station codes assigned.

A read package has been developed in which a day's data for several networks can be read and stored in memory. All the analysis programs can then access the data from memory instead of from disk, thus saving a considerable amount of run time once the data are read in initially. As a trade-off for run time, enough memory to accommodate 1440 minutes of data for 36 stations each having 10 sensors must be available.

However, if a direct access disk storage format were developed, equally fast run time data access could be achieved without large memory requirements and without an initial delay to read in the entire dataset. The development of this format and the corresponding read and write packages is definitely recommended.

C. Data "Quick-Look" Utilities

Several utility programs were written as a part of the data analysis effort to enable the user to examine the data in both graphic and tabular formats. With the use of these utilities, several sensor problems have been identified and resolved.

1. Tabular Inventory

An inventory program was developed to determine the overall success of the data collection effort. It provides an index of the total available data for each day as characterized by:

      a. a table of percent missing data for each station,
      b. a table of percent missing data for each sensor,
      c. the total average percent missing data for the day, and
      d. a list of times each station failed to report.

This inventory program is routinely used to summarize both raw and "edited" data availability. The results of each day's inventory are kept in a single disk file, so that the data collection performance for an entire season can be evaluated (see Chapter VII).

2. 24-hour Time Series Plots

Once the raw mesonet and/or LLWAS data have been translated into CIDF, 24-hour time series plots for each sensor at each station are produced. This capability allows for the early detection of problems with sensors or stations before the data are used for analysis and before too many data are collected with faulty equipment. Examples of these plots are presented in VII.B.3.

3. List

A command-driven data listing utility was written to list any combination of mesonet or LLWAS variables vs. time for a given station. This utility is an excellent "quick look" capability, providing legible hard copy of the actual data values. Examination of this numerical output revealed the "bad" data problem described in Section D below.

D. Data Editing

Upon examination of the initial raw mesonet data, it was found that several of the sensors were malfunctioning and were reporting erroneous data. If these data were used in, for example, an automatic microburst detection algorithm, the results would certainly be contaminated. Thus an editing capability was designed.

1. Software Structure

The "editor" is a modular program which allows various algorithms for each of the sensors to be tested in order to eliminate "bad" data. A command-driven interface allows the user to specify the sensors, the platforms and the time period over which "bad" data are to be sought. The output is a file of times at which the specified sensors at the specified platforms were reporting erroneous data, according to the user-specified algorithm. This file is later used as input into a program which produces a data base of "bad" data. This process is shown in Figure VI-2 and the comparison of raw and edited wind speed data is shown in Figure VI-3.

2. Algorithms

a. Peak Wind Speed

The peak and average wind speed and wind direction data are flagged as "bad" in the following cases:

EDITOR

EDITS 'BAD' DATA FOR

TEMPERATURE
HUMIDITY
PRESSURE
WINDS
PRECIPITATION

COMMON FORMAT FILE

↓

EDITOR

↓

FILE OF BAD DATA

↓

DATA BASE PROGRAM

↓

DATA BASE OF 'BAD' DATA
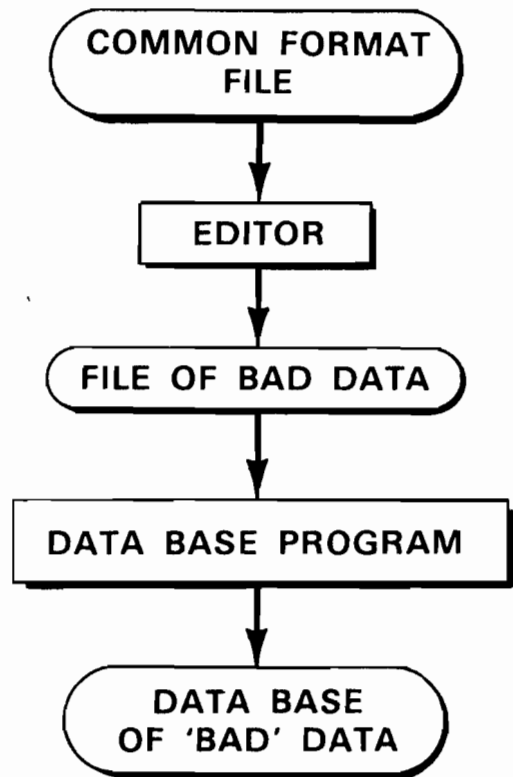
Figure VI-2.   Block diagram of mesonet data editing capability.

STATION 16 DAY 291 10/17/1984

RAW DATA

TIME (UT)	DIRECTION (deg)	AVERAGE SPEED (m/s)	PEAK SPEED (m/s)
00:00	141.11	0.46	0 46
00:01	152.77	1.21	4.27
00:02	153.58	0.66	2.79
00:03	150.45	0.80	3.19
00:04	161.65	1 14	3.81
00:05	146.55	0.52	1.09
00:06	143.82	0.46	0.46
00:07	140.03	0.46	0.46
00:08	129.28	0.46	0.46
00:09	136.05	0.46	0.46
00:10	153.02	0.69	2.65
00:11	155.23	1.19	3.98
00:12	156.46	1.39	2.87
00:13	163.49	0.78	2.51
00:14	159.91	1.46	4.55
00:15	168.75	0.85	2.48
00:16	168.75	0.85	2.48
00:17	159.19	2.08	31.80
00:18	200.60	0.46	0.46
00:19	196.09	0.71	1.71
00:20	211.12	0.69	2.33
00:21	239.97	1.31	4.18
00:22	246.84	7.61	12.00
00:23	256.13	8.46	15.26
00:24	249.43	5.21	9.38
00:25	242.12	6.81	9.68

BAD DATA

Year	Day	Time	Station	Flag
1984	291	00:00	116	AWS
				PWS
1984	291	00:01	116	PWS
1984	291	00:02	116	PWS
1984	291	00:03	116	PWS
1984	291	00:04	116	PWS
1984	291	00:05	116	PWS
1984	291	00:06	116	AWS
				PWS
1984	291	00:07	116	AWS
				PWS
1984	291	00:08	116	AWS
				PWS
1984	291	00:09	116	AWS
				PWS
1984	291	00:10	116	PWS
1984	291	00:11	116	PWS
1984	291	00:12	116	PWS
1984	291	00:13	116	PWS
1984	291	00:14	116	PWS
1984	291	00:15	116	PWS
1984	291	00:16	116	PWS
1984	291	00:17	116	AWS
				PWS
1984	291	00:18	116	AWS
				PWS
1984	291	00:19	116	PWS
1984	291	00:20	116	PWS

EDITED DATA

DIRECTION (deg)	AVERAGE SPEED (m s)	PEAK SPEED (m s)
141.11	- - - - -	- - - - -
152.77	1.21	- - - - -
153.58	0 66	- - - - -
150.45	0 80	- - - - -
161.65	1 14	- - - - -
146.55	0 52	- - - - -
143.82	- - - - -	- - - - -
140 03	- - - - -	- - - - -
129.28	- - - - -	- - - - -
136.05	- - - - -	- - - - -
153.02	0.69	- - - - -
155.23	1 18	- - - - -
156.46	1 39	- - - - -
163.49	0 78	- - - - -
159.91	1 46	- - - - -
168.75	0 85	- - - - -
168.75	0 85	- - - - -
159.19	- - - - -	- - - - -
200.60	- - - - -	- - - - -
196.09	0.71	- - - - -
211.12	0.69	- - - - -
239.97	1.31	4.18
246.84	7 61	12.00
256.12	8.46	15 26
249.43	5 21	9 38
242.12	6 81	9 68

76652-1

Figure VI-3. Comparison of raw (left) and edited wind speed data (right). Between them are the "bad data" time intervals identified by the editor. At time 00:01, the editor flagged the peak wind speed of 4.27 m/s as "bad" because the average wind speed of 1.21 m/s is small ($\leq$ 3 m/s) and the peak wind speed is greater than twice the average wind speed (See VI.D.2.a.vii).

i.   if either of the wind speeds are reported as
      missing data,

ii.   if the difference between the peak and average wind
      speed is greater than 15 m/s,

iii. if the average wind speed is greater than the peak
      wind speed,

iv.   if the average wind speed is equal to the smallest
      possible average wind speed sensor reading, and

v.   if either wind speed is greater than 60 m/s.

The erroneous data rejected by these tests were primarily caused by sensor malfunctions and the peak wind speed "chatter" problem. Since these tests did not completely eliminate the "chatter", further editing was necessary.

In this additional editing, an average of 10 points about each average wind speed is taken. The data are additionally flagged as "bad" in the following case:

vi.   if this average is small ($\leq$3 m/s) and the difference
      between the peak wind speed and the average wind
      speed is greater than 5 m/s.

Just the peak wind speed is flagged "bad" in the following cases:

vii. if this average is small ($\leq$3 m/s) and peak wind
      speed is greater than twice the average wind
      speed (see Figure VI-3),

viii. if this average is small ($\leq$3 m/s) and the difference
      between the peak wind speed and the average wind
      speed is between 4 and 5 m/s, and

ix.   if the average wind speed is less than 1 m/s
      and the difference between the peak wind speed and
      the average wind speed is greater than 1 m/s.

b. Temperature

The temperature data greater than 48°C are flagged as "bad".

c. Relative Humidity

Relative humidity values that rose more than 15% or fell more than 12%, or rose between 12% and 15% while the temperature dropped more than .45°C from one minute to the next are flagged as "bad".

d. <u>Barometric Pressure</u>

Barometric pressure data values greater than 1070 mb or less then 930 mb are flagged as "bad". Also, pressure values that were "erratic", swinging up and down by more than .8 mb more than twice in ten minutes are rejected.

e. <u>Precipitation</u>

Rain gage measurements of less than 0 mm or greater than 300 mm are flagged as "bad". Also erratic values, more than 2 rises of 2 mm and 2 falls of 1.5 mm in a ten minute interval are rejected. If the rain data dipped slightly (1.0 mm) in low winds (average wind speed <10 m/s), or dipped more then 1.5 mm or rose more then 7 mm in one minute, then these data, too, are rejected.

E. <u>Data Calibration</u>

Several of the measured variables, particularly the pressure, need to be calibrated before they are used in detailed analyses of low-altitude wind shear events. Also, wind speeds can be corrected to compensate for large and small scale obstructions (see Chapter V). Thus software was developed to facilitate sensor calibration as illustrated in Figure VI-4.

1. <u>Software Structure</u>

The calibration database for mesonet and LLWAS sensors was designed to be a file of multiplicative and additive constants ordered according to the CIDF platform (station) number, the sensor code, and the calibration time. Each variable was allowed a multiplicative and an additive constant to be applied to the sensor value as follows:

Multiplicative constant * Sensor value + Additive constant

Additionally, average wind speed and peak wind speed were allowed 360 calibration constant pairs, one for each degree of wind direction. In this case, the pair of calibration constants which applies to a particular wind speed measurement is determined by the wind direction. If a more sophisticated wind correction scheme is developed where the applicable calibration constants are a function of both the wind direction and wind speed, then minor modifications to this software structure would be necessary.

In the database, a pair of calibration constants is tagged with its CIDF platform number, its sensor number and the calibration time specified by minutes, Universal day, and year. Calibration constants are valid from their calibration date to the date at which the sensor is recalibrated (if ever).

CALIBRATOR

FOR EACH PLATFORM:

- ## LINEAR CORRECTION

  CALIBRATED = A (Time, Sensor) $\times$ RAW + B (Time, Sensor)
  VALUE   VALUE

  ### FOR WINDS:

  CALIBRATED = A (Time, Sensor, Azimuth) $\times$ RAW + B (Time, Sensor, Azimuth)
  VALUE   VALUE

- ## DATA BASE MANAGER

  SORTS CALIBRATION CONSTANTS ACCORDING TO

  PLATFORM
  SENSOR
  TIME
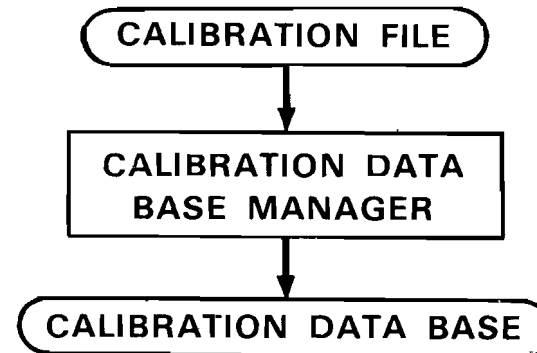
Figure VI-4. Linear equations used in calibrating the data, and the creation of the calibration database are shown.

2. Specification of Calibration Constants

The user specifies the calibration constants for mesonet and LLWAS sensors with a set of commands which are entered into a file via the editor. As the sensors are recalibrated command lines are appended to this file.

If only the multiplicative constant is specified, the additive constant defaults to 0. If only the additive constant is specified, the multiplicative constant defaults to 1. If a sensor for a particular station is declared "bad", it will appear as "missing data" on the CIDF file until it is recalibrated, i.e., if it becomes "good", a multiplicative value of 1 must be inserted in the file even if it does not have to be calibrated.

This file of commands is read by the calibration constant "compiler" and the calibration database is created. This database is recreated each time sensors are recalibrated.

F. Final Translation of Data

A "final" translator was designed in which "raw" CIDF data can be edited and calibrated and derived products can be calculated. The output from this final translator is a CIDF file of data that can be used by all of the data analysis utilities.

1. Access to "Bad" Data Database

The "bad" data database is read in by the final translator, and for each platform, sensor, and time combination, a bit is set in the database if the data is "bad". The final translator converts "bad" data into "missing" data on the final CIDF file.

2. Access Routines for Calibration Constants

A subroutine package has been written to enable the user to access calibration constants in the mesonet and LLWAS database. The subroutine package must first be initialized; the calibration constants for a particular platform and sensor at a specified time can then be accessed by calling a routine which returns the most recent applicable constants (if any).

These access routines were designed with an internal cache to prevent unnecessary disk read operations while converting large amounts of data. The database is read once and the constants are stored in the cache for each sensor on each station present. Information about the time that these constants become invalid (when the sensor is recalibrated) is also stored internally in a look-up table format.

Each time a request to access calibration constants is made, a table look-up is performed to determine whether the constants are in the cache and whether they are valid. If they are not in the cache, the disk is read and constants are stored in the cache. If constants are in the cache but are invalid (the given time is past the valid time), the data base is read again and new values are either added to the cache or are written over the present values in the cache.

The final translator accesses these constants, computes the calibrated data, and outputs the data onto the final CIDF file.

3. Derived Variables

The derived variables are computed during the final translation after the data have been edited and/or calibrated. These, as well as the original variables are output onto the final CIDF file.

a. Dew Point

The dew point, or the temperature to which humid air has to be cooled to achieve condensation, characterizes the absolute humidity in the air. It is derived from the temperature and the relative humidity, as follows:

$$\text{DEW POINT (°C)} = \frac{\text{TEMP (°K)}}{(-4.25 \times 10^{-4} \times \text{LOG}_{10}(\text{Relative Humidity}/100) \times \text{TEMP(°K)} + 1)} - 273.15$$

In the above equation, the temperature has been calibrated and the relative humidity value has been both mathematically compensated for any incorrect calibration, as discussed in section III.A.3.d, and calibrated. Any values of relative humidity greater than 100% were first set equal to 100%. These corrected relative humidity data are output to the final CIDF file.

b. Rain Rate

The rainfall data value recorded each minute represents the total amount of precipitation in the rain gage bucket, but it is often the rain rate that is of primary interest. The rain rate is estimated as the difference in measured precipitation between the current and the previous minute.

c. Smoothed Pressure

The barometric pressure can be smoothed by using a Hamming weighted function:

$$w(n) = 0.54 - 0.46 \cos\left(\frac{2\pi n}{N-1}\right) \qquad 0 \le n \le N-1$$

where N is a selectable time interval in minutes. A 15 minute interval is typically used and the raw pressure is replaced by the smoothed pressure on the final CIDF output file.

d. Potential Temperature

The potential temperature of air at a given temperature and pressure is the temperature that air would have if it were brought dry adiabatically to a pressure of 1000 mb:

$$\theta(°K) = TEMP\ (°K) \left[\frac{1000\ mb}{PRESS(mb)}\right]^{R/C_p}$$

where: θ = potential temperature
R = Ideal Gas Constant for air (287 Joules/Kg-K)
C_p = specific heat of air at constant pressure (1005 Joules/Kg-K).

e. Equivalent Potential Temperature

The equivalent potential temperature is the temperature air would have if all its moisture was condensed and the heat of condensation retained, and then brought dry-abiabatically to 1000 mb:

$$\theta_e\ (°K) = \theta(°K)\ exp\left[\frac{L_v\ r_s}{C_p\ T_c}\right]$$

where θ_e = equivalent potential temperature
θ = potential temperature (defined above)
L_v = latent heat of vaporization of water (2.5×10^6 J/kg, depends on temperature)
r_s = saturated water vapor mixing ratio, or the mass of water vapor per unit mass of dry air when the air is saturated with respect to water
C_p = specific heat of air at constant pressure (1005 J/kg-K, also depends on temperature)
T_c = temperature (°K) at which condensation occurs as the sub-saturated air is lifted dry-adiabatically.

G. Data Analysis Utilities

1. Single Station Microburst Detection Algorithm

The algorithm used was proposed and used by Fujita for microburst detection based on mesonet data in the NIMROD and JAWS Projects (see Figure VI-5). The steps are as follows:

    i. Search the peak wind measurements for a value greater than 15 m/s. Label this point W(C), where C is for center.

FUJITA'S MICROBURST DETECTION ALGORITHM
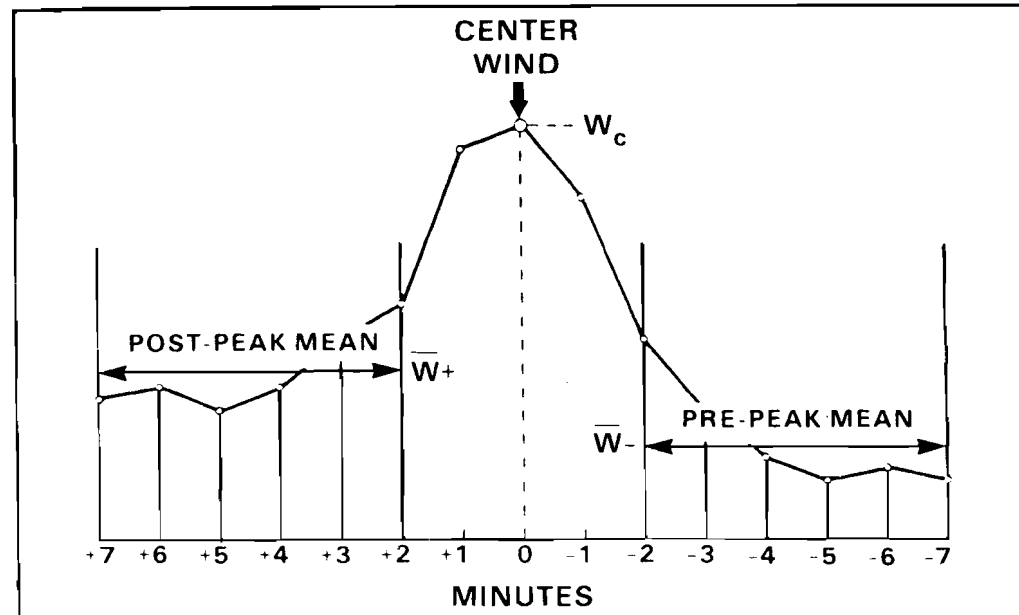
- INITIAL SEARCH BASED ON 1 min. PEAK WINDS
- MUST SATISFY THE FOLLOWING CONDITIONS

  CONDITION 1, $W_c \geqslant$ 10 m/s = 19.4 kts

  CONDITION 2, $W_c \geqslant \overline{W}- +$ 5 m/s

  CONDITION 3, $W_c \geqslant \overline{W}+ +5$ m/s

  CONDITION 4, $W_c \geqslant$ 1.55 $\overline{W}-$

  CONDITION 5, $W_c \geqslant$ 1.55 $\overline{W}+$

  CONDITION 6, $\overline{W}+ \leqslant$ 1.5 $\overline{W}-$

- FINAL VERIFICATION BASED ON ALL VARIABLES AND EXPERT JUDGEMENT

Figure VI-5. Single station microburst detection algorithm by Fujita (1984).

ii. Once such a point is found, compute the pre- and post-peak means. If the center point is the origin, the post-peak mean is the average of minutes 2-7 (six values). Note that the values one minute prior to and after the peak are not used in computing the means.

iii. Then, if the pre- and post-peak average winds are both at least 5 m/s less and at least 55 percent less than the peak, and additionally the post-peak winds are within 50 percent of the pre-peak winds, the point is considered a potential microburst. The time of each peak is noted in an output file during the algorithm run.

This method of microburst detection had a false alarm rate of 95% but a probability of detection close to 100% on the 1984 data, although occasionally microbursts were detected as gust fronts and vice versa. The triple station algorithm described below is currently under investigation.

2. Triple Station Microburst Detection Algorithm

A triple station algorithm for microburst detection suggested by Wilson and Flueck (1985) is based on a triangulation of the network geometry and an estimation of the mass flux across the boundary of each triangle in the network. The divergence can be computed by a vector cross-product formula which takes into account the spatial relationship of the winds at the three stations in a triangle. In this algorithm it is the triangles, rather than the stations, that are designated as having divergent winds. This method is in the process of being investigated to determine its detection and false alarm probabilities.

3. Single Station Gust Front Detection Algorithm

The gust front algorithm is nearly identical to the single station microburst algorithm but allows those winds after the initial jump to remain high. Thus the gust front center point has the pre-peak average wind down by at least 5 m/s and 55 percent, but requires that the post-peak winds (average) be at least 50 percent greater than the pre-peak winds.

H. Data Display Utilities

1. Synoptic Plots

a. Mesonet Only

The synoptic plots are generated in order to show the analyst what the surface wind field looks like at a given point in time over the entire mesonet (Figure VI-6). These plots reveal the spatial relationship between the same variable recorded at each of the stations and help the analyst in determining the existence of microbursts and gust fronts.
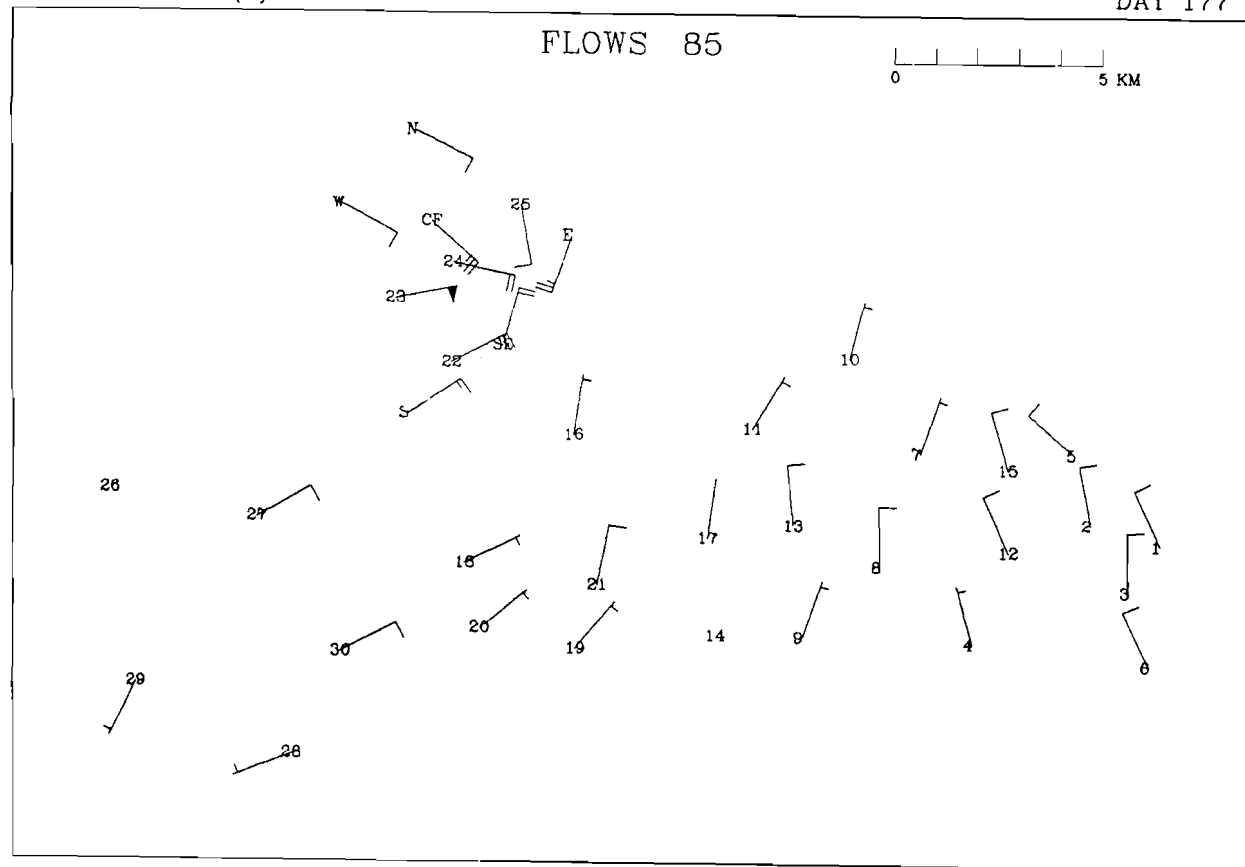
Figure VI-6. Synoptic plot of the winds over the entire FLOWS mesonet.

b. Mesonet and Radar Combined

This utility generates plots such as the one shown in Figure VI-7.
This is simply the mesonet synoptic plot with radar data overlayed as a set
of contours. These contours can represent reflectivity, velocity, or
spectrum width and can be drawn at any user specified interval.

2. Time Series Plots

a. 21-minute

These plots, illustrated in Figure VI-8, show a trace of the tem-
perature, equivalent potential temperature, dew point temperature,
pressure, peak wind, and rainfall rate for a 21-minute interval centered
about the time a microburst had been detected at a specified mesonet or
LLWAS station (LLWAS only records wind speed and direction). These plots,
along with the mesonet synoptic plots, and/or mesonet and radar plots, pro-
vide the information necessary for an analyst to determine the validity of
a suspected microburst or gust front event.

b. 24-hour

These plots, which were described previously in section VI.C.2 as a
quick-look inventory type of utility, can also be effectively used to show
the various meteorological traces over an expanded time interval.
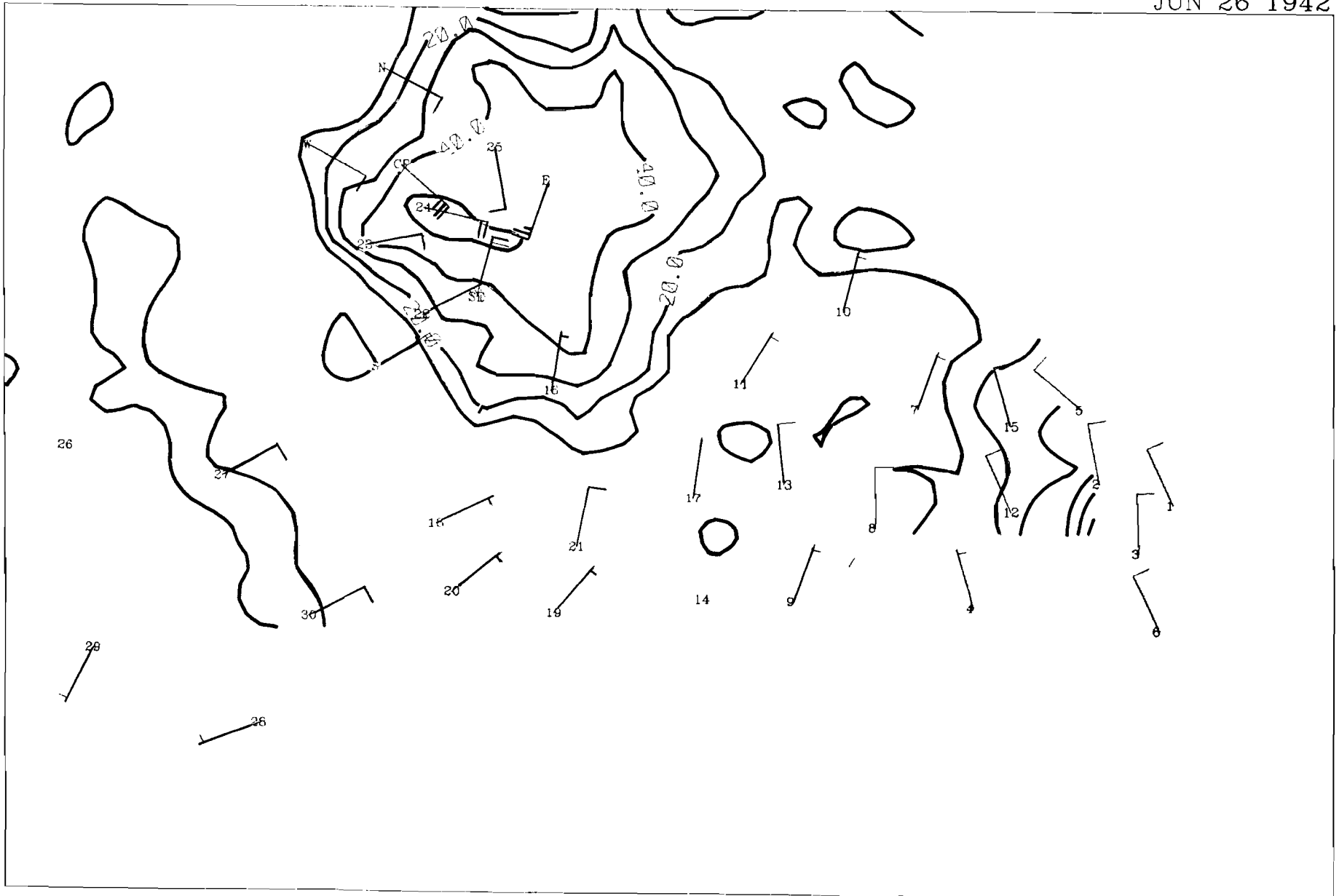
Figure VI-7. Synoptic plots of winds over FLOWS mesonet overlayed with
FL-2 radar reflectivity contours.
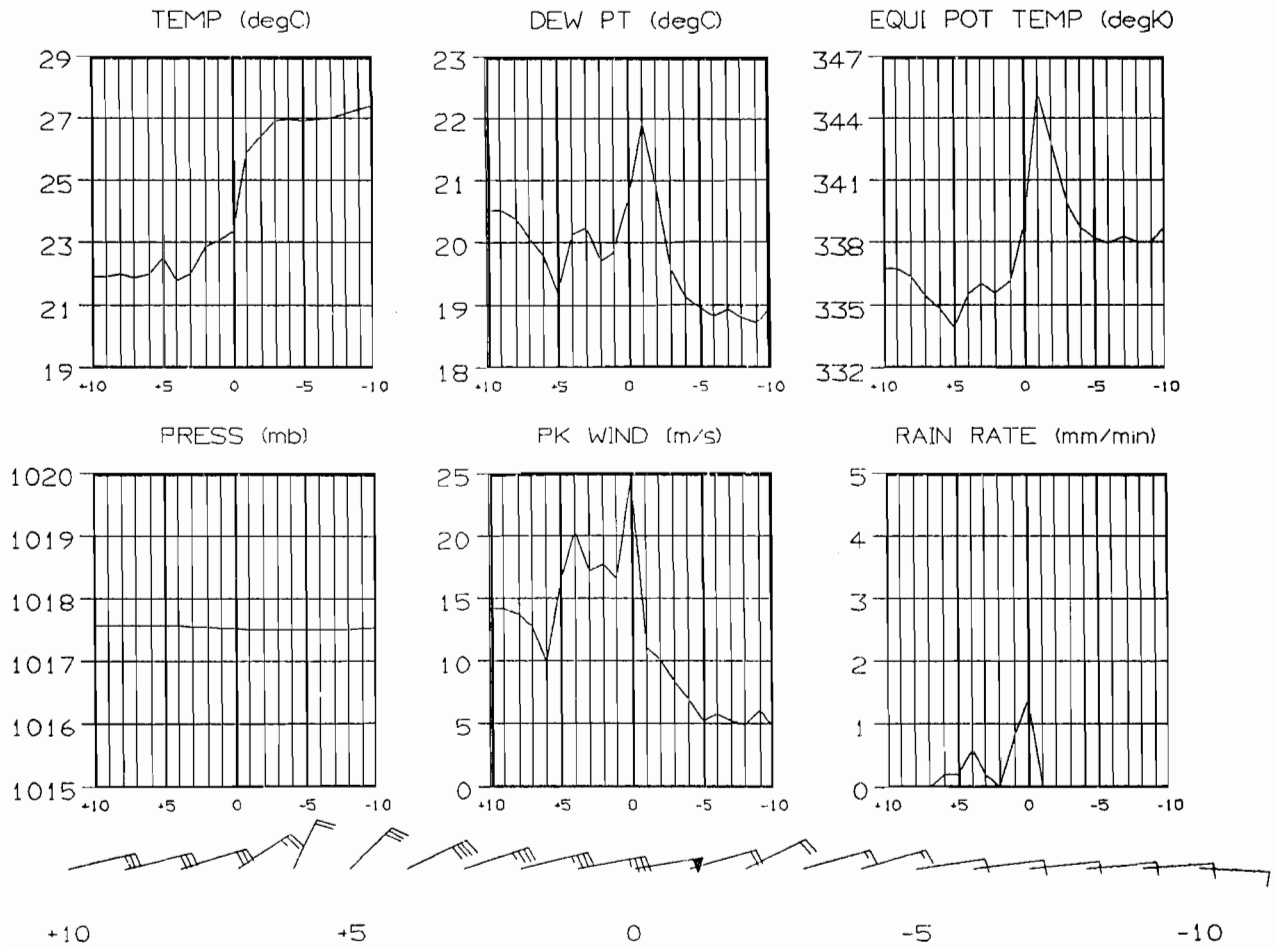
Figure VI-8. 21-minute time series plot of temperature, dew point temperature, pressure, peak wind, and rain rate for station No. 23.

VII. PERFORMANCE EVALUATION

The performance of the automatic weather station network is evaluated in terms of its operational reliability and its overall data quality. An entire day's data collected from each station in 1984 are used to illustrate the general characteristics and problems with the data.

A. Operational Reliability

The evaluation of the operational reliability of the weather station network takes into consideration the performance of the individual stations' transmission systems, the GOES satellite system, the commercial down-link service, and our field repair staff (one person only, whenever necessary). These various factors are not analyzed separately in the following section but in some cases they can be isolated. For example, when no data were recorded from any of the stations, the down-link service was not functioning; the satellite itself never failed. Also, site repair is discussed separately in section 2., below.

1. Missed Transmissions

The missed transmissions are evaluated by assuming that data would be available for every minute of every day from each of 30 stations in the network if no transmissions were missed. Seven meteorological variables are assumed to be present each minute including two for the wind speed (peak and average).

If, for example, the barometer was the only sensor not working at a particular station, then 14.3% (1/7) of the data for that station would be missing. The station percentages calculated in this way are used to characterize the overall percentage of data missing for the network.

Figure VII-1 shows the total average percentage of data missing for the network (all sensors) as a function of day of the year for 1984. Two curves are shown: the lower curve represents the percentage of raw data missing and is relevant to the evaluation of missed transmissions. The spike of 100% raw data missing near day number 240 occurred when the ground station receiving the data went down for maintenance. (The weather was clear and calm in Memphis so no wind shear data were lost.) The upper curve represents the percentage of data missing after the final editing and calibration steps have been performed. The difference between these two curves reflects the overall quality of data recorded and is discussed in detail in section B. of this chapter.

For the entire 1984 data collection season, an average of only 2.1% of the data were not recorded. These figures surpass the goal of at least 95% average data retrieval set in 1983. Examination of a similar data summary for the FAA's operational Low Level Wind Shear Alert System (LLWAS) at the Memphis International Airport helps to put the FLOWS mesonet record in perspective. As shown in Figure VII-2, the 6-station anemometer system missed an average of 4.5% of the possible data in 1984.

7-1

1984 FLOWS MESONET
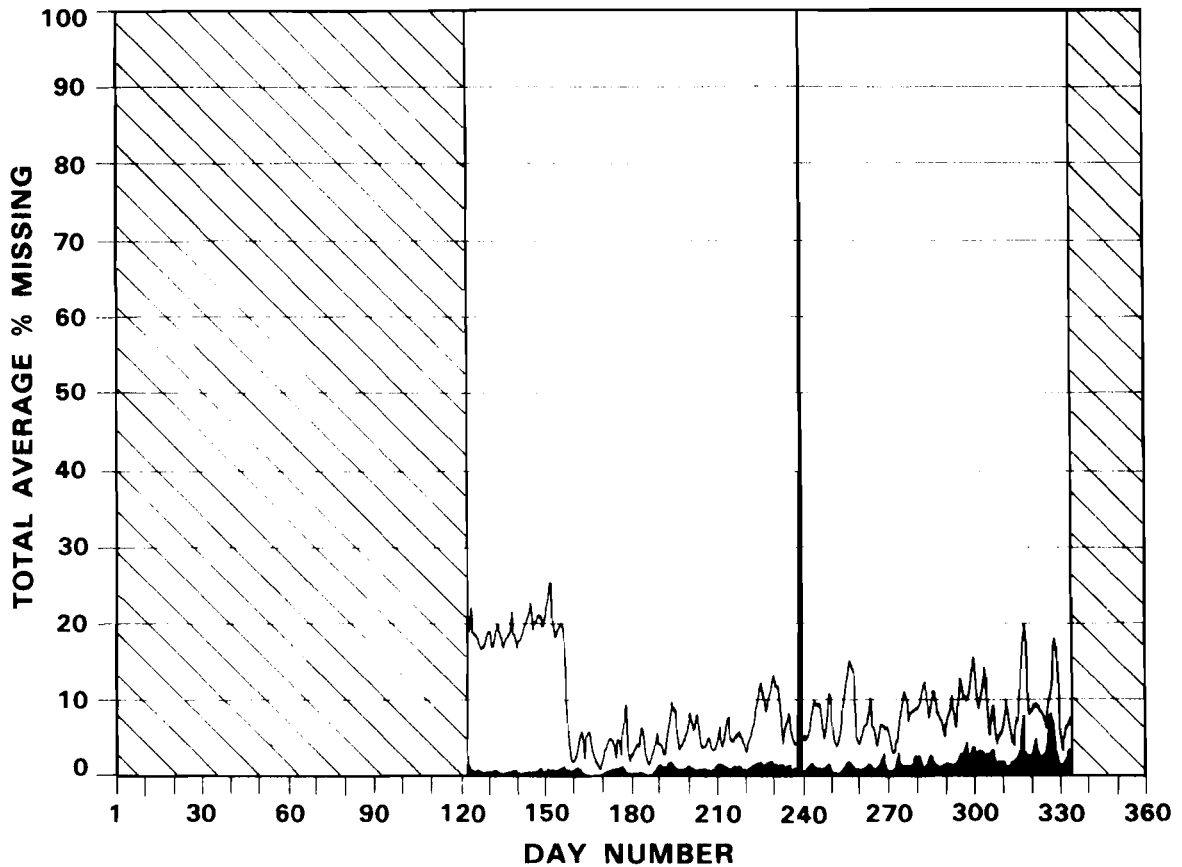
Figure VII-1. Total average percentage of data missing for the FLOWS Memphis network as a function of day of the year in 1984. The days on which the network was not operating are shown as hatched regions. The lower, solid black curve shows the percentage of raw data missing and the upper curve shows the percentage of data missing after the editing and calibration steps have been performed.

1984 FAA MEMPHIS LLWAS SYSTEM
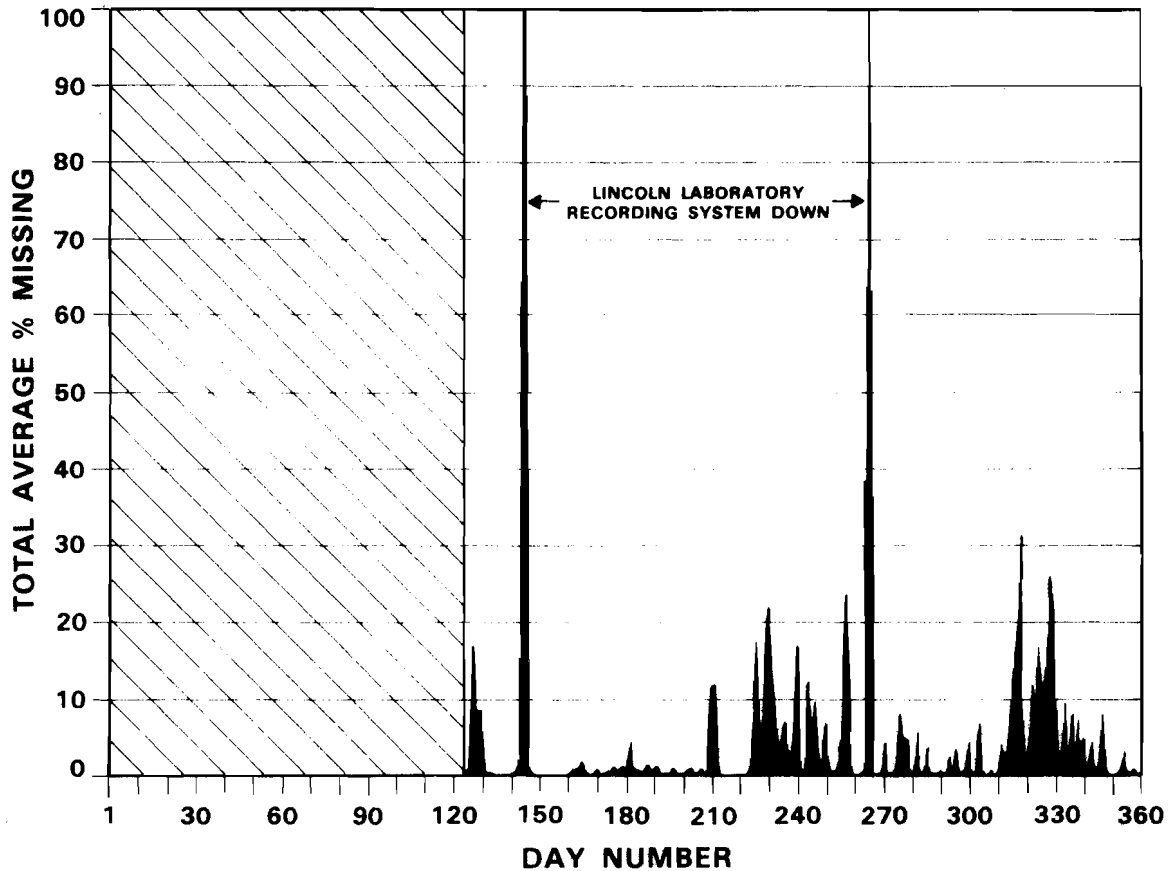
Figure VII-2. Total average percentage of data missing for the FAA
Memphis Low Level Wind Shear Alert System (LLWAS). The time before
Lincoln installed the recording system is shown as a hatched region.
When the LLWAS data were missing, either the station reported the "bad
data" flag, or the winds were perfectly calm there. At the two times
when all of the data were missing, the Lincoln recording system had
lost power.

The percentage of data missing can also be displayed for individual stations. For example, station No. 26 was not activated until late in 1984 when the additional five stations were acquired. The performance record for station No. 26 is shown in Figure VII-15.

2. Site Repair

Another measure of the reliability of the stations is how often they have to be visited, on average, to keep them in operational condition. Table VII-1 shows the total number of site visits per station in 1984 and through August, 1985, and specifically shows the number of visits for repair, maintenance, and installation (after the original station deployment). Station maintenance at a site can consist of, for example, cutting down the weeds or emptying the rain gage bucket, while repairs usually involve sensor or Data Collection Platform (DCP) replacements. In 1984, the then-25 station network was deployed initially without barometers; the one "installation" visit shown for each site involved installing the barometers and editing the DCP software to include the equations to calculate pressure. In 1985, gas-discharge tubes were installed on most of the DCPs for lightning protection and these visits, too, were classified as "installation" visits.

Results from both 1984 and 1985 show that, on average, less than one visit per station per month was required to keep the mesonet operational. Moreover, this average value has been improved by 42% in the 1985 data collection period owing to better sensor calibration, stabilization of the mesonet system, and more familiarity with the individual sites.

B. Data Quality

The issue of data quality pertains to the raw data collected and archived from the automatic weather station network. First, the quality of the data from each sensor is characterized by examining the amount of data edited out on the average and on a daily basis throughout the data collection period. Then, the quality of data from the individual stations is examined, revealing not systematic but specific, chronic sensor problems. Finally, detailed plots of 24 hours of data for each of the individual stations on 11 August 1984 are given to illustrate some of the known problems, as well as the high resolution and quality of the data. Most of the illustrated problems were satisfactorily corrected before the mesonet sensosrs were redeployed in 1985, as discussed in Chapter III and in the following sections.

1. Sensors

Each sensor, when coupled with the sensor interface and timing limitations of the DCP, exhibited some kind of problem. Many of these affected the quality of a limited amount of data only with the rest of the data usually intact and calibrated. The average percentage of data rejected in the editing step for each sensor is the difference between the average percentage missing for the raw and edited data, given in Table VII-2.

	1984 25 stations - 7 mo. (2 May-28 Nov) 5 stations - 2 mo.				1985 6.5 months (15 Feb-31 Aug)			
Station #	Total	Instal.	Maint.	Repair	Total	Instal.	Maint.	Repair
1	2	1	1	0	1	1	0	0
2	6	1	1	4	5	2	0	3
3	6	1	2	3	*5	1	0	4
*4	13	1	3	9	4	2	0	2
5	3	1	1	1	1	1	0	0
*6	2	1	0	1	3	1	1	1
7	3	1	2	0	2	1	0	1
8	4	1	1	2	0	0	0	0
9	10	1	1	8	*7	1	0	6
10	6	1	2	3	2	1	0	1
11	3	1	1	1	1	1	0	0
12	5	1	1	3	0	0	0	0
13	2	1	1	0	2	1	0	1
14	4	1	2	1	3	1	0	2
15	3	1	1	1	3	1	0	2
16	5	1	1	3	2	0	0	2
17	3	1	2	0	1	0	0	1
18	4	1	0	3	2	1	0	1
19	5	1	2	2	1	1	0	0
20	6	1	4	1	3	1	1	1
21	6	1	5	0	2	0	0	2
22	3	1	0	2	2	1	0	1
23	1	1	0	0	3	1	0	2
24	2	1	0	1	2	1	1	0
25	1	1	0	0	0	0	0	0
26	0	0	0	0	4	1	0	3
†27	1	0	0	1	3	1	0	2
28	1	0	0	1	3	1	0	2
29	3	1	0	2	2	1	0	1
30	2	0	0	2	1	0	0	1
+ Totals	108:7	25:1	34:0	49:6	70	25	3	42
X Average per site per month	.63	.14 (22%)	.16 (25%)	.33 (52%)	.36	.13 (36%)	.02 (3%)	.22 (61%)

Key to Symbols

* hit by lightning

† wrecked by vandals

+ The totals for 1984 are listed with two numbers, e.g., 108:7. The first number is the total for 25 stations over 7 months, the second for 5 stations over 2 months.

X The average number of visits per site per month was computed for 1984 by weighting the two "network" totals 5 to 1.

Table VII-1. Summary of mesonet site visits, excluding original installation and final removal, for 2 May - 28 November 1984 and for 15 February - 31 August 1985.

Data Type	% Missing Raw	% Missing Edited	Difference
Temperature	2.51	2.53	0.02
Barometric Pressure	0.59	22.09	21.50
Average Wind Speed	0.59	5.55	4.96
Peak Wind Speed	1.07	6.90	5.83
Wind Direction	0.69	5.55	4.86
Relative Humidity	3.37	12.19	8.82
Precipitation	5.50	8.70	3.20
Total Average	2.05	9.07	7.03

Table VII-2. Average percentage of missing data for each sensor in 1984. Percentages missing of raw and edited data are given separately. The difference between the two is the percentage of received data rejected in the editing procedure and is an inverse measure of data quality.

a. Temperature

The temperature data had the smallest difference of all between the raw and edited percentages missing in Table VII-2. When the temperature statistics are viewed graphically as a function of day of the year (Figure VII-3), no perceptable difference between the two curves exists. The only problem occured around day 220 when the sensor malfunctioned at station No. 11 and reported temperatures around 50°C (see also Figure VII-29). The large amount of missing raw data in November occurred when the ambient temperature fell below freezing; the down-link computer had not been programmed to handle negative integers and so instead reported temperatures in the thousands. This problem has since been corrected, and negative temperatures were successfully recorded in early 1985.

b. Pressure

The pressure data had the lowest quality of all with 21% edited out, although nearly all of the raw data were recovered. Part of this poor record is certainly due to the fact that the barometers were not deployed until June, 30-40 days into 1984 the data collection period. The raw data for this time appear to have been recovered (Figure VII-4), but zeroes were actually transmitted to help in the initial network shakedown. The zero values were then edited out in the final processing steps.

However, most of the poor performance of the barometers must be attributed to the sensors themselves. The output signal is very weak, especially when only 5V excitation is used as was done in 1984, and because a gain of 100 is applied, the noise component is also amplified. The thermostatically controlled heaters do not effectively regulate the temperature, and unless the internal barometer temperature is greater than the thermostat setting (90°F), an oscillation can be seen in the data.

c. Winds

The wind data were contaminated primarily by the "peak wind speed chatter" problem described in Chapter III. This problem gave rise to erroneously high peak wind speeds (defined as the maximum of all the 5 s wind speed samples each minute) which, in turn, contaminated the one-minute average wind speeds. This problem occurred primarily at station Nos. 4, 16 and 22 as is discussed in section B.2. of this chapter. Also, if the wind direction was missing for a given minute, the corresponding peak and average wind speed measurements could not be calibrated (Chapters V and VI) and thus they were considered missing as well. Therefore, a similarity can be seen between the curves for missing data in Figures VII-5, VII-6, and VII-7 for, respectively, average wind speed, peak wind speed, and wind direction.

1984 FLOWS MESONET — TEMPERATURE
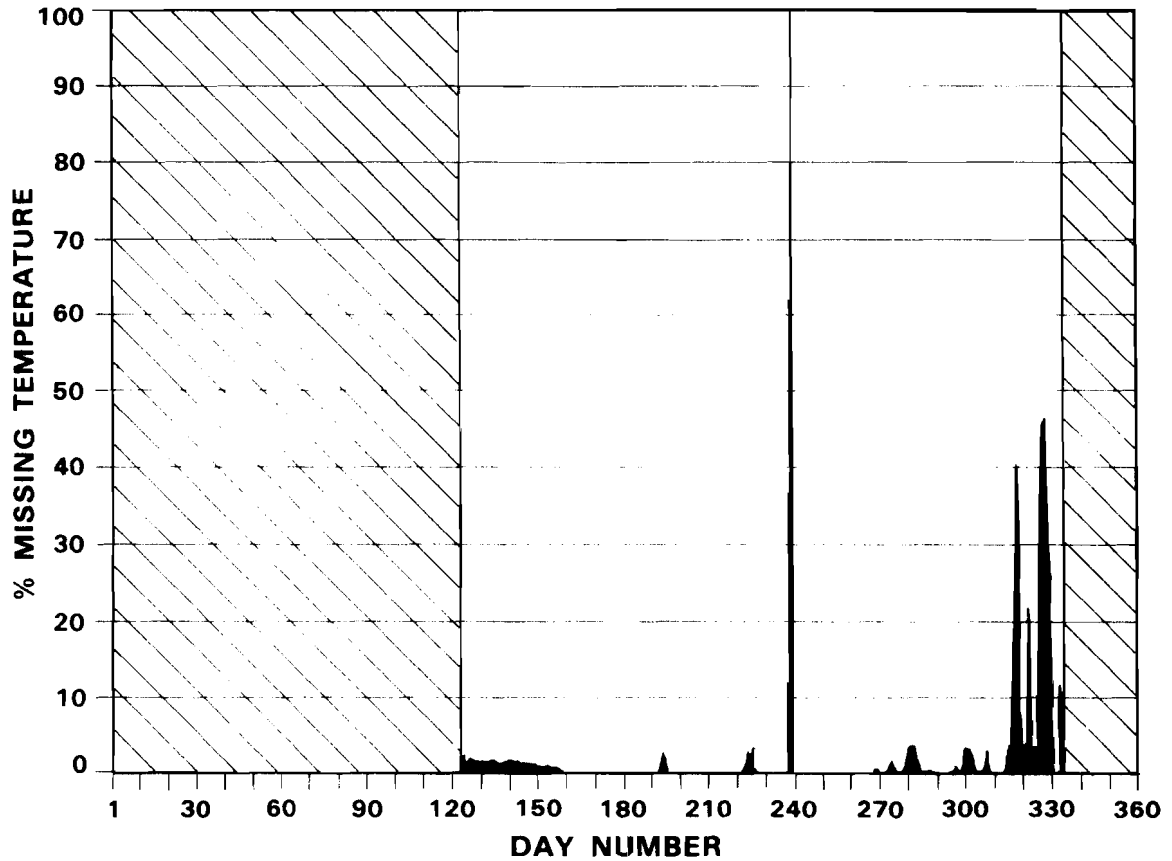
Figure VII-3. Percentage of temperature data missing for 1984. Notice that if the data were received, they were usually good values for the difference between the raw data curve (black) and the edited data curve (above) cannot be seen.

1984 FLOWS MESONET — PRESSURE
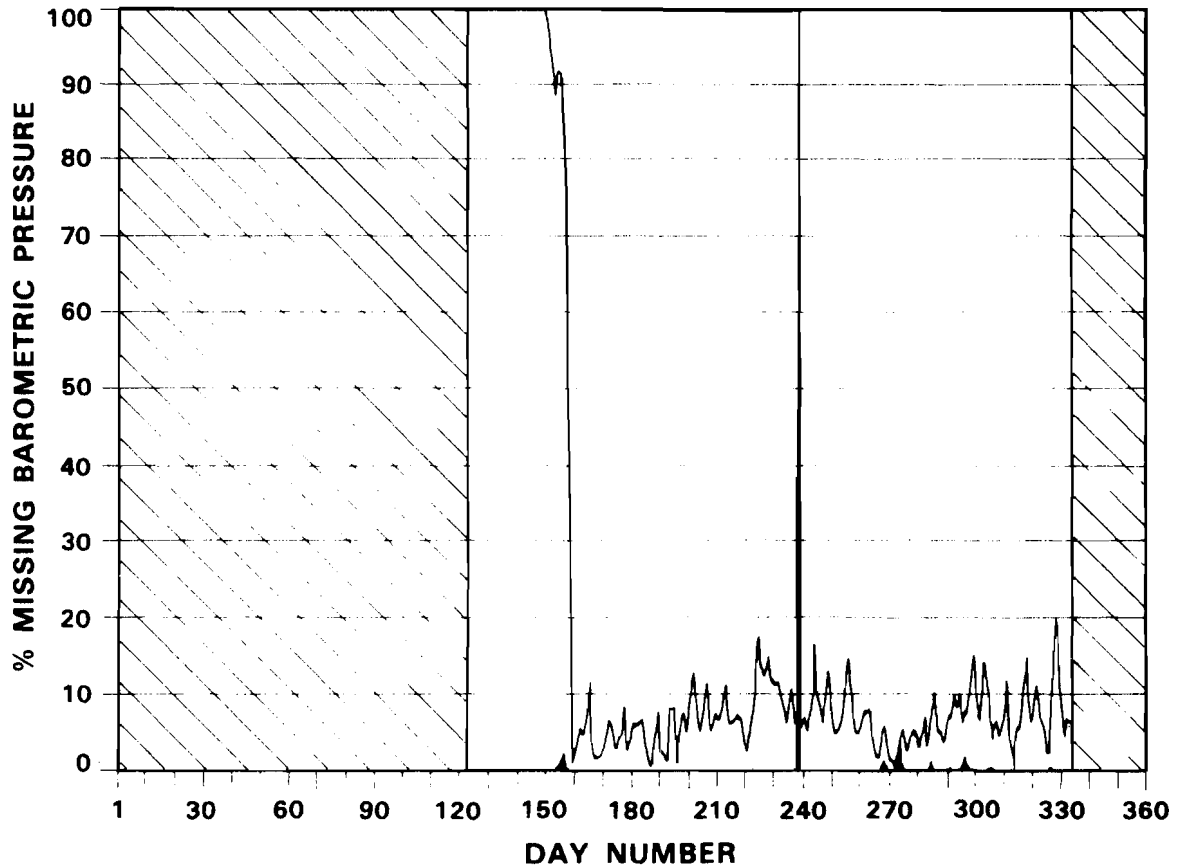
Figure VII-4. Percentage of pressure data missing for 1984. During the first month the barometer readings were all zeroes, so although all the raw data were received, they were edited out.

1984 FLOWS MESONET — AVERAGE WIND SPEED
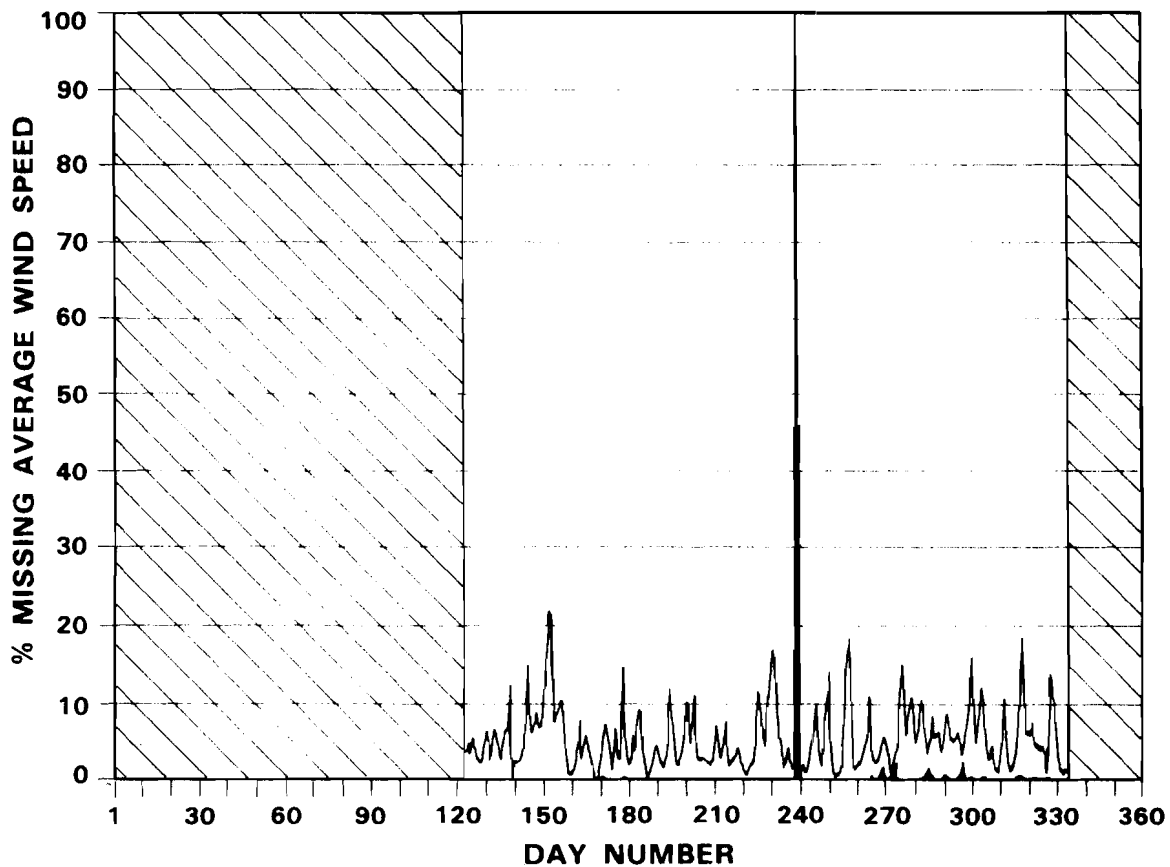
Figure VII-5. Percentage of one-minute averaged wind speed data missing for 1984.

1984 FLOWS MESONET — PEAK WIND SPEED
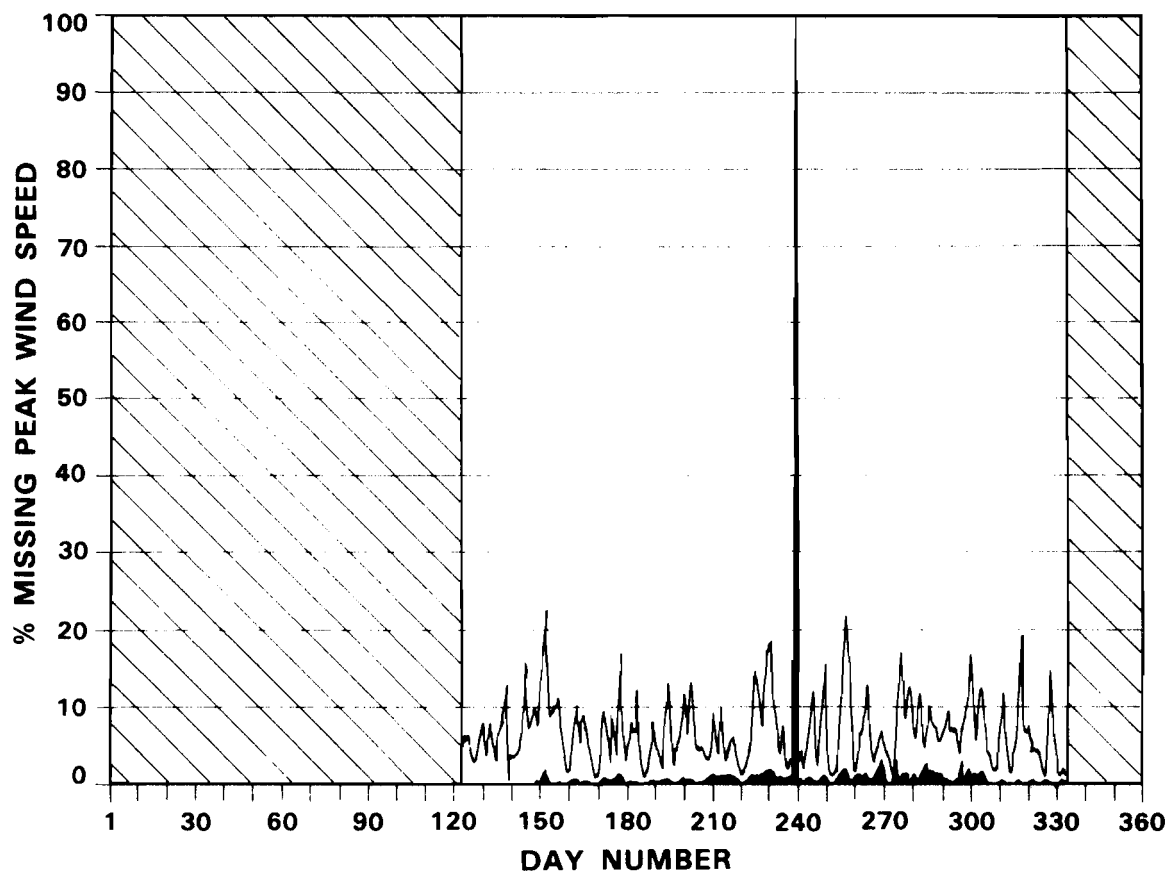
Figure VII-6. Percentage of one-minute peak wind speed data missing for 1984.

1984 FLOWS MESONET — WIND DIRECTION
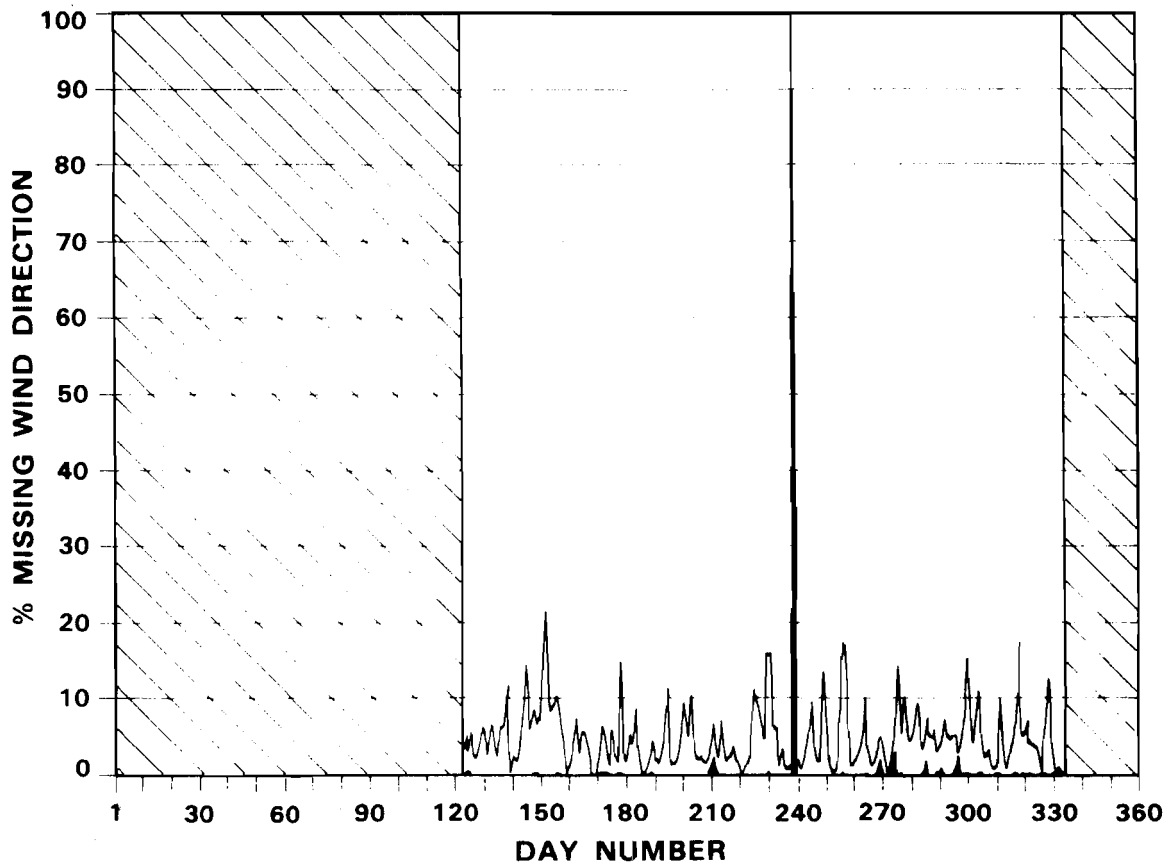
Figure VII-7. Percentage of wind direction data missing for 1984.

d. <u>Relative Humidity</u>

The relative humidity probes were not correctly calibrated at the beginning of 1984 for the high humidity environment encountered in the Memphis area, and because of this, measurements well above 100% were commonly recorded. It was possible to mathematically correct most of these data by compensating for the miscalibration, but when the humidity reading was very high (~124%) the sensor would "overload" and shut itself down. At these times the data would appear at extremely low values (~4%) and had to be rejected although in analysis it would be safe to assume the air was saturated. Figure VII-8 shows how the amount of data rejected varied significantly from day to day and increased as the summer progressed.

e. <u>Precipitation</u>

The percentage of raw data missing for the rain gages was higher than for all the other sensors primarily because station No. 22 did not have a sensor from July through November. Minor amounts of noisy data were edited out (Figure VII-9) and, later in the season when the potentiometers failed in some of the gages, much more data had to be rejected.

2. <u>Stations</u>

The missing data summaries for the individual weather stations are quite revealing, and help explain some of the features of the various sensor summaries discussed in the previous section. Table VII-3 lists these values for all 30 weather stations. For example, station Nos. 4, 16 and 22 (Figures VII-10, VII-11, and VII-12) show large, variable differences between the missing raw and edited data amounts, due to the erroneously high peak wind measurements recorded during light wind conditions. When a multiple of 14% of the raw data is missing over a prolonged period of time such as it is between days 190 and 310 at station No. 22, one or more of the sensors at that station had stopped working. (In this case the rain gage was out.) The limited availability of spare parts in 1984 prolonged problems of this sort.

The station with the best data quality was No. 3, where only 3% of the data were rejected in the editing step (Figure VII-13), most of which can be attributed to the late barometer deployment. The larger percentage of missing raw data near the end of the data collection period was caused by the down-link software problem in handling negative temperatures.

Station No. 8 was extremely reliable except for the relative humidity probe. The calibration was far from correct and on very humid days the probe would completely shut down. Figure VII-14 shows the variability of the percentage of data rejected through editing; nearly all of that rejected was humidity data. This summary for station No. 8 illustrates well how the poor humidity probe calibration impacted the data quality at a single station.

1984 FLOWS MESONET — RELATIVE HUMIDITY
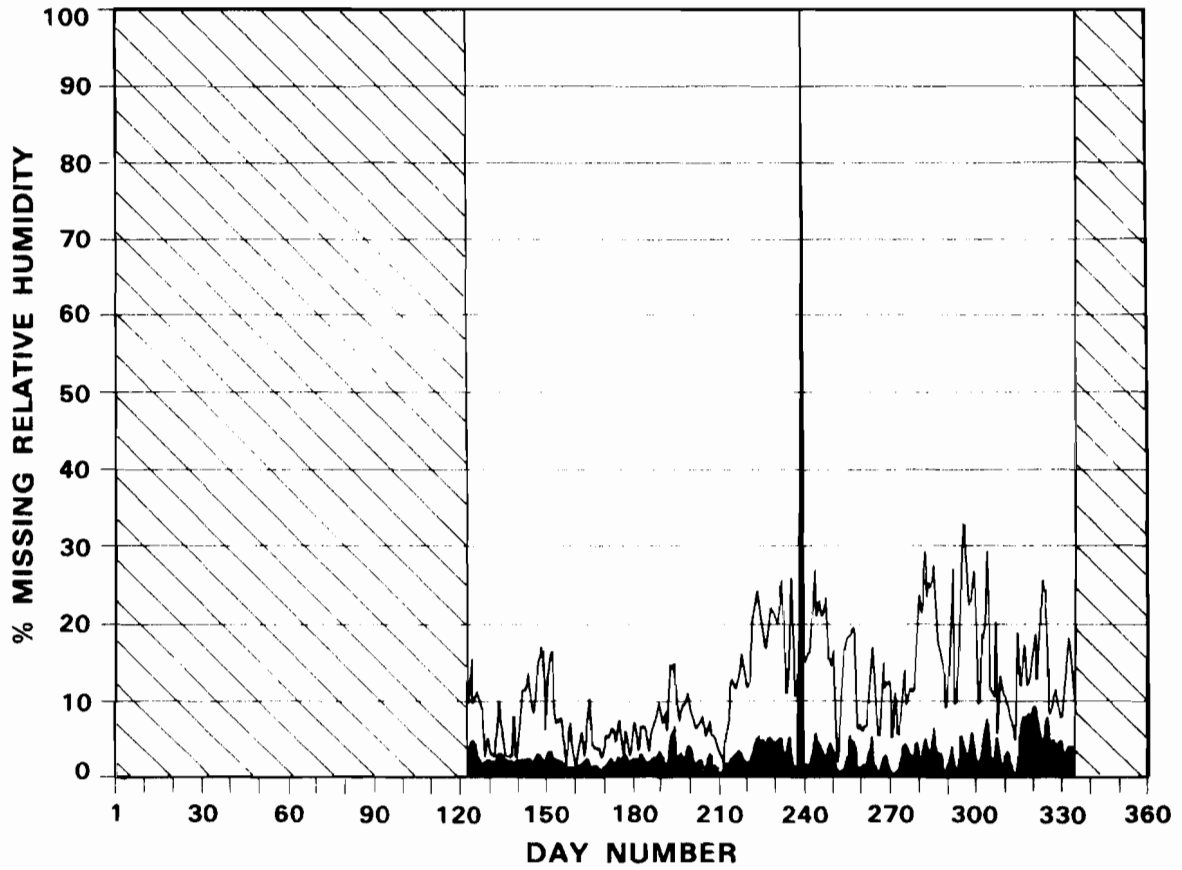
Figure VII-8. Percentage of relative humidity data missing for 1984.

1984 FLOWS MESONET — PRECIPITATION
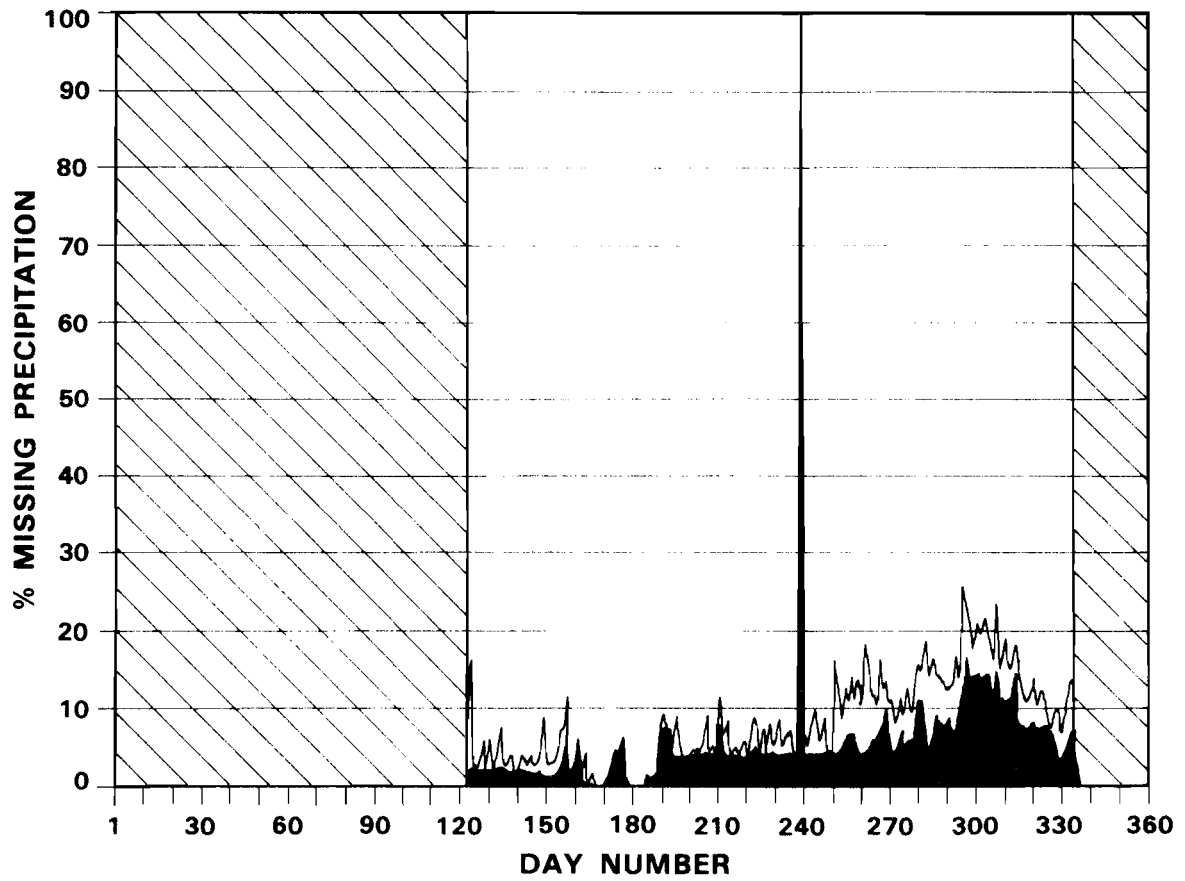
Figure VII-9. Percentage of precipitation data missing for 1984.

Station	% Missing Raw	% Missing Edited	Difference
1	1.01	5.17	4.16
2	1.18	5.89	4.71
3	0.85	3.82	2.97
4	3.32	15.32	12.00
5	0.89	4.70	3.81
6	1.06	11.93	10.87
7	1.26	9.50	8.24
8	1.63	9.61	7.98
9	2.75	10.88	8.13
10	1.95	7.99	6.04
11	1.26	5.21	3.95
12	0.93	5.72	4.79
13	1.77	7.13	5.36
14	1.54	13.11	11.57
15	2.42	13.08	10.66
16	0.79	14.96	14.17
17	1.61	4.99	3.38
18	3.80	10.46	6.66
19	1.65	10.58	8.93
20	0.81	3.98	3.17
21	0.96	4.64	3.68
22	11.55	21.94	10.39
23	1.09	5.35	4.26
24	2.13	8.83	6.70
25	0.96	6.48	5.52
26	13.49	18.14	4.65
27	0.48	14.24	13.76
28	2.38	9.68	7.30
29	0.37	6.76	6.39
30	1.31	11.01	9.70
Total Average	2.24	9.37	7.13

Table VII-3. Average percentage of missing data for each automatic weather station in 1984. Percentages missing of raw* and edited data are given separately. The difference between the two is the percentage of received data rejected in the editing procedure and is an inverse measure of data quality.

*The total average percentage of raw data missing is higher here than in Table VII-2 because here it is assumed that each station reported each day. In Table VII-2, stations that did not report at all on a given day were not figured into the average.

1984 FLOWS MESONET — STATION 4
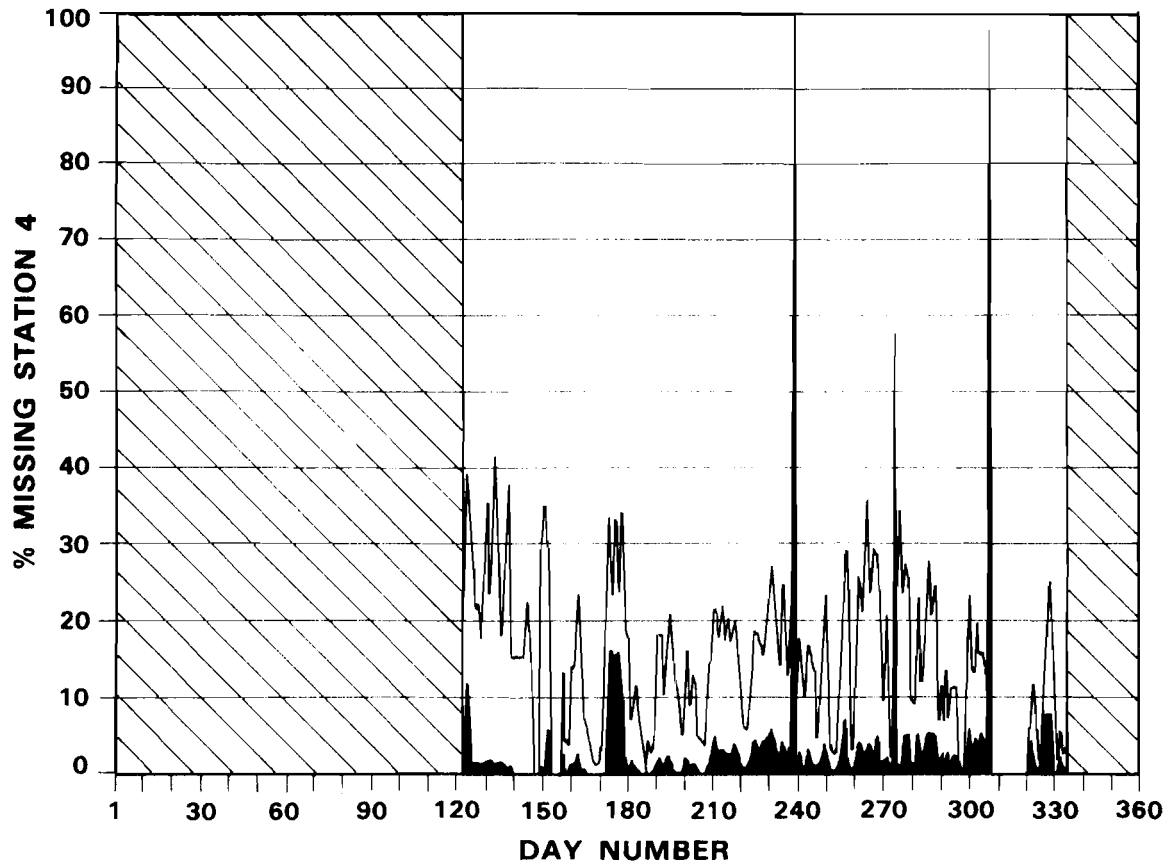
Figure VII-10. Percentage of all types of data missing at station No. 4 in the FLOWS Memphis mesonet in 1984.

1984 FLOWS MESONET — STATION 16
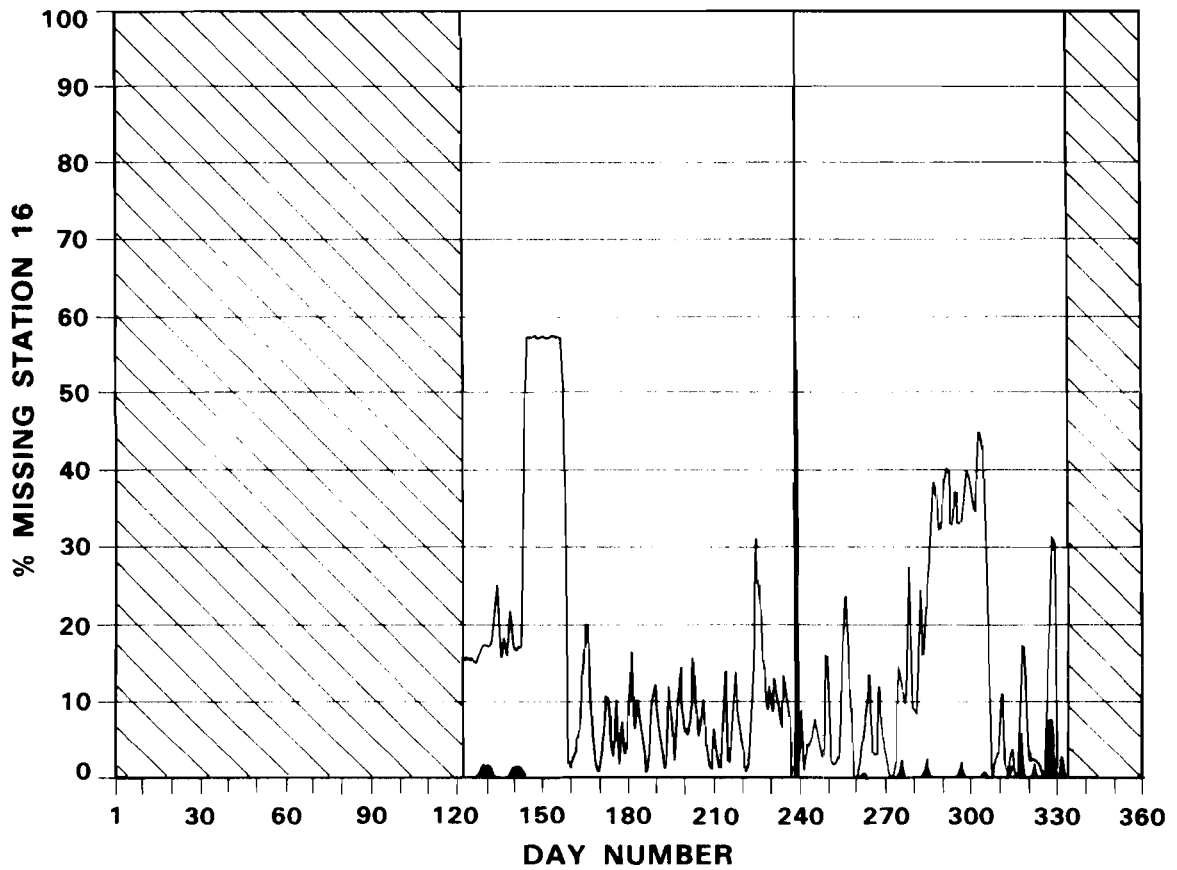
Figure VII-11. Percentage of all types of data missing at station No. 16 in the FLOWS Memphis mesonet in 1984.

1984 FLOWS MESONET — STATION 22
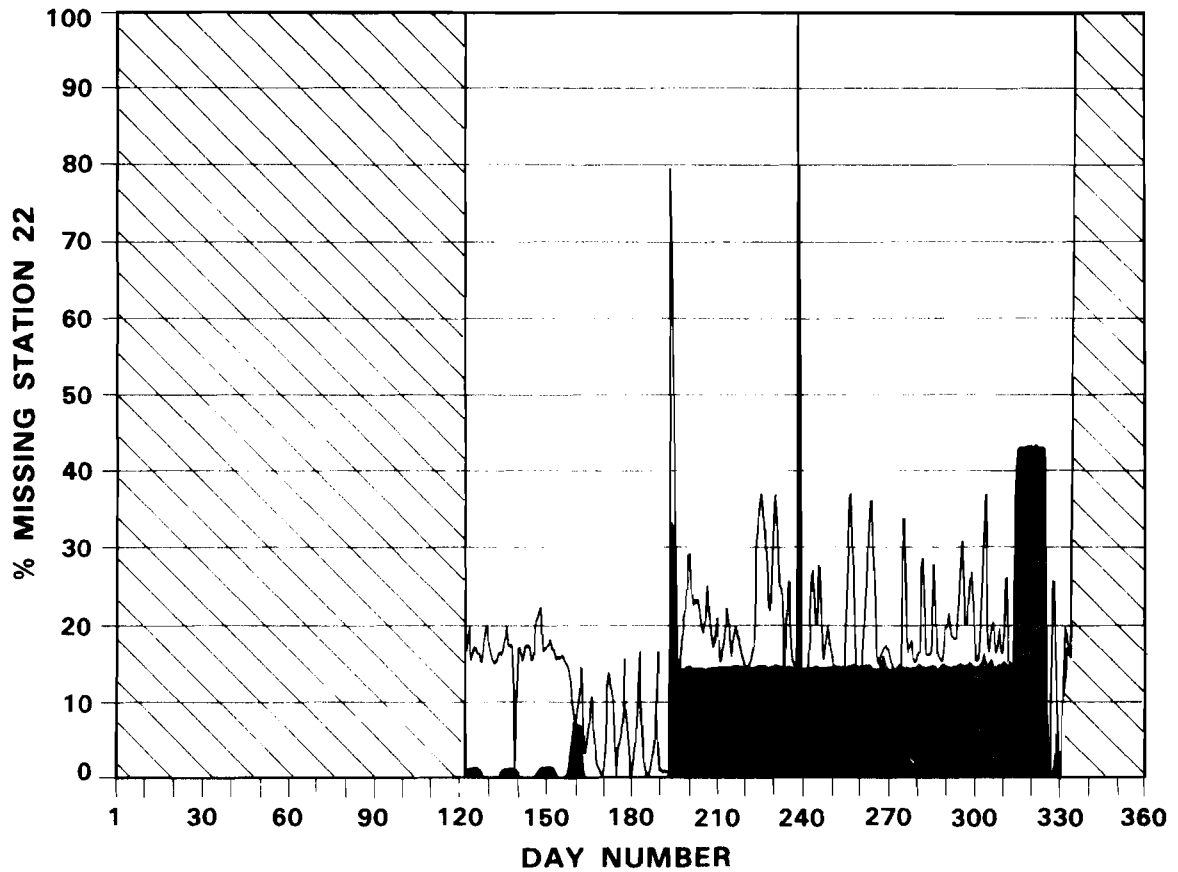
Figure VII-12. Percentage of all types of data missing at station No. 22 in the FLOWS Memphis mesonet in 1984.
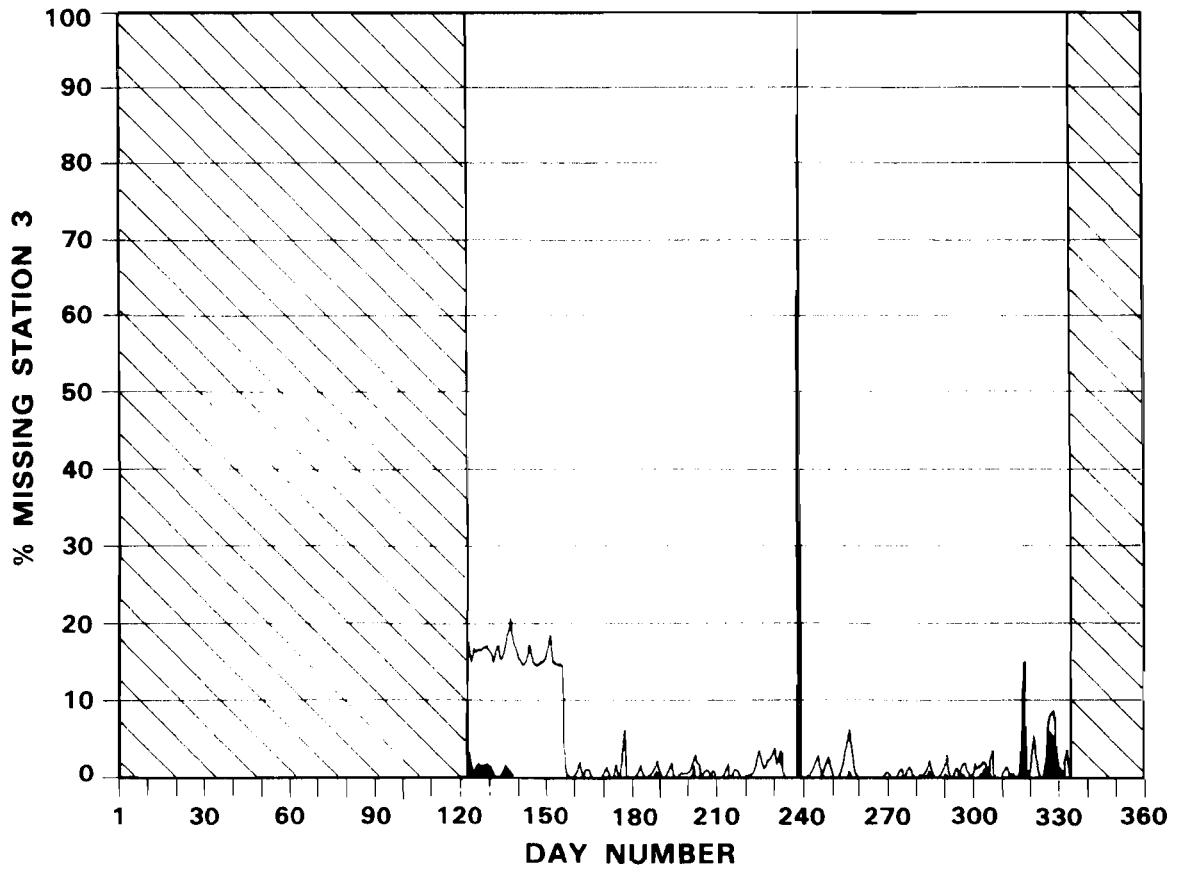
Figure VII-13. Percentage of all types of data missing at station No. 3 in the FLOWS Memphis mesonet in 1984.

1984 FLOWS MESONET — STATION 8
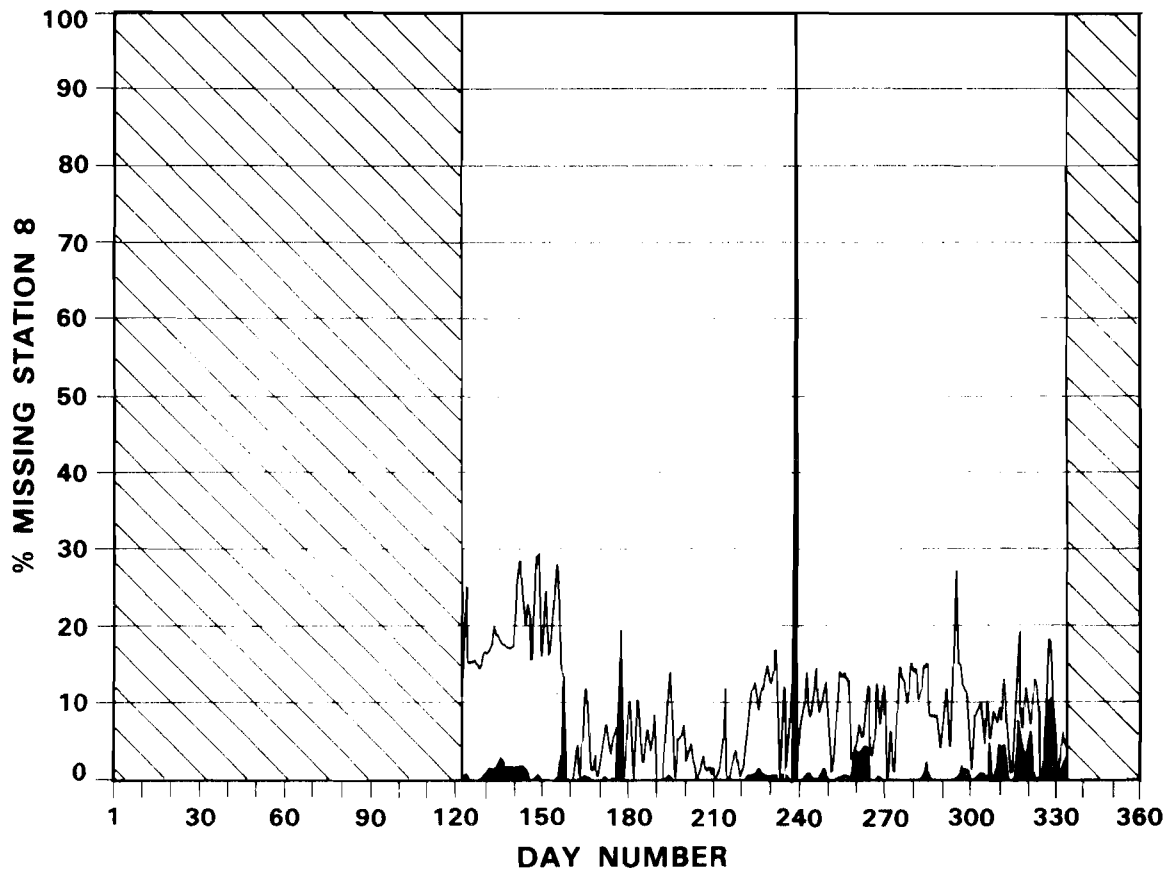
Figure VII-14. Percentage of all types of data missing at station No. 8 in the FLOWS Memphis mesonet in 1984.

Station Nos. 26-30 were not added to the network until late September (around day 290) as can be seen in the data summaries for station Nos. 26 and 27 (Figures VII-15 and VII-16). Notice how the data quality at No. 27 gets very bad and then disappears altogether (stippled area in Figure VII-16). This station was vandalized and not reactivated in 1984.

3. Examples of Individual Station Data

The data from 11 August 1984 have been selected to illustrate in detail the quality of measurements from the various sensors at each station. All of the known problems as well as the features of the automatic weather station data are contained in this dataset.

This dataset also contains a microburst, which first impacted the mesonet at 1815 (GMT, as are all future times). Figure VII-17 shows the microburst with its strongly divergent wind pattern detected between station Nos. 11, 13, and 17, about 3 km apart, at 1820. The boundary of the microburst, shown as a barbed front in Figure VII-17, was evident not only in wind field, but in the temperature field as the edge of the thermal gradient accompanying this event. The rain fall rate reached 70 mm/hr (3 in/hr) at station No. 11, just north of the microburst center (MB). As shown in Figure VII-18, at 1826 the microburst remained highly divergent and associated with even higher rainfall rates of 100-110 mm/hr (4-5 in/hr) as the outflow front continued to spread and high winds, rain, decreasing temperatures, and saturated relative humidity conditions were reported by many more of the mesonet stations.

a. Explanation of the Time Series Plots

Figures VII-19 through VII-43 are time series plots showing all of the data collected on 11 August 1984 (GMT) at station Nos. 1-25, respectively. Station Nos. 26-30 were not yet part of the network. Each plot is labelled at the top with the platform number used internally in the software which is simply the weather station number plus 100. Each grid space in the horizontal direction represents one hour; the heavier vertical lines are at 600, 1200, and 1800 hours. Memphis local time (CDT) is five hours earlier than GMT. Each data point represents a one-minute average so that, if no data were missing, 60 points would be plotted within one horizontal grid interval. Missing data are simply not plotted, accounting for gaps such as the one in Figure VII-21 between 1903 and 1933. The units on the vertical axes are labelled differently for each variable with the name of the plotted variable and the units that apply printed under the individual graphs. Both the one-minute peak and average wind speeds are plotted in the same window. In most cases the two curves are quite closer together, but far enough apart so that they can be individually resolved. Since there is not always enough space to plot the full range of a particular variable, a "wrap-around" scale has been used. Thus, when the trace goes off the top of the scale it reappears at the bottom. The scale from then on should be interpreted so that the bottom line is equal to the highest labelled line, and the higher lines are still higher by increments equal to those originally set. In Figure VII-19 the peak wind speed wraps around between 1800 and 1900, reaching a value of 18.5 m/s. The curve can also wrap around by going off the bottom of the scale as it does with a few of the pressure values in that same figure during the last three hours of the day.

1984 FLOWS MESONET — STATION 26
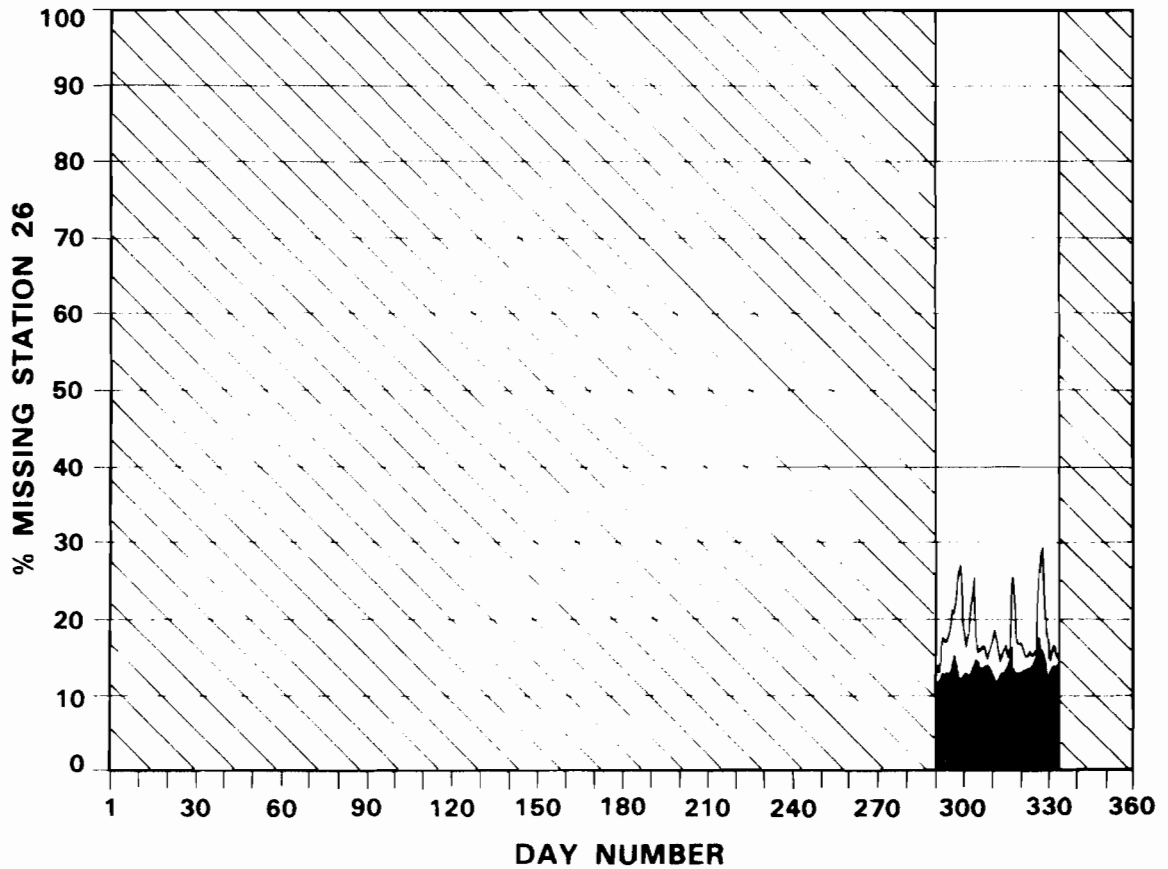
Figure VII-15. Percentage of all types of data missing at station No. 26 in the FLOWS Memphis mesonet in 1984.

1984 FLOWS MESONET — STATION 27
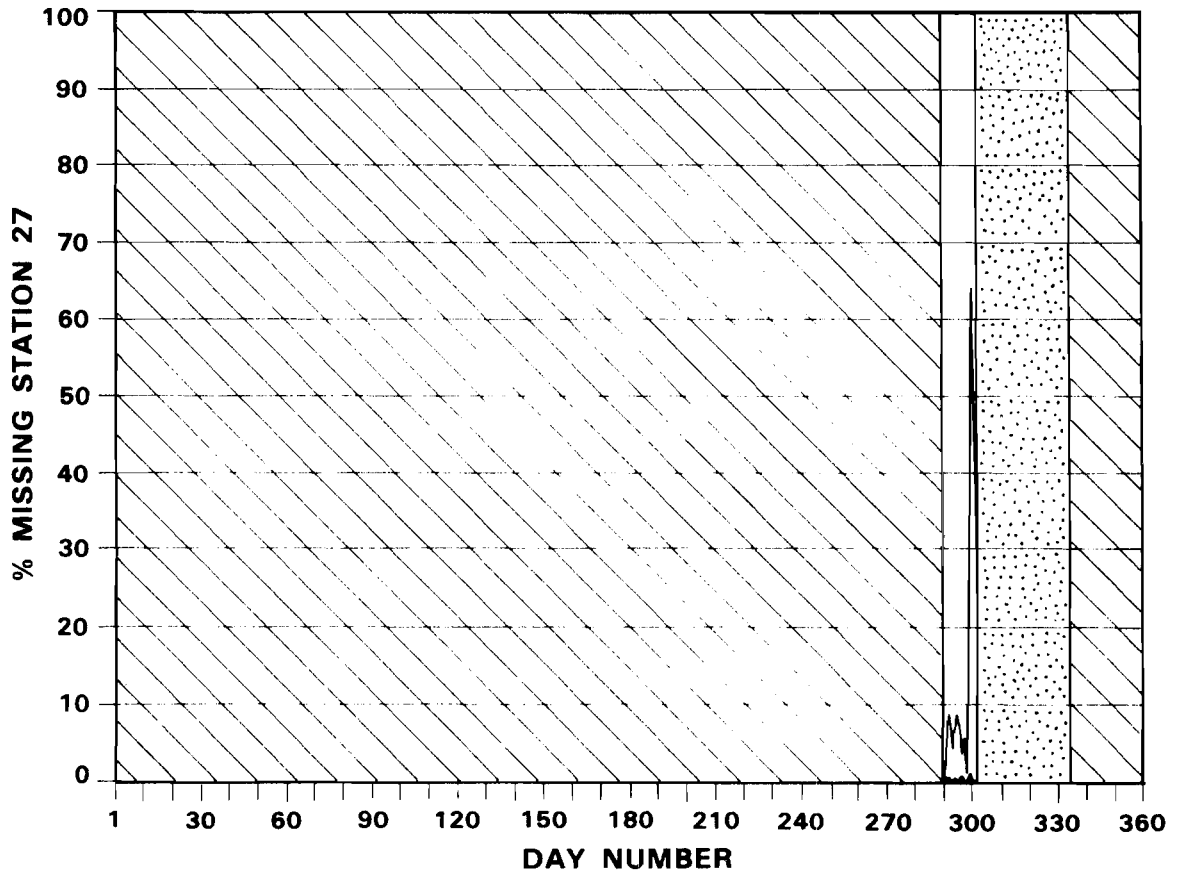
Figure VII-16. Percentage of all types of data missing at station No. 27 in the FLOWS Memphis mesonet in 1984.
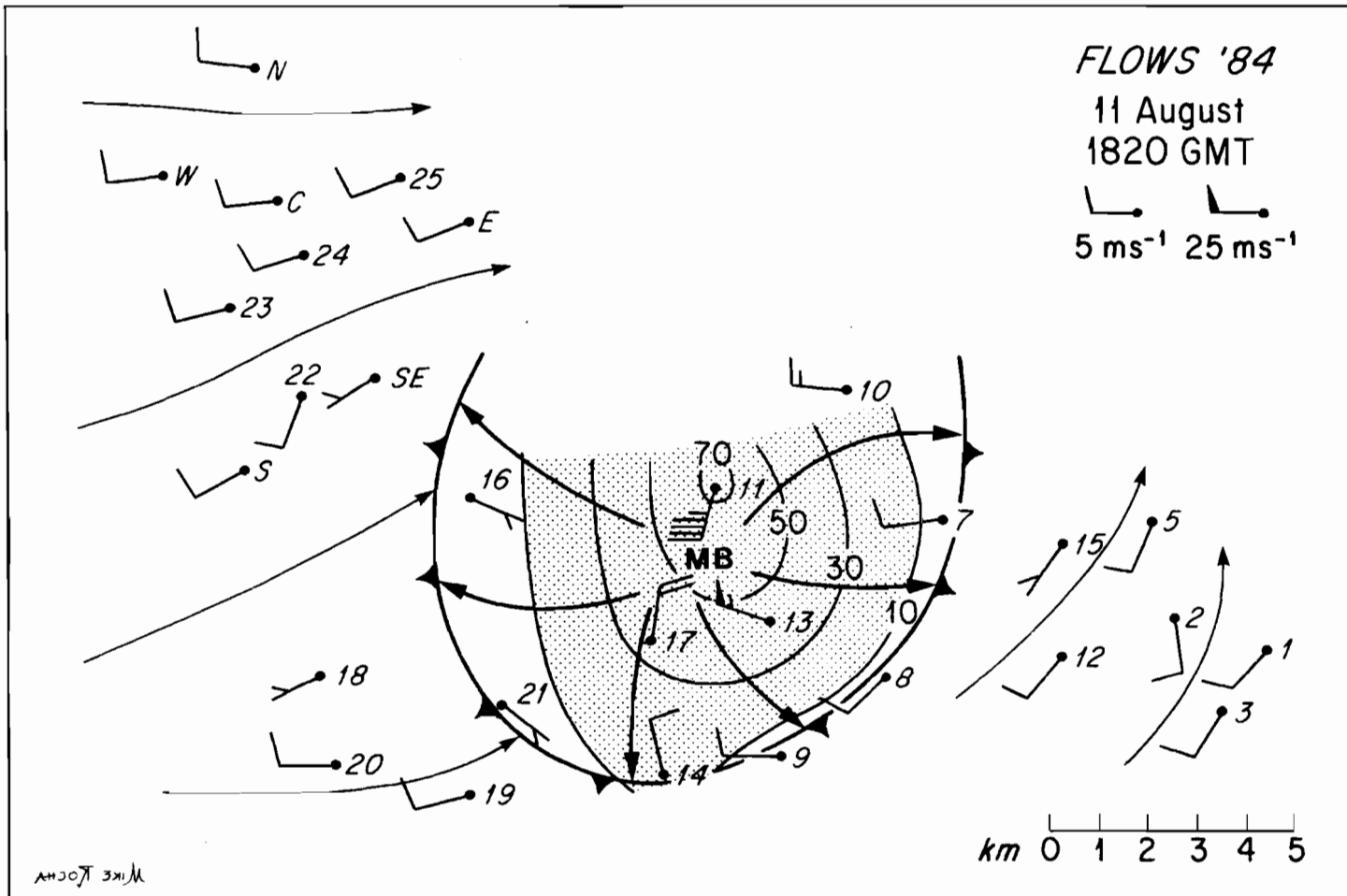
Figure VII-17. A strong microburst is centered between station Nos. 11, 13, and 17 of the FLOWS Memphis mesonet on 11 August 1984 at 1820 (GMT). Solid contours are rain rates in mm/hr (values >10 mm/hr are stippled).
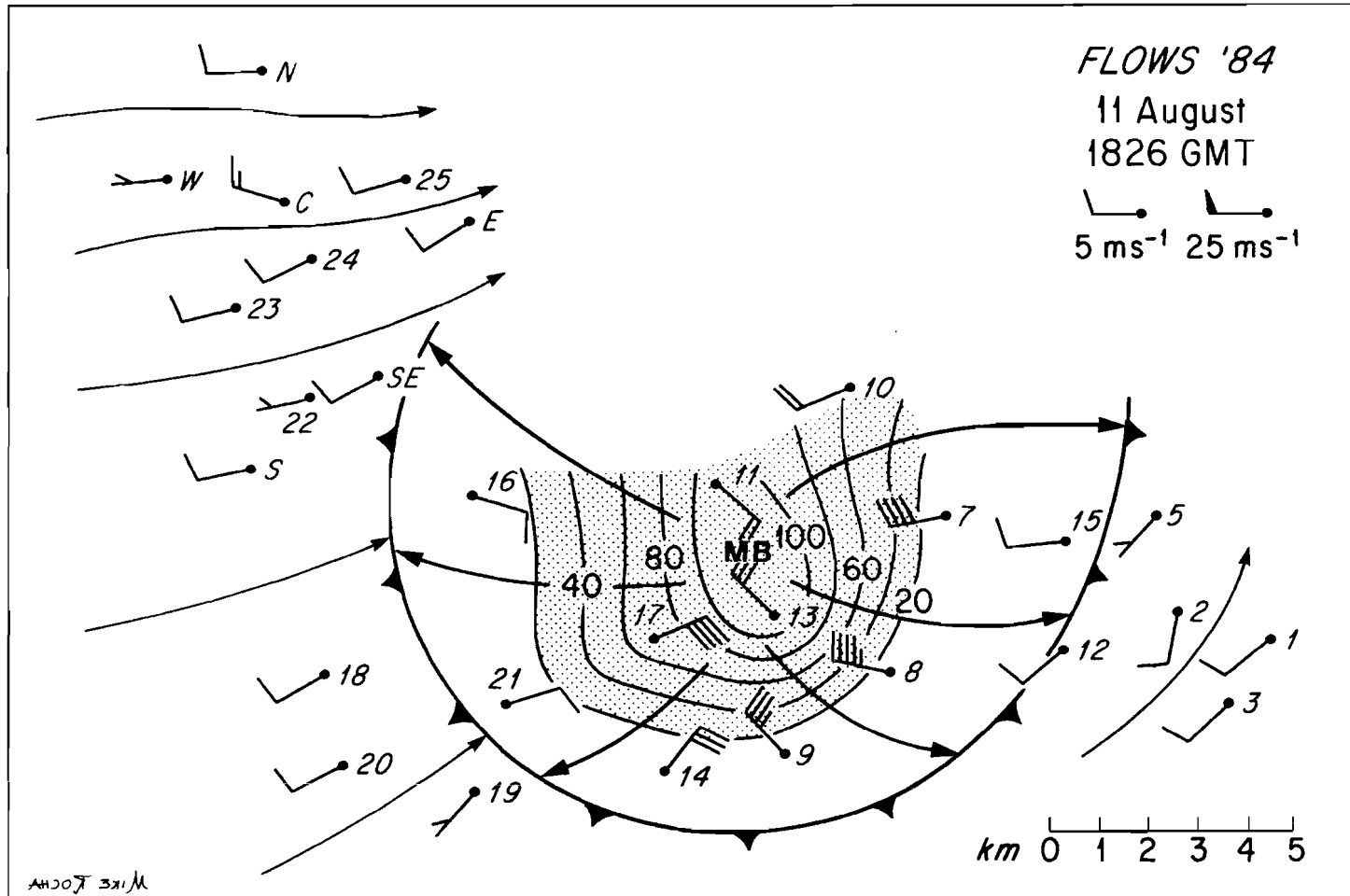
Figure VII-18. The same microburst shown in Figure VII-17 is now centered between station Nos. 11 and 13, six minutes later at 1826 (GMT). Solid contours are rain rates in mm/hr (values >20 mm/hr are stippled). Note that the microburst and rain core centers are coincident.
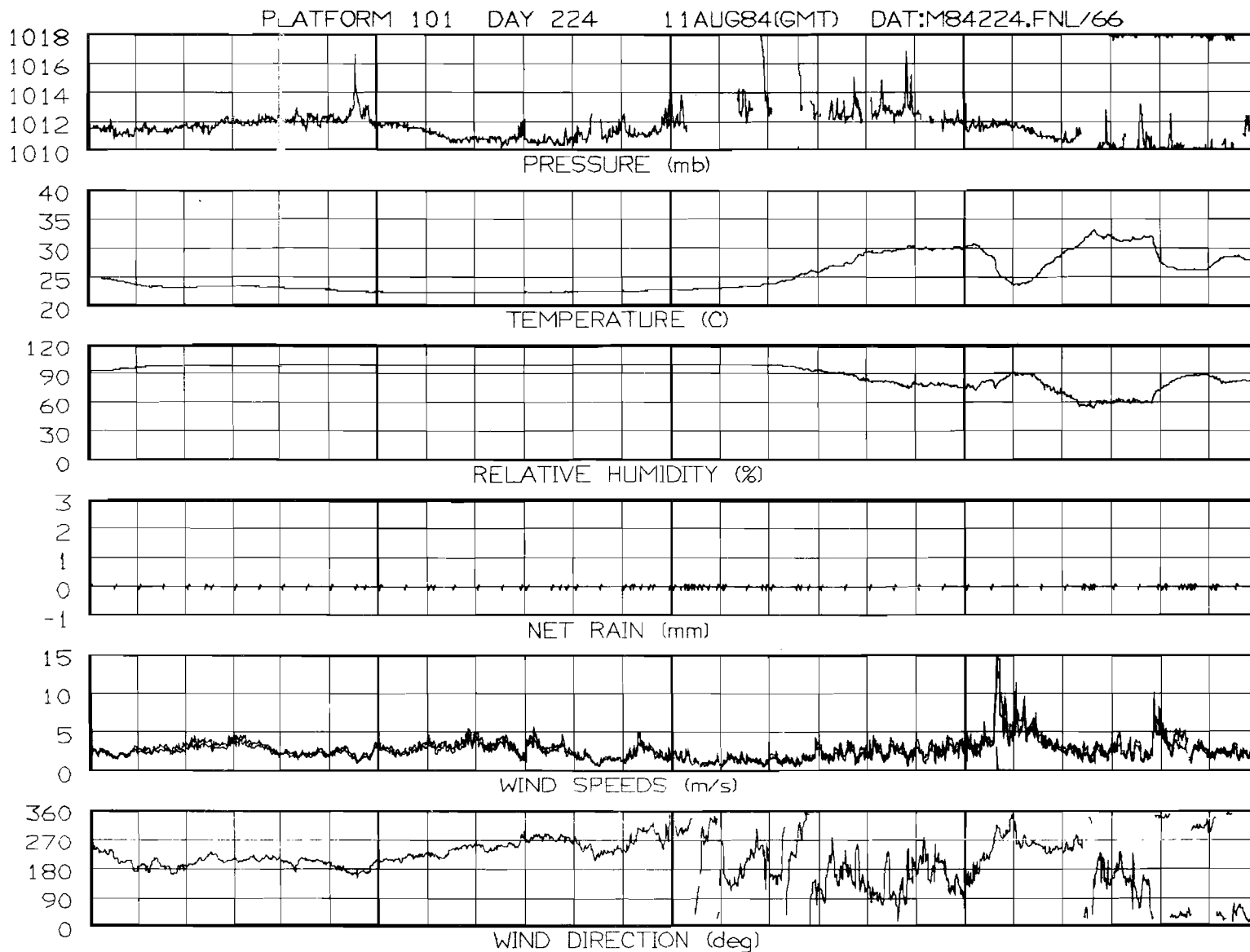
Figure VII-19. Data from station No. 1 in the FLOWS Memphis mesonet on 11 August (Day 224) 1984. Data from 0000 (GMT) to 2359 (GMT) are shown. Refer to text for full explanation of the figure.
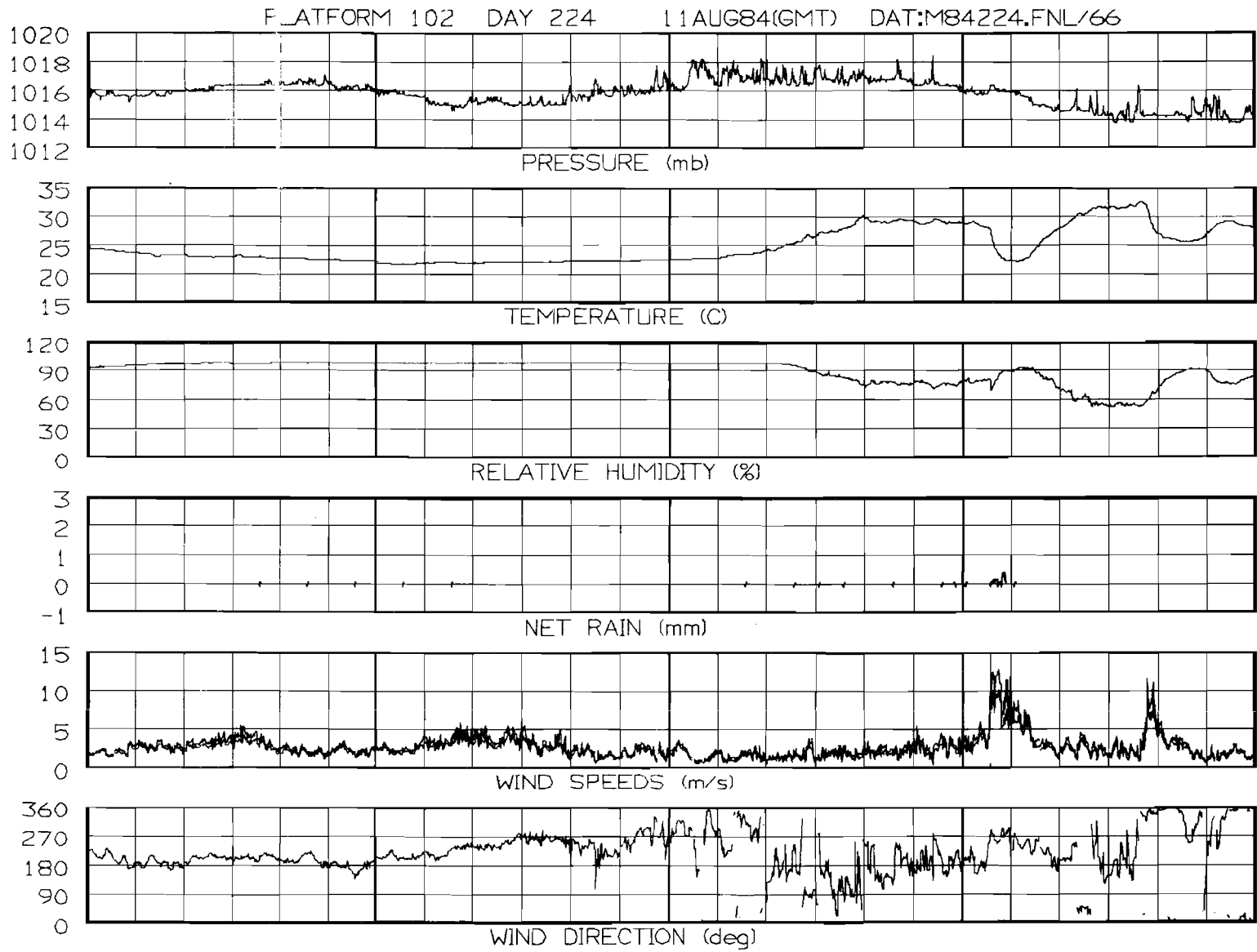
Figure VII-20. Data from station No. 2 in the FLOWS Memphis mesonet.

7-28

PLATFORM 103   DAY 224   11AUG84(GMT)   DAT:M84224.FNL/66

PRESSURE (mb)

TEMPERATURE (C)

RELATIVE HUMIDITY (%)

NET RAIN (mm)

WIND SPEEDS (m/s)

WIND DIRECTION (deg)
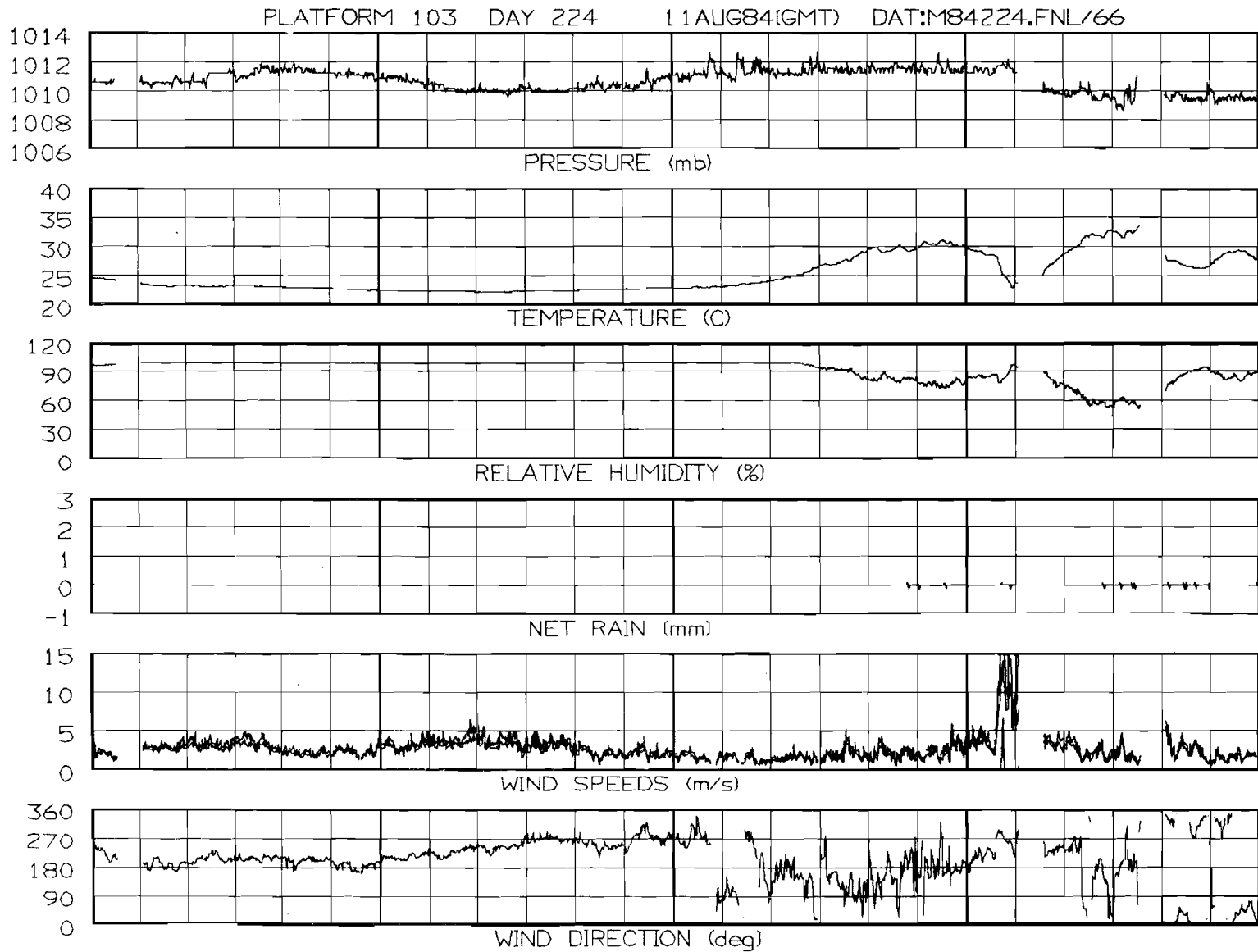
Figure VII-21.   Data from station No. 3 in the FLOWS Memphis mesonet.

PLATFORM 104   DAY 224   11AUG84(GMT)   DAT:M84224.FNL/66

PRESSURE (mb)

TEMPERATURE (C)

RELATIVE HUMIDITY (%)

NET RAIN (mm)

WIND SPEEDS (m/s)

WIND DIRECTION (deg)
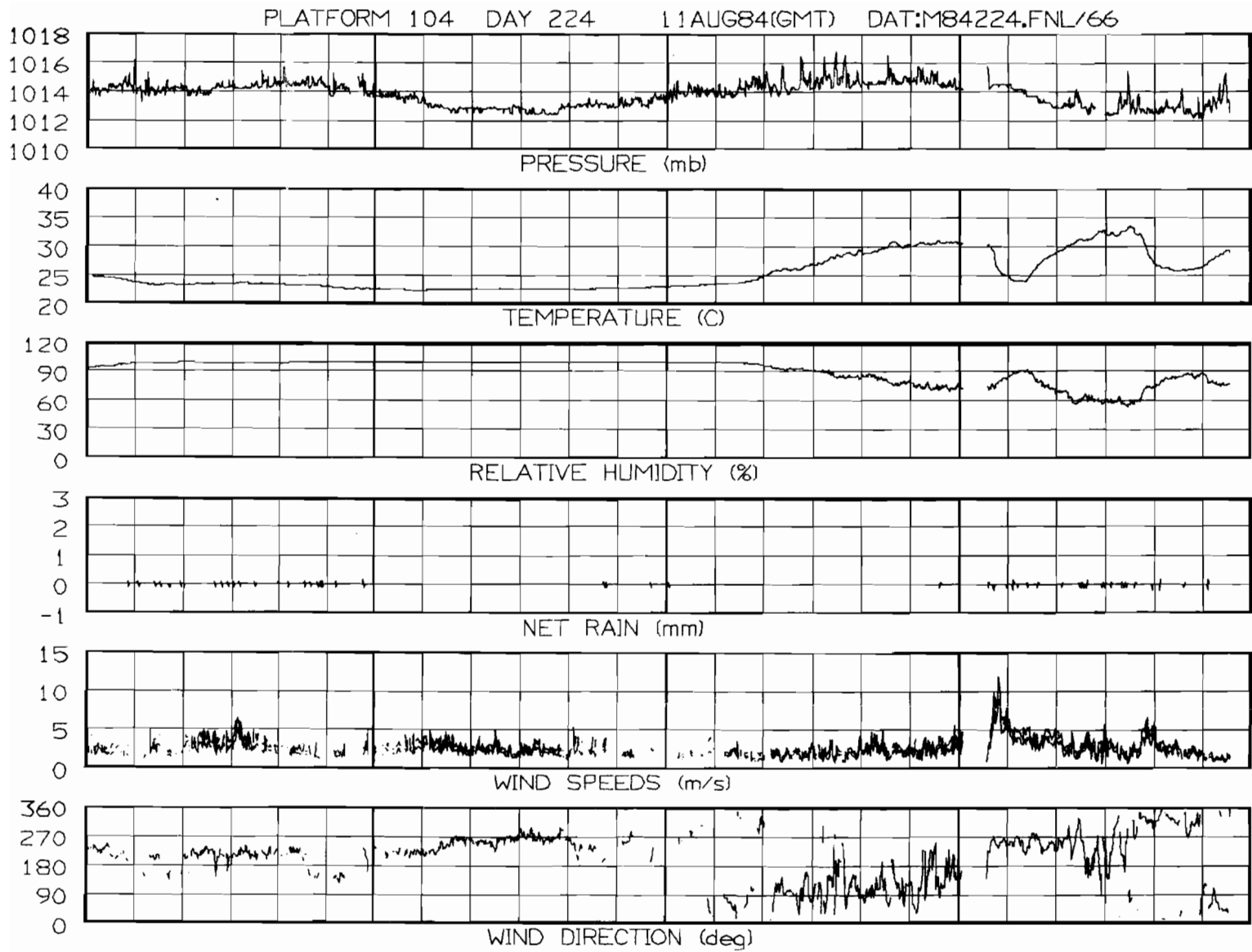
Figure VII-22.   Data from station No. 4 in the FLOWS Memphis mesonet.
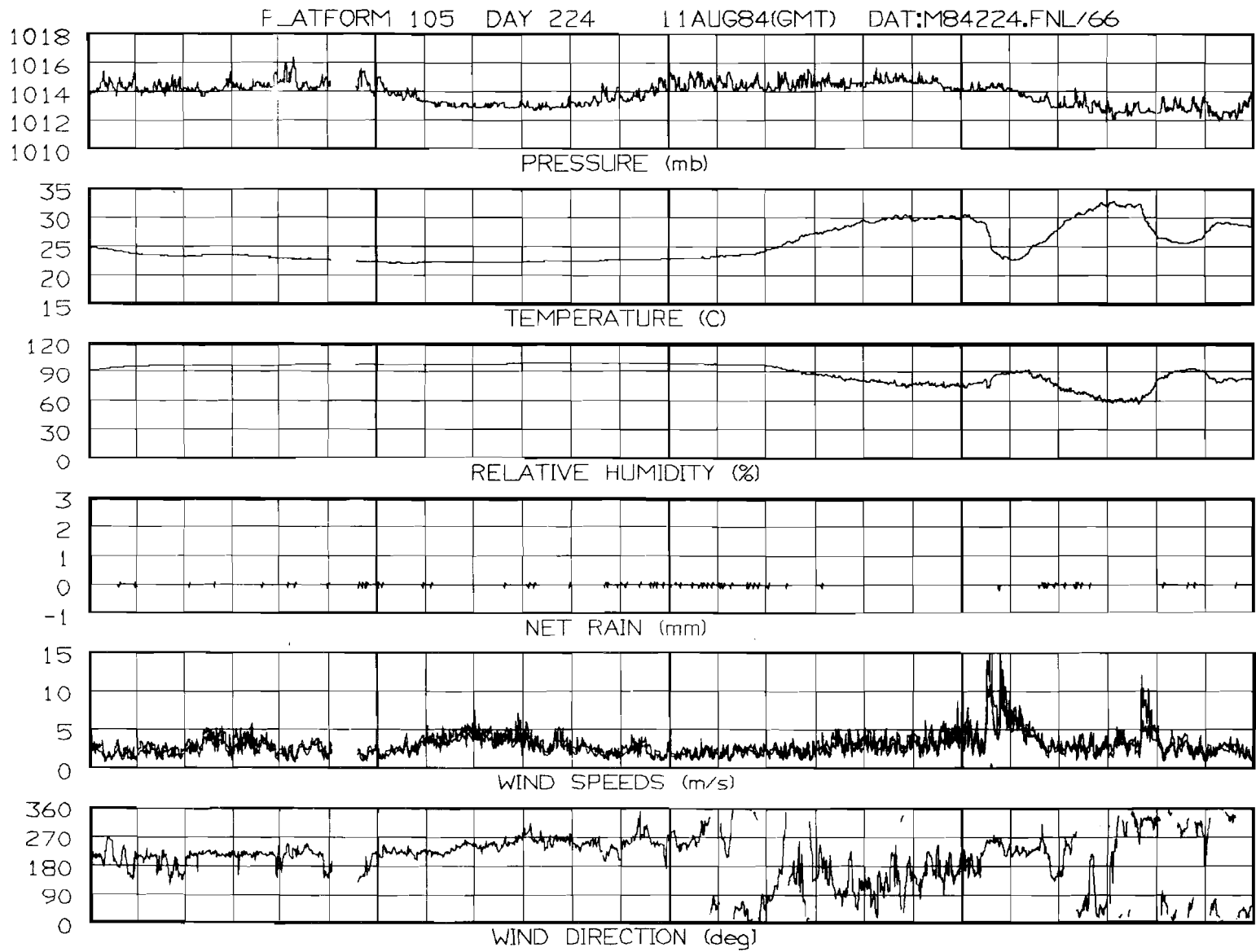
Figure VII-23. Data from station No. 5 in the FLOWS Memphis mesonet.

NO   PRESSURE (mb)   DATA

NO   TEMPERATURE (C)   DATA

NO RELATIVE HUMIDITY (%) DATA

NO   NET RAIN (mm)   DATA

NO   WIND SPEEDS (m/s)   DATA

NO   WIND DIRECTION (deg) DATA

Figure VII-24. Data from station No. 6 in the FLOWS Memphis mesonet.

PLATFORM 107   DAY 224   11AUG84(GMT)   DAT:M84224.FNL/66

PRESSURE (mb)

TEMPERATURE (C)

RELATIVE HUMIDITY (%)

NET RAIN (mm)

WIND SPEEDS (m/s)

WIND DIRECTION (deg)
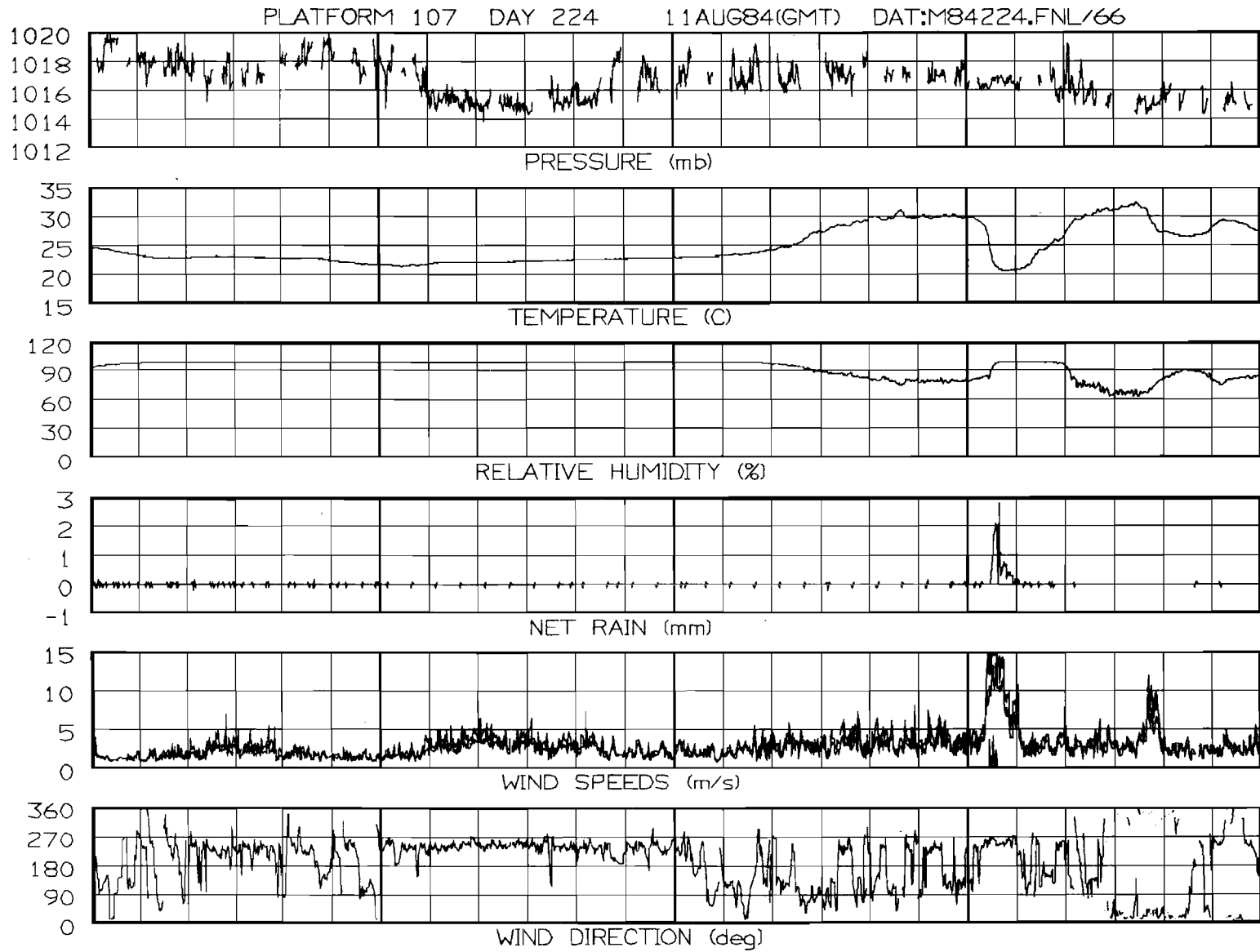
Figure VII-25.   Data from station No. 7 in the FLOWS Memphis mesonet.

PLATFORM 108   DAY 224   11AUG84(GMT)   DAT:M84224.FNL/66

PRESSURE (mb)

TEMPERATURE (C)

RELATIVE HUMIDITY (%)

NET RAIN (mm)

WIND SPEEDS (m/s)

WIND DIRECTION (deg)
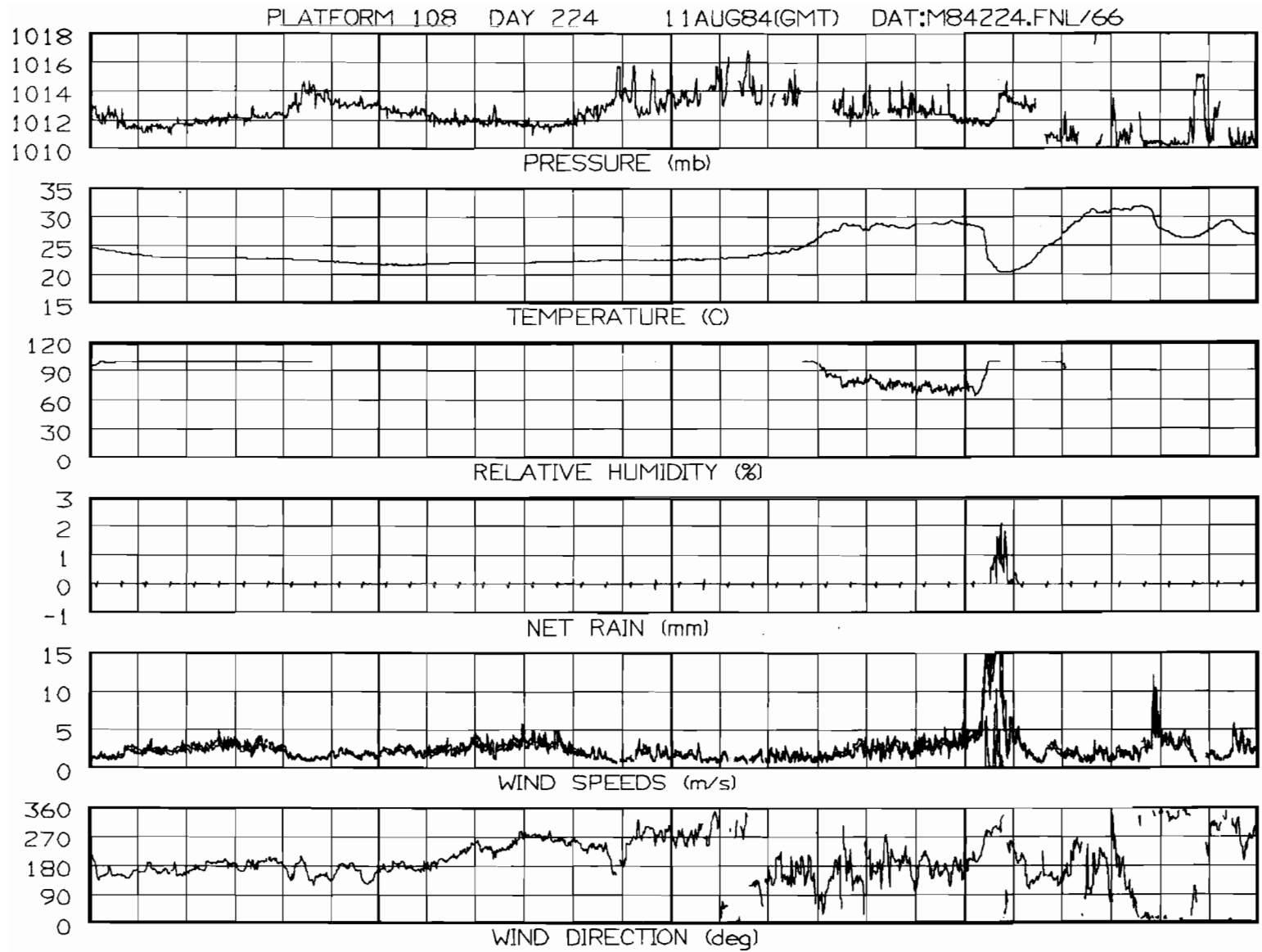
Figure VII-26.   Data from station No. 8 in the FLOWS Memphis mesonet.
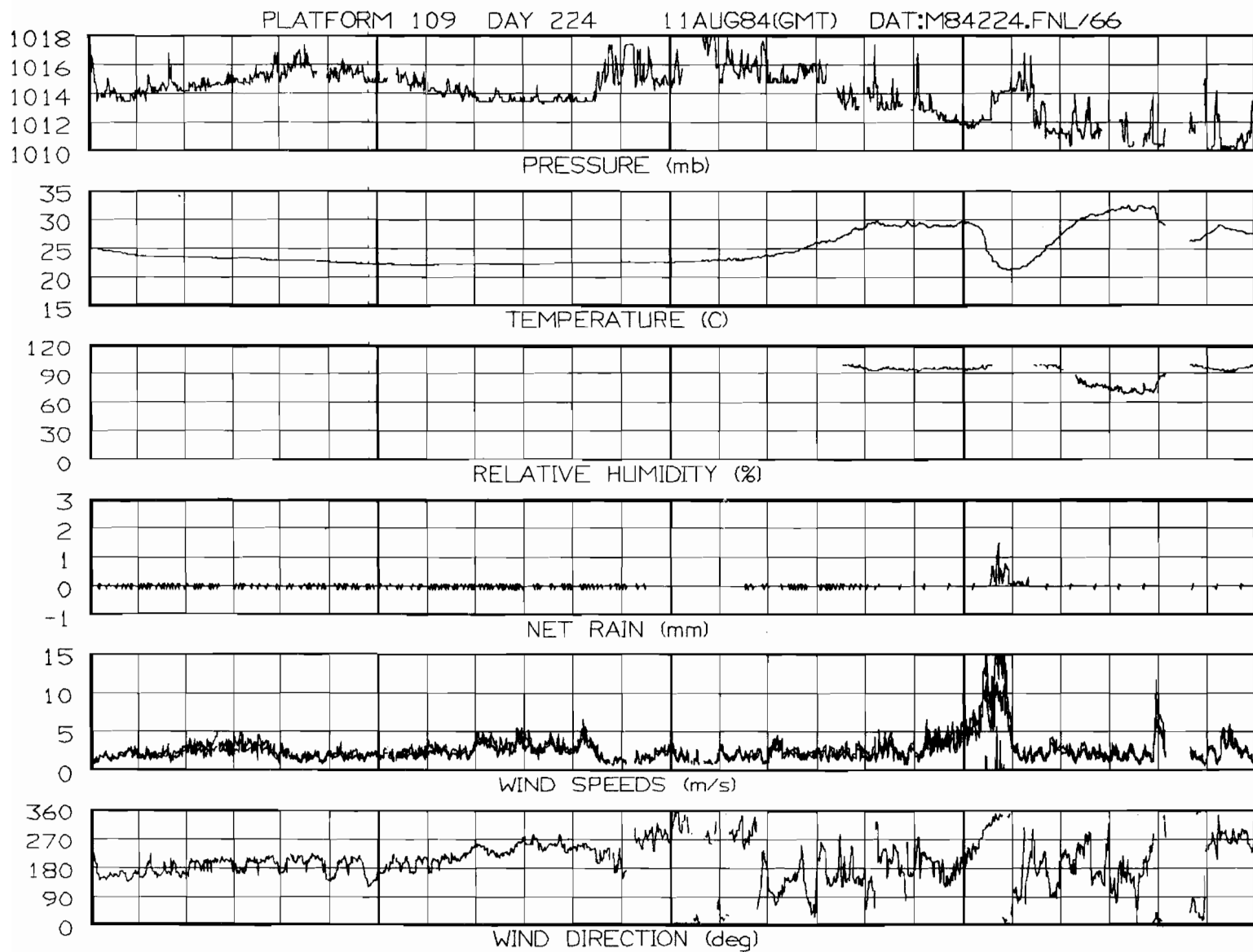
Figure VII-27. Data from station No. 9 in the FLOWS Memphis mesonet.
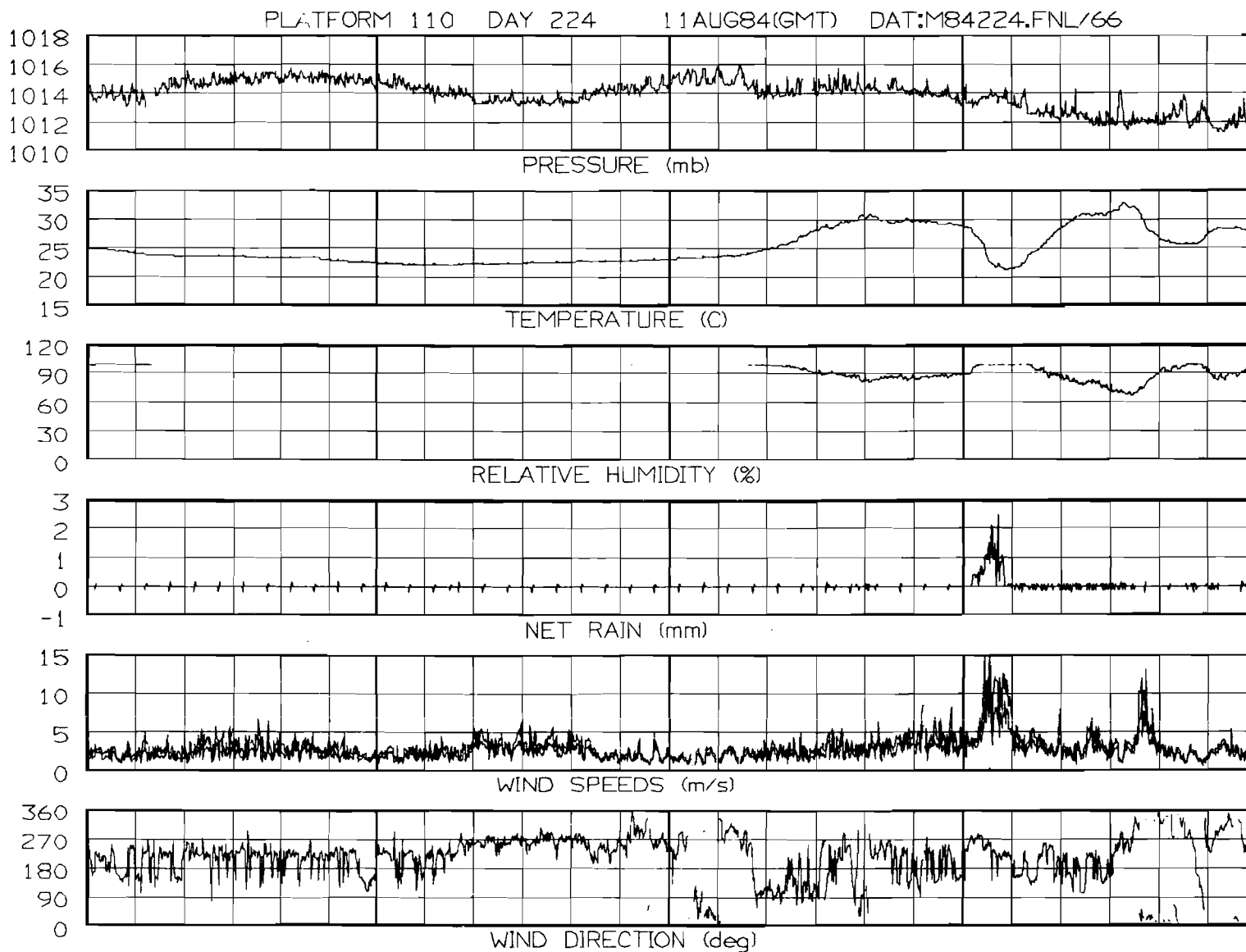
Figure VII-28. Data from station No. 10 in the FLOWS Memphis mesonet.

PLATFORM 111   DAY 224   11AUG84(GMT)   DAT:M84224.FNL/66

PRESSURE (mb)

TEMPERATURE (C)

RELATIVE HUMIDITY (%)

NET RAIN (mm)

WIND SPEEDS (m/s)

WIND DIRECTION (deg)
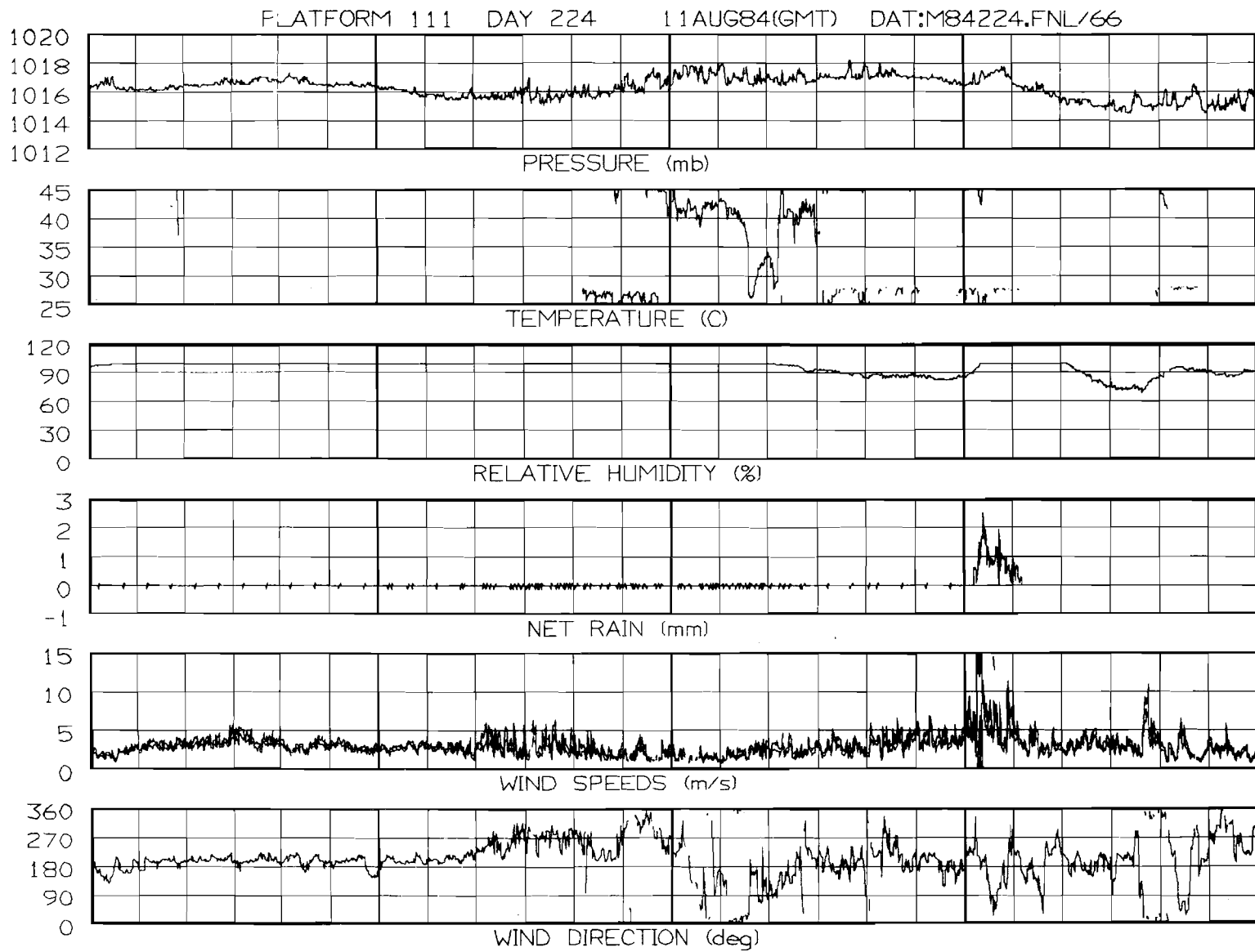
Figure VII-29.   Data from station No. 11 in the FLOWS Memphis mesonet.

PLATFORM 112   DAY 224   11AUG84(GMT)   DAT:M84224.FNL/66

PRESSURE (mb)

TEMPERATURE (C)

RELATIVE HUMIDITY (%)

NET RAIN (mm)

WIND SPEEDS (m/s)

WIND DIRECTION (deg)
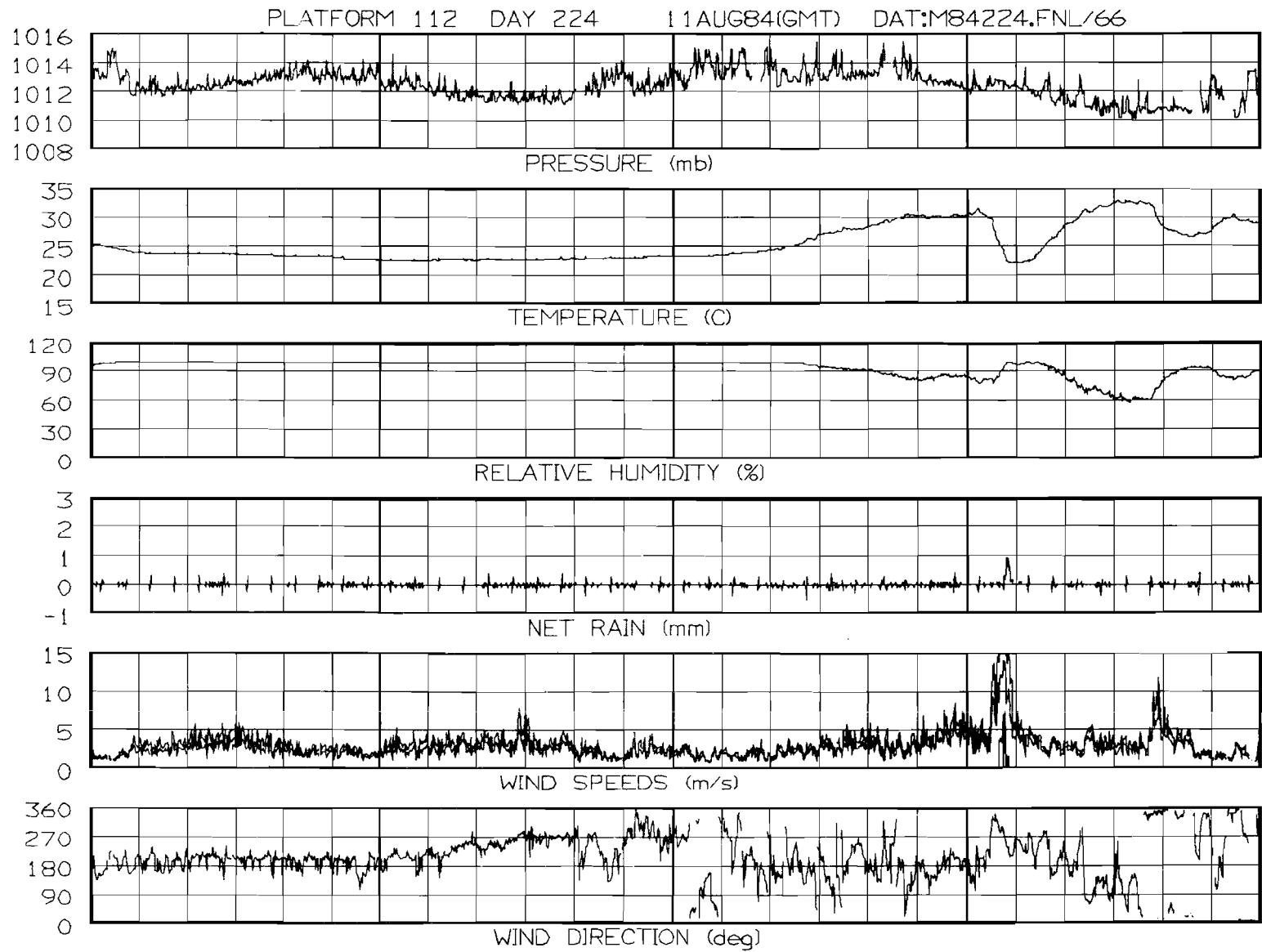
Figure VII-30.   Data from station No. 12 in the FLOWS Memphis mesonet.

PLATFORM 113   DAY 224   11AUG84(GMT)   DAT:M84224.FNL/66

PRESSURE (mb)

TEMPERATURE (C)

RELATIVE HUMIDITY (%)

NET RAIN (mm)

WIND SPEEDS (m/s)

WIND DIRECTION (deg)
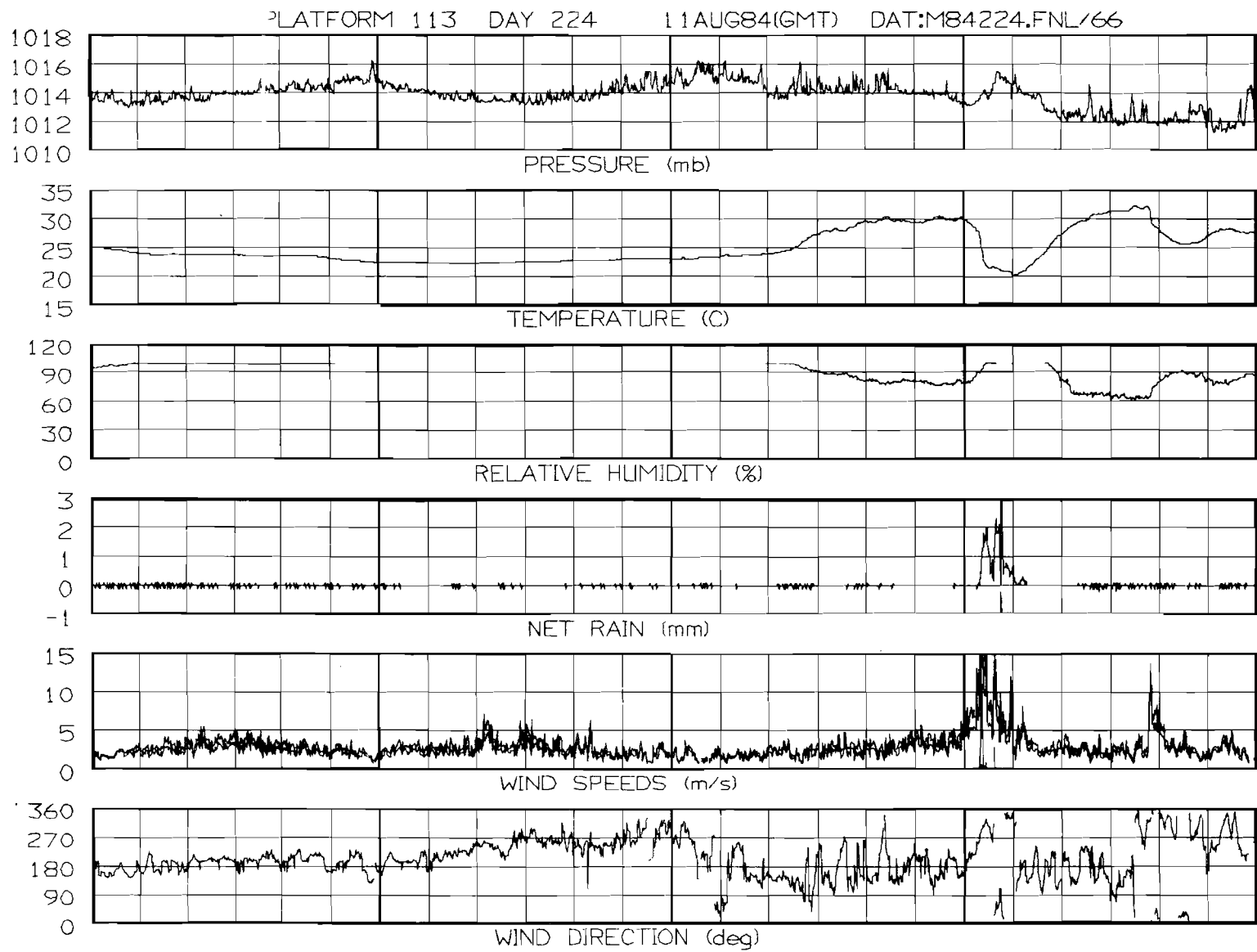
Figure VII-31.   Data from station No. 13 in the FLOWS Memphis mesonet.

PLATFORM 114   DAY 224   11AUG84(GMT)   DAT:M84224.FNL/66

PRESSURE (mb)

TEMPERATURE (C)

NO RELATIVE HUMIDITY (%) DATA

NET RAIN (mm)

WIND SPEEDS (m/s)

WIND DIRECTION (deg)
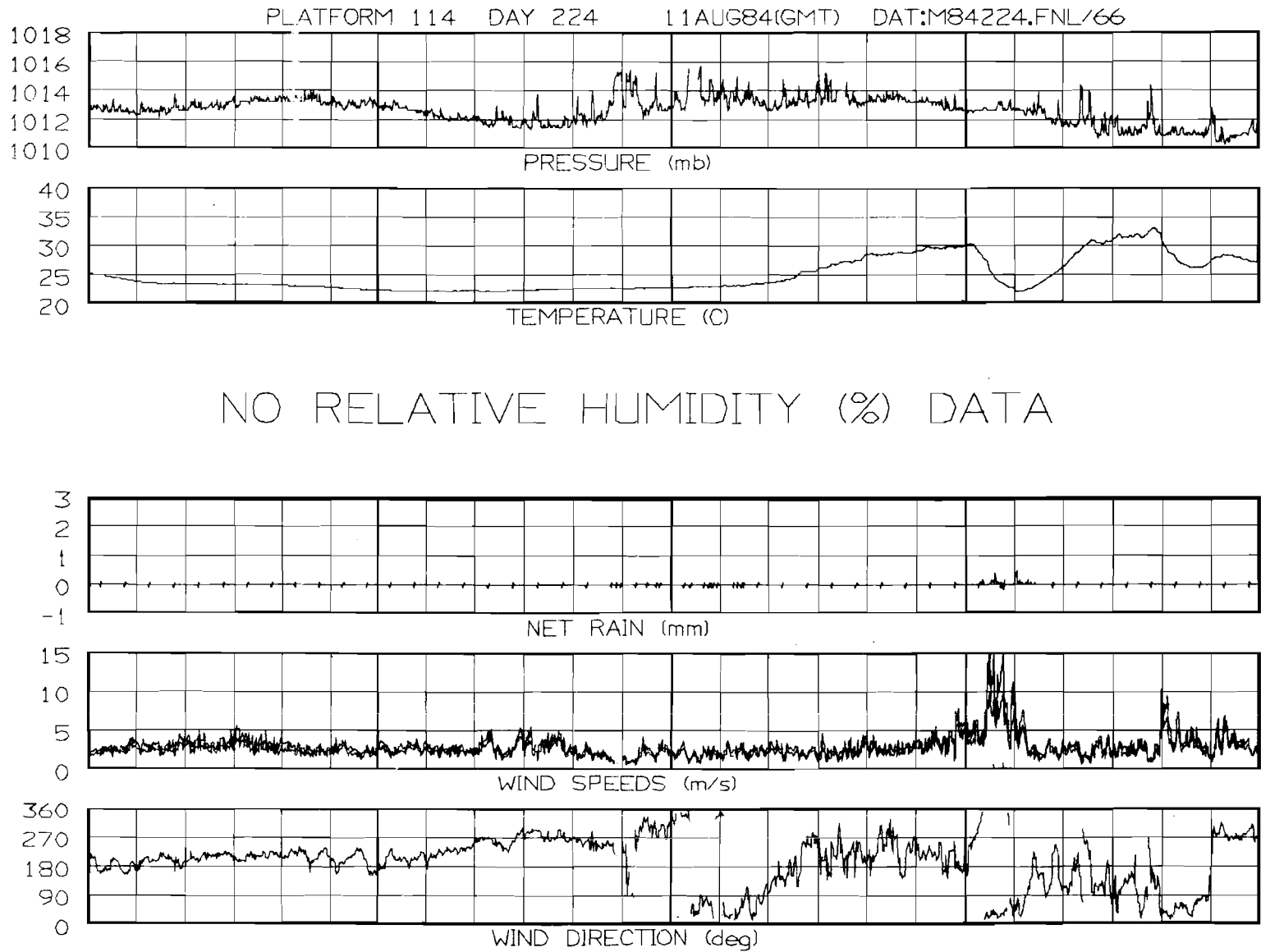
Figure VII-32.   Data from station No. 14 in the FLOWS Memphis mesonet.

PLATFORM 115   DAY 224   11AUG84(GMT)   DAT:M84224.FNL/66

PRESSURE (mb)

TEMPERATURE (C)

NO RELATIVE HUMIDITY (%) DATA

NET RAIN (mm)

WIND SPEEDS (m/s)

WIND DIRECTION (deg)
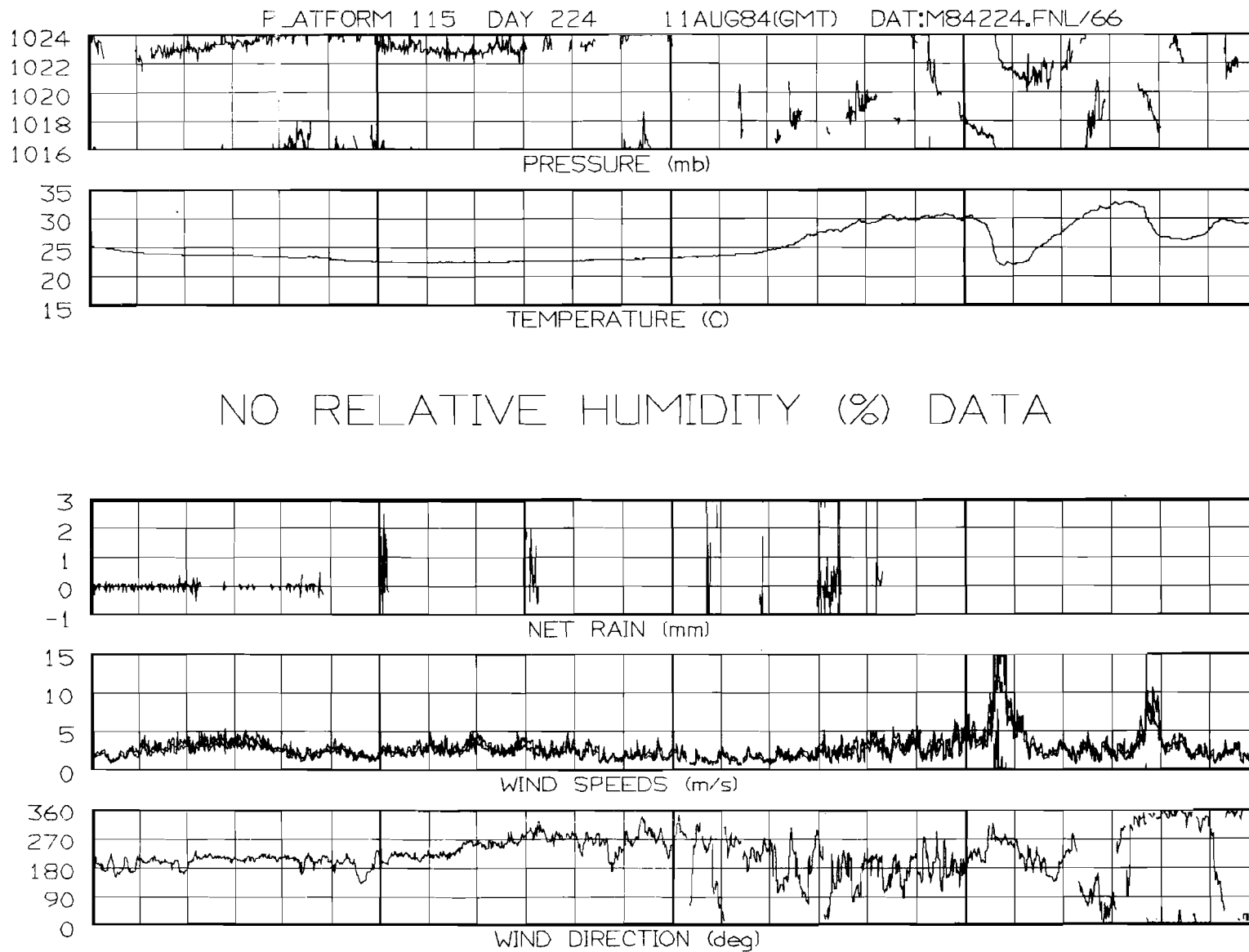
Figure VII-33.   Data from station No. 15 in the FLOWS Memphis mesonet.
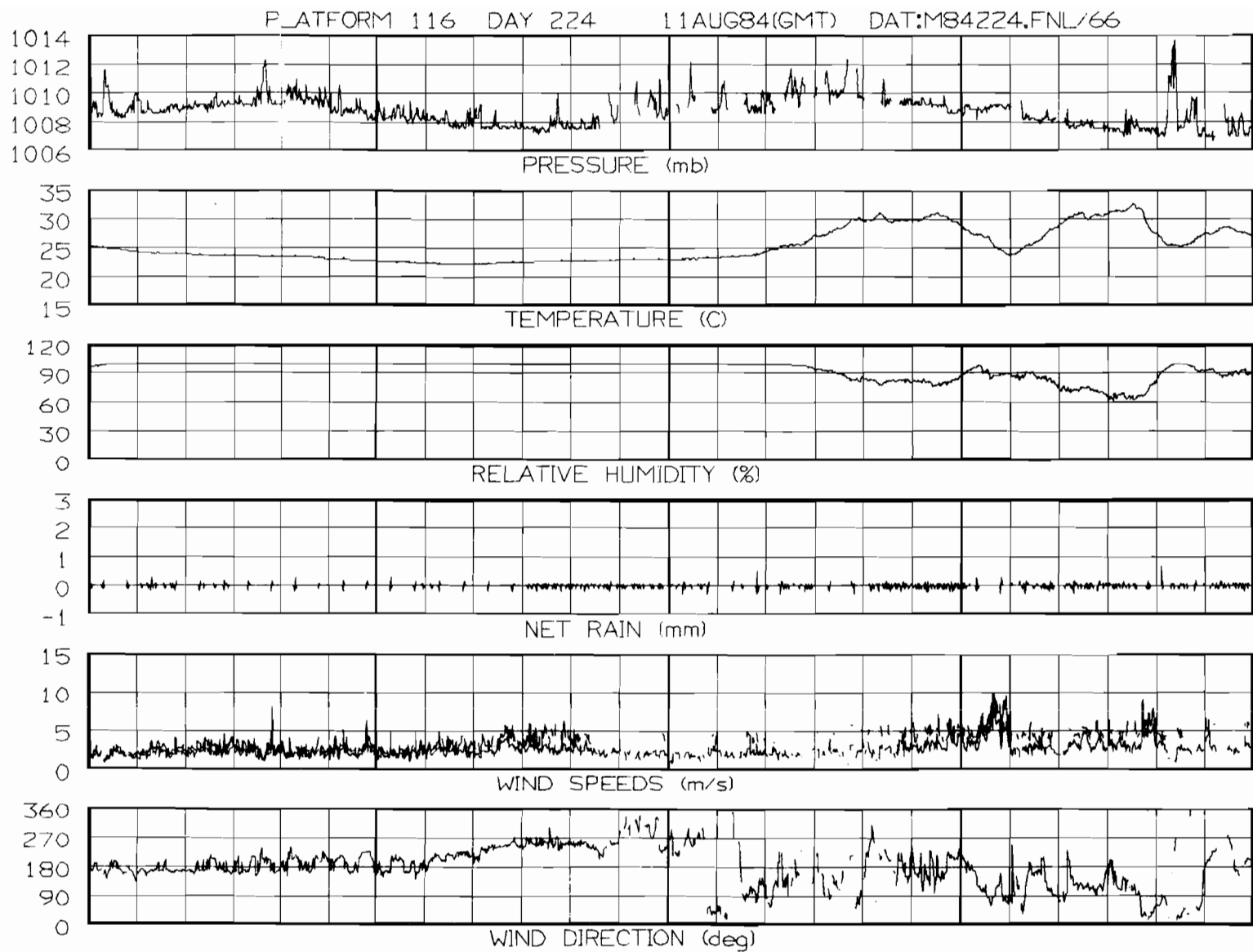
Figure VII-34. Data from station No. 16 in the FLOWS Memphis mesonet.
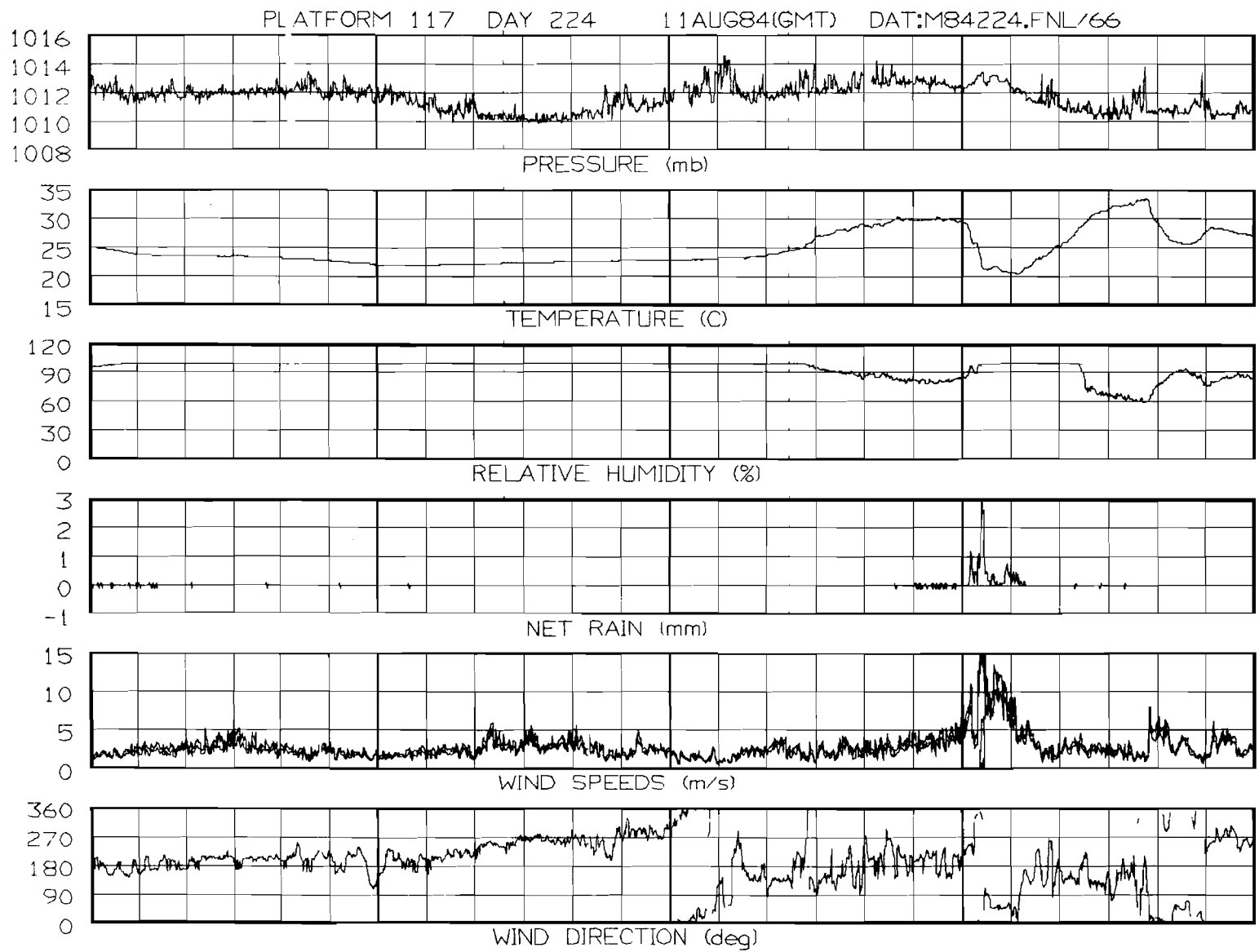
Figure VII-35. Data from station No. 17 in the FLOWS Memphis mesonet.

PLATFORM 118   DAY 224   11AUG84(GMT)   DAT:M84224.FNL/66

PRESSURE (mb)

TEMPERATURE (C)

RELATIVE HUMIDITY (%)

NET RAIN (mm)

WIND SPEEDS (m/s)

WIND DIRECTION (deg)
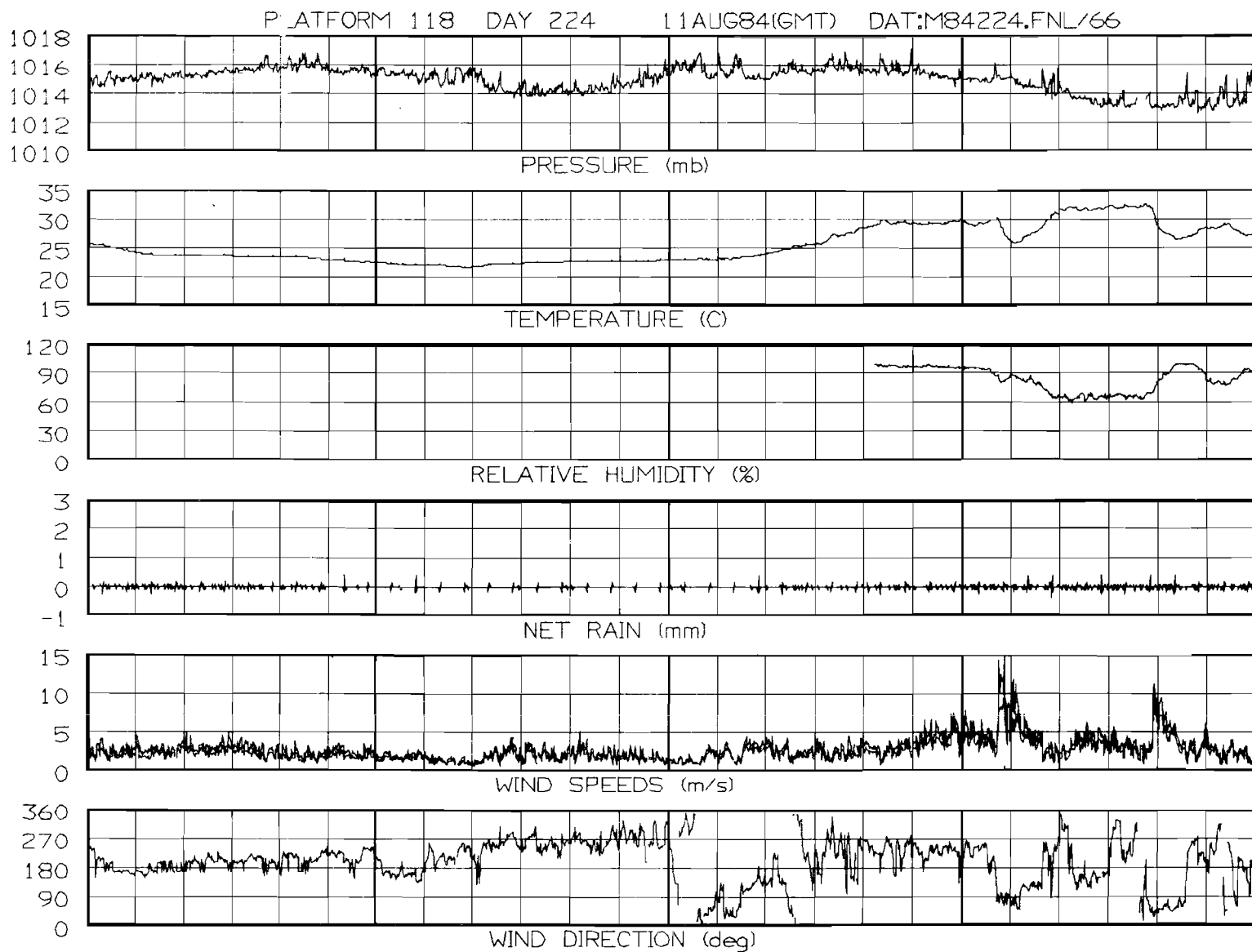
Figure VII-36. Data from station No. 18 in the FLOWS Memphis mesonet.
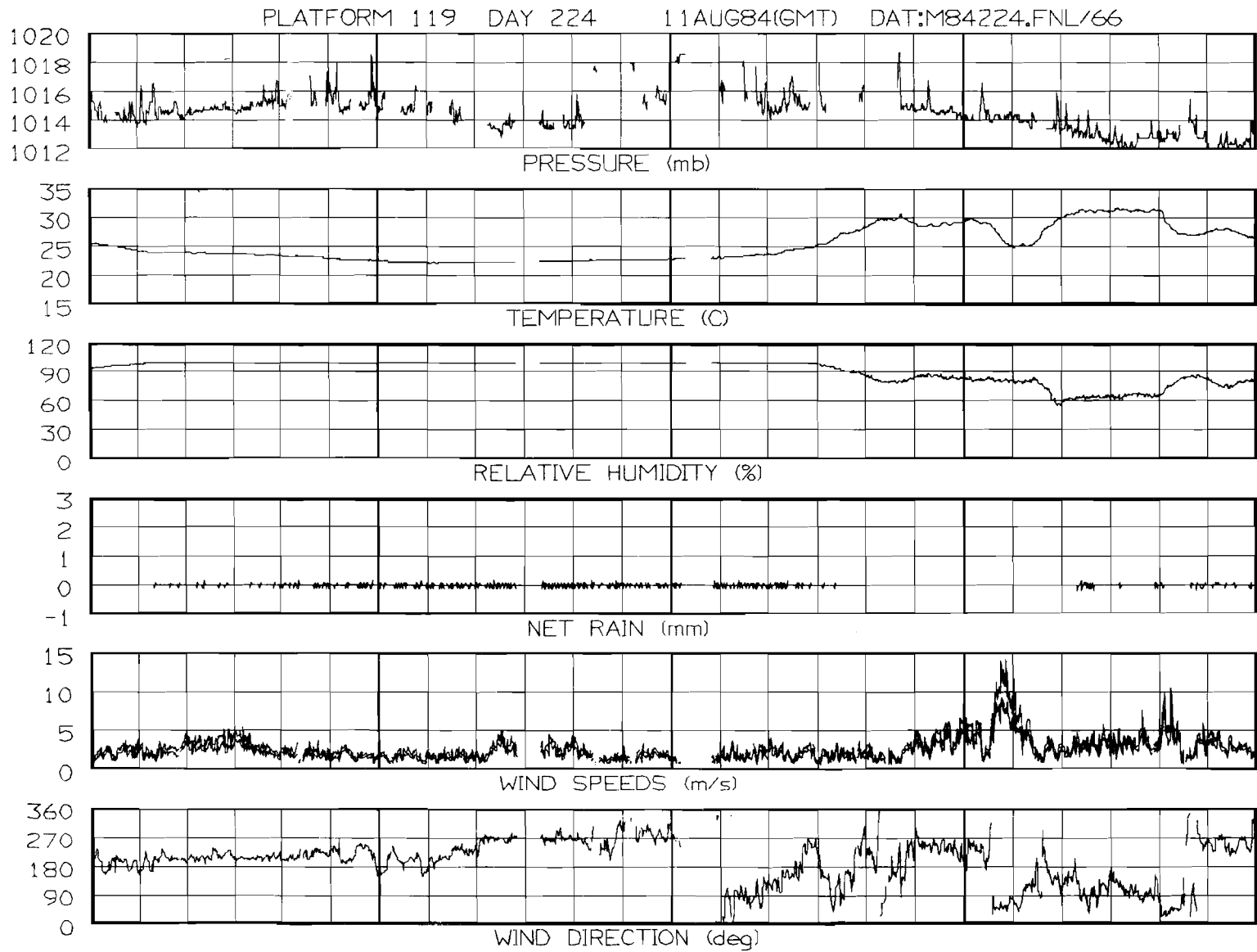
Figure VII-37. Data from station No. 19 in the FLOWS Memphis mesonet.

PLATFORM 120   DAY 224   11AUG84(GMT)   DAT:M84224.FNL/66

PRESSURE (mb)

TEMPERATURE (C)

RELATIVE HUMIDITY (%)

NET RAIN (mm)

WIND SPEEDS (m/s)

WIND DIRECTION (deg)
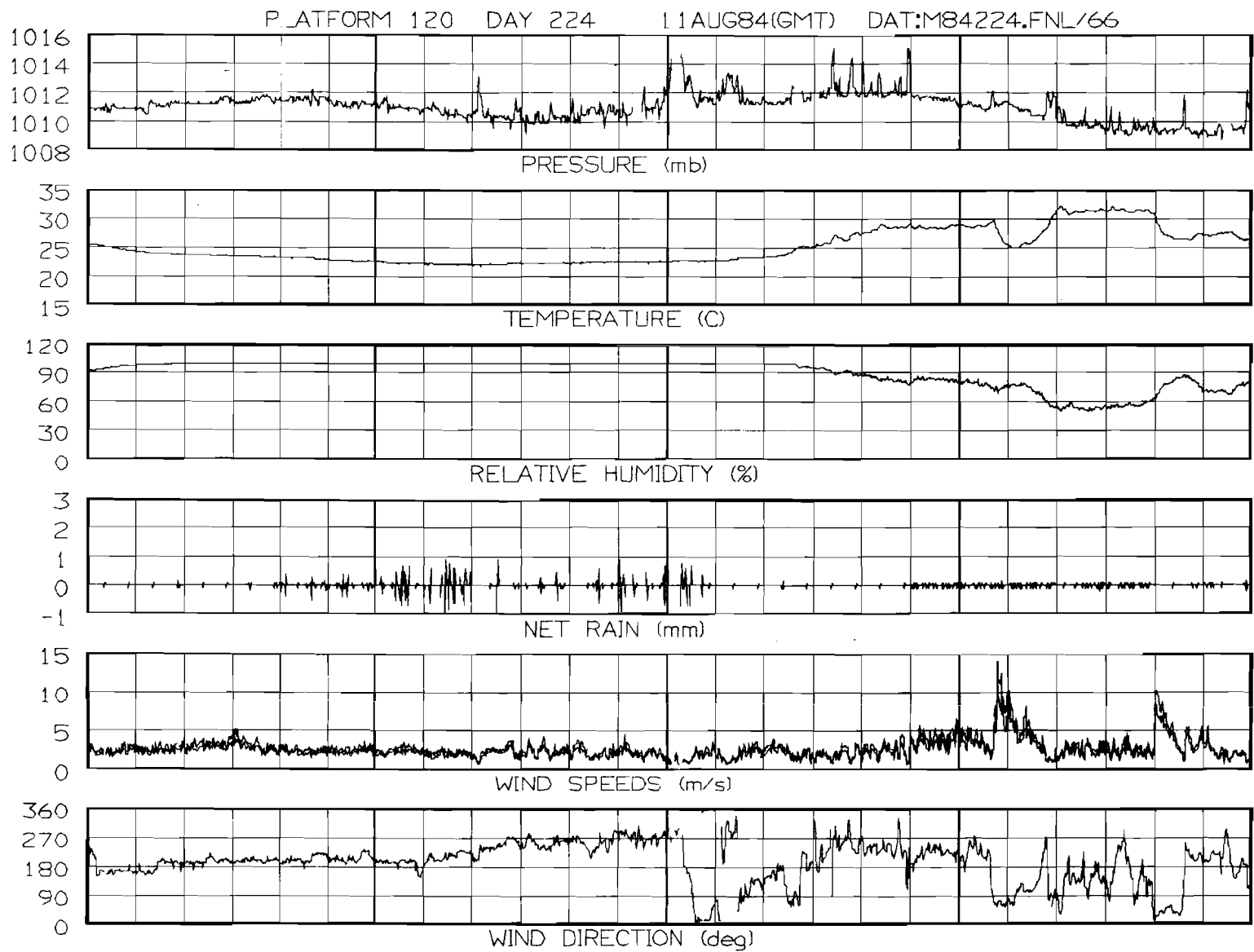
Figure VII-38.   Data from station No. 20 in the FLOWS Memphis mesonet.

PLATFORM 121   DAY 224   11AUG84(GMT)   DAT:M84224.FNL/66
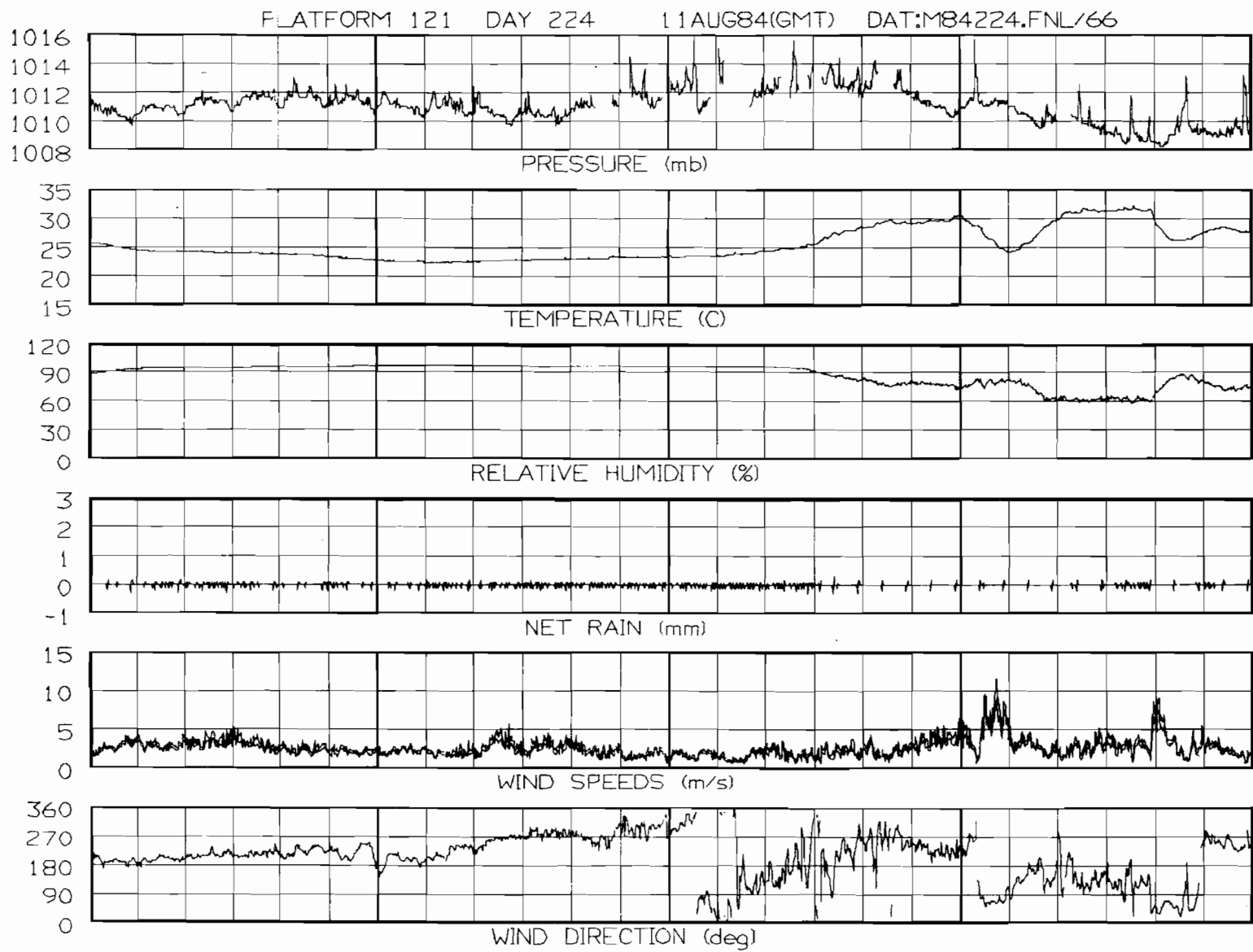
Figure VII-39.   Data from station No. 21 in the FLOWS Memphis mesonet.

PLATFORM 122   DAY 224   11AUG84(GMT)   DAT:M84224.FNL/66

PRESSURE (mb)

TEMPERATURE (C)

RELATIVE HUMIDITY (%)

NO   NET RAIN (mm)   DATA

WIND SPEEDS (m/s)

WIND DIRECTION (deg)
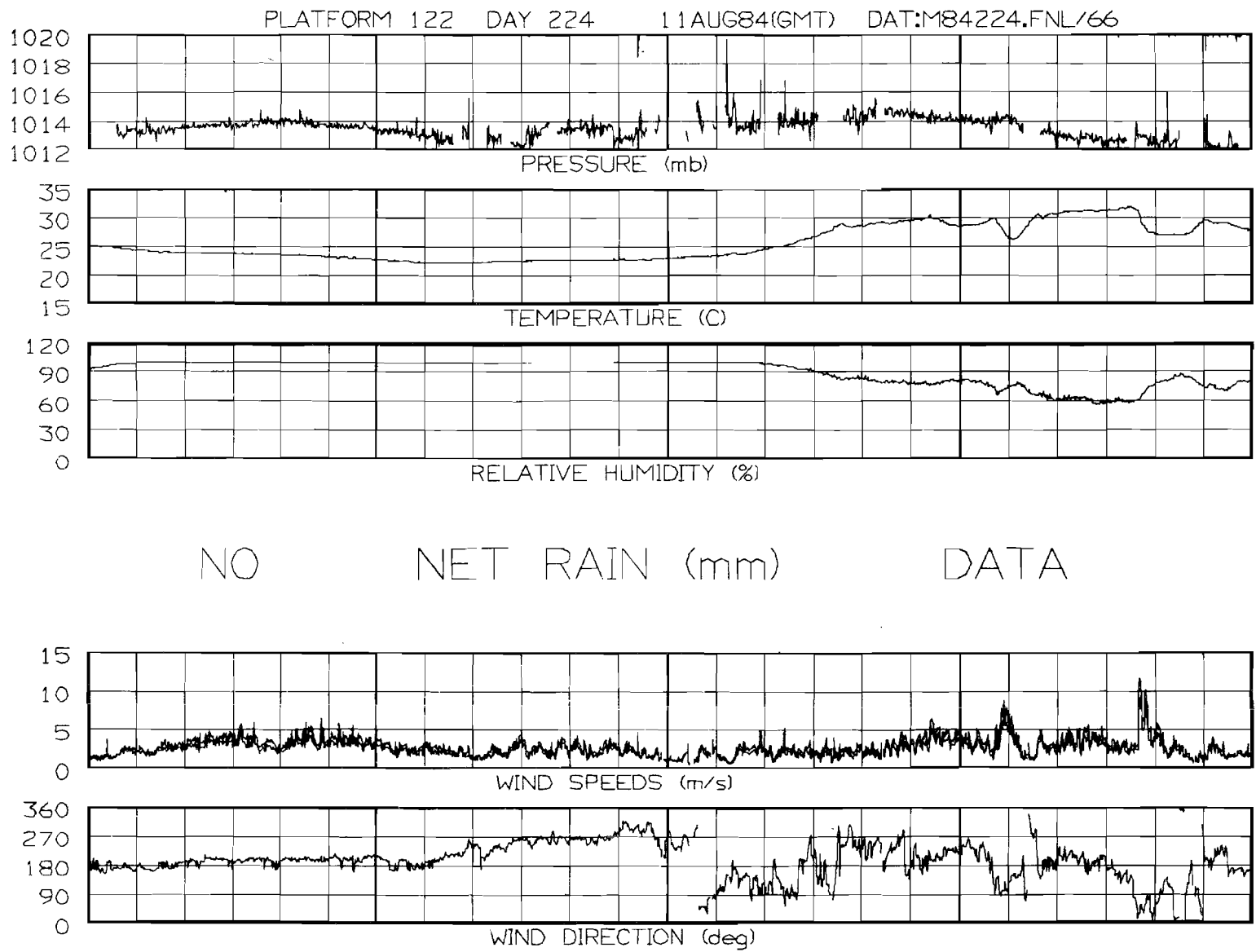
Figure VII-40.   Data from station No. 22 in the FLOWS Memphis mesonet.
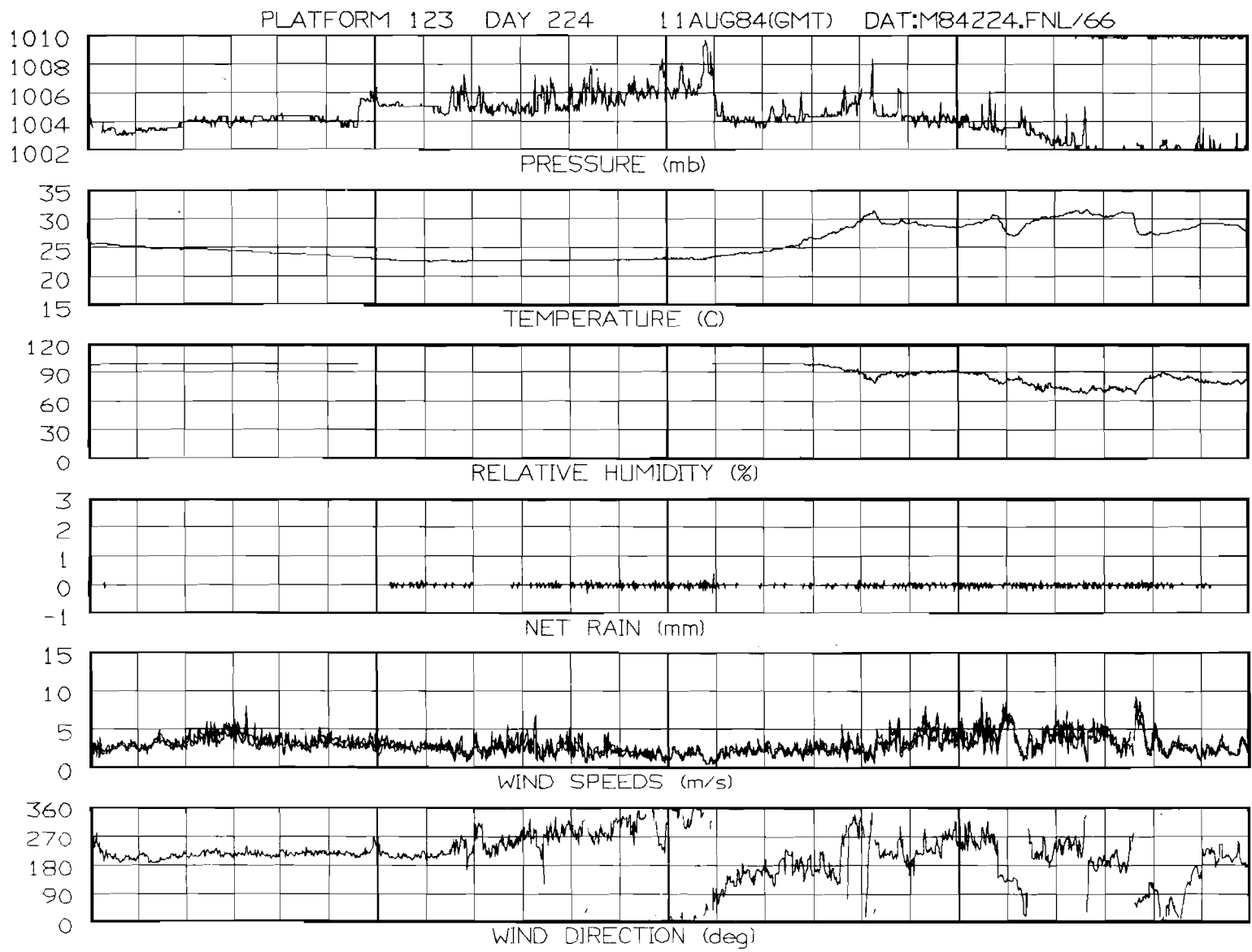
Figure VII-41. Data from station No. 23 in the FLOWS Memphis mesonet.

PLATFORM 124   DAY 224   11AUG84(GMT)   DAT:M84224.FNL/66

PRESSURE (mb)

TEMPERATURE (C)

RELATIVE HUMIDITY (%)

NET RAIN (mm)

WIND SPEEDS (m/s)

WIND DIRECTION (deg)
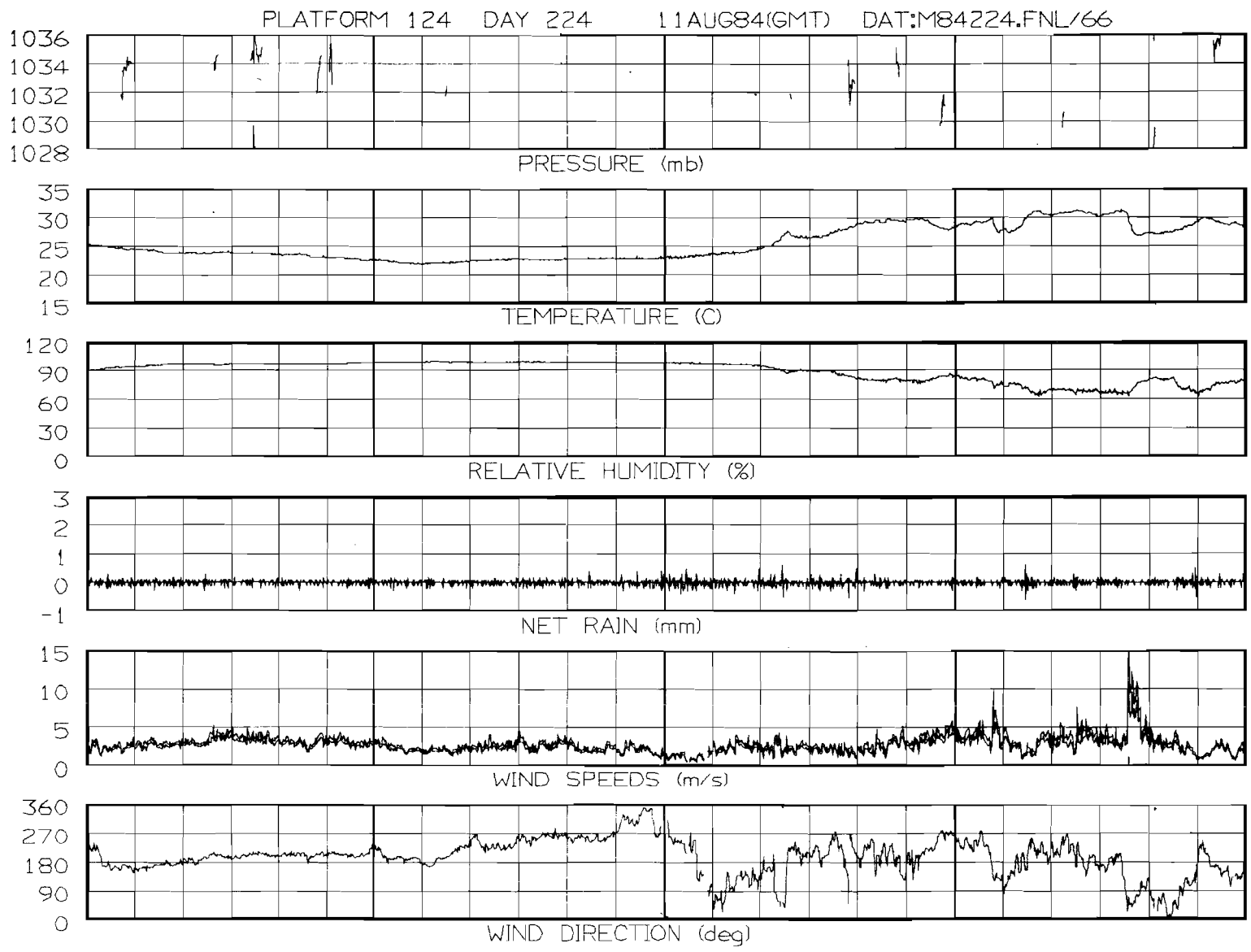
Figure VII-42.   Data from station No. 24 in the FLOWS Memphis mesonet.
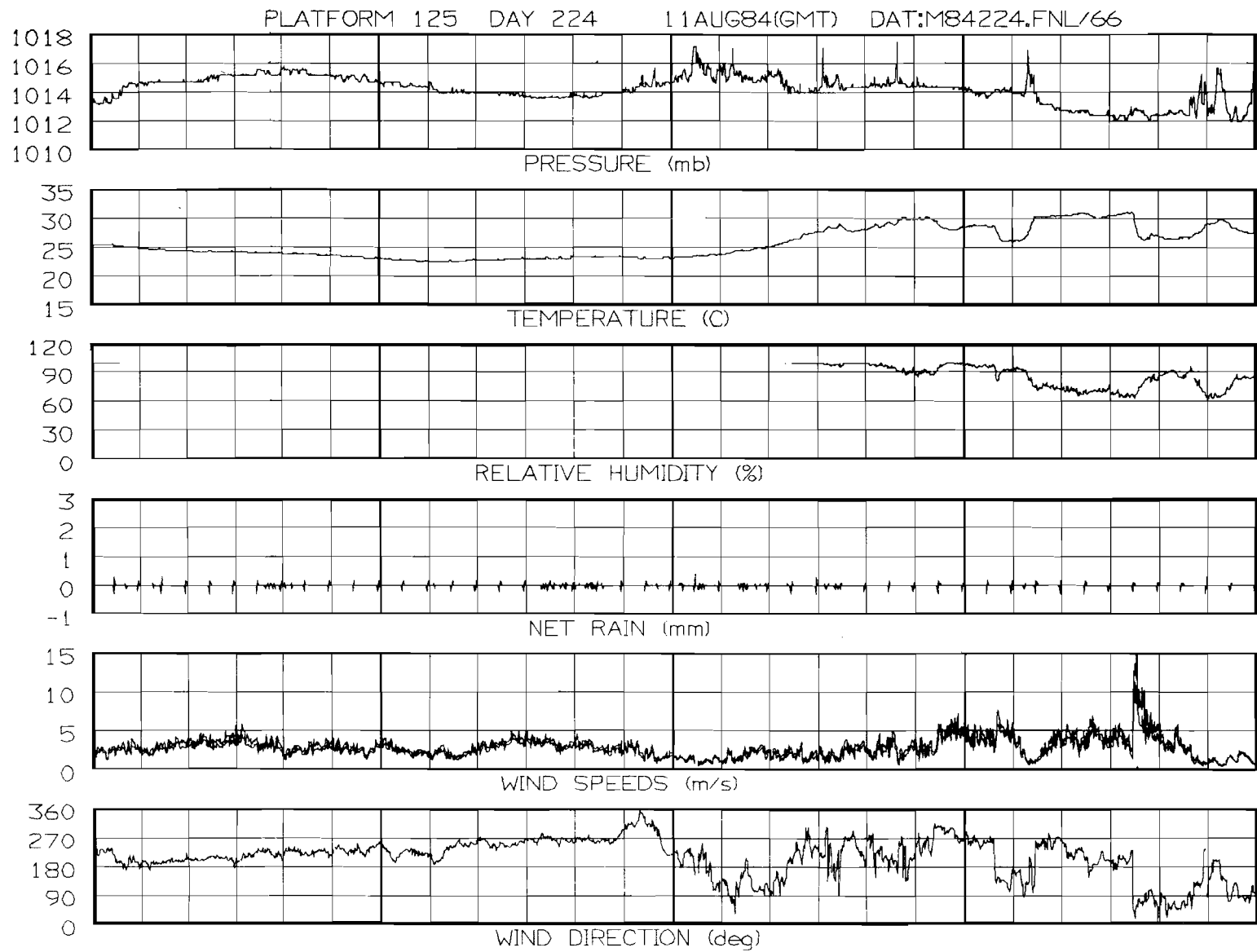
Figure VII-43.   Data from station No. 25 in the FLOWS Memphis mesonet.

b. General Characteristics

In glancing through Figures VII-19 through VII-43, it is immediately apparent that station No. 6 (Figure VII-24) failed to report at all on this day, that the relative humidity probe was non-functional at station No. 15, (Figure VII-33) and that the rain gage was missing at station No. 22 (Figure VII-40). The temperature sensor at station No. 11 (Figure VII-29) was broken, as can be seen by the few scattered data points below 50°C left after the editing. The rain gage at station No. 15 (Figure VII-33) was also malfunctioning. It is also clear that a rainshower accompanied by high winds and relatively cool saturated air impacted the entire network between 1800 and 1900 hours. The analyses presented in Figure VII-17 and VII-18 showed that this shower could be classified as a microburst in its initial stages. Notice the generally fine resolution of the data and the high-frequency atmospheric variations captured, especially in the temperature, humidity, and wind fields. These plots illustrate how essential the 1-minute averaging period is in revealing this variability and how much information would have been lost with the 3-5 minute averaging periods to which the old DCPs were limited.

c. Problems with the Data

In section B.1.b. of this chapter, it was stated that 21% of the pressure data, on the average, was discarded in the editing process and that this was the worst of all the sensors. The pressures shown in the top graphs in Figures VII-19 through VII-43 are what is left after editing, and they are still so poor that little if any use can be made of them. Gaps where the editing has removed wildly varying pressure values appear at a number of times, for example, in Figures VII-25, VII-33, VII-37, and VII-42.

The next thing to notice is that the absolute pressure values differ by 10 to 15 mb, even during the earlier calm part of the day (e.g., compare station No. 23 (Figure VII-41) and station No. 7 (Figure VII-25)). This miscalibration on an absolute scale, however, can be corrected through post data-collection analysis and software calibration. Furthermore, it is often the time variation of the pressure field that is of key meteorological interest. But in this data the noise signal is so contaminating that even after filtering, derivatives on the 1-minute or even 5-minute timescale could not be trusted.

The noise inherent in the sensor output signal is amplified by a factor of 100 along with the signal itself before it is sampled and digitized. It should be emphasized that simply by increasing the barometer excitation voltage from 5V to 9V, the true signal became enough greater than the noise that most of the noise in the digitized output disappeared. Another source of noise became immediately apparent when the higher voltage was used; a sort of "cross-talk" was occurring in the DCP between the anemometer and barometer signals so that when the wind speed was low, the pressure was noisy and as the winds picked up, the barometer noise level died down. This was fixed by changing the input port configuration on the DCP. The
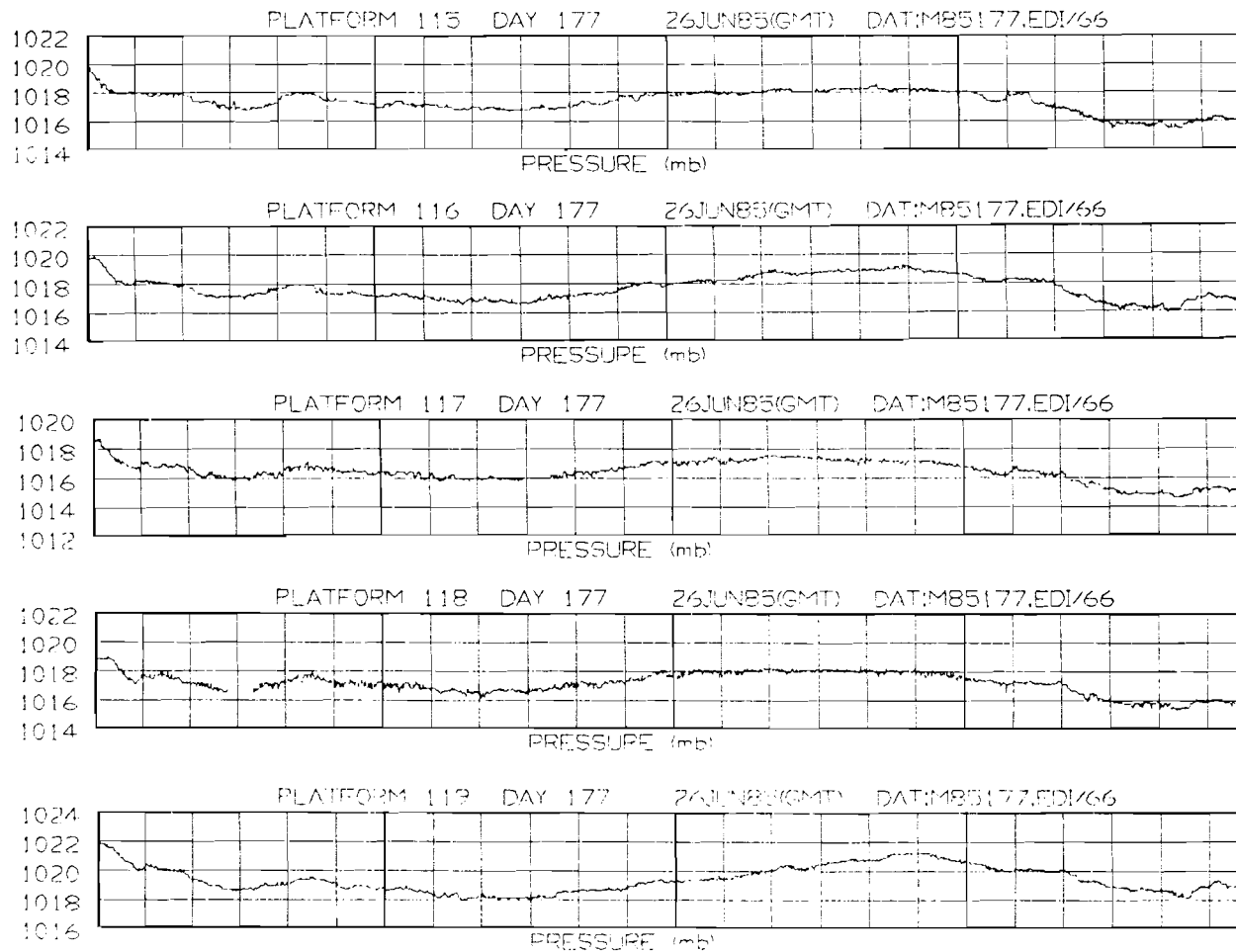
Figure VII-44. Pressure traces from 5 stations (Nos. 15-19) on
26 June 1985 (GMT). The signals are far less noisy for all stations in
1985 than they were in 1984 because of the increase in barometer excitation
voltage from 5V to 9V.

9V excitation voltage was used beginning in February 1985 and, as can be seen in Figure VII-44, the pressure time series traces became much more solid. Thus only the data collected in 1984 and early 1985 are excessively contaminated by noise.

Erratic fluctuations in the pressure field are also created when the heaters are activated. These spurious spikes are more evident in the data from some stations (e.g., Nos. 1, 7, 9, etc.) than from others (e.g., Nos. 3, 5 and 10). Occasionally, though, a believable mesoscale pressure signature does appear. The 1-hour local pressure rise at station No. 13 between 1800 and 1900 hours (Figure VII-31) superimposed on a 6-hour trend of falling pressure and occuring with very heavy rain and high winds is an example of this.

The temperature data are of high quality and consistently calibrated (to within 1°C) at every station except No. 11, where the sensor was broken. The two-element thermistor is a very stable sensor. The sensitivity of the relative humidity sensor is apparent when the data are below 100%, but because of the mathematical correction applied to compensate for the original miscalibration, the data occasionally appear artificially capped at 100% (e.g., Figure VII-25, 1830-2000 hours). Also, some probes such as the one at station No. 8 (Figure VII-26) stopped working under saturation conditions, but the assumption of saturation can be used in place of the missing data in specific analyses.

The rain rate (net rain) data for that same station (Figure VII-26) show a "glitch" every 30 minutes of a loss and then gain of 0.1 mm. This is an artifact of the nearly one minute-long satellite transmissions made for this station at 8 and 38 minutes after every hour, and is present to some degree in the data from each of the sensors. During the transmission minute, the sensor sampling function ceases as the other DCP activity monopolizes the control module. The sensor sampling requests are collected and executed in rapid succession when the transmission is completed, creating variability in the 1-minute averaged data values. A noise level of ±0.1 mm in the rain gage data is, however, the rule rather than the exception, and at some stations such as No. 12 (Figure VII-30) the noise level is even higher. High gusty winds often create noise in the rain gage data.

Anemometers at station Nos. 4 and 16 exhibited the peak wind speed chatter problem during light wind conditions on this day, but the algorithm has successfully eliminated most of these points (see Figures VII-22 and VII-34). Otherwise the anemometer data are very good.

The main problem with the wind vane data is the loss of resolution near 180° and 360° (see IV.A.3). It is barely evident at some stations while at others it is evidenced by wide oscillations in direction around these angles (see station No. 10 (Figure VII-28) during the first 6 hours). When the vanes move through 360°, it appears as if data are missing; this is simply an artifact of the plotting and is done because connecting the points would mean drawing full-scale vertical lines that would obscure the actual data values.

C. Conclusions

The 1984 performance of the FLOWS automatic weather station network has been evaluated. Many data quality problems, such as absolute scale calibrations, were evident that can be corrected through post-data collection analysis and recalibration. Other problems, such as the relative humidity sensor miscalibration, the large noise component in the barometer signal, and the wind direction loss of resolution near 180° and 360°, had been corrected before the sensors were redeployed in 1985. It is recommended that detailed performance analysis of the 1985 dataset be given a high priority before the 1986 network deployment gets underway, both to derive software corrections for the 1985 data and to expose any additional problems that could be easily corrected before the 1986 data collection operation begins.

The operational reliability of the FLOWS weather station network was near 98% for raw data collection and recording, a level considered quite acceptable for further use. One easy way to improve this level is to have about six spares of each of the sensors in good condition at the start of the 1986 data collection period. When raw data were not recorded, it was usually because spare sensors were not available for installation, not because the field personnel were unaware of the problems. Delivery of sensors can often take 4-8 weeks after the order has been placed, so advance planning is essential.

VIII. DETERMINATION OF A WIND SHEAR EVENT OVER THE NETWORK

Once the mesonet data have been received at Lincoln Laboratory and converted to common format, they are inventoried and plotted for immediate system performance analysis. From this initial look at the data and from the FLOWS field log reports, the days on which wind shear events may have occurred over the mesonet are determined. Several steps, involving both objective and subjective analysis, are then taken to confirm and classify the event(s).

To illustrate this procedure, the data collected on 26 June 1985, a day on which more than one wind shear event impacted the network within a short period of time, are examined in some detail. It is shown through this analysis exactly how the various forms of data, both synoptic scale (large scale) and mesoscale (approximate scale of the FLOWS weather station network), are used to decide first if, and then what type(s), of wind shear event(s) occurred.

A. Overview of the 24-hour Weather Situation

Analysis of the synoptic scale NWS surface weather maps for 26 June 1985 revealed the presence of a slow moving cold front which stretched from Minnesota south-southwestward through western Texas. A warm front extended from the cold front in Minnesota, south-southeastward into North Carolina. Western Tennessee and the surrounding mid-southern states remained free of any frontal storms during the day. However, GOES satellite imagery showed scattered convection that began to develop by 1830 GMT (all times in GMT) over Arkansas, southwestern Tennessee, and northern and eastern Mississippi. This airmass convection was apparently triggered by a combination of surface heating and an observed perterbation in the upper levels of the atmosphere.

It will be shown in the following sections of this chapter how these convective events of the 26th affected the FLOWS weather station network. First, the 24-hour time series plots of mesonet and LLWAS (winds only) data are analyzed to give a quick look at the weather situation over the network during the entire day. This helps to identify the specific time periods in which possible wind shear events occurred, and in which more detailed, mesoscale analyses should be performed.

1. Analyzing the Mesonet 24-hour Time Series Plots

The 24-hour time series plots were analyzed to see if any perturbations in the various fields which might point to a shear event were present. Microbursts and gust fronts are the two types of wind shear events of main concern. The microburst signature, as defined by the characteristic changes in the surface meteorological parameters during the NIMROD and JAWS projects, was very complicated. During these microbursts, both increases and decreases were observed in air temperature, dew point

temperature, relative humidity, and surface pressure (Fujita, 1985). However, during the 1984 FLOWS program, the majority of the microbursts were characterized by decreases in temperature and dew-point and increases in the relative humidity. These signatures, as seen from the 1984 data set in Memphis, were used as guidance during 1985. The typical surface wind signatures for both the microburst and gust front were described in Chapter VI.

Figure VIII-1 shows the 24-hour plot for mesonet station No. 1 (platform 101) on 26 June 1985*. The wind field was rather unperturbed for the first three quarters of the day until shortly after 1900. After that time, the wind sharply increased to approximately 10 m/s and stayed anomalously high for about 40 minutes. The temperature field depicted a steady fall from 31°C to 25°C within a 30 minute time span, and the relative humidity rose by 15%. From these traces, a preliminary assessment of this event would suggest that a gust front passed over the site. The main reasoning behind this was the slow recovery of the high peak winds.

The meteorological traces for mesonet station Nos. 2 and 3 resembled those for station No. 1 in their overall pattern, except that the magnitude of the relative humidity trace for station No. 2 was greater. Station No. 4 (Figure VIII-2) showed two separate wind events. The first appeared at approximately 0015 and was accompanied by precipitation (see the rain rate trace) and a pressure fall. The second was at 1915 and was probably related to the same event that affected station Nos. 1-3. Both events, as seen by station No. 4, were relatively weak (<10 m/s), and neither would qualify as microbursts when compared with Fujita's definition (Fujita, 1985).

Station No. 6 (Figure VIII-3) showed a sharp drop in temperature, some precipitation, and an increase in the wind speed between 1900 and 2000 hours. The wind direction shifted abruptly from south to northwest during the onset of this event and then remained out of the northwest through the duration of the event. The sharp rise in wind speed was observed to have occurred approximately 8-10 minutes later than the similar rise at station No. 1. This suggested that the possible gust front (as evidenced by the signature at station No. 1 and also station No. 6) was moving southward across the eastern portion of the network. To ultimately determine the classification of this event, the surrounding stations had to be investigated (both individually and as a network).

---

*The 1985 FLOWS automatic weather station network is configured such that stations with lower numbers are mainly toward the east end and those with higher numbers, toward the west (see Fig. II-9). Mesonet station Nos. 22-25 and the LLWAS stations surround the Memphis International Airport.

PLATFORM 101   DAY 177   26JUN85(GMT)   DAT:M85177.RAW/17

PRESSURE (mb)

TEMPERATURE (C)

RELATIVE HUMIDITY (%)

NET RAIN (mm)

WIND SPEEDS (m/s)

WIND DIRECTION (deg)

8-3
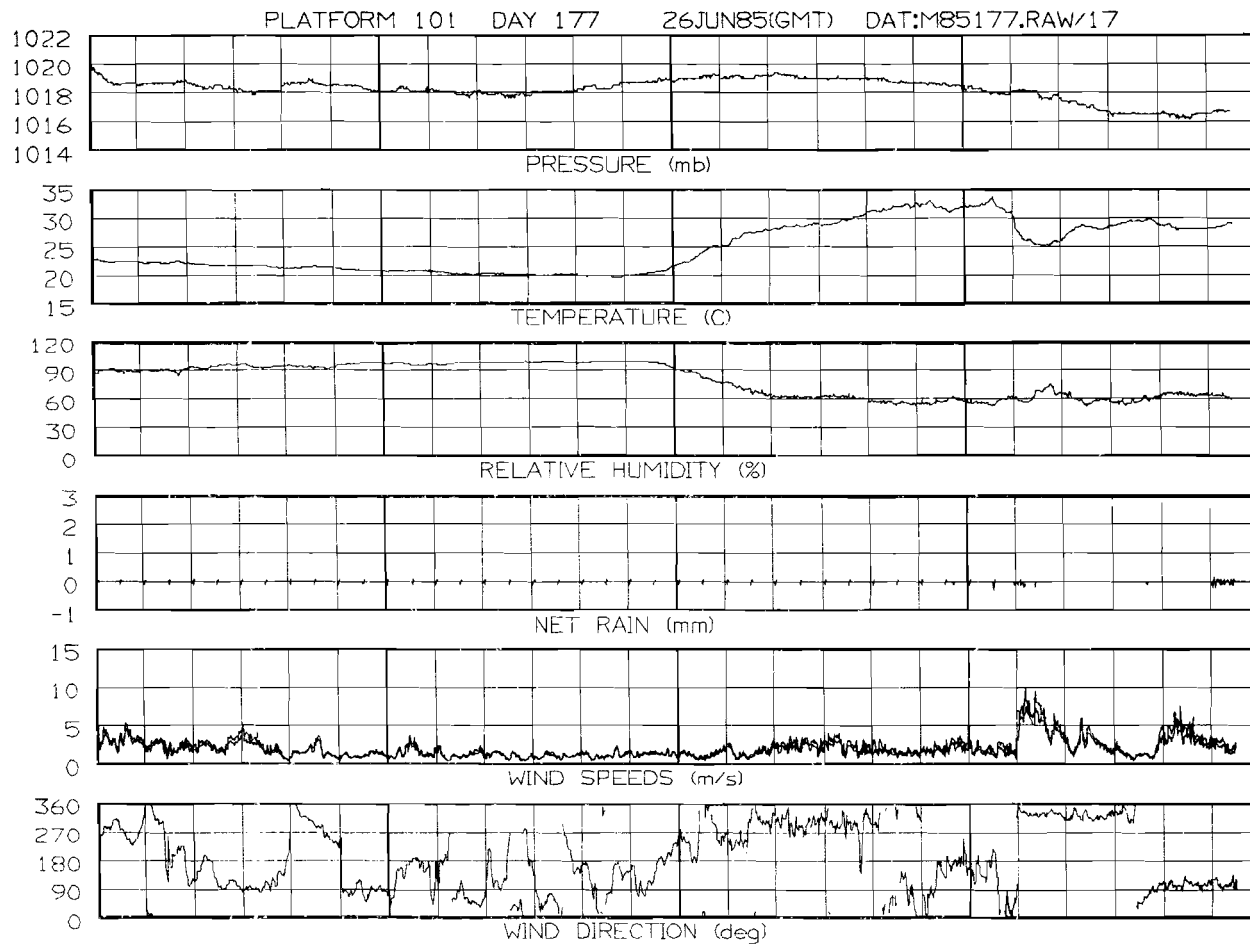
Figure VIII-1.   24-hour time series plot for mesonet station No. 1 on June 26, 1985.
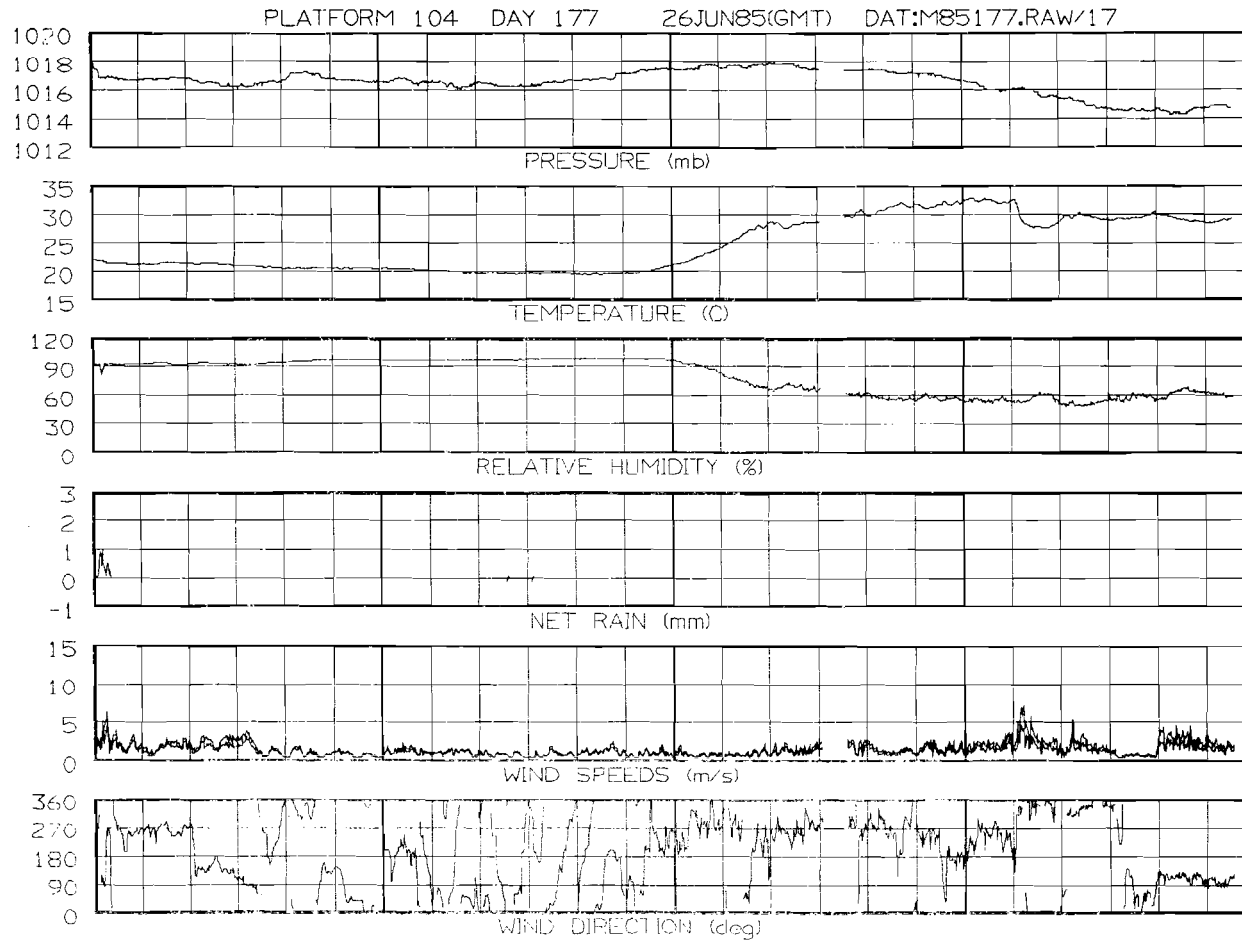
Figure VIII-2. 24-hour time series plot for mesonet station No. 4 on June 26, 1985.

PLATFORM 106   DAY 177   26JUN85(GMT)   DAT:M85177.RAW/17

PRESSURE (mb)

TEMPERATURE (C)

RELATIVE HUMIDITY (%)

NET RAIN (mm)

WIND SPEEDS (m/s)

WIND DIRECTION (deg)
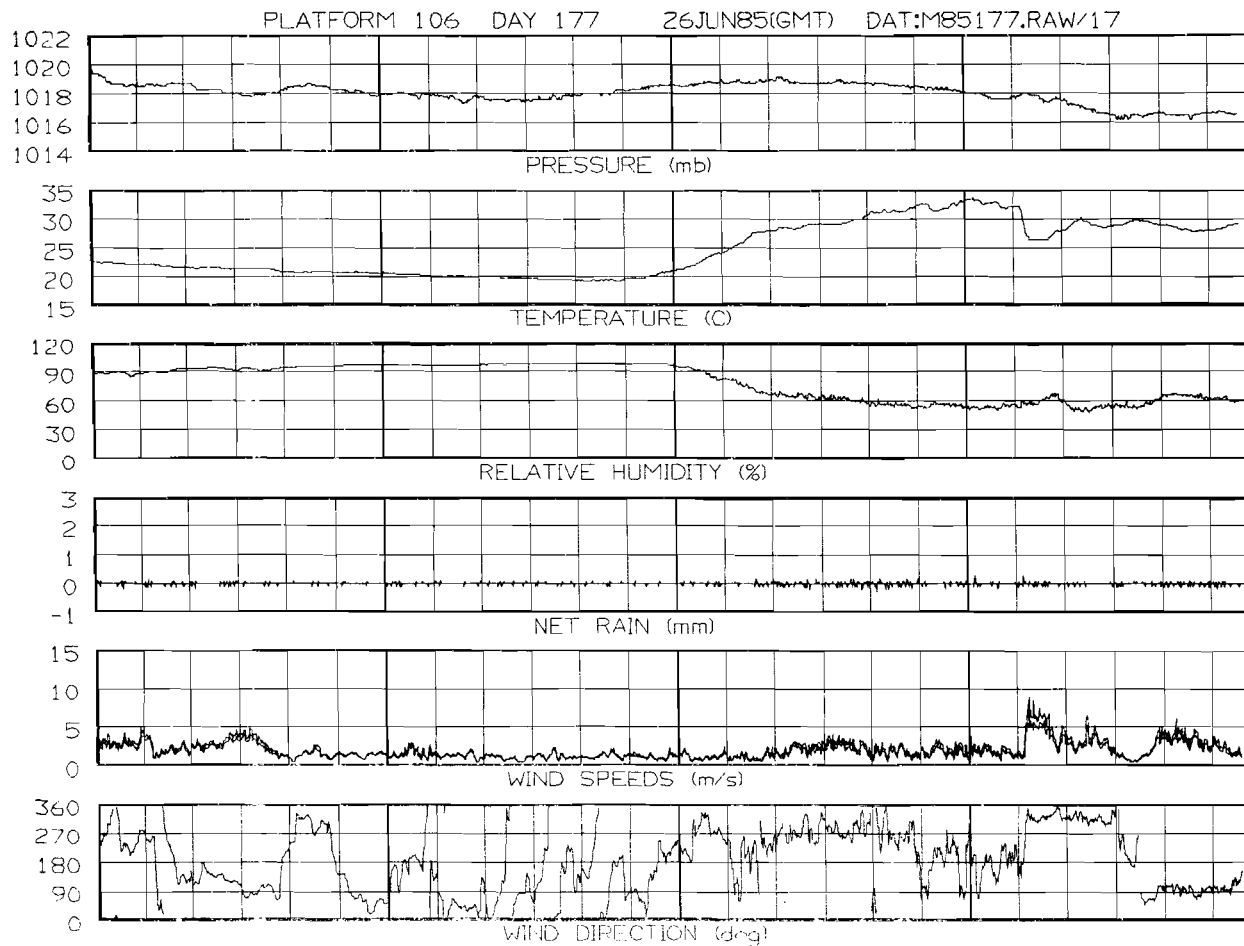
Figure VIII-3.   24-hour time series plot for mesonet station No. 6 on
June 26, 1985.

Mesonet station Nos. 7 and 8 also identified a wind event between 1900 and 2000 hours. The traces for these stations showed tendencies similar to those for stations Nos. 1-6 during the same time period. Now station No. 9, in Figure VIII-4, depicted only a slight perturbation in the wind speed field, but showed a 5°C drop in the temperature field at 1900. It was evident that microburst winds did not affect this station but that the event itself, which affected most of the mesonet's eastern portion, did manage to impact station No. 9.

Station No. 10 (Figure VIII-5) showed the strongest wind speed peak to be 15 m/s shortly after 1900. Precipitation was falling and the temperature fell 10°C within 20 minutes. The wind direction was from the north-northeast during the peak of the event. The strongest perturbations in the wind and temperature over the eastern half of the mesonet were observed at station No. 10. With the wind direction being from the north, it was obvious that the center of this weather event was north of the mesonet but closest to station No. 10. The pattern of the wind speed trace for the 15-30 minute period centered about the peak, which occurred shortly after 1900, resembled that of a typical microburst (Fujita, 1985).

Stations Nos. 11-13 showed minor perturbations in the wind and temperature fields at 1900, while station No. 15 in Figure VIII-6 recorded a sharp peak of 12.5 m/s at approximately 1930. Station No. 15 also exhibited wind speed "chatter" (see III.A.1.b.iii), or spurious peak winds, as evidenced by the wind speed trace. While obvious to an analyst, these spikes, if not filtered out, could cause false alarms to be triggered by an automatic microburst detection algorithm. Station Nos. 16-21 showed no evidence of high winds.

Shortly before 2000 hours, mesonet station Nos. 22 and 23, which are situated at the Memphis International Airport, recorded peak winds of 18.0 and 20.5 m/s, respectively (see Figures VIII-7 and VIII-8). Sharp temperature drops along with precipitation were also noted. Station No. 22 recorded a slight pressure rise which may indicate the close proximity to a microburst center (Fujita, 1985). Station Nos. 24 and 25 (Figures VIII-9 and VIII-10) depicted similar traces, although their wind peaks were weaker (but still greater than 10 m/s). The remaining mesonet stations (Nos. 26-30) showed only minor perturbations in the wind and temperature fields during this same time period.

So, according to the 24-hour time series plots for station Nos. 1-30, there appeared to be two weather events accompanied by significant surface wind shear. Most stations were affected by the events in some way or another, although station Nos. 1,7,10,15 and 22-25 were the only ones to record peak winds greater than 10 m/s. The strongest event of the day, according to these stations, occurred over the Memphis International Airport.

PLATFORM 109   DAY 177   26JUN85(GMT)   DAT:M85177.RAW/17

PRESSURE (mb)

TEMPERATURE (C)

RELATIVE HUMIDITY (%)

NET RAIN (mm)

WIND SPEEDS (m/s)

WIND DIRECTION (deg)
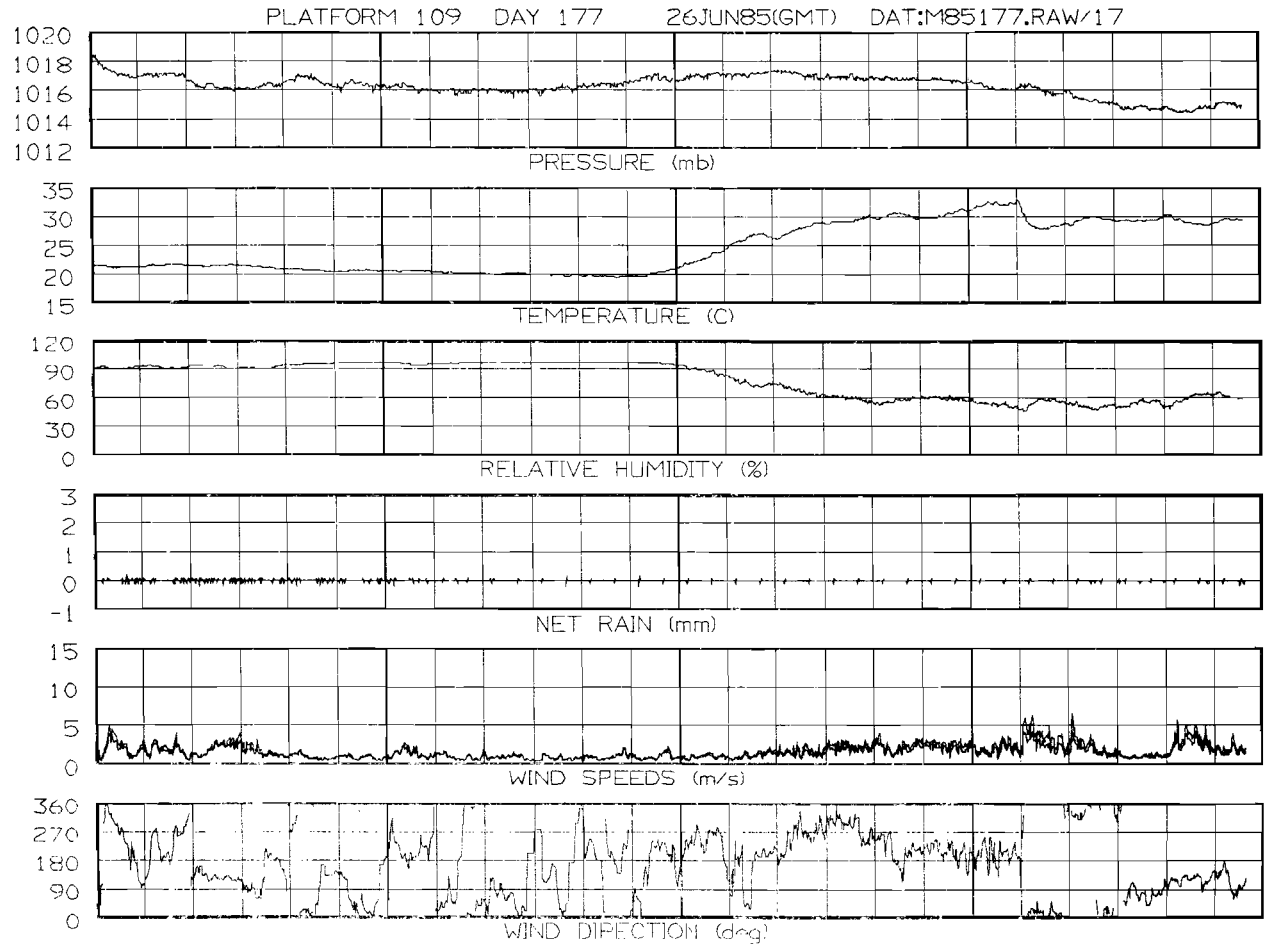
Figure VIII-4.   24-hour time series plot for mesonet station No. 9 on
June 26, 1985.

PLATFORM 110   DAY 177   26JUN85(GMT)   DAT:M85177.RAW/17

PRESSURE (mb)

TEMPERATURE (C)

RELATIVE HUMIDITY (%)

NET RAIN (mm)

WIND SPEEDS (m/s)

WIND DIRECTION (deg)
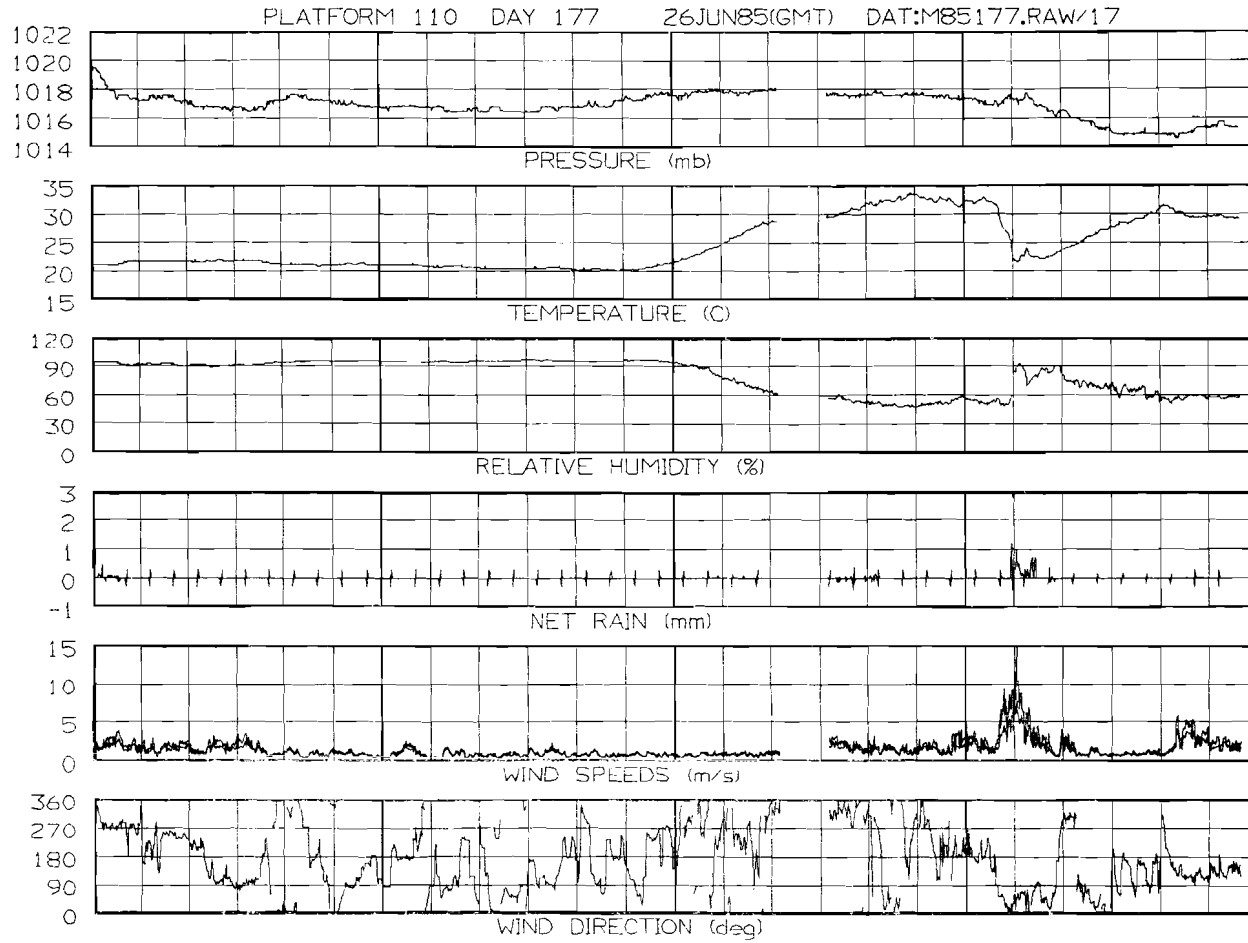
Figure VIII-5.   24-hour time series plot for mesonet station No. 10 on June 26, 1985.

PLATFORM 115   DAY 177   26JUN85(GMT)   DAT:M85177.RAW/17

PRESSURE (mb)

TEMPERATURE (C)

RELATIVE HUMIDITY (%)

NET RAIN (mm)

WIND SPEEDS (m/s)

WIND DIRECTION (deg)
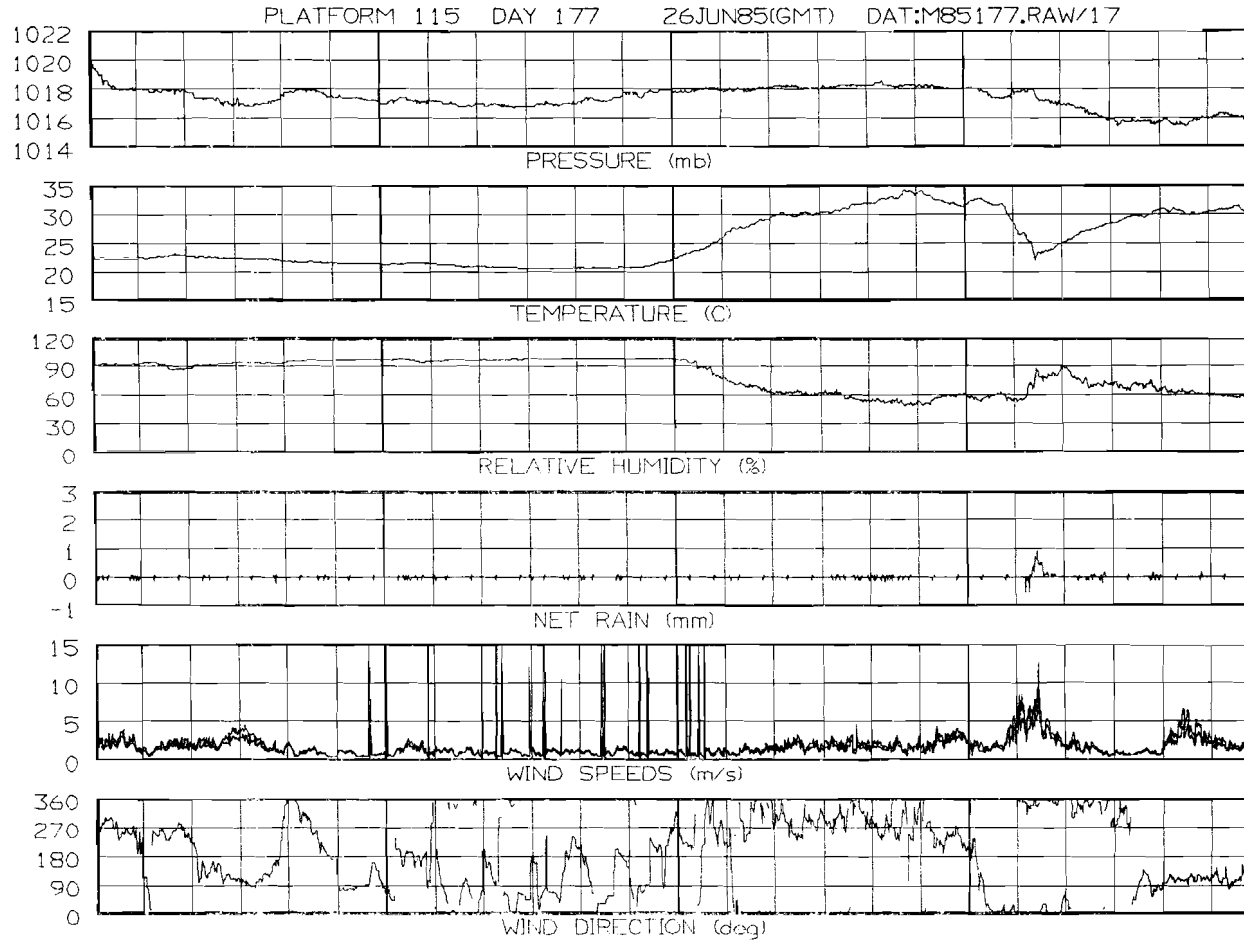
Figure VIII-6.   24-hour time series plot for mesonet station No. 15 on June 26, 1985.

PLATFORM 122   DAY 177   26JUN85(GMT)   DAT:M85177.RAW/17

PRESSURE (mb)

TEMPERATURE (C)

RELATIVE HUMIDITY (%)

NET RAIN (mm)

WIND SPEEDS (m/s)

WIND DIRECTION (deg)
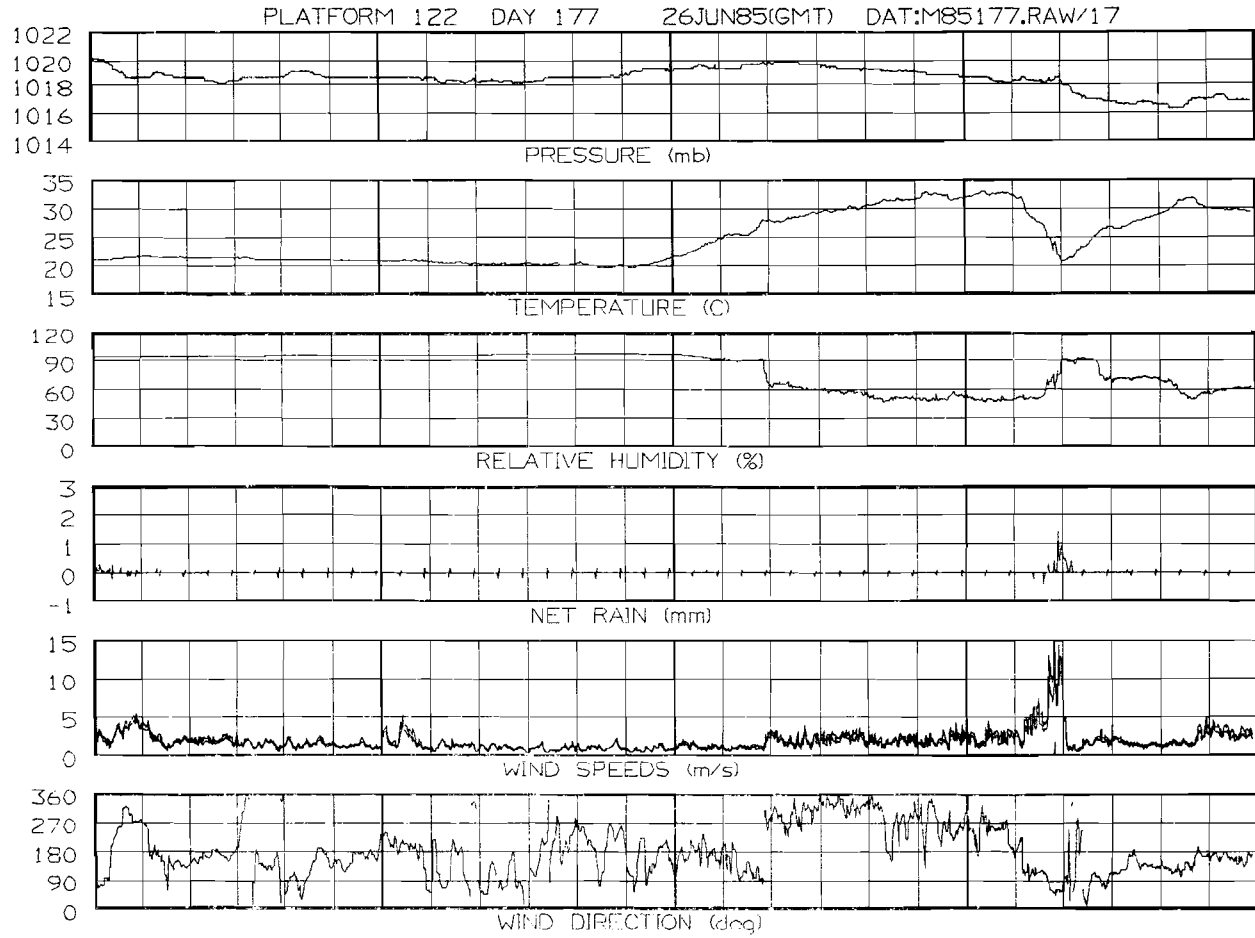
Figure VIII-7.   24-hour time series plot for mesonet station No. 22 on June 26, 1985.

PLATFORM 123 DAY 177   26JUN85(GMT)   DAT:M85177.RAW/17

PRESSURE (mb)

TEMPERATURE (C)

RELATIVE HUMIDITY (%)

NET RAIN (mm)

WIND SPEEDS (m/s)

WIND DIRECTION (deg)
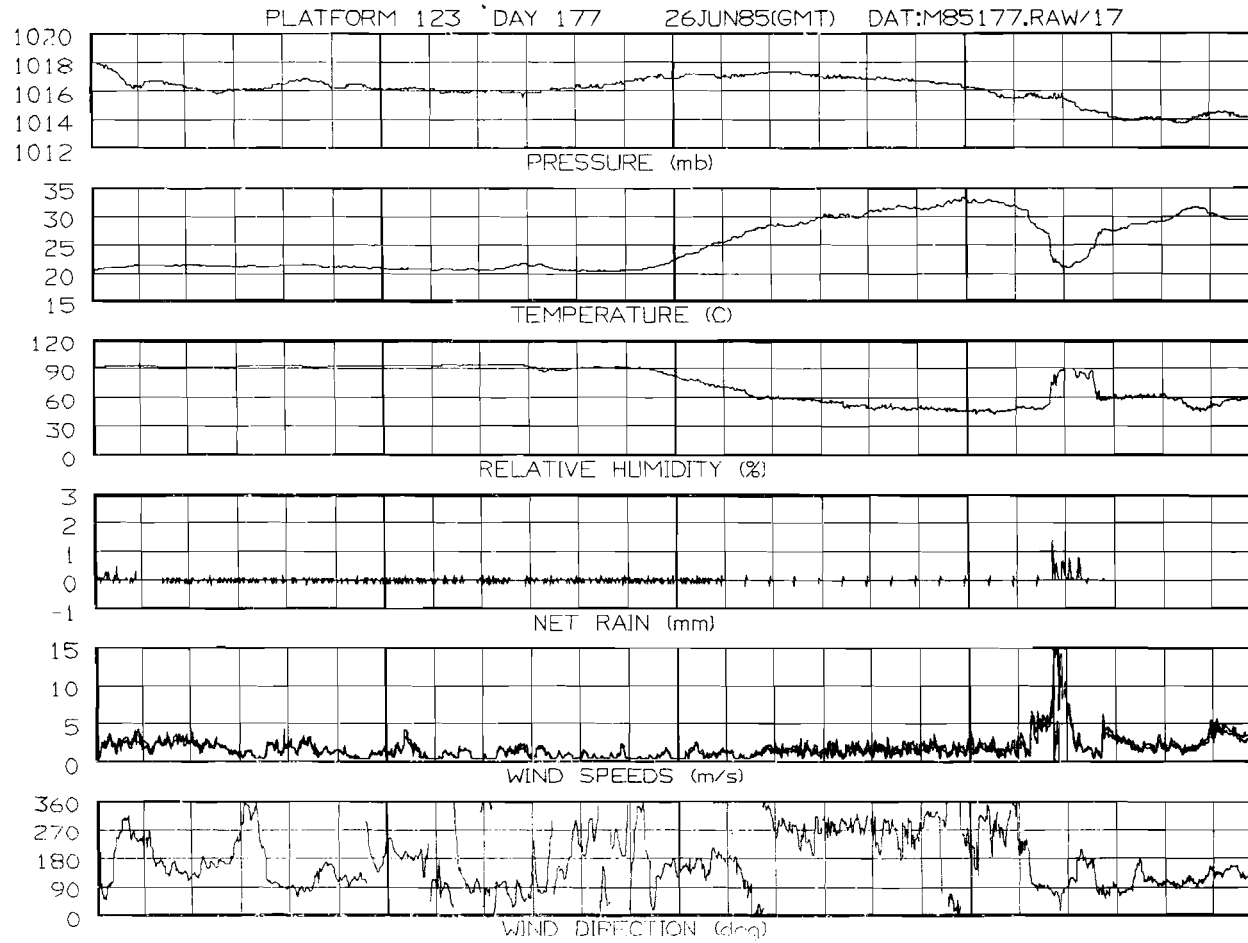
Figure VIII-8.   24-hour time series plot for mesonet station No. 23 on
June 26, 1985.

PLATFORM 124   DAY 177   26JUN85(GMT)   DAT:M85177.RAW/17

PRESSURE (mb)

TEMPERATURE (C)

RELATIVE HUMIDITY (%)

NET RAIN (mm)

WIND SPEEDS (m/s)

WIND DIRECTION (deg)
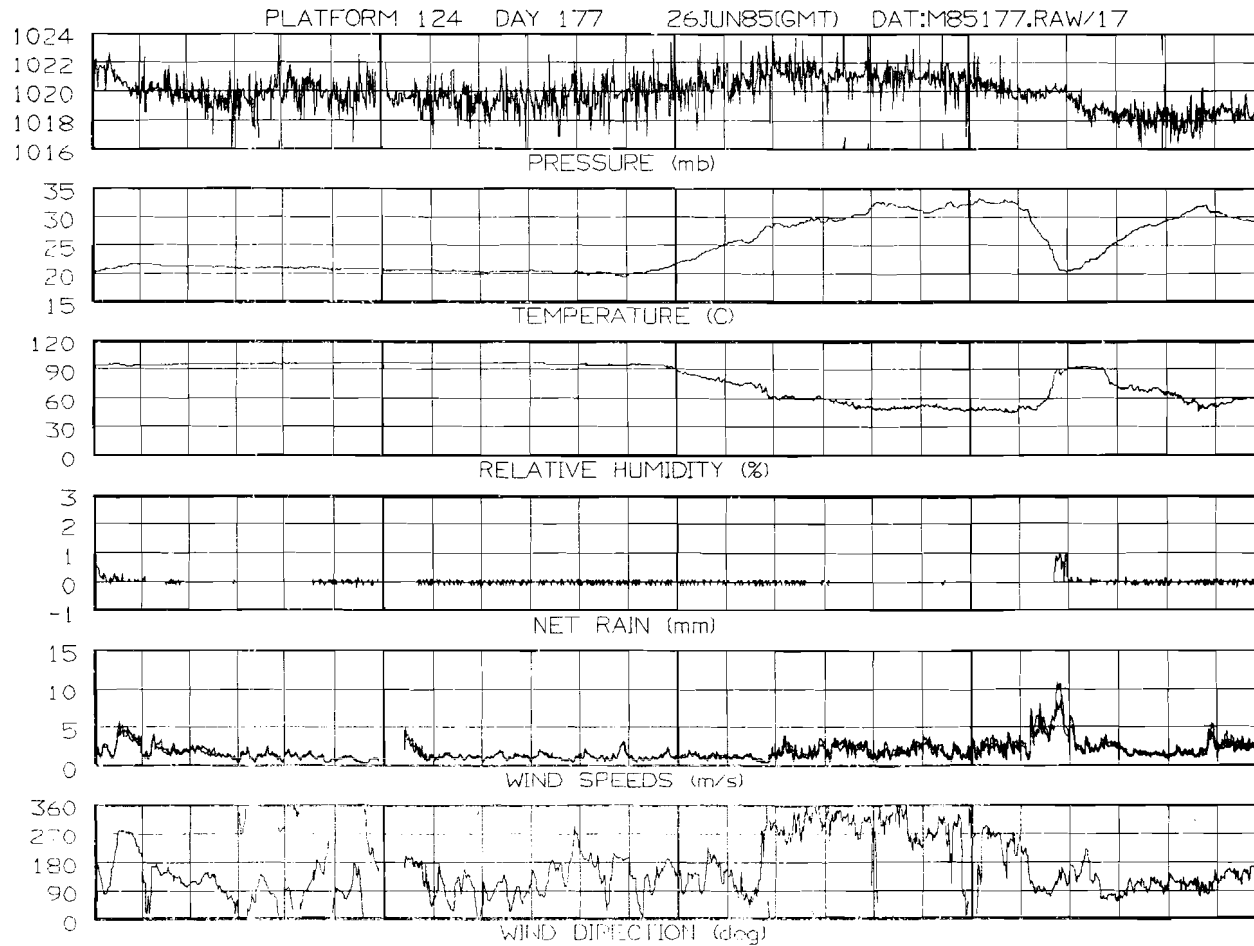
Figure VIII-9.   24-hour time series plot for mesonet station No. 24 on June 26, 1985.

PLATFORM 125   DAY 177   26JUN85(GMT)   DAT:M85177.RAW/17

PRESSURE (mb)

TEMPERATURE (C)

RELATIVE HUMIDITY (%)

NET RAIN (mm)

WIND SPEEDS (m/s)

WIND DIRECTION (deg)
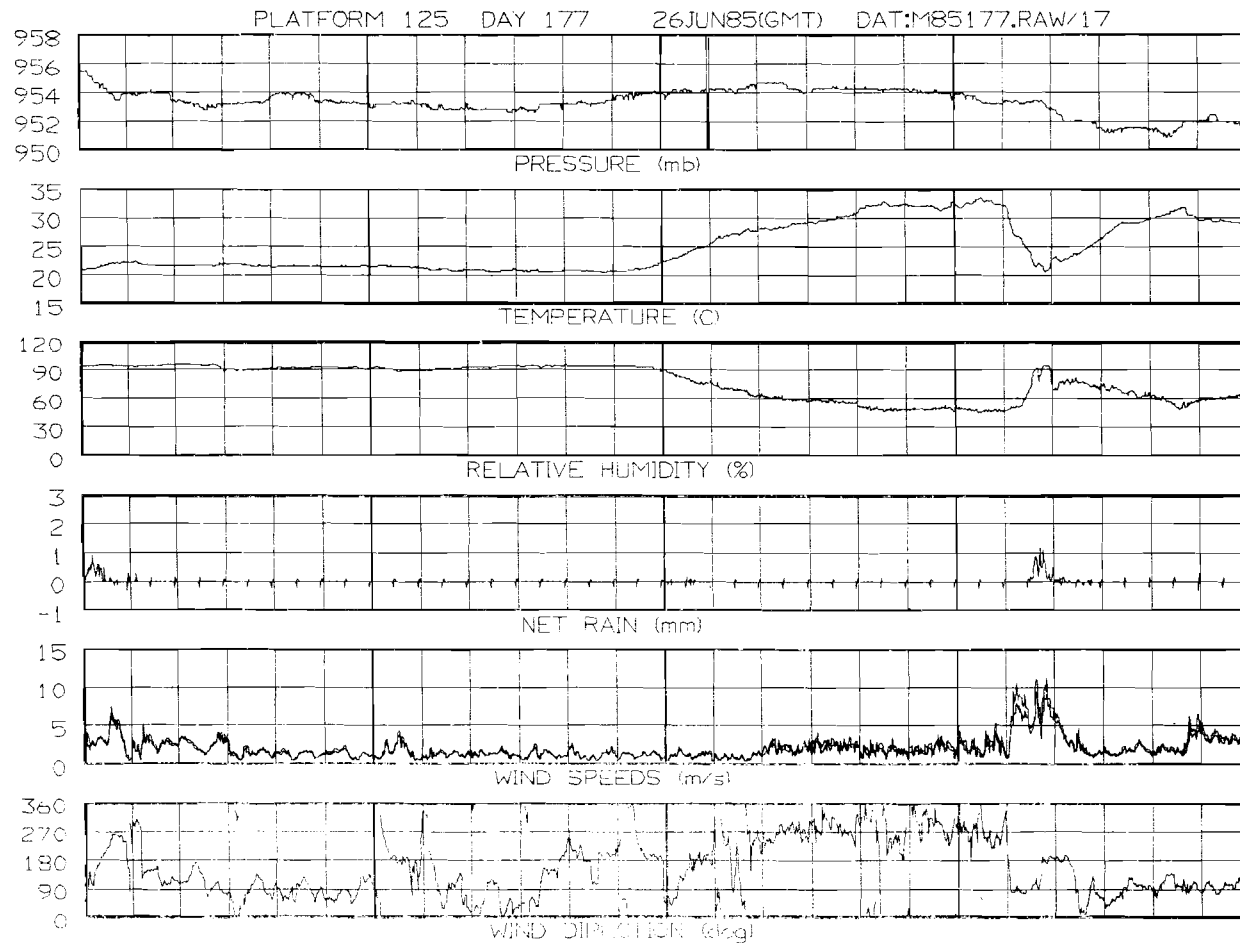
Figure VIII-10.   24-hour time series plot for mesonet station No. 25 on June 26, 1985.

2. Analyzing LLWAS 24-hour Time Series Plots

The 24-hour time series plots for the LLWAS are depicted in figures VIII-11 through VIII-16 as platforms 201-206 which represent, respectively, the center field (CF), north (N), east (E), southeast (SE), south (S), and west (W) sensors. All of these sensors recorded a wind event between 1900-2000 hours. Only CF, E, and SE had wind peaks which attained speeds greater than 10 m/s. These same three stations showed a sharp rise in the winds between 1900-1915 and then a separate peak at approximately 1945.

It seemed apparent that the LLWAS stations were also affected by two separate events which were separated by approximately 30 minutes. The second of the two wind shear events was the stronger, with a 15 m/s peak recorded at the SE sensor.

B. The Automatic Detection Technique

After analyzing the 24-hour time series plots, it was evident that the two identified weather events produced peak winds which attained or exceeded that of microburst peaks. Running Fujita's single station microburst detection algorithm allowed us to determine automatically if any of the stations had experienced a microburst (see VI.G.1).

It was shown by the algorithm, that at 1902 a microburst occurred at mesonet station No. 10. This was the only microburst detection. The gust front algorithm, which was run simultaneously with the microburst algorithm, flagged the times of 1943 and 1944 at station No. 23 as having had a gust front present.

As will be shown in the sections that follow, these automated algorithms have serious deficiencies, and cannot begin to identify and categorize wind shear events as well as analysts. When the 24-hour time series plots (described in the previous section) are available, the times at which wind shear events occurred become obvious and the need for an automatic detection technique, at least in this application, is greatly diminished.

C. Mesoscale Analysis

After identifying the possible wind shear events through analysis of the 24-hour time series plots (and having output from the single station microburst and gust front detection algorithms), the data over the scale of the mesonet must be examined. Using the mesonet data display utilities (described in VI.H), it was possible to investigate, minute by minute, the periods in which wind shear events possibly occurred.

1. Analyzing the Mesonet Plots

This more thorough investigation primarily involved the analysis of the wind field over the mesonet for a specified period of time. For each minute

PLATFORM 201   DAY 177   26JUN85(GMT)   DAT:L85177.RAW/17

WIND SPEEDS (m/s)

WIND DIRECTION (deg)
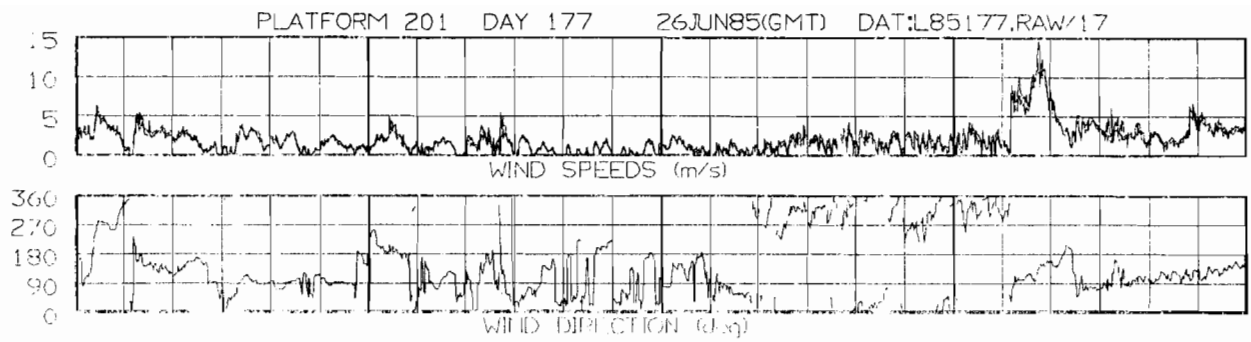
Figure VIII-11.   24-hour time series plot for LLWSAS station "CF" on
June 26, 1985.

PLATFORM 202   DAY 177   26JUN85(GMT)   DAT:L85177.RAW/17

WIND SPEEDS (m/s)

WIND DIRECTION (deg)
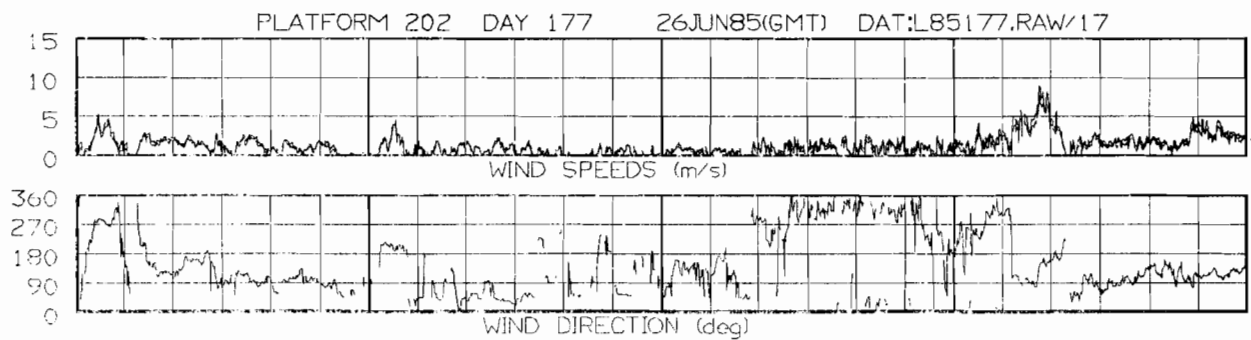
Figure VIII-12.   24-hour time series plot for LLWSAS station "N" on
June 26, 1985.

PLATFORM 203   DAY 177   26JUN85(GMT)   DAT:L85177.RAW/17

WIND SPEEDS (m/s)

WIND DIRECTION (deg)
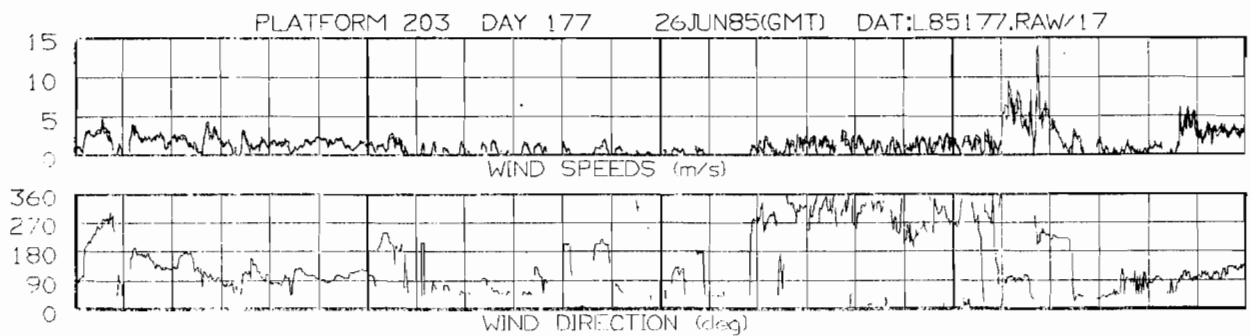
Figure VIII-13.   24-hour time series plot for LLWSAS station "E" on
June 26, 1985.

PLATFORM 204   DAY 177   26JUN85(GMT)   DAT:L85177.RAW/17

WIND SPEEDS (m/s)

WIND DIRECTION (deg)
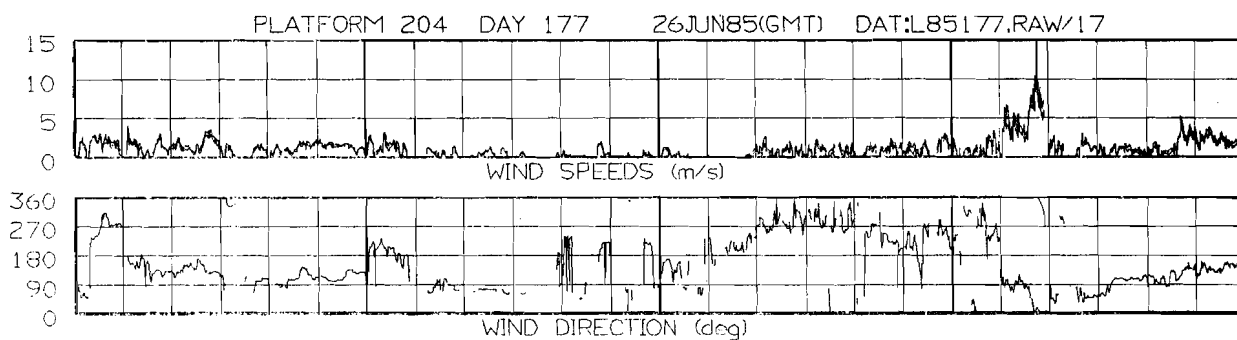
Figure VIII-14.   24-hour time series plot for LLWSAS station "SE" on June 26, 1985.

PLATFORM 205   DAY 177   26JUN85(GMT)   DAT:L85177.RAW/17

WIND SPEEDS (m/s)

WIND DIRECTION (deg)
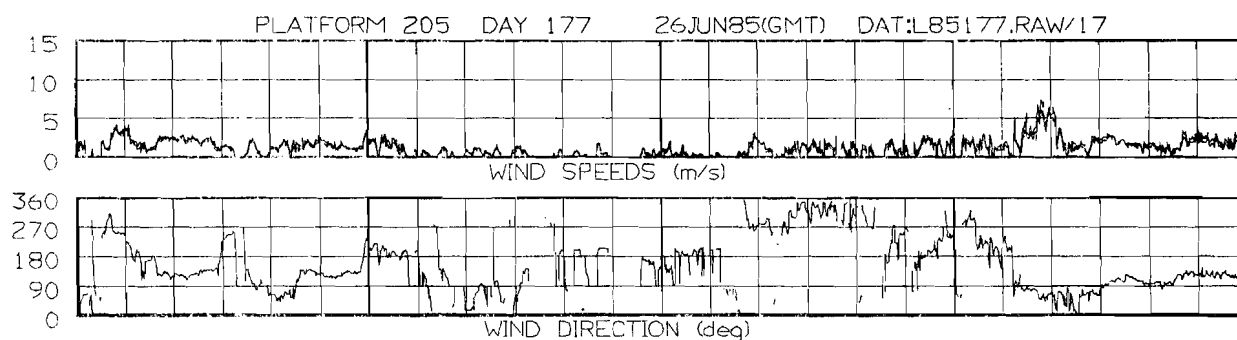
Figure VIII-15.   24-hour time series plot for LLWSAS station "S" on June 26, 1985.

PLATFORM 206   DAY 177   26JUN85(GMT)   DAT:L85177.RAW/17

WIND SPEEDS (m/s)

WIND DIRECTION (deg)
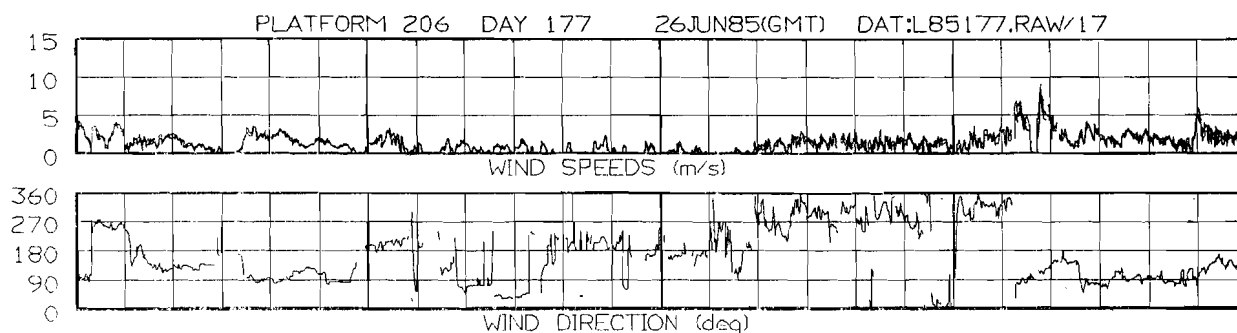
Figure VIII-16.   24-hour time series plot for LLWSAS station "W" on June 26, 1985.

during the specified time interval, the winds for both the mesonet and LLWAS sensors were plotted. This period was chosen, based on the times for which the 24-hour time series plots revealed possible wind events (both microbursts and gust fronts), was 1830-2030.

During this time period, two distinct wind shear events were observed. The first event began to affect the mesonet shortly before 1900 and persisted through 1930, although by this time it had weakened considerably. Figures VIII-17 through VIII-26 show this event as it expanded over the mesonet.

This first event appeared to be centered north of station Nos. 5, 7, and 15. By 1906, as shown clearly in Figure VIII-20, divergence was present between station Nos. 5 and 10, indicating possibly the center of the event. The outflow boundary expanded radially outward from this center point. This boundary, delineated by the dashed line, was seen clearly at station Nos. 22-25 and the LLWAS stations during the period between 1900 and 1918. All of these stations showed winds shifting into the east with its passage. By 1930, this outflow edge had not reached station Nos. 26-30 in the extreme southwest corner of the mesonet.

By 1933, a divergent area was observed over the mesonet in the area of the Memphis International Airport. At 1939, a purely divergent wind shear was seen between station No. 25 and LLWAS station E. Figures VIII-27 through VIII-36 show this second wind shear event as it took shape over the mesonet. For the period between 1940 and 2000, a distinct divergent wind shear event (obviously a microburst) was seen centered over the airport. The maximum wind speed peak of 25 m/s was observed at 1943 at station No. 23. This was the strongest recorded peak wind speed over the entire mesonet for this day. Also, by the end of this period, the accompanying outflow had expanded to cover the western two-thirds of the mesonet.

These two wind shear events, as seen by the mesonet plots, can be classified as microbursts. They both had divergent outflows with peak winds in the microburst range. The center of the first microburst was located outside the network of weather stations, whereas the second event was centered over the Memphis Airport.

2. Analyzing the Wind Event Time Series Plots

Another method used in determining the type of wind shear events present over the mesonet is the analysis of 21-minute time series plots. In this specific case of 26 June 1985, the wind shear events could quite easily be categorized as microbursts based on the overall wind patterns revealed by the mesonet plots. However, the examination of other variables may be necessary in more ambiguous cases, and always provides additional useful information. The 21-minute time series plots of all recorded variables at a single station reveal the fine scale structure of the weather event in question, and can help to discriminate microburst or gust front events from less significant forms of wind shear, especially when the validity of the wind speed profile is in question.
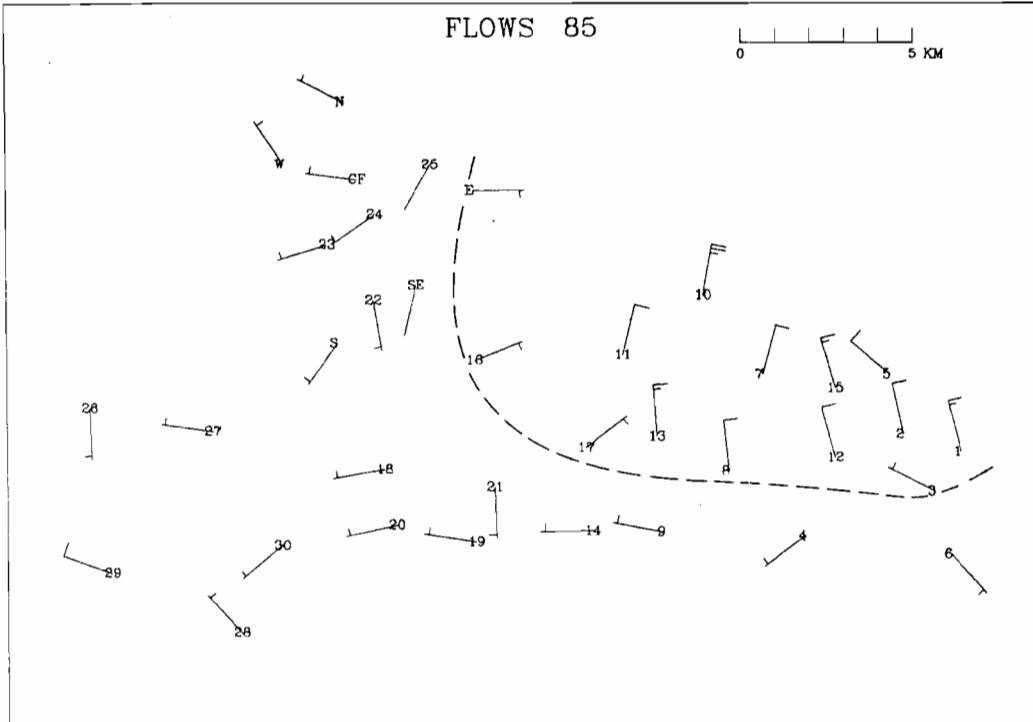
Figure VIII-17. Mesoscale plot showing the surface wind field over the
Memphis mesonet at 1900 (GMT) on June 26, 1985. Dashed line represents
microburst outflow boundary, half barbs (2.5 m/s), full barbs (5.0 m/s),
and flags (25.0 m/s).
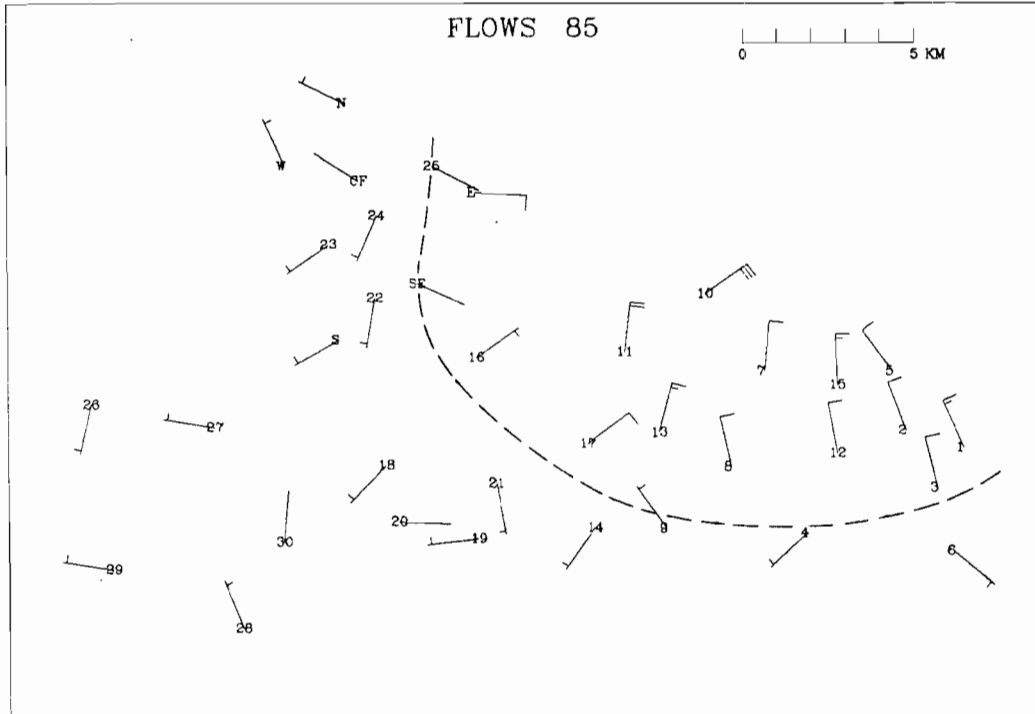
Figure VIII-18.   Same as Figure VIII-17, but for 1902 (GMT).
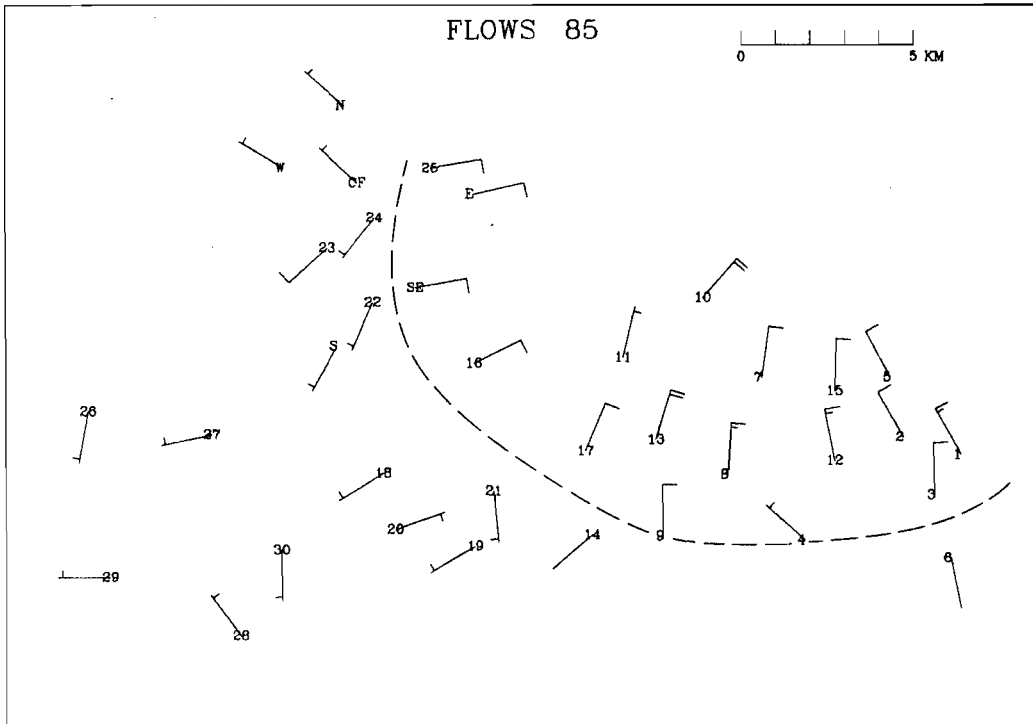
Figure VIII-19.   Same as Figure VIII-17, but for 1904 (GMT).
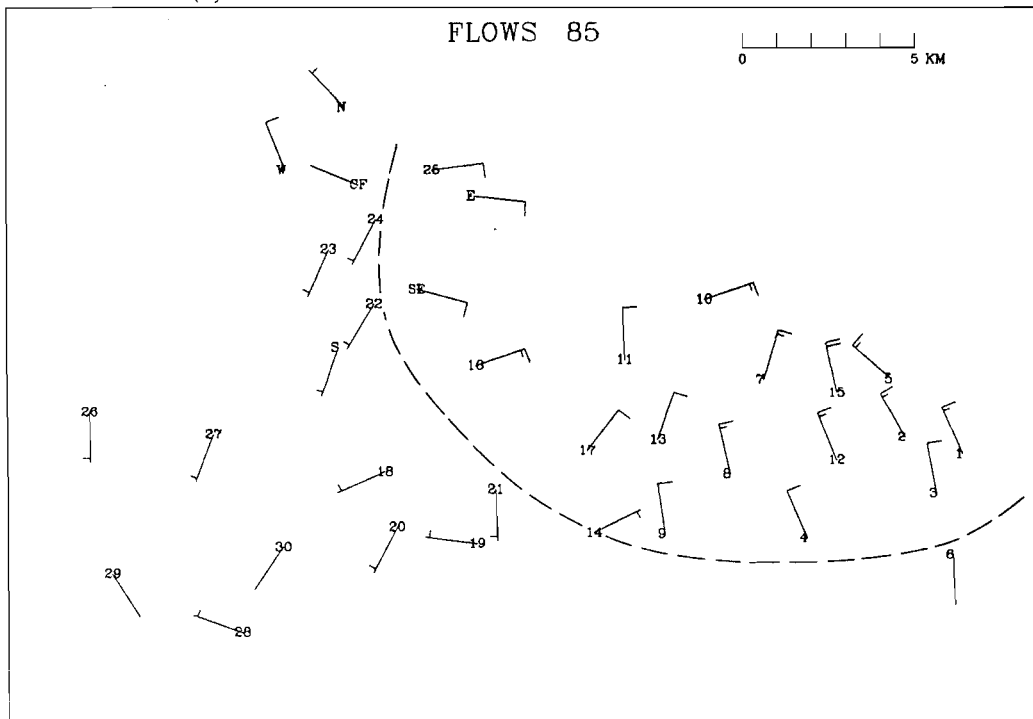
Figure VIII-20.   Same as Figure VIII-17, but for 1906 (GMT).
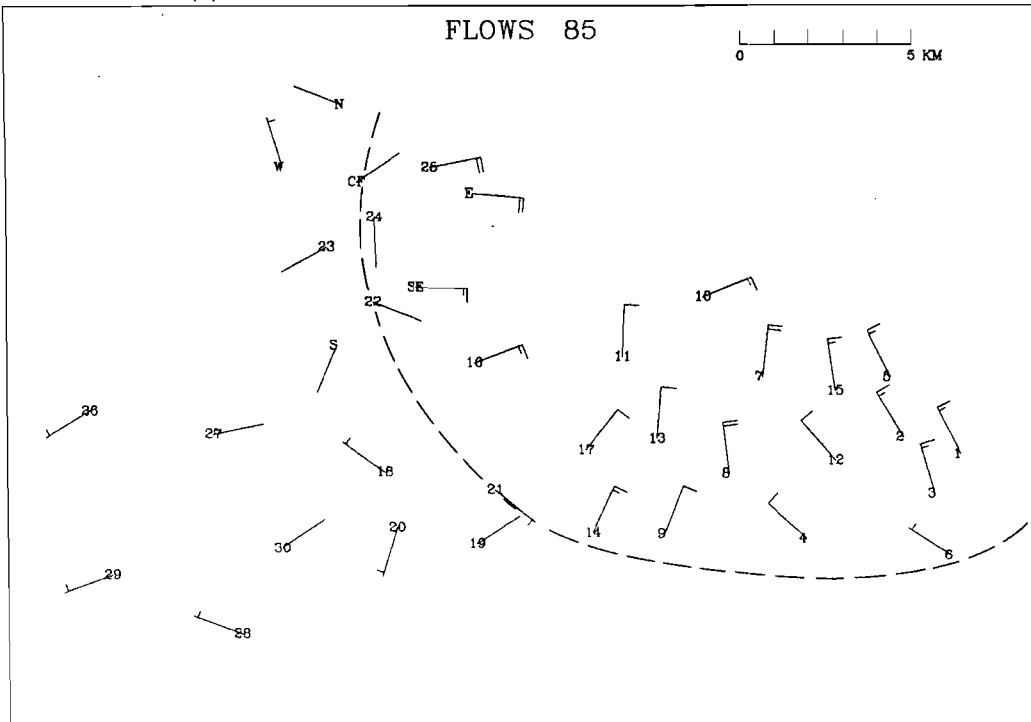
Figure VIII-21. Same as Figure VIII-17, but for 1908 (GMT).
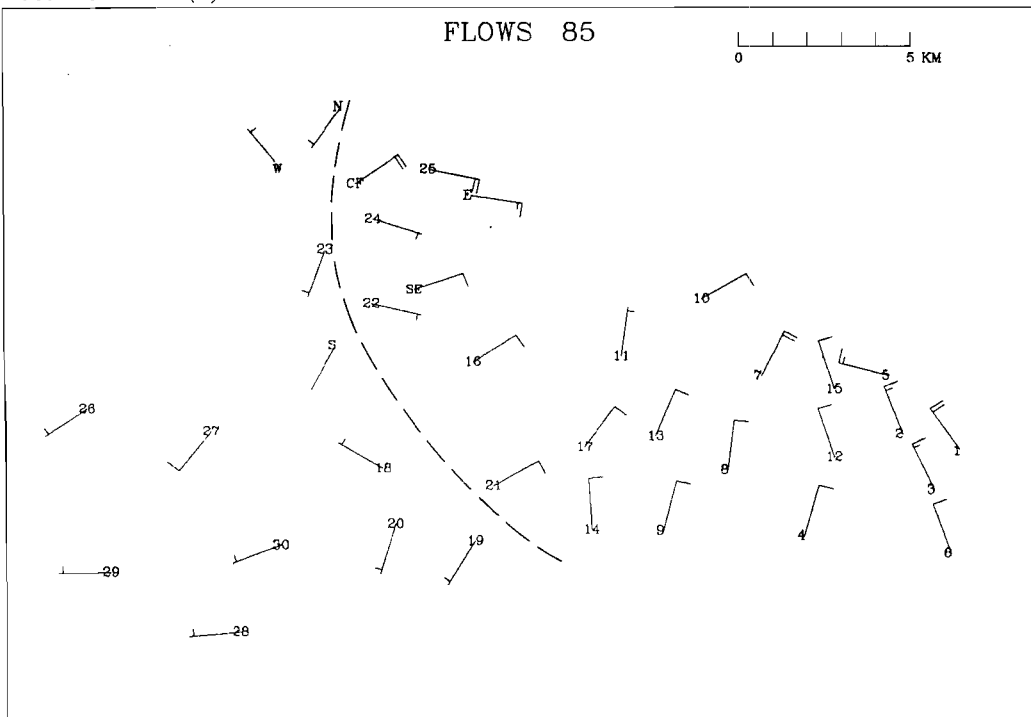
Figure VIII-22. Same as Figure VIII-17, but for 1910 (GMT).
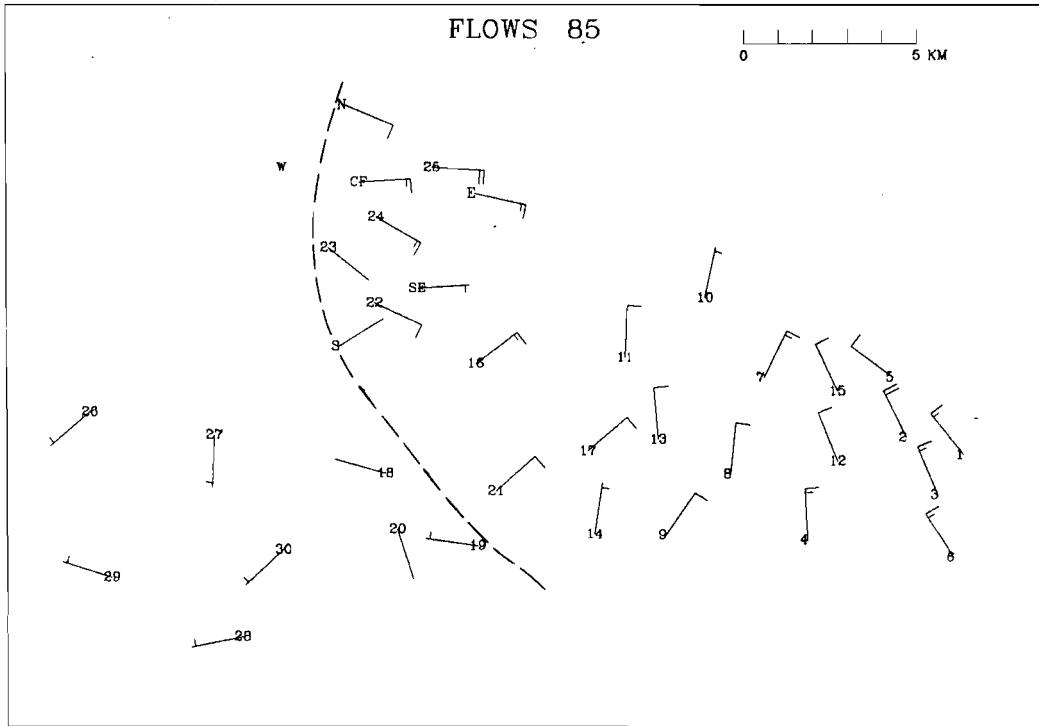
Figure VIII-23. Same as Figure VIII-17, but for 1912 (GMT).
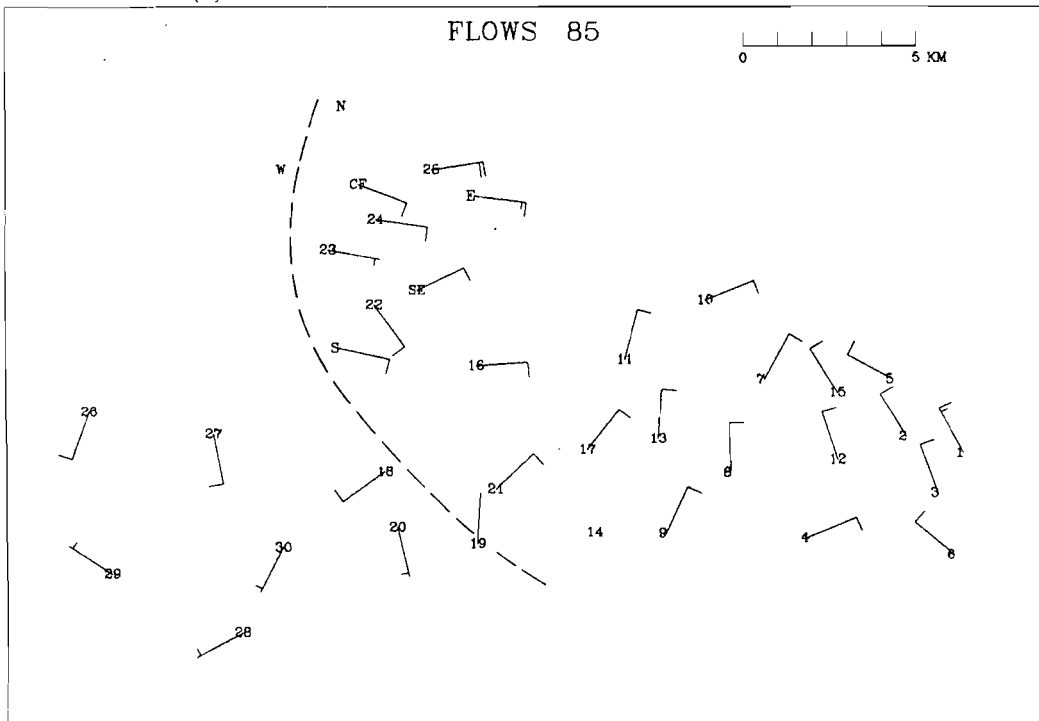
Figure VIII-24. Same as Figure VIII-17, but for 1914 (GMT) .

FLOWS 85
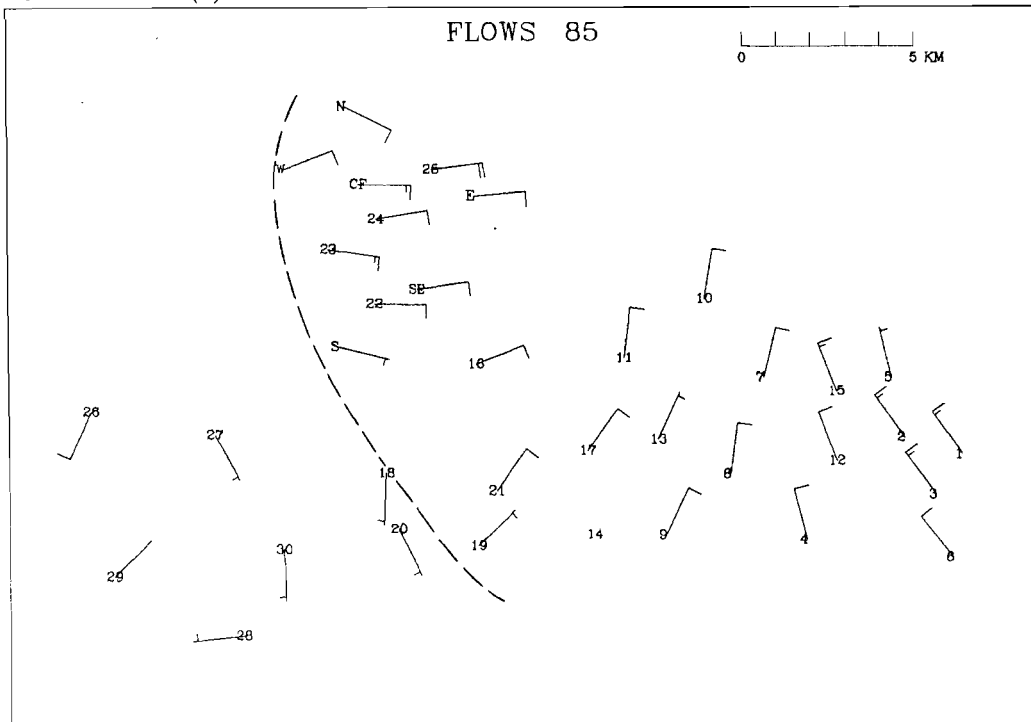
Figure VIII-25. Same as Figure VIII-17, but for 1916 (GMT).

FLOWS 85
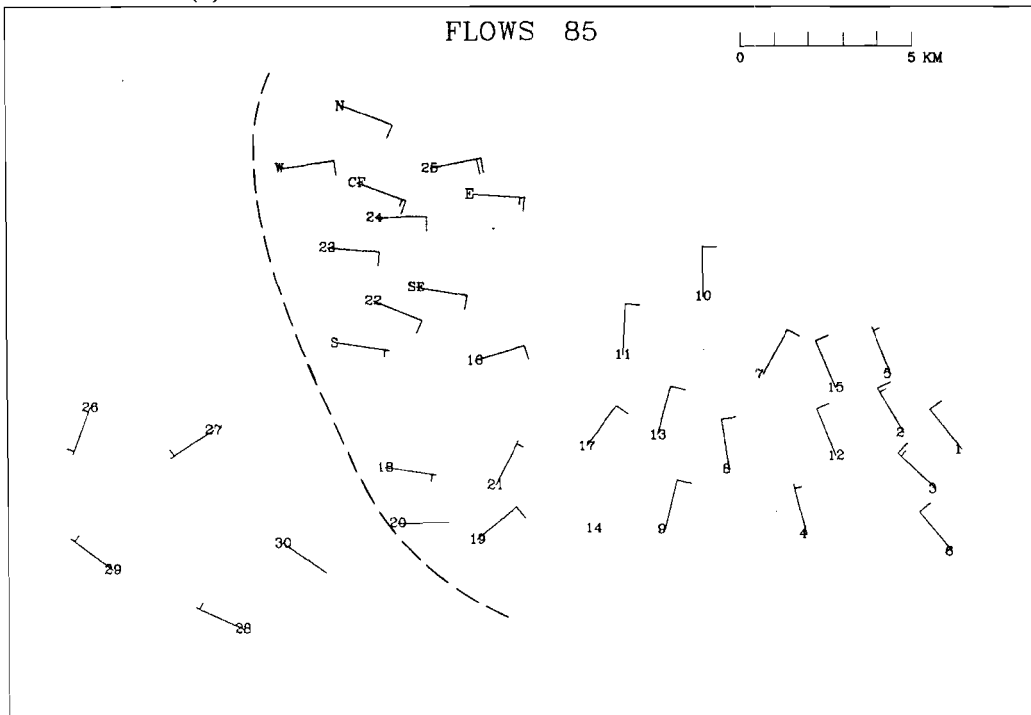
Figure VIII-26. Same as Figure VIII-17, but for 1918 (GMT).

FLOWS 85
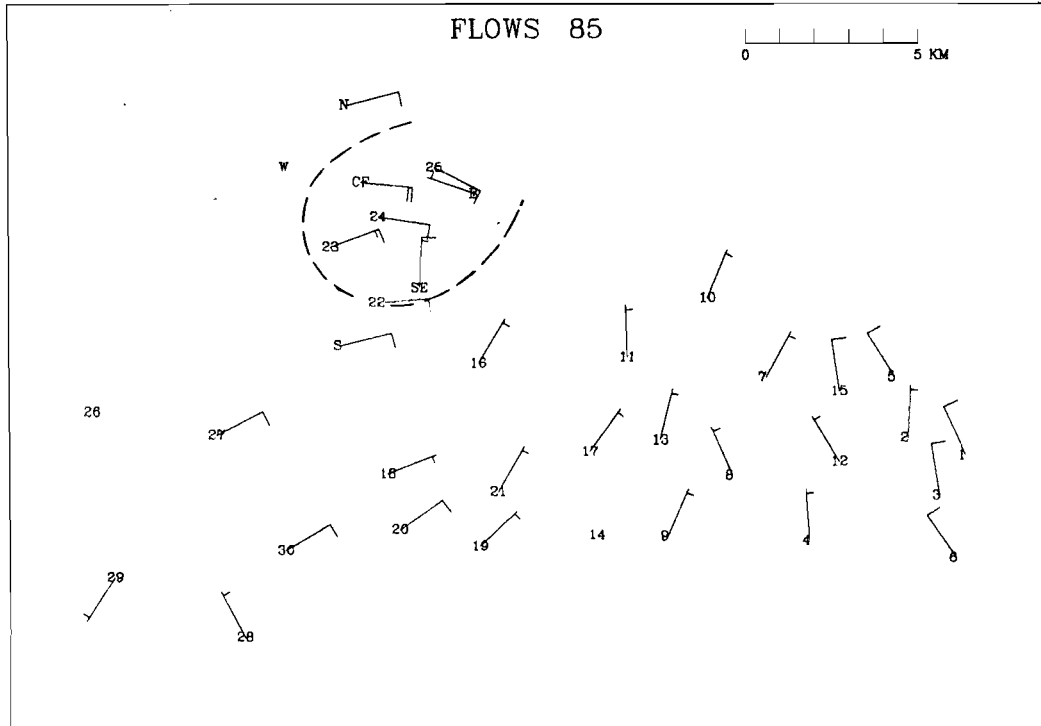
Figure VIII-27. Same as Figure VIII-17, but for 1939 (GMT).

FLOWS 85
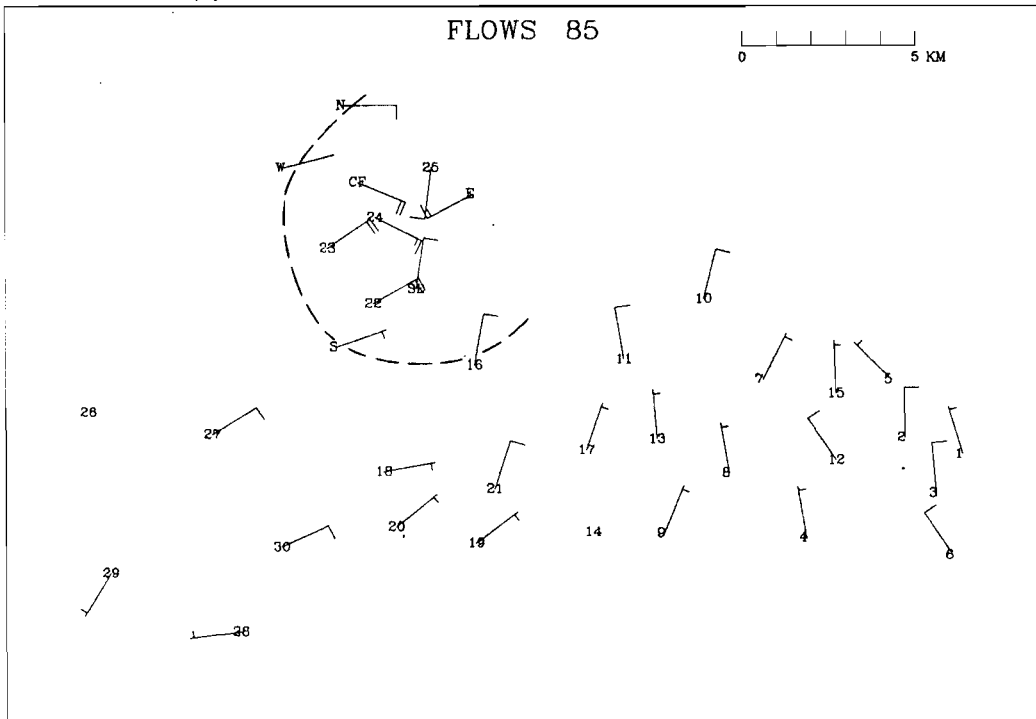
Figure VIII-28. Same as Figure VIII-17, but for 1941 (GMT).
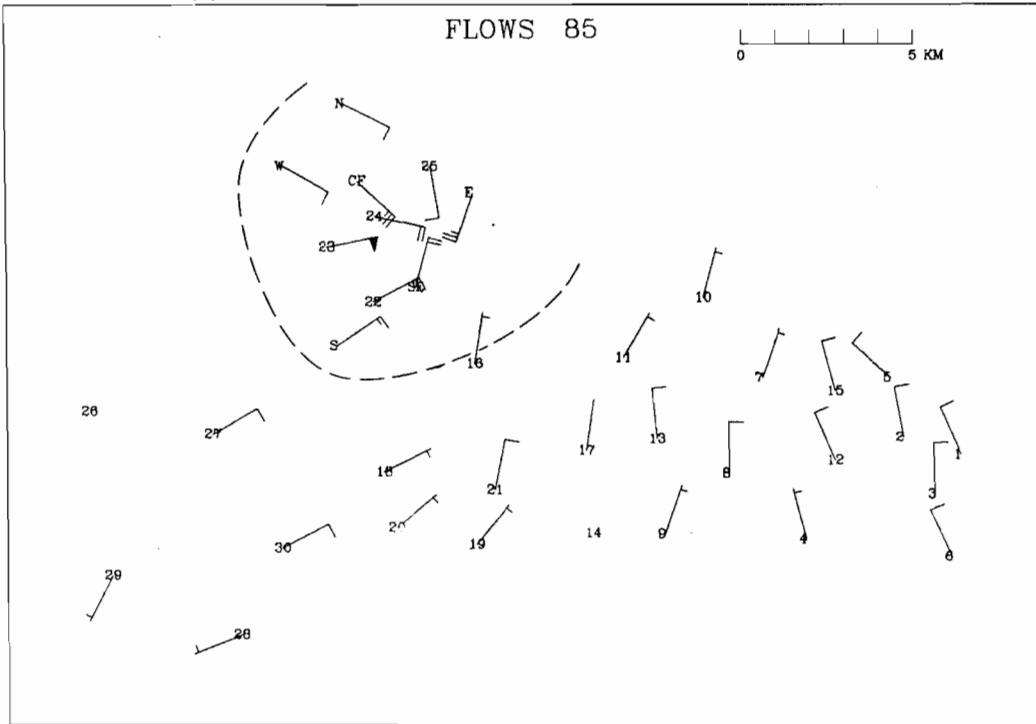
Figure VIII-29. Same as Figure VIII-17, but for 1943 (GMT).
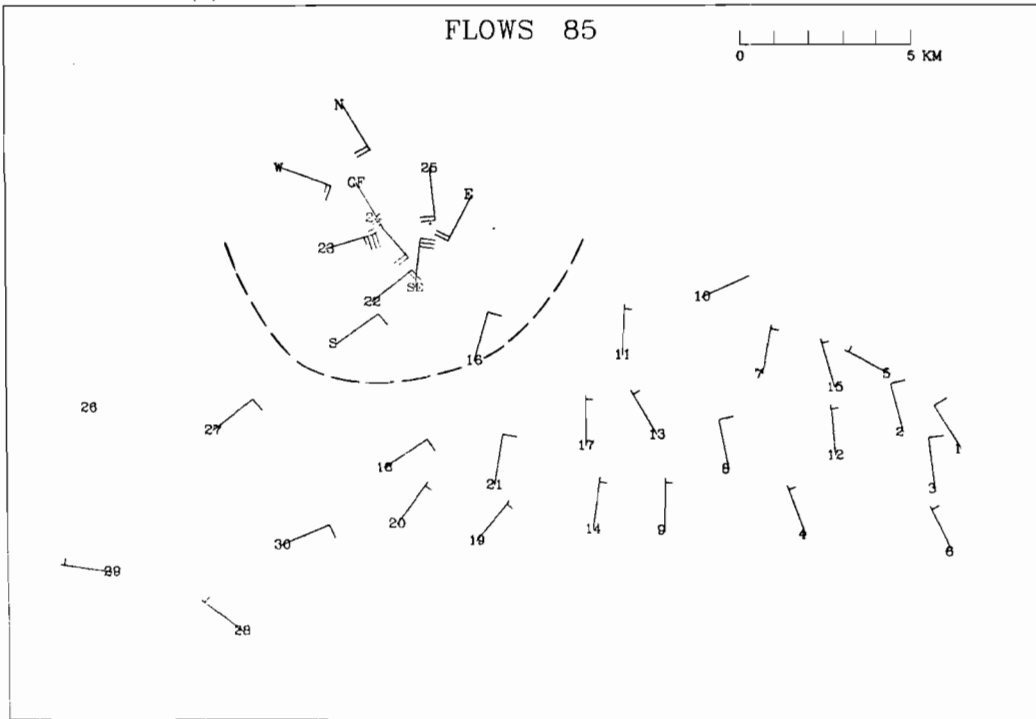
Figure VIII-30. Same as Figure VIII-17, but for 1945 (GMT).
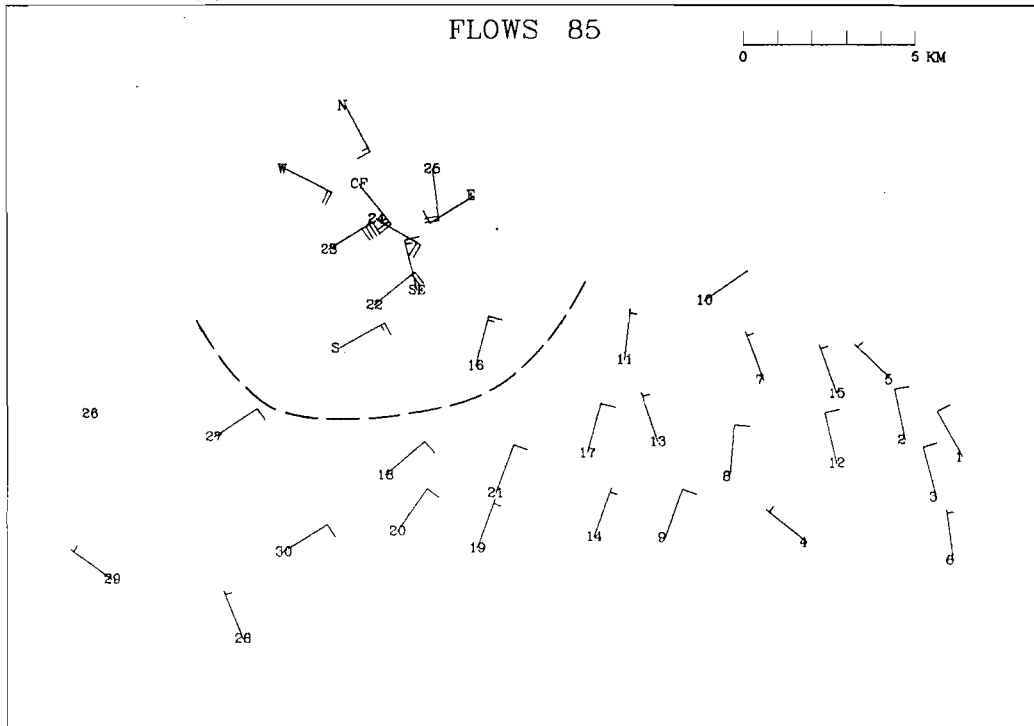
Figure VIII-31. Same as Figure VIII-17, But for 1947 (GMT).
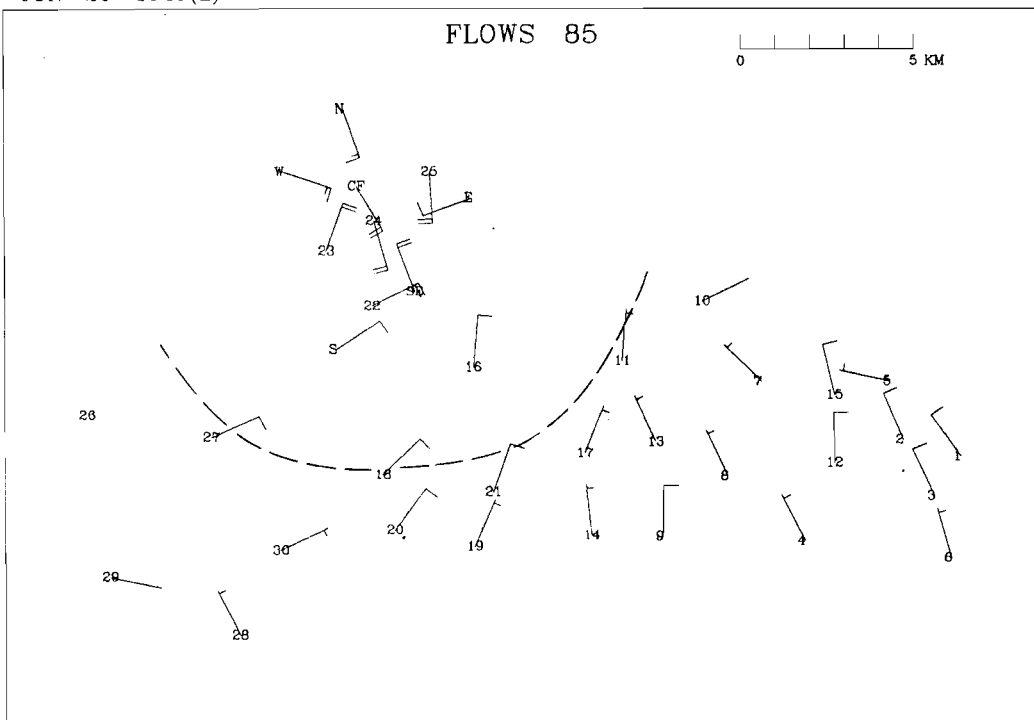
Figure VIII-32. Same as Figure VIII-17, but for 1949 (GMT).
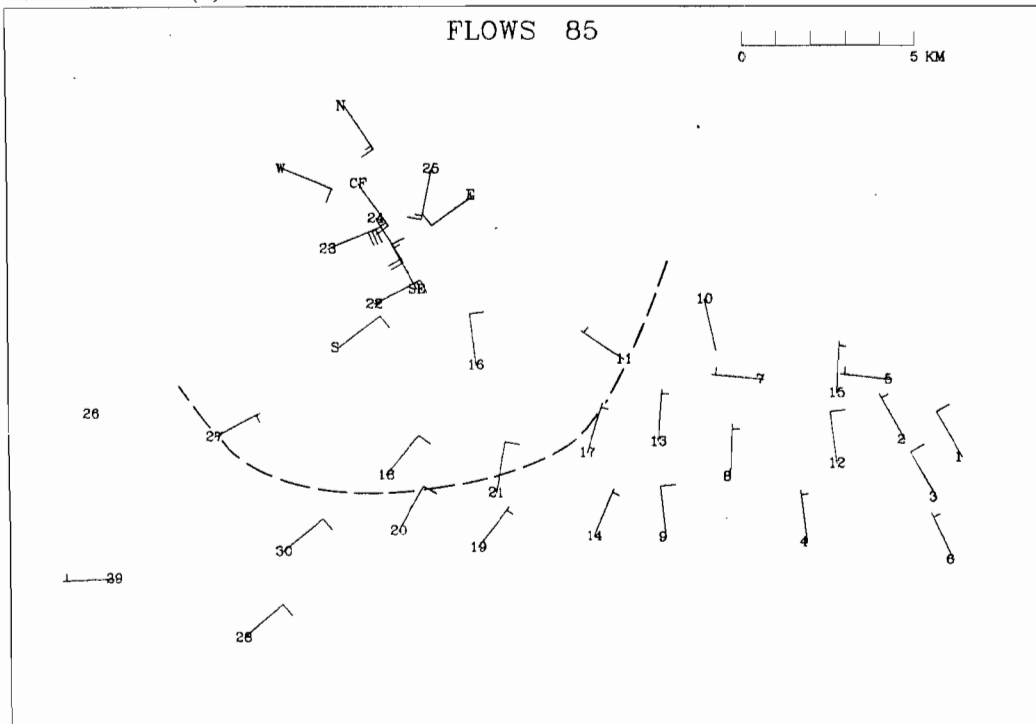
Figure VIII-33.   Same as Figure VIII-17, but for 1951 (GMT).
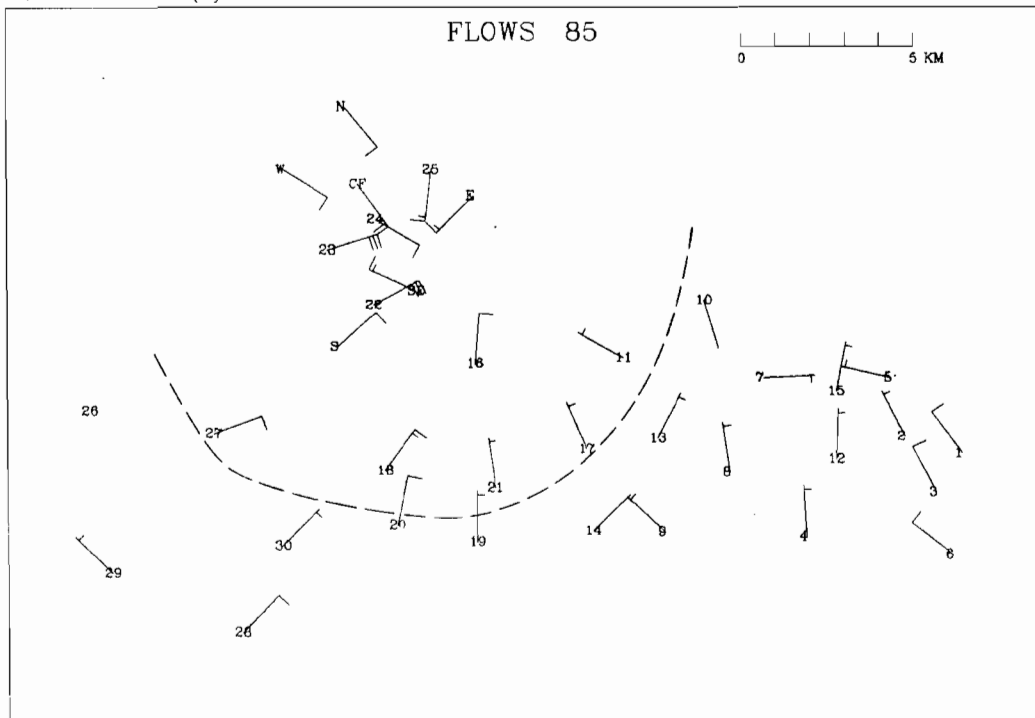
Figure VIII-34.   Same as Figure VIII-17, but for 1953 (GMT).
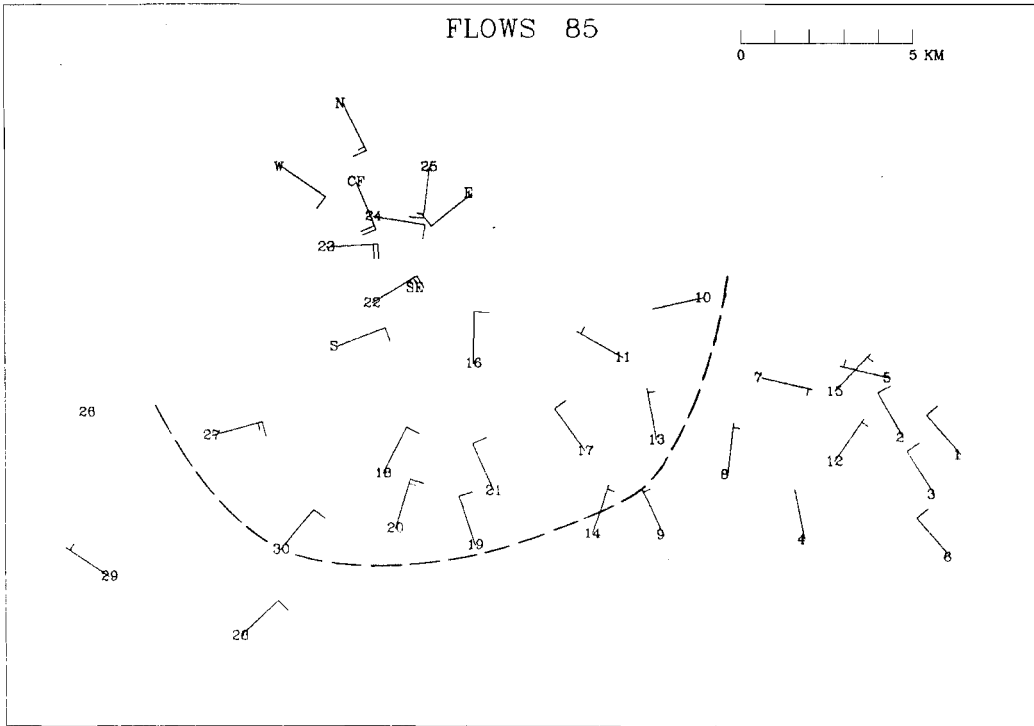
Figure VIII-35.   Same as Figure VIII-17, but for 1955 (GMT).
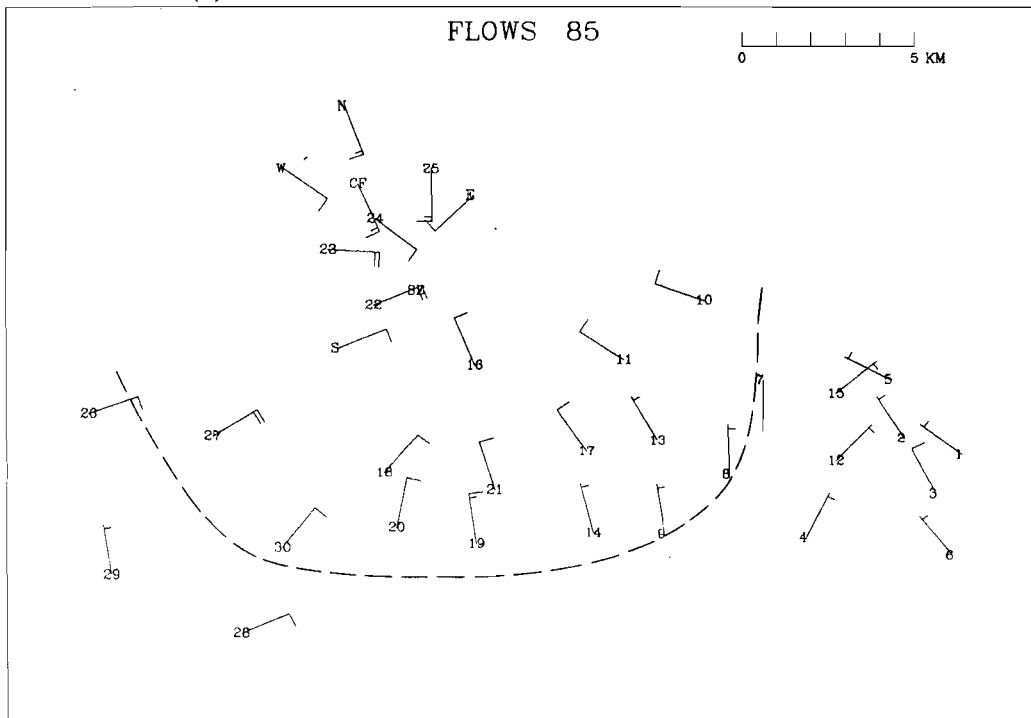
Figure VIII-36.   Same as Figure VIII-17, but for 1957 (GMT).

Recall that the single station microburst and gust front algorithms flagged station Nos. 10 and 23 as having experienced a microburst and gust front, respectively. Their time series can be seen in Figures VIII-37 and VIII-38. Station No. 10 showed a peak of 15 m/s at 1902, which was preceded for 9 minutes by a temperature fall. Precipitation also fell during this event and the wind direction was mainly from the north-northeast. With the temperature drop occurring several minutes before the peak wind, it is probable that the effects of the microburst were being felt earlier in the area to the north (this was verified by the mesonet plots).

The time series for station No. 23 for the event centered about 1943 is shown in Figure VIII-38. It can be seen from the peak wind profile why the single station detection algorithms flagged this incorrectly as a gust front and not as a microburst. This event which occurred over the airport was quasi-stationary and remained strong for several minutes. It was for this reason that the post-peak winds, which occurred from 1945-1950, were too high to comply with the conditions set forth in the specification of the microburst detection algorithm.

D. Conclusions

The 24-hour time series plots, for both the mesonet and LLWAS stations, showed distinct perturbations in the wind, temperature, and precipitation fields on 26 June 1985 during the time from 1900-2000. Two separate events were flagged and then verified by the microburst/gust front detection algorithm and the mesonet plots.

The first event was detected at approximately 1900 just north-northeast of station No. 10. This was detected by the microburst algorithm, verified through analysis of the mesoscale plots and classified accordingly as a microburst. Several stations during this event depicted wind traces similar to those typical of gust fronts. Although not detected as such by the algorithm, it was seen that these traces were associated with the passage of the first microburst's outflow boundary.

The second event occurred in the vicinity of the Memphis International Airport at approximately 1945. It was detected as a gust front by the algorithm, but verified as a microburst through analysis of the mesonet plots. It was shown that because of its intensity and almost non-existent translational motion, the wind speed trace, as seen in the 21-minute time series plot, resembled that of a gust front and thus failed to pass the conditions set forth in the microburst algorithm.

Depending on the case in question, varied amounts of emphasis will be placed on the different analysis utilities. For this case, the microburst algorithm failed to detect the airport microburst. It was the 24-hour time series plots that pointed to the event and the mesoscale analysis that allowed its verification.
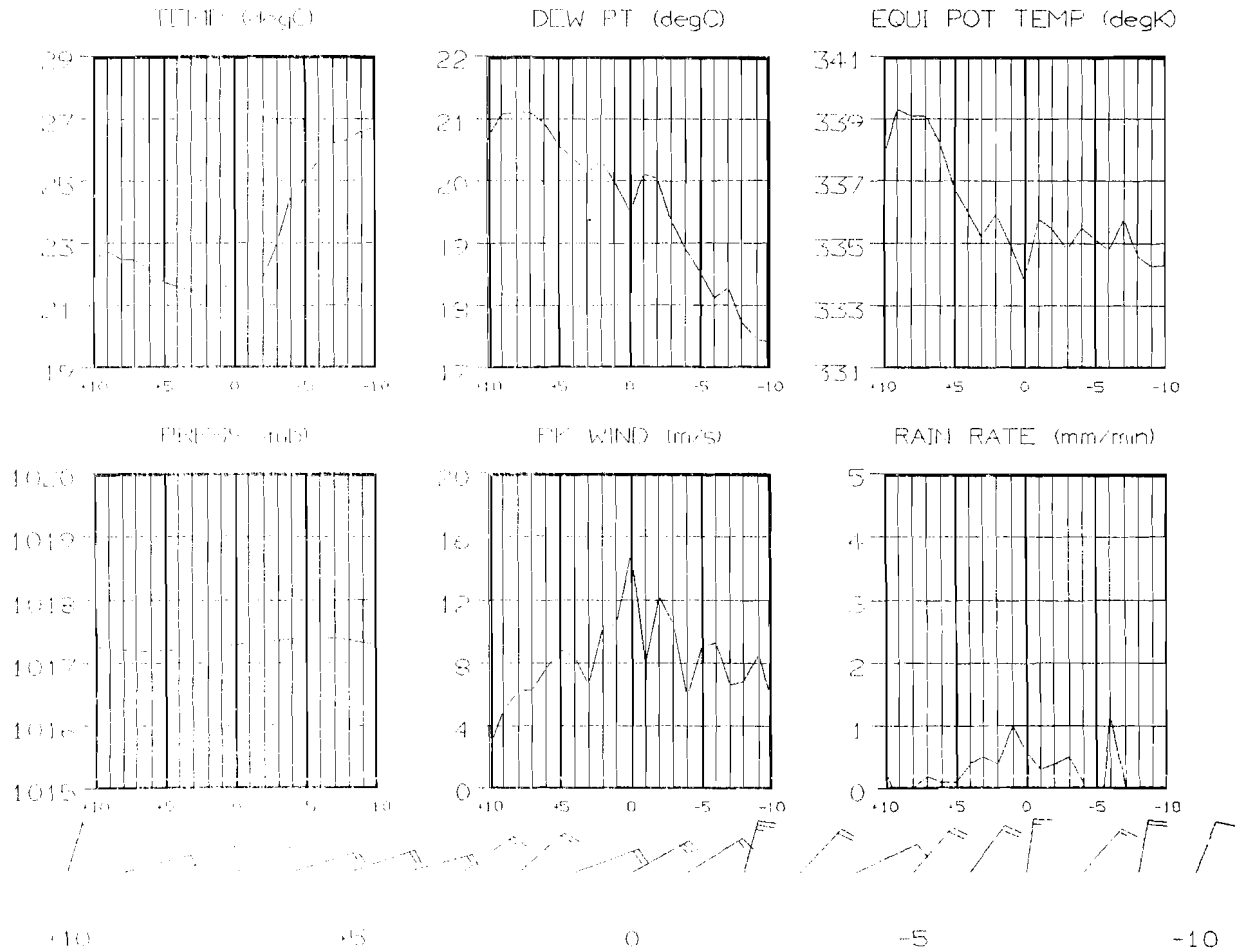
Figure VIII-37. 21-minute time series plot for mesonet station No. 10 on June 26, 1985. Time is centered at 1902 (GMT). Half barb (2.5 m/s), full barb (5.0 m/s), and flag (25.0 m/s).
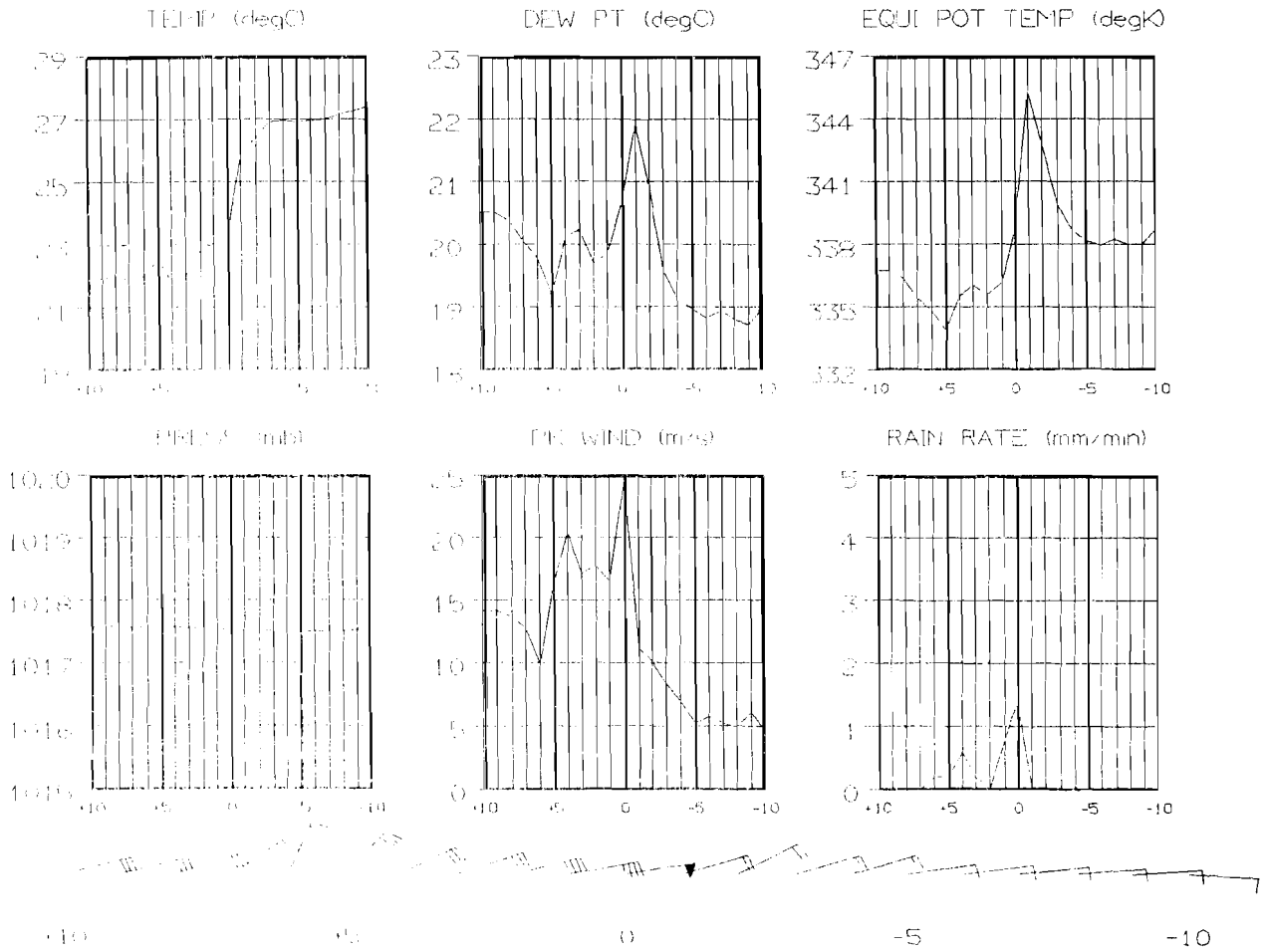
Figure VIII-38.   Same as Figure VIII-37, but for the time centered at 1943 (GMT) at mesonet station No. 23.

IX. SUMMARY

This report has presented a wide variety of information and results pertaining to the operation of the FLOWS automatic weather station network in the Memphis, TN area in 1984 and most of 1985. After a brief introduction to the goals of the FLOWS project, some background on the problem of low-altitude wind shear for aviation and on the history of the automatic weather stations was presented, along with a description of the FLOWS 1984-1985 network near Memphis, TN. It was noted that the microburst, a small scale divergent surface wind event originating from the outflows of commonplace localized thunderstorms, posed a major threat for aviation. Thus the design of the weather station system and network as well as the entire FLOWS data collection program has focused on the accurate detection of microburst phenomena.

The third and fourth chapters described, respectively, the weather station system including sensor calibration procedures and modifications, and the transmitted and archived data. These systems are still evolving, but the major advancements and developments to date, as well as remaining problems were detailed. The recommendations for future improvements mentioned in these and other chapters are summarized in the final chapter of this report.

Next a technique to mathematically compensate recorded winds for the effects of site obstructions was explored (Chapter V). The negative correlation between the wind speed deficit (transmission) at all azimuths at a particular station and the observed obstructions there was so high that a causal relationship between them could not be overlooked. It is possible that a more sophicated version of the technique presented here could be developed for operational use, for example, with the FAA LLWAS anemometer system.

In Chapter VI an overview of the software system developed at Lincoln Laboratory for the off-line data processing and analysis of mesonet data was given, and the various forms of graphical output were illustrated. The calibration system was designed so that wind speed correction factors, derived from a technique such as that described in Chapter V, could be easily and automatically included.

Once the details of the FLOWS automatic weather station network had been described, an evaluation of the overall system performance throughout the 1984 data collection period was given (Chapter VII). In the final section of that chapter, detailed examples of the individual station data from a day on which a microburst occurred were presented that illustrated most of the problems as well as the quality and resolution of the dataset. The performance not only of the automatic weather station system, but of the satellite and data archival system was evaluated as well.

The FLOWS automatic weather station network has proven to be a relatively trouble-free, consistent system for continuously collecting surface meteorological information in a given region. Its basic role in the FLOWS

project is that of a support system for the Doppler radar data collection effort, to be used, as illustrated in Chapter VIII, to locate and reveal the surface characteristics of microbursts. These analyses can then be used to confirm shear in the Doppler data or to detect events undetected in the radar data. Yet as has been shown in this report, the mesonet data, even alone, can go a long way in furthering the meteorological understanding of small scale low-altitude wind shear events such as microbursts that pose a threat to jet aircraft and that must be detected in a timely manner by the operational Doppler radars. The recommendations for future improvements to the weather station system given in the following chapter are put forth as practical solutions to known problems or inadequacies; these improvements can now be prioritized and their relative merits considered.

X. RECOMMENDATIONS

Recommendations for solving some of the known problems, for increasing the measurement accuracy of the automatic weather station system, and for data processing and analysis software enhancements are given in this chapter. No attempt has been made at prioritization; in some cases the recommendations can be implemented simply by adopting a slightly different operational procedure, while in other cases significant cost and effort would be involved. All of these factors should be considered in the decision to implement any of these recommendations for future data collection seasons.

A. Weather Station System

1. Do not use the rubber O-rings to additionally protect the upper anemometer bearings from water. They deteriorate rapidly and crack; when they finally break they can prevent the anemometer cups from spinning. The bearings probably are adequately protected from water exposure by the Teflon bushing attached to the anemometer cup hub. If O-rings are not used, the anemometers at a few of the sites should be checked after approximately two months of service for any signs of fouled bearings.

2. Use a flow coefficient of 1.7 m/rev instead of the 1.8 m/rev (6 ft/rev) specified by MRI, the manufacturer of the anemometers.

3. The anemometer bearings should all be replaced every two years.

4. Explore the option of calibrating the barometers as a function of output signal and temperature at the strain gage bridge. This would allow removal of the thermostatically controlled heaters which cause erratic behavior of the output signal and ultimately fail to keep the internal temperature constant as intended. Thermistors would have to be placed next to each sensor and sampled by the DCP for use in the calibration equations.

5. If an accurate calibration can be found for the barometers, it may be worth investigating the use of a new port that reduces the dynamic pressure fluctuations from the wind. Also, if the noise component of the signal is still too high (even after the heaters have been removed), additional signal conditioning electronics could be built, or the pressures could be sampled at a much lower rate by the DCP software.

6. If an accurate calibration cannot be found for the barometers, the purchase of new ones should be seriously considered. The signal strength, resolution, reliability, and the pressure port are all important factors.

7. The inventory of sensors should be increased until at least three working spares are available for each sensor. At least six spare temperature-relative humidity probes should be available in advance to be calibrated with the other probes. In the case of the rain gages, only spare parts (e.g., potentiometers) have been kept on hand in the past but it is now recommended that a total of 33 rain gages be part of the inventory. The purchase of spare barometers of the same type should be delayed until after recommendation Nos. 4-6 have been considered.

8. The purchase of new 0°-360° or 0°-540° potentiometers for the wind vanes should be considered. The true wind direction could be obtained at all azimuths. The Synergetic DCP automatically performs vector wind averages when 0°-360° potentiometers are used making this an attractive option.

9. The sensor calibration work should continue to be contracted out to professional instrumentation firms. New permanent shipping cartons should be obtained that are designed for shipment of these sensors in particular.

10. The inside of a vane aspirator should be painted white and tested along with an unmodified aspirator for evidence of improved reflection of low incidence angle solar radiation (see Chapter III.B.1.). If the paint is effective, then all of the vane aspirator openings should be painted.

11. The white armored boxes in which the DCP electronics and the barometers are housed are rusting badly. Since it is probable that the mesonet system will be in use through 1987, these boxes should be stripped and repainted before deployment in 1986.

B. Satellite and Down-Link System

1. The biggest improvement in this area would be to obtain an additional satellite channel (or even two) on which to transmit data. Many of the frustrating problems associated with the long 53 second transmission period could be alleviated. If a total of three channels were available, real-time mesonet data display would become a practical and useful consideration.

2. It has been suggested that, with the small size of the network and the lack of transmit time on the one GOES satellite channel, it might be better to transmit data directly to a ground based receiving system. This would impose a line-of-sight restriction on the remote weather station locations and would ensure that the network could only be operated in a spatially small configuration. The satellite transmission system is preferable in every way, and it is strongly recommended that any changeover to a ground transmission system be resisted.

C. Data Processing and Analysis System

1. Development of a direct-access disk file format for the meso-net data should be considered. Since, in general, less than 10% of the data are missing on a given day, little space would be wasted. A direct-access format would allow very rapid retreival of the data values for analysis or display.

2. New algorithms for detecting microbursts and gust fronts in the mesonet data that recognize the horizontal flow patterns and perhaps change in other measured variables such as tem-perature should be implemented. The number of false detec-tions should be reduced greatly if more information than just a 15-minute time series at each individual station is used. A method for computing the divergence within triangles whose vertices are the locations of the mesonet and LLWAS stations has been suggested (Wilson and Flueck, 1985).

3. Additional software utilities for the display of mesonet data need to be developed. Contour plots of any variables would be useful, and interpolation of the data to a regularly spaced grid would allow easy calculation of derived fields, smoothed fields, etc.

4. Additional software to facilitate the data quality checks should also be developed. Often problems only emerge when averaged data from a number of days or months is examined through histograms or other bulk statistics. Analyses of this type will help to better identify malfunctioning sensors, and to better determine the corrections to be used in post-data collection calibration.

REFERENCES

Brock, F.V. and P.K. Govind, "Portable Automated Mesonet in Operation", J. Appl. Meteor., 16, pp. 299-310 (1977).

Evans, J.E. and D. Johnson, "The FAA Transportable Doppler Weather Radar", Preprints, Twenty Second Confernce on Radar Meteorology, pp. 246-250, American Meteorological Society, Boston, MA (1984).

Evans, J.E. and D.H. Turnbull, "The FAA/MIT Lincoln Laboratory Doppler Weather Radar Program", Preprints, Second International Conference on the Aviation Weather System, pp. 76-79, American Meteorological Society, Boston, MA (1985).

Fredrickson, S., Personal Communication, October (1984).

Fujita, T.T., Manual of Downburst Identification for Project NIMROD, University of Chicago, Department of Geophysical Sciences, Satellite and Mesometeorology Research Project. SMRP Research Paper 137, The University of Chicago, IL. (1978).

Fujita, T.T., "Downbursts and Microbursts - An Aviation Hazard". Preprints, Ninth Conference on Radar Meteorology, pp. 94-101, American Meteorological Society, Boston, MA (1980).

Fujita, T.T., Microburst Wind Shear at New Orleans International Airport, Kenner, Louisiana on July 9, 1982. University of Chicago, Department of Geophysical Sciences, Satellite and Mesometeorology Research Project. SMRP Research Paper 199, The University of Chicago, IL (1983).

Fujita, T.T., The Downburst - Microburst and Macroburst. Department of Geophysical Sciences, The University of Chicago, IL, 122 p. (1985).

Fujita, T.T., DFW Microburst, Department of the Geophysical Sciences, The University of Chicago, IL, 154 p., (1986).

Fujita, T.T. and H.R. Byers, "Spearhead Echo and Downburst in the Crash of an Airliner", Mon. Wea. Rev., 105, (1977).

Fujita, T.T. and F. Caracena, "An Analysis of Three Weather-related Aircraft Accidents", Bull. Amer. Meteor. Soc., 58, pp. 1164-1181, (1977).

Fujita, T.T. and R.M. Wakimoto, "Effects of Miso- and Meso-scale Obstructions on PAM Winds Obtained During Project NIMROD", J. Appl. Meteor., 21, pp. 840-858 (1982).

Goff, R.C., "Vertical Structure of Thunderstorm Outflows", Mon. Wea. Rev. 104, pp. 1429-1440 (1976).

Harrison, W.F., B.A. Silverman, and T. Engel, "The HIPLEX Mesonetwork: Design and Description", Seventh Conference on Inadvertent and Planned Weather Modification, Alberta, Canada, pp. 112-113, American Meteorological Society, Boston, MA (1979).

Holman, L. and J. McInerney, "CCOPE PROBE Mesonet, Calibration and Maintenance Measures", Technical Report to the U.S. Department of Interior Bureau of Reclamation, June (1983).

MacCready, P.J., "Mean Wind Speed Measurements in Turbulence", J. Appl. Meteor., 5, pp. 219-225 (1966).

Naegeli, W., "Investigations on the Wind Conditions in the Range of Narrow Walls of Reed", Mitt. Schweiz, Anst. Forstl. Versuchswes, 29, pp. 213-266 (1953).

National Research Council, Low-Altitude Wind Shear and its Hazard to Aviation. National Academy Press, 112 pp., (1983).

Ott, J., "Inquiry Focuses on Wind Shear as Cause of Delta L-1011 Crash", Aviation Week and Space Technology, 12 August 1985.

Shrager, J.J., The Analysis of NTSB Large Fixed-Wing Aircraft Accident/ Incident Reports for the Potential Presence of Low-Level Wind Shear. Report No. FAA-DD-77-169. Federal Aviation Administration, Washington, D.C. (1977).

Wilson, F.W., Jr. and J.A. Flueck, A Study of the Methodology of Low-Altitude Wind Shear Detection with a Special Emphasis on the LLWAS Concept. JAWS NCAR Report No. 02-85, (1985).

Wilson, J.W., R.D. Roberts, C. Kessinger, and J. McCarthy, "Microburst Wind Structure and Evaluation of Doppler Radar for Airport Wind Shear Detection", J. Climate and Appl. Meteor., 23, pp. 898-915 (1984).

Wolfson, M.M., J.T. DiStefano, and D.L. Klingle, An Automatic Weather Station Network for Low-Altitude Wind Shear Investigations, Lincoln Laboratory, M.I.T., Project Report ATC-128 (18 September 1984).

Wolfson, M.M., J.T. DiStefano, and T.T. Fujita, "Low-Altitude Wind Shear Characteristics in the Memphis, TN Area Based on Mesonet and LLWAS Data", Preprints, Fourteenth Conference on Severe Local Storms, pp. 322-327, American Meteorological Society, Boston, MA (1985).

World Meteorological Organization, "Guide to Meteorological Instruments and Methods of Observation", WMO Report No. 8, 5th Edition, Geneva, Switzerland, 1983.

Wurtele, M.C., "Meteorological Conditions Surrounding the Paradise Airline Crash of March 1, 1964", J. Appl. Meteor., 9, pp. 787-794, (1970).

APPENDIX A

WEATHER STATION LOGISTICS

In this appendix, suggested guidelines are given for selecting new sites for the FLOWS automatic weather stations, a number of pre-deployment requirements are listed, and procedures for deployment of the weather station network are discussed.

A. Selecting Sites

Experience to date with locating the mesonet in new areas has led to the development of a few guidelines to follow when selecting new sites.

1. Select and confirm the Doppler radar site(s). The location of the stations in the network will depend on this choice.

2. Choose a two-person team to select and negotiate contracts for the 30 mesonet sites. Since site selection can take from one to three weeks, and since there is often a continuing need for a local contact representing Lincoln Laboratory prior to full installation of all the test facilities, it helps if someone living locally can be hired on a consulting basis to be part of this team.

3. A preliminary network, based on detailed topographic maps and visual appearance from public roadways should be established prior to contacting landowners about individual sites.

4. The mesonet site rental fee and length of stay must be decided upon. It is always wise to write the rental contract for a longer stay than is anticipated. In any case, the contracts must terminate at the end of the Lincoln Laboratory fiscal year, at which time they can be renewed if necessary. A sample of the landowner contract used in 1984 and 1985 appears in Figure A-1.

5. Establish a local telephone number that will be answered by a consultant, secretary, or at least an answering service. This will be required so that messages can be taken for the site-selection team while they are out investigating new sites, and to facilitate communication between prospective landowners and Lincoln personnel. It will also be required, until the permanent radar site number is established, as the number citizens are instructed to call "IN EVENT OF DAMAGE, OR IN CASE OF EMERGENCY" by the sign on each mesonet station.

6. The site selection effort should be short and intense, rather than long and drawn out, primarily because confirmation of certain sites may depend on others becoming available and the quicker these decisions are resolved, the easier the negotations are for all parties involved. Also, by accomplishing all of the work on one trip, Lincoln personnel can avoid making numerous trips to the area.

Massachusetts Institute of Technology
Lincoln Laboratory
P.O. Box 73
Lexington, MA   02173

Gentlemen:

In accordance with your recent request, _____
(hereinafter call the Owner), grants MIT Lincoln Laboratory (hereinafter
called MIT) permission to erect and operate an automatic weather station
on a portion of land located

1.   MIT will pay a monthly rental fee of $_____/per month, payable
     monthly, from _____ until completion of the project,
     probably about _____.

2.   MIT personnel will have access to the weather station at any time
     to service equipment.

3.   MIT will restore the land to its original state on completion of
     the project.

4.   MIT agrees to hold the Owner harmless against any and all claims
     by others for damages (including damages to property or bodily
     injury and death) resulting from MIT's use of the property, pro-
     vided, however, that if any damages result from the negligence of
     the Owner or his employees, then MIT shall not be so obligated.

5.   All MIT personnel and their associates using the property will
     take special considerations in their activities for the safety,
     convenience and rights of privacy of the people living in the
     area.

If this permit is acceptable to you, please sign below and return one
copy to Owner.

                              Very truly yours,

                              _____

Accepted and agreed to this
    th day of

MASSACHUSETTS INSTITUTE OF TECHNOLOGY
Lincoln Laboratory

By: _____
    Assistant Director

Figure A-1. Mesonet site lease contract.

7. Once a general location for each station has been decided upon (based on the preliminary network map) care should be taken in choosing the individual sites. For an area to qualify as an acceptable site, the following characteristics should be considered:

    a. The field should be open pasture or crop land, and of 4 to 5 acres in horizontal extent. This insures adequate station exposure to wind and precipitation and reduces the influence of nearby buildings or trees on the measurements.

    b. Since valleys, hills, or nearby lakes could produce microscale effects on the local weather, more representative sites away from steep topography and water sources should be chosen.

    c. The public should have limited or no access to the selected field to guard against vandalism. It is best if the station cannot easily be seen from public roadways.

    d. The site should have roads nearby, for access must be obtainable by work crews to deploy and maintain the station. Fields in which the work crews can drive right up to the weather station have proven to be the best sites.

8. Once all the potential sites have been located, the proposed network should be mapped and the inter-station spacing critically examined. Any adjustments deemed necessary should be attempted. Before the actual deployment of station hardware begins, approval of each site, as appropriate for providing representative meteorological measurements, by a Lincoln staff member or other expert should be obtained.

9. A detailed set of directions for each final mesonet site should be compiled into a notebook, complete with the name, address and telephone number of the landowner. Copies of this notebook should be readily available for the mesonet deployment team, radar site personnel, and the Lincoln Laboratory group office. Any instructions about, for example, when not to visit the site, should be included as well as any particular features about that installation (e.g., electric fence present).

B. Pre-deployment Requirements

There are a number of requirements that should be accomplished prior to deployment of the mesonet station hardware which are listed and explained below.

1. Storage space, such as an open hangar or a corner of a warehouse
    should be rented in time to receive the mesonet hardware when it
    arrives. A forklift will be necessary to unload the equipment
    from the trailer. The storage area may well be used as an indoor
    workspace by mesonet technicians in which to assemble the hardware
    or perform final equipment tests and troubleshooting. Therefore,
    the space should be climate-controlled and provided with adequate
    power and lighting. A telephone line is also extremely useful.

2. One four-wheel drive pick-up truck should be leased locally for
    the full period of the intended mesonet operation in the area. It
    should be available in time for use in mesonet hardware deployment
    and may have to be ordered two or three months in advance.

3. If time is of the essence (it often is), then plans may be made to
    use two teams of workers to deploy the mesonet stations. In that
    case, an additional pick-up truck or van, preferably four-wheel
    drive, will be needed. Again, this may have to be arranged months
    in advance.

4. A local "petty cash" bank account, to which at least one member of
    the mesonet deployment team has access, should be opened at least
    two weeks prior to beginning the mesonet work. Most banks require
    a hold of at least this long before allowing withdrawals on a new
    account. This fund is necessary to permit personnel to effi-
    ciently obtain any maps, tools, mechanical parts, or equipment
    necessary to keep the site deployment work on schedule.

5. Self-stick weather-proof signs about 12" long with the local phone
    number (or radar site number) printed in black 1" high figures
    should be requested from graphic arts. These should be pasted on
    each station's sign prior to deployment.

6. The official GOES Platform Data Files, which identify for NOAA the
    exact location, platform code, and transmit time of each station
    in the FLOWS network, should be filled out and mailed at least two
    weeks prior to activation of the network. A status report
    describing the new network should be sent as a cover letter.
    Also, the GOES satellite channel allocation agreement between the
    FAA and NOAA periodically expires. It is Lincoln's responsibility
    to ensure that the agreement is in force before transmitting on
    the GOES system.

7. A terminal/modem connection capable of producing hardcopy output
    will be required to check the initial test transmissions and to
    begin daily data quality checks as the stations are activated. If
    the FL-2 Doppler radar testbed is assembled, the standard proce-
    dures can be followed; if not, a DecWriter or Silent 700 terminal
    and a 300-baud modem will have to be used. A telephone line that
    can be monopolized for one to two hours at a time must be
    available.

8. Each landowner should be contacted and arrangements made for a permissable time to install the weather station.

C. Deployment of the Network

In this section, some of the major operational procedures involved in taking down, moving to a new site, and setting up the mesonet stations are discussed.

1. Taking Down the Network

As soon as stations start to be deactivated, the utility of the mesonet dataset begins rapidly to decline. It is best to set a date, after which no mesonet data will be considered to be available, even though all transmitted data will actually be archived.

Access by truck to the fields in which the stations are located is much easier when the ground is dry and, in fact, may be nearly impossible after one or two days of heavy rain; it is therefore preferable to have two teams of personnel available when taking down the mesonet. It is best to have a two-person team just to remove the electronic equipment and the sensors and another three-person team, in a separate truck, to remove the mechanical structures. This division of responsibilities permits the more fragile electronics to remain apart from the rugged equipment, and allows enough room for immediate packing of sensors from a number of stations.

Once all of the equipment has been retrieved, the sensors are packed in specially designed protective crates and shipped back to Lincoln Laboratory (except the raingages and any other sensors that are to be calibrated by field personnel), and the other equipment is carefully packed into a trailer (Figure A-2). The DCPs and raingages are packed in protective cartons, the hardware pieces are boxed up, the batteries are bolted to the floor, and everything is secured in place before the trailer is driven by a hired cab to the next site.

2. Setting Up the Network

Setting up the new weather station network is very much like taking down the old; two teams are preferable but in any case the station hardware should be deployed first, and separately. The entire operation is much easier if a good-sized indoor workspace is available into which all of the equipment can be unloaded and segregated.

Each morning the sites to be set up should be identified and only the necessary equipment loaded into the truck(s). Landowner permission to work on the sites should be obtained, if possible. That evening, if any stations have been activated, a dump of the data being downlinked should be performed. Daily data quality checks should commence immediately upon activation of the first weather stations.

When the station hardware is being set up, the corner of the triangular base to which the wind sensor mast is guyed should be pointed toward magnetic north, so that the solar panels end up facing south.

Figure A-2. View looking into the truck trailer used to transport FLOWS mesonet equipment. Flourescent lighting and a heater (upper left) have been added. Note the long wind sensor masts (right), the white armored boxes (left), and the batteries (front).

APPENDIX B

ABBREVIATED DCP SOFTWARE GLOSSARY

This appendix gives an abbreviated list of the operators and functions in the Synergetics SCADA-SOFT (FORTH) language. The entries chosen for this list are those needed to understand the current DCP software given in Appendix C.

INTRODUCTION

This glossary contains definitions of the words used in SCADA-SOFT® Ver. 1.0.X/X, presented in the order of their ASCII sort.

Parameter Notation

The first line of each entry is a symbolic description of the the procedure's action. The symbols on the left indicate the order in which the word expects its input parameter(s). The three dashes, " - - - ", indicate the execution point; parameters returned after execution are shown on the right.

Words used in SCADA-SOFT® may pass parameters via two methods. The first and most commonly used in FORTH-like systems is a "last-in, first-out" (LIFO) parameter stack. The parameters are entered post-fix (RPN) and are indicated by lower case symbols (i.e., n, d, f. . . .).

The second method of parameter-passing uses internal system variables. Words that operate in this manner extract their input parameters from variables that have been set up by previously executed commands. Parameters passed in this manner are indicated by capital letters (i.e., Tn, Sn).

Stack Parameter-Passing

Symbol	Definition
f	Boolean flag ($\emptyset$=false, non-zero = true)
ff	Boolean false flag (flag=$\emptyset$)
tf	Boolean true flag (flag= non-zero)
n, n1, . . .	16-bit signed integer number
un, un1, . . .	16-bit unsigned integer number
d, d1, . . .	32-bit signed integer number
ud, ud1, . . .	32-bit unsigned integer number

System Variable Parameter Passing

Symbol	Definition
Tn	Name of processing equation
Sn	Name of scan event
Hn	Name of header number (record separator)

Word Usage

Following the parameter notation on the first line of each definition is a word usage index. This index consists of five levels:

Level	Usage Level Indicator	Indicator
Command	COMMAND?	C
Equation	<- (user entered)	E
Output	T1 - 60, H$\emptyset$ - 63 OR DONE?	O
Process	T1 - 60 OR DONE?	P
Scan	Sn - 25 OR DONE?	S

The word usage index indicates the level(s) at which the word may be used. For example, the usage for the word ON is CE, indicating that it may be used at the command and equation levels.

Pronunciation

The natural language pronunciation of SCADA-SOFT names is given in double quotes ("). In words such as Tn and Sn the pronunciation is; T2 "t-two", S10 "s-ten".

Integer Format

Unless otherwise noted, all references to numbers are for 16-bit signed integers. For 32-bit signed double numbers, the most significant 16 bits (with the sign) are on top of the parameter stack.

Examples

Command and operator examples are intended to show correct syntax and use. Parameters that are passed to and from commands on the parameter stack are displayed to facilitate visualizing the actual stack contents.

Glossary Entry Format

Word Name	Parameter Notation Word Use
	Pronunciation
	Definition
	Example

*

n1 n2 - - - n3
"times"
Multiply two 16-bit signed numbers, n1 and n2, leaving their 16-bit signed product, n3.
2 3 * 6

*/

n1 n2 n3 - - - n4
"times-divide"
Multiply the 16-bit signed numbers, n1 and n2, to form a signed 32-bit intermediate product. Divide this result by the 16-bit signed number, n3, leaving the 16-bit signed quotient, n4. The quotient is truncated, and the remainder is lost. The intermediate 32-bit product provides greater precision than the equivalent sequence, "n1 n2 * n3 /".
16000 4 3 */ 21333

+

n1 n2 - - - n3
"plus"
Add two 16-bit signed numbers, n1 and n2, leaving their 16-bit signed sum, n3.
2 3 + 5

-

n1 n2 - - - n3
"minus"
Subtract n2 from n1, each 16-bit signed numbers. Leave the difference as a 16-bit signed number, n3.
5 3 - 2

/

n1 n2 - - - n3
"divide"
Divide n1 by n2, each 16-bit signed numbers. Leave the 16-bit signed quotient, n3. The quotient is truncated, and the remainder is lost.
8 3 / 2

;

- - -
"semicolon"
Signal the end of the processing equation definition.
T1 <- T1 1 + SAVE ;

<

n1 n2 - - - f
"less-than"
Leave a true flag if the 16-bit signed number, n1, is less than the 16-bit signed number, n2; otherwise leave a false flag.
-1 -2 < ff

<-

Tn - - -
"is"
Signals the beginning of a processing equation. The equation will be assigned to the last accessed Tn. This operator changes the Data Structure assigned to Tn to the default type, which saves no data. It is important to note that if an error occurs while editing a processing equation, the actual Data Structure may not coincide with the displayed equation. When this occurs, the processing equation should be redefined immediately.
T3 <- 1 0 INPUT HISTO ;

=	n1 n2 - - - f "equals" Leave a true flag if the top two 16-bit signed numbers are of equal value; otherwise leave a false flag. 1 1 = tf
>	n1 n2 - - - f "greater-than" Leave a true flag if the 16-bit signed number, n1, is greater than the 16-bit signed number, n2; otherwise leave a false flag. 2 1 > tf
DIM	n1 n2 - - - "dimension" Specify the Data Structure for this processing equation to be a DIM type with depth n2. The depth, n2, may range from 1 to 60. When the equation is executed, the 16-bit signed value, n1, is stored in the DIM Data Structure, overwriting the oldest data. This feature allows the storage of the n2 most current values of n1. When accessed for processing, the most current value of n1 is returned. Access for outputting causes all n2 entries to be returned with the most recent value first. T5 <- T3 3 DIM ;
DONE	- - - "done" Exit the setup loop prompted by ; . . . OR DONE?. DONE
ELSE	- - - "else" Used in the following form: IF . . . ELSE . . . ENDIF When the test performed by IF is false, the words after the ELSE are executed. See IF. 1 2 < IF 3 ELSE 4 ENDIF
ENDIF	- - - "endif" ENDIF marks the end of the IF-ELSE-ENDIF control structure. Execution of the conditional words after IF or ELSE is followed by a jump to ENDIF where execution resumes. 4 1 2 > IF DROP 3 ENDIF
IF	f - - - "if" Used in the form: IF . . . ENDIF (or) IF . . . ELSE . . . ENDIF

IF (cont.)	IF selects execution based on the boolean flag on top of the stack. If the flag is true (non-zero), the words following IF are executed and the words after ELSE are skipped. A false flag (zero) causes the words after the IF to be skipped and the words following ELSE to be executed. After either branch, execution resumes following the ENDIF.

Note that the ELSE portion of this control structure is optional. If it is eliminated, a false flag will cause execution to continue following the ENDIF.

When the IF-ELSE-ENDIF control structure is used, the resulting stack change in each of the branches must be equal. For example, "IF 1. ENDIF" is illegal because the true branch places the double number "1." on the stack and the false branch does not change the stack.

IF-ELSE-ENDIF control structures may be embedded (nested) to any level.
1 2 = IF 3 ELSE 4 ENDIF

INPUT

n1 n2 --- n3
"input"
The INPUT operator is used to read data, n3, from an S-34 Bus® module. The top stack value, n2, is the address of the S-34 Bus® module from which the data will be input. The input channel number that will provide the data is n1. Users should consult an input channel list to determine the valid module addresses and channel numbers for their specific DCP configurations. Invalid channel numbers or module addresses will cause n3 to be returned as 0.
10 64 INPUT 7

OR

n1 n2 --- n3
"or"
Perform a bit-wise logical OR on the 16-bit numbers, n1 and n2. The result is a 16-bit number, n3.
1 2 OR 3

OUTPUT

n1 n2 n3 ---
"output"
This operator is used to output 16-bit signed data, n1, to the module data channel, n2, at S-34 module address n3. Valid module addresses for OUTPUT are 64-254. This command performs no operation if applied to a module whose address is outside this range or to a channel number that is not an output channel. The user should consult an output channel list to determine valid module addresses and channels.
3 0 64 OUTPUT

SAVE

n ---
"save"
Specify the Data Structure associated with the processing equation as being a SAVE type. When the equation is executed, the 16-bit signed number, n, is stored in the SAVE Data Structure. If the data structure is accessed for output or processing, the last value of n is returned.
T7 ← 2 SAVE ;

Tn   - - - n   (or)
                      - - -
"t - n"

Tn is the generic name for a user-definable data storage and processing operator. Once assigned to an equation, use of Tn allows:

1. Access to processed data in equation -- 10 T1 +
2. Access to processed data for output -- T7 T1 DONE
3. Access to processed data from the terminal — T7 VIEW
4. Assigning new equation -- T2 <- . . .
5. Listing equation -- T1 ?EQ
6. Testing equation -- T2 CYCLE

Tn will leave a 16-bit signed value, n, on the stack only when accessed in an equation. This value is determined by the Data Structure type assigned to the equation and is the last calculated value.

T1 <- T1 1 + SAVE ;

APPENDIX C

DCP SOFTWARE

The software that is in use in the FLOWS automatic weather stations is described. The two separate "scans" executed each minute by the DCPs are explained, and annotated listings of each part of the program are given.

1. Scan 1 (S1)

a. Description

The first scan, S1, is executed every minute but the lengthy equation it contains, which programs the sensor interface to sample the various sensor voltages, is executed only during the first minute. A complete explanation of the port process numbers, autosample group numbers, and processing request codes can be found in the manual for the Synergetics sensor interface module (3252A). However, a brief illustration will be given here.

The following lines of code (listed on the left and explained in detail on the right) set up the sensor interface to sample temperature:

Temperature

10 0 96 OUTPUT

10 = Port/Process number. Says signal for temperature is at port 10, and is a single ended, analog input (see Table C-1).
0 = First channel in autosample group 0-5 (see Table C-2).
96 = Module #96, the 3252A sensor interface module.
OUTPUT = outputs port process number to first autosample channel of 0-5

10 1 96 OUTPUT

10 = sample rate, every 10 seconds
1 = sends sample interval to 2nd channel in autosample group 1.
96 = Module #96 (as above)

60000 0 96 OUTPUT

60000 = Final processing request to continue sampling.
0 = Autosample channel group

The Port/Process number can also specify the gain to be applied to the signal before it is used in the equation for engineering units or that the

TABLE C-1.   COMPOSITION OF DCP PORT/PROCESS NUMBERS.

Hundreds,Tens and Units Digits		
1-48	Analog (Main Mux)	1-32 are single-ended inputs 33-48 are differential pairs
101-132	Digital(Main Mux)	subtract 100; result is a single-ended Main Mux input
201-248	Frequency(Main Mux)	subtract 200; result is a single-ended or diff. pair
249-250	Serial(Serial Port)	(consult factory)
251-254	Freq. (Timer Mux)	subtract 250; result is Timer Mux input (1-4)

Ten Thousands and Thousands Digits

```
Analog:    0 = DC, Gain=1   (-6.14 to +6.14 V., 1 unit=1 mv)
        1000 = DC, Gain= 10 (-1.22 to +1.22 V., 1 unit=0.1 mv)
        2000 = DC, Gain=100 (-0.12 to +0.12 V., 1 unit=0.01 mv)
        4000 = AC, Gain=1   (-6.14 to +6.14 V., 1 unit=1 mv)
        5000 = AC, Gain= 10 (-1.22 to +1.22 V., 1 unit=0.1 mv)
        6000 = AC, Gain=100 (-0.12 to +0.12 V., 1 unit=0.01 mv)

      Add 10,000 for 540 degree wind direction pot only
```

```
Digital:   1000 = 1 bit
           2000 = 2 bits
             .      .
             .      .
          16000 = 16 bits
```

```
Freq.   0 =    1 period,  1 unit = 100 microseconds (0-3.2 sec.)
     1000 =   16 periods, 1 unit =  10 microseconds (0-320 msec.)
     2000 =  256 periods, 1 unit =   1 microsecond  (0-32 msec.)
     3000 =  256 periods, 1 unit = 0.1 microseconds (0-3.2 msec)
     4000 =    1 period,  1 unit = 0.01 Hertz       (0-320.00 Hz.)
     5000 =   16 periods, 1 unit =  0.1 Hertz       (0-3.2000 Khz.)
     6000 =  256 periods, 1 unit =   1 Hertz        (0-32.000 Khz.)
     7000 =  256 periods, 1 unit =  10 Hertz        (0-65.000 Khz.)
```

TABLE C-2. DCP AUTOSAMPLE CHANNEL INTERPRETATION.

AUTOSAMPLE CHANNELS

Channel Number	Group
0-5	1
6-11	2
12-17	3
18-23	4
24-29	5
30-35	6
36-41	7
42-47	8
48-53	9
54-59	10
60-65	11
66-71	12
72-77	13
78-83	14

Sampling Requests

n = send OUTPUT Port/ Process number

$n+1$ = send output interval in seconds

Read Final Data

n = not used

$n+1$ = number of samples

$n+2$ = minimum

$n+3$ = maximum

$n+4$ = average or mean

$n+5$ = standard deviation

input is to be counted as frequency. The Port/Process numbers for baro-metric pressure and wind speed are given below. Table C-2 contains the information needed to compose these Port/Process numbers. See the example on the following page for a listing of S1 as it is currently set up.

<u>Pressure</u>

```
2047 12 96 OUTPUT          2047 = 2000 - DC gain of 100
                                    47 - analog differential input
                                         at port (47-32)=15
                              12 = Autosample group
```

<u>Wind Speed</u>

```
5212 18 96 OUTPUT          5212 = 5000 - Frequency, 0.1 Hz, from
                                         0 to 3.2 KHz
                                   200 - Frequency (Main Mux).
                                         Indicates that the 5000
                                         pertains to frequency
                                         resolution, not analog DC
                                         (gain 10) or digital
                                         (5 bits).
                                    12 - Analog, single ended, #12
                              18 = Autosample group
```

b. Example

Listed here is the first scan of the program being run in each FLOWS automatic weather station DCP. The text and indentation have been added for clarification, and are not actually stored as part of the program. The scan consists of "T-equations" or storage locations/program statements, which are executed in the order in which they were entered. The T-numbers cannot be reused in different scans, and a maximum of 60 may be used altogether.

EXAMPLE OF CURRENT DCP SOFTWARE SCAN 1

```
           DAY   HR   MIN   SEC
S1          0    0    1     0      (INTERVAL)
                 0    0     5      (TIME)
==================================================

T1 <- ;
T2 <- ;

T3 <- T3 0 = IF
         10 0  96 OUTPUT      Temperature
         10 1  96 OUTPUT
       2043 6  96 OUTPUT      Relative Humidity
         10 7  96 OUTPUT
       2047 12 96 OUTPUT      Barometric Pressure
         10 13 96 OUTPUT
       5212 18 96 OUTPUT      Average & Peak Wind Speed
          5 19 96 OUTPUT
         13 24 96 OUTPUT      Sine of Wind Angle
          5 25 96 OUTPUT
         14 30 96 OUTPUT      Cosine of Wind Angle
          5 31 96 OUTPUT
         16 36 96 OUTPUT      Precipitation
         10 37 96 OUTPUT
            1 SAVE ENDIF ;

T4 <- 60000 0  96 OUTPUT
      60000 6  96 OUTPUT
      60000 12 96 OUTPUT
      60000 18 96 OUTPUT
      60000 24 96 OUTPUT
      60000 30 96 OUTPUT
      60000 36 96 OUTPUT ;

DONE
```

2. Scan 2 (S2)

a. Description

It is in the second scan, S2, that the one minute averaged values (and peak value in the case of wind speed) are converted into engineering units and stored in arrays for transmission. The arrays each hold 30 integer values, one for each minute data was collected in the half-hour interval between transmissions.

Separate T-equations have been used for each of the voltage signals as they are read from the appropriate channels because when setting up the stations in the field, it is often more valuable to be able to see the signal directly than it is to see the engineering units or derived values. Examples of the statements that read the channel input values for temperature, average wind speed, and peak wind speed are given below. Use of these input statements in the context of the rest of the DCP program is illustrated in the example on the following page.

Temperature

4 96 INPUT
    4 = Autosample channel n+4 where n=0 for temperature. This contains the average or mean for the scan interval (1 min). (see Table C-2).
    96 = Module #96
    INPUT = Reads value in selected channel; (here channel 4).

Average wind speed

22 96 INPUT
    22 = Autosample channel n+4 where n=18 (n+4 = average value).

Peak wind speed

21 96 INPUT
    21 = Autosample channel n+3 where n=18 (n+3 = max value).

b. __Example__

Throughout S2 are the "INPUT" statements described in the previous section. The temperature, barometric pressure, and rainfall equations all require input calibration constants denoted here simply by "A", "B", or "C". For the temperature probes, only two sets of constants are required - one set for the 80° range probes and a different set for the 100° range probes. Each barometer and raingage, however, has a unique set of constants. The barometer constants are determined during calibration and by the correction to mean sea level at each site and the rain gage constants are determined in the field by using a set of weights to simulate different known amounts of rain in the bucket. The software is recorded on a micro-cassette with zeroes in place of these constants, and the actual values are entered in the field during set-up.

Listed here is the second scan of the program being run in each DCP. The text and indentation have been added for clarification, and are not actually stored as part of the program. See Appendix B for the definitions of the operators, symbols, and functions used.

<u>EXAMPLE OF CURRENT DCP SOFTWARE SCAN 2</u>

```
        DAY   HR   MIN   SEC
S2       0    0     1     0      (INTERVAL)
                    0    15      (TIME)
============================================
```

T5 <- ;

      Temperature (°C * 100)

```
T6 <- ;
T7 <- "A" SAVE ;                (Intercept e.g. 9579)
T8 <- "B" SAVE ;                (Slope e.g. 4087)
T9 <- 4 96 INPUT SAVE ;
T10 <- T7 T8 T9 1000 */ - 30 DIM ;
```

      Relative Humidity (% * 100)

```
T11 <- ;
T12 <- 10 96 INPUT SAVE ;
T13 <- T12 30 DIM ;
```

      Barometric Pressure (millibars * 10)

```
T14 <- ;
T15 <- "A" SAVE ;              (Slope  e.g. 19266)
T16 <- "B" SAVE ;              (Intercept e.g. 4087)
T17 <- "C" SAVE ;              (Correction to mean sea level)
```

```
T18 <- 16 96 INPUT SAVE ;
T19 <- T15 T18 10000 */ SAVE ;
T20 <- T16 T17 T19 + + 30 DIM ;
```

Average Wind Speed (m/s * 100) (not transmitted)

```
T21 <- ;
T22 <- 22 96 INPUT SAVE ;
T23 <- 18 200 T22 + 100 */ SAVE ;
```

Peak Wind Speed (m/s * 100)

```
T24 <- ;
T25 <- 21 96 INPUT SAVE ;
T26 <- 18 200 T25 + 100 */ 30 DIM ;
```

Average Sine of Wind Direction (millivolts)

```
T27 <- 28 96 INPUT SAVE ;
```

Average Cosine of Wind Direction (millivolts)

```
T28 <- 34 96 INPUT SAVE ;
```

Test to see if the Cosine is below 732 or above 4268. This
represents angles between 315° and 45° to the north, and
135° and 225° to the south. If it is, T29 will be true, and
the Sine instead of the Cosine will be transmitted. Likewise,
the Cosine instead of the Sine will be tested for
being greater than, less than, or equal to zero (2500).

```
T29 <- T28 732 <
       T28 4268 > OR SAVE ;
```

Determine the transmitted variable. If the Sine is transmitted,
add 10,000 to signal this fact. T30 is always transmitted.

```
T30 <- T29 IF T27 10000 +
          ELSE T28
          ENDIF 30 DIM ;
```

Determine the tested variable. If the Cosine is transmitted, the
Sine is tested, and vice versa. T31 is always the one checked.

```
T31 <- T29 IF T28
          ELSE T27
          ENDIF SAVE ;
```

Constant dependent on sign of T31 (sine or cosine).

```
T32 <- T31 2500 > IF 10000
                ELSE T31 2500 < IF 20000
                              ELSE 0
                              ENDIF
           ENDIF SAVE ;
```

Average Wind Speed + Constant

```
T33 <- ;
T34 <- T23 T32 + 30 DIM ;
```

Rain (millimeters * 10)

```
T35 <- ;
T36 <- "A" SAVE ;                    (Slope  mm/V)
T37 <- "B" SAVE ;                    (mv when no rain)

T38 <- 40 96 INPUT SAVE ;
T39 <- T36 T37 100 */ SAVE ;
T40 <- T36 T38 100 */ SAVE ;
T41 <- T40 T39 - 30 DIM ;
```

Status Word

```
T42 <- ;
T43 <- 12 0 INPUT SAVE ;
```

DONE

3. Headers

The headers, H1-H8 represent the data that is actually transmitted. Notice that all variables (T-equations) being transmited, except Status, are dimensioned to 30.

Transmitted variables H1 - H8

```
H1 T10   Temperature
H2 T13   Relative Humidity
H3 T20   Barometric Pressure
H4 T34   Average Wind Speed + Constant
H5 T26   Peak Wind Speed
H6 T30   Cosine -or- Sine of Wind Direction
H7 T41   Rain
H8 T43   Status
```

APPENDIX D

ALGORITHM FOR DECODING WIND DIRECTION

```
    DIRECTION = Transmitted variable representing SINE or COSINE
    AWSPD = Average wind speed in meters per second

 If DIRECTION > or = to 10000. then:

    SINE = DIRECTION - 10000.
    Sine = (SINE - 2500.)/2500.
    ANGLE = Arcsine (Sine) (in degrees)

    If AWSPD > or = to 200. then:
       AWSPD = AWSPD - 200.
       COSINE < 0.
       Average wind angle = 180. - ANGLE
    Else
       If AWSPD > or = to 100. then:
          AWSPD = AWSPD - 100.
       Endif
       COSINE > or = 0.
       If ANGLE < 0 then:
          Average wind angle = 360. + ANGLE
       Else
          Average wind angle = ANGLE
       Endif
    Endif

 Else

    COSINE = DIRECTION
    Cosine = (COSINE - 2500.)/2500.
    ANGLE = Arccosine (Cosine) (in degrees)

    If AWSPD > or = to 200. then:
       AWSPD = AWSPD - 200.
       SINE < 0.
       Average wind angle = 360. - ANGLE
    Else
       If AWSPD > or = to 100. then:
          AWSPD = AWSPD - 100.
       Endif
       SINE > or = 0.
       Average wind angle = ANGLE
    Endif

 Endif
```

The following examples illustrate how to find the average wind speed and direction given AWSPD and DIRECTION values on the Synergetics data file.

Example 1.

AWSPD = 204.14   DIRECTION = 3147.

Since DIRECTION is less than 10000, know COSINE was transmitted. Subtract 200. from AWSPD:

    Sine is negative
    ================================
    Average wind speed = 4.14 m/s
    ================================

Compute arccosine of rescaled COSINE:

    Cosine = (COSINE - 2500.)/2500. = 0.259
    Arcosine (Cosine) = ANGLE = 75.0°

Then, since the sine is negative:

    Average wind direction = 360.° - ANGLE
    ==
    Average wind direction = 285.°
    ==

Example 2.

AWSPD = 221.73   DIRECTION = 11727.

Since DIRECTION is greater than 10000, know SINE was transmitted. Subtract 200. from AWSPD:

    Cosine is negative.
    ==
    Average wind speed = 21.73 m/s
    ==

Compute arcsine of rescaled SINE:

    Sine = [(SINE - 10000.) - 2500.]/2500. = -0.309
    Arcsine (Sine) = ANGLE = -18.0°

Then, since the cosine is negative:

    Average wind direction = 180° - ANGLE
    ==
    Average wind direction = 198.°
    ==

APPENDIX E

INTERPRETATION OF DCP STATUS WORD

The DCP Status Word contains 16 bits of encoded information about the DCP internal temperature, the forward power, the battery voltage and error codes. One DCP Status Word is sent with each message, once each half-hour. It represents the status of the DCP just before transmission.

Interpretation of the DCP Status requires writing the decimal number in its binary form, and numbering the bits from 0 (lsb) to 15 (msb). Table E-1 on the following page shows how to interpret the various bit positions.

Example: DCP Status = 1974

Rewrite as binary:

15	14	13	12	11	10	9	8	7	6	5	4	3	2	1	0
32768	16384	8192	4096	2048	1024	512	256	128	64	32	16	8	4	2	1
0	0	0	0	0	1	1	1	1	0	1	1	0	1	1	0

```
    0     0     0     0     0
_____
Status Error Code = 0

                        1    1    1
                 Battery Voltage > 13.49 V

                            1    0    1    1
                    Forward Power 40.-41.9 dBm

                                      0
                   Ratio Forward/Reverse Power > 10

                                      1    1    0
                       DCP Temperature 35.- 47.4 C
```

Status Word																
Bit No.	15	14	13	12	11	10	9	8	7	6	5	4	3	2	1	0
		Error Codes				Battery Voltage			Forward Power				F/R Flag	DCP Temperature		

DCP Temperature						
Bit No.			Code	Temperature in degrees		
2	1	0				
0	0	0	0	-27.6	or	below
0	0	1	1	-27.5	to	-14.9
0	1	0	2	-15.0	to	-2.4
0	1	1	3	-2.5	to	9.9
1	0	0	4	10.0	to	22.4
1	0	1	5	22.5	to	34.9
1	1	0	6	35.0	to	47.4
1	1	1	7	47.5	or	above

Forward Transmitter Power											
Bit				Code	Power in dBm	Bit				Code	Power in dBm
7	6	5	4			7	6	5	4		
0	0	0	0	0	<20.0	1	0	0	0	8	38-35.9
0	0	0	1	1	20-21.9	1	0	0	1	9	36-37.9
0	0	1	0	2	22-23.9	1	0	1	0	10	38-39.9
0	0	1	1	3	24-25.9	1	0	1	1	11	40-41.9
0	1	0	0	4	26-27.9	1	1	0	0	12	42-43.9
0	1	0	1	5	28-29.9	1	1	0	1	13	44-45.9
0	1	1	0	6	30-31.9	1	1	1	0	14	46-47.9
0	1	1	1	7	32-33.9	1	1	1	1	15	≥48

Battery Voltage							
Bit No.			Code	Battery Voltage Range			
10	9	8					
0	0	0	0	<10.5			
0	0	1	1	10.50	to	10.99	
0	1	0	2	11.00	to	11.49	
0	1	1	3	11.50	to	11.99	
1	0	0	4	12.00	to	12.49	
1	0	1	5	12.50	to	12.99	
1	1	0	6	13.00	to	13.49	
1	1	1	7	>13.49			

Status Error Codes						
Bit No.				Decimal Error Code	ASCII Character	Meaning
15	14	13	12	11		
1	1	1	0	1	29	~(7E)	Low battery voltage (<10.5 V) during transmission
1	1	0	1	1	27	} (7D)	ADR timeout error
1	1	0	1	0	26	} (7D)	Hydro module did not turn on
1	1	0	0	0	24	| (7C)	XMT error, phase-lock not achieved in 1 second
1	0	1	1	1	23	{ (7B)	XMT error, no power amp (PA) acknowledge
1	0	1	1	0	22	{ (7B)	XMT error, no synthesizer acknowledge
1	0	1	0	1	21	z (7A)	XMT error, transmission attempted within 70 seconds of last one
1	0	1	0	0	20	z (7A)	XMT error, status incorrect
1	0	0	1	1	19	y (79)	XMT error, circular buffer fill error
1	0	0	1	0	18	y (79)	GOES channel read back error
0	1	1	1	1	15	G (47)	Transmitter time out error
0	1	1	1	0	14	G (47)	XMT error, hardware buffer underflowed
0	1	0	1	0	10	E (45)	Format error, software buffer overflowed
0	1	1	0	1	13	F (46)	Undefined interrupt error
0	1	1	0	0	12	F (46)	undefined S-34 Bus* interrupt